Renormalization group flow of the Higgs sector

Dissertation

zur Erlangung des akademischen Grades
doctor rerum naturalium (Dr. rer. nat.)

vorgelegt dem Rat der Physikalisch-Astronomischen Fakultät
der Friedrich-Schiller-Universität Jena

von M. Sc. René Sondenheimer
geboren am 19.08.1988 in Weimar

Gutachter

1. **Prof. Dr. Holger Gies (Friedrich-Schiller-Universität Jena)**
2. **Prof. Dr. Axel Maas (Karl-Franzens-Universität Graz)**
3. **Prof. Dr. Jan Pawlowski (Ruprecht-Karls-Universität Heidelberg)**

Tag der Disputation: 17.02.2016

Renormierungsgruppenfluss des Higgs-Sektors

Zusammenfassung

Im Rahmen dieser Arbeit werden nicht-störungstheoretische Renormierungsgruppenflüsse in verschiedenen Higgs-Yukawa Modellen untersucht, welche bestimmte Eigenschaften des Higgs-Sektors des Standardmodells der Teilchenphysik imitieren. Dafür hinterfragen wir kritisch die konventionellen Argumente, die eine untere Schranke an die Masse des Higgs-Bosons mit dem Problem der Stabilität des Vakuums in Verbindung bringen. Für diese Analyse nutzen wir die funktionale Renormierungsgruppe als nicht-störungstheoretische Methode. Darüber hinaus leiten wir analytische Resultate für die Beiträge der fermionischen Determinante zum Higgs Potential her. In beiden Fällen finden wir bei beliebigem endlichem Cutoff keine Hinweise, dass Top-Quark Fluktuationen eine Instabilität oder Metastabilität des Vakuums erzeugen, falls man sich auf die Klasse von störungstheoretisch renormierbaren Theorien beschränkt. Weiterhin erlaubt der vorgenommene nicht-störungstheoretische Zugang beliebige nackte Kopplungen zu betrachten, sodass auch der Fall starker Kopplungen untersucht werden kann.

Ein endlicher Massenbereich für das Higgs-Boson ergibt sich im Infraroten in natürlicher Weise aus dem Renormierungsgruppenfluss im Falle der gewöhnlichen Klasse von ϕ^4 Potentialen an der ultravioletten Cutoff-Skala. Higgs-Massen außerhalb dieser Schranken können in keiner Weise mit physikalisch sinnvollen nackten Parametern innerhalb der Klasse von ϕ^4 Potentialen in Verbindung gebracht werden. Die untere Higgs-Massenschranke folgt aus der Forderung einer wohldefinierten Zustandssumme. Dies setzt ein stabiles nacktes Potential voraus. Allerdings kann die Schranke aus dieser Konsistenzbedingung wesentlich verschoben werden, indem allgemeinere nackte Potentiale an der Cutoff-Skala des Standardmodells zugelassen werden, ohne dass In- oder Matestabilitäten erzeugt werden. Wir identifizieren einen einfachen Renormierungsgruppenmechanismus zur Erklärung dieser Verringerung der unteren Higgs-Massenschranke. Sollte dieser Mechanismus auch im vollen Standardmodell der Teilchenphysik vorhanden sein, führen Higgs-Massen unterhalb der konventionellen unteren Schranke nicht notwendigerweise zu einem In-/Metastabilitätsproblem.

Wir beginnen unsere Untersuchungen in einem einfachen Higgs-Yukawa Modell, welches den Higgs-Top Sektor des Standardmodells imitiert. Im Folgenden erweitern wir dieses einfache Modell, indem wir sukzessive weitere Teile des Standardmodells berücksichtigen und untersuchen deren phänomenologische Einflüsse auf die untere Higgs-Massenschranke sowie den Mechanismus der Verringerung dieser. Schlussendlich geben wir eine nicht-störungstheoretische Flussgleichung für das Higgs-Potential im vollen Standardmodell an.

Renormalization group flow of the Higgs sector

Abstract

We investigate nonperturbative renormalization group flows of various Higgs-Yukawa models mimicking the Higgs sector of the standard model of particle physics. We reanalyze the conventional arguments that relate a lower bound for the Higgs mass with vacuum stability in the framework of the functional renormalization group as well as in the light of exact results for the regularized fermion determinant. In both cases, we find no indication for vacuum instability nor metastability induced by top fluctuations if the cutoff is kept finite but arbitrary for standard bare actions which are perturbatively renormalizable. Moreover, the nonperturbative approach allows for treating arbitrary bare couplings such that we are also able to approach the strong coupling limit.

For the class of standard bare potentials of ϕ^4 type at a given ultraviolet cutoff scale, we show that a finite infrared Higgs mass range emerges naturally from the renormalization group flow itself. Higgs masses outside the resulting bounds cannot be connected to any conceivable set of bare parameters in this standard model ϕ^4 class. A lower bound for the Higgs mass arises from the requirement of a well-defined partition function, i.e., stability of the bare potential. This consistency bound can, however, be relaxed considerably by more general forms of the bare potential without necessarily introducing new metastable minima. We identify a simple renormalization group mechanism for this diminishing of the lower bound. If this depletion is also active in the full standard model, Higgs masses smaller than the conventional infrared window do not necessarily require new physics at low scales or give rise to instability problems.

Starting our analysis from a simple Higgs-Yukawa model, which mimics the Higgs-top sector, we successively take more standard model degrees of freedom into account and study their phenomenological influence on both, the calculation of a lower Higgs mass consistency bound from the nonperturbative flow equations as well as on the mechanism of diminishing this consistency bound. Finally, we present a nonperturbative flow equation for the full standard model Higgs potential.

Contents

1 Introduction

The recent discovery of a Higgs boson at the LHC by the ATLAS [1] and CMS [2] collaborations completed our current version of the standard model of particle physics. This observation counts as a remarkable success for experiment as well as theory and is a paradigm for the fruitful interplay between both. So far, the standard model succeeded in describing particle experiments up to a few TeV, the energy range tested by the LHC. Its phenomenological development already started in the early sixties. In 1961, Glashow pointed out that there is the possibility to combine the weak interaction with the electromagnetic one [3]. However, gauge theories which are used to describe the interactions between particles have a major deficit. They can be only constructed for massless gauge fields which contradicts the fact that the weak gauge bosons are massive. The situation is even worse. In fact, weak interactions violate parity maximally. Thus, a mass term for all matter particles which take part in the weak interaction is forbidden. A way to circumvent the problem of massless gauge bosons was found by Brout and Englert [4], Higgs [5–7], and also a few months later by Guralnik, Hagen, and Kibble [8] in 1964. They introduced a mechanism based on spontaneous symmetry breaking which finally leads to massive gauge bosons. Similar techniques were used in solid state physics by Anderson in order to describe superconductors [9]. However, it took another three years until Weinberg [10] and Salam [11] applied the mechanism provided by Brout, Englert, Higgs, Guralnik, Hagen, and Kibble to the electroweak unification of Glashow. Further, Weinberg and Salam realized that the Higgs mechanism is able to generate the masses of the leptons as well. This consideration was generalized to quarks a few years later [12]. Thus, the electroweak sector obtained its modern form.

In addition, a theoretical description of the strong force was developed at this time. The introduction of color as a supplemental quantum number [13–17] allowed to consider hadrons as composites of quarks which are particles with a fractional number of electric charge. These quarks are glued together to form mesons and baryons by the force carrying particle of the strong interaction, the gluon [18]. Thus, the standard model of particle physics acquired its final form as a gauge theory in the seventies. The gauge bosons mediate the fundamental forces of the electroweak and strong interactions between the matter particles, which are fermions, while the Higgs mechanism provides a technique to introduce masses into the theory without spoiling the gauge symmetry.

After its theoretical formulation, all particles and various processes predicted by the standard model were confirmed by experiment, for instance, the occurrence of weak neutral currents [19],

the discovery of the W and Z bosons [20–22] with their predicted masses, or the discovery of the top quark [23, 24]. Finally, the Higgs boson was the long-term missing piece. Actually, strong evidence is accumulated that the new bosonic particle that was found at the LHC in 2012 has the properties which the standard model predicts for the Higgs boson, e.g., the quantum numbers [25–27], coupling to weak gauge bosons [28], leptons [29], as well as down-type quarks [30]. Hence, it is likely that this boson is the standard model Higgs boson indeed.

Further experimental tests will figure out whether the confirmation of the standard model will continue or indications for new physics beyond the standard model will be found. Though, there is no experimental observation within particle physics for physics beyond the standard model after LHC Run 1 so far. One of the few noteworthy deviations are discovered in the decay of a B_s^0 meson [31]. While the angular observables of the decay products are in agreement with standard model predictions, the branching fraction is 3.5 standard deviations below the standard model prediction. Currently, it is an open question, if this result is only a statistical fluctuation, an underestimated hadronic effect, or indicates physics beyond the standard model. However, without any strong hint for new phenomena, the standard model is the most successful theory in particle physics at present.

Despite the unprecedented achievement of the standard model in explaining the LHC experiments, it has some shortcomings. In fact, we know that the standard model is not the end of the story. There are indications for an even more fundamental theory. Most of the experimental indications are found in astrophysics and cosmology, for instance, the existence of dark matter to explain the motions of the galaxies, the accelerated cosmic expansion found in supernova data, or inflation which may be visible in the cosmic microwave background. None of the standard model forces or particles are able to describe these mechanisms in an appropriate manner. Furthermore, there are also open issues from a theoretical point of view.

The interactions described by the standard model do not include gravity. Currently, the best theory of gravity is general relativity [32] while the other three fundamental forces are described in terms of quantum field theories. A conventional quantization for gravity fails due to the fact that gravity is perturbatively nonrenormalizable. The fact that we do not have a consistent quantum theory of gravity is not a problem at energy scales tested presently and in the near future. Compared to the other interactions, the gravitational interaction between subatomic particles is extremely weak at scales far below the Planck scale. Therefore, gravity can be completely neglected in phenomenological considerations. However, at least at the Planck scale quantum effects arising from gravity will be comparable to the other interactions. For this reason, the pure standard model should be considered as an effective field theory which is valid at most up to the Planck scale. Beyond this cutoff a more fundamental theory appears to be required that also treats gravity appropriately. Actually, two strategies are pursued. Either this theory describes gravity and the other forces of nature within the usual framework of quantum field theory or involves a rather different principle beyond the concepts of quantum field theory. An example for the latter is string theory [33–36]. Other possible approaches to treat gravity on

a quantum level are loop quantum gravity [37], supergravity [38], or asymptotic safety [39–41]. Whether these methods describe gravity and the other forces of nature in a unified setting or only offer a route to quantize gravity consistently, depends on the precise details and particular models which are considered. Furthermore, there are unsolved problems within the standard model itself. Three urgent problems are directly related to the Higgs sector: the triviality problem, the hierarchy problem, and the vacuum (in-/meta-)stability problem.

The hierarchy problem states that there is an unnatural large separation between the Planck and the Fermi scale, such that a high degree of fine-tuning of the Higgs parameters is necessary to obtain this separation. There is no symmetry which protects the mass parameter of the Higgs against large radiative corrections. Thus, it would be natural to expect that the Higgs mass parameter is of the order of the standard model cutoff scale. Of course, it is likely that the scale of maximal UV extension of the standard model is even below the Planck scale. For instance, the three gauge couplings for the three standard model interactions appear to become of similar size near a scale of 10^{16}GeV. This fact can be viewed as an indication for a possible unification of the strong and electroweak interaction [42, 43]. Then, new physics would set in at this GUT scale. Even if the underlying theory of the standard model is not far away from the Fermi scale such that only a small amount of fine-tuning is needed, the standard model has 26 free parameters which differ by ten orders of magnitude at least. The standard model has no explanation for this hierarchy for the different coupling strengths between the particles. Although unsatisfactory from a phenomenological point of view, this is more an aesthetic question rather than a fundamental problem of the theory. In principle there is no reason why nature should not be fine-tuned.

A reason for concern about the standard model is rather, that the pure Higgs sector can predict its own failure by studying the renormalization group (RG) flow at high energies. Thus, a possible scale of maximal UV extension can be deduced which restricts the standard model to an effective field theory. These considerations are linked to the mass of the standard model Higgs particle. While the Higgs mass is a free parameter in the classical theory, renormalization group arguments were used to obtain bounds on the Higgs mass long before its discovery.

So far, strong evidence is accumulated that the only consistent quantum field theory of a scalar field in four spacetime dimensions is a free field theory [44, 45]. In perturbation theory this behavior manifests in the Landau pole of the quartic self interaction, i.e., the running coupling diverges at a finite RG scale. Thus, a pure scalar field theory seems perturbatively only valid on scales below the Landau pole and cannot be a fundamental theory of nature or has to be noninteracting. This fact can be summarized as the triviality problem. Of course, perturbative techniques break down for strong couplings. Nonperturbative effects could change the renormalization group flow in the strong coupling regime in such a way that the coupling does not diverge at finite but arbitrarily large scales. However, even nonperturbative methods support the statement that a fundamental scalar field theory is trivial and has to be defined with an intrinsic cutoff [46–51].

Though, the situation is less clear in case of interactions between a scalar field with other particles. For instance, the occurrence of a non-Gaußian fixed point could render the RG flow in the deep UV finite. Currently, it is under consideration, if bosonic and fermionic fluctuations in Higgs-Yukawa models can balance each other in such a way that the cutoff of the theory can be send to infinity [52–54]. Furthermore, asymptotic safety [55] as well as asymptotic freedom [56–58] in gauged Higgs models point out that the triviality problem could be circumvented. If a non-Gaußian fixed-point exists, also the hierarchy problem might be weakened or solved, depending on the critical exponents of this fixed point. Unfortunately, it is not straightforward to generalize the results from these toy models to the complex structure of the standard model. Therefore, the triviality of the scalar sector serves to obtain an upper bound on the mass of the standard model Higgs boson [59–64]. However, the triviality bound is not a problem for energy scales below the Planck scale due to the observed light Higgs.

Also, a lower bound on the Higgs mass can be obtained from RG arguments. In particular, this bound is directly related to the vacuum stability problem of the effective Higgs potential [65–81]. The precise shape of the effective potential depends on accurate measurements of various parameters. The most important quantities are the Higgs mass, the mass of the top quark, and the value of the strong coupling constant. Whether the mass of the Higgs satisfies or violates the lower bound has important consequences. These range from upper bounds for the scale of new physics and constraints on the underlying UV theory to the prediction of the decay of our universe as we know it. Currently, the measured Higgs mass seems to violate the lower bound at high energy scales. However, there is still the opportunity that the Higgs mass is close to or even on top of the lower bound due to the uncertainty in the measurement of the top mass [82]. Therefore, a thorough understanding of the lower Higgs mass bound within the standard model is clearly mandatory.

The vacuum stability problem is given by the fact that the effective scalar potential can obtain a second minimum at large scales besides the one at the Fermi scale depending on the values and the ratio of the Higgs and top mass. The effective potential is called metastable if the second minimum is the lowest energy state and the inverse decay rate from the false electroweak vacuum to the true vacuum state exceeds the lifetime of our universe. For larger decay rates, or even the case that the potential is unbounded from below, the potential becomes unstable. In case of a stable potential, the electroweak minimum is the ground state of the theory.

In the standard perturbative approach, the stability issue is directly related to the running of the scalar quartic self-coupling. The RG flow equations allow to extrapolate the standard-model running couplings to high energies. For current measured values of the couplings, the quartic Higgs coupling λ_2 drops below zero at a scale of approximate 10^{10}GeV due to top fluctuations [83]. Combining this result with the assumption that the RG improved effective potential is well approximated by $U_{\text{eff}} \sim \lambda_2(\mu = \phi)\phi^4$ for large field values, one would conclude that the effective potential becomes unstable, first of all. In fact, the quartic coupling becomes positive

again at very high energies due to the electroweak gauge boson fluctuations. Thus, the scalar potential develops a second global minimum far beyond the Planck scale [84]. Of course, the position of this global minimum is ambiguous due to the fact that at least close to the Planck scale new degrees of freedom are expected to enter the game. Indeed, gravitational corrections are able to deform the running in such a way that the second minimum appears at field values below the Planck scale [85]. In a similar manner this discussion can be generalized to several theories beyond the standard model such as supersymmetry [86–88], theories with additional heavy particles [89, 90] and dark matter candidates [91–94], as well as in the context of inflation and the early universe [95–104] or curved spacetime [105, 106]. The main idea is, that new degrees of freedom could modify the running of the standard-model couplings in such a way that the effective potential is stable for all field values.

In the standard line of reasoning, the metastability is associated with the large Yukawa coupling of the top quark. This Yukawa coupling dominates the β function of the scalar quartic coupling and is responsible that it becomes negative. Nevertheless, the standard approach to this metastability has been questioned by different methods. As mentioned before, typical computations of mass bounds are often done with perturbative methods, although the problem is generically nonperturbative. This is obvious for the upper Higgs mass bound which is related to a strongly coupled Higgs sector in the UV. But also the lower bound involves nonperturbative information. First of all, the prediction of infrared (IR) quantities such as Higgs and top masses involve a proper description of threshold effects. Second, an investigation of stability issues requires the computation of a full effective potential for arbitrary field amplitudes.

First nonperturbative studies of the vacuum stability problem were done in a simple Higgs-Yukawa model. This toy model shares analogous features of the emergence of the lower Higgs mass bound with the standard model. The quartic scalar self-coupling turns negative at high energies due to top fluctuations for a too light Higgs. Therefore, the effective potential has an instability and is unbounded from below in the usual perturbative treatment. As a result, a lower bound on the Higgs mass is obtained by requiring that the effective potential should be stable. However, this observation is in conflict with nonperturbative lattice simulations [64, 107, 108]. The effective potential resulting from lattice calculations does not show an instability at all. Of course, it is difficult on the lattice to separate the IR physics from the UV cutoff scale over a wide range of scales. Hence, the lattice simulations have been criticized that they possibly do not cover a large enough scale separation in order to get the information about the relevant part of the effective potential [109].

The aim of this work is to investigate the properties and the emergence of Higgs mass bounds at a nonperturbative level by means of the functional renormalization group in order to cover a wide range of energy scales. In particular, we concentrate on the lower bound for phenomenological reasons. Results for a nonperturbative upper Higgs mass bound are a by-product of our method. Besides lattice results, also functional methods indicate that the occurrence of the instability is questionable. In fact, the instability can be traced back to

an implicit renormalization condition which is not compatible with a well-defined partition function for the theory [110, 111]. Furthermore, our functional renormalization group (FRG) studies show that no instability in the effective potential occurs during the RG flow as long as the bare theory is well-defined [112]. A lower mass bound arises from the renormalization group flow itself as a consistency condition on the UV potential.

Additionally, a route to diminish this lower Higgs mass consistency bound is found by allowing for a generalized class of bare potentials beyond the ϕ^4-type class. We will show that the sole consideration of bare potentials of ϕ^4 type is actually too restrictive. In fact, if the standard model is viewed as a low-energy effective theory, there is no reason to exclude higher-dimensional operators from the bare potential. Their occurrence is actually expected as they are generically generated at the UV cutoff scale of the standard model from the underlying theory. Whereas Wilsonian renormalization group arguments of course suggest that low-energy observables remain almost completely unaffected by the higher-dimensional operators, we demonstrate that Higgs mass bounds can in fact exhibit a significant dependence on the bare potential as higher order operators are able to stabilize the Higgs potential [113–115].

In the perturbative set up, the occurrence of the metastability is connected to the sign of the quartic Higgs self-coupling evaluated at different energy scales. Thus, only the running of a particular coupling in the scalar potential is used to determine the stability of the Higgs potential in the UV as well as in the IR. The details of such a connection between a UV potential $U_\Lambda \sim \lambda_2(\Lambda)\phi^4$ defined at an UV cutoff scale Λ and the shape of the effective potential via $U_{\text{eff}} \sim \lambda_2(\mu = \phi)\phi^4$ at large field values beyond the electroweak minimum has to be tested carefully. In principle, the RG evolution of the Higgs potential is a multiscale problem, depending on the field amplitude as well as on the RG scale. The FRG takes these aspects into account by describing a scale-dependent effective average potential $U(k, \phi)$ which takes all quantum fluctuations up to an IR scale k into account. This effective average potential interpolates smoothly between the bare potential $U(\Lambda, \phi)$ and the effective potential $U(k = 0, \phi)$. Thus, we are able to investigate the RG flow of the entire scalar potential as an arbitrary function of the field amplitude in a Wilsonian sense by integrating out quantum fluctuations momentum shell wise. In this sense, the (meta-)stability properties of the effective potential can be followed in a scale-dependent manner.

The investigation of the RG flow of the scalar potential in various models is carried out with the functional renormalization group as a nonperturbative continuum method. In contrast to lattice simulations, the mutual backreactions between bosonic and fermionic fluctuations can be considered over a wide range of scales. The price to pay for these advantages is the necessity to truncate the effective action. Thus, we carefully study the impact of truncation errors on our results by use of systematic expansions. Starting the investigations in the simple Higgs-Yukawa model, we take successively further standard model degrees of freedom into account. For instance, we will generalize the results of the simple Yukawa model to the full chiral structure of the standard model [116].

The investigation of upper and lower Higgs mass bounds as well as the phase structure of a chiral invariant Higgs-Yukawa model was also performed in nonperturbative lattice calculations [117–121]. Again, the lower Higgs mass bound is given by the consistency condition that the underlying lattice partition function should be well-defined. Once this condition is fulfilled, the effective potential is stable. Constraints on the existence of a potential heavy fourth flavor generation were obtained in the same line of argument [122, 123], also see [124] for a conventional analytical study. Moreover, the mechanism of lowering the lower mass bound by adding higher dimensional operators to the bare potential was confirmed by the lattice [125, 126]. Further, this mechanism was successfully used in a model that involves a dark matter scalar to diminish the lower Higgs mass bound [127].

In order to study the phenomenological implications of generalized bare potentials, we discuss the scale of new physics under the influence of higher dimensional operators. We demonstrate how this scale, at which new physical degrees of freedom beyond the standard model occur, can be shifted by 2-3 orders of magnitude due to stabilizing effects of bare potentials beyond the quartic type. An interesting behavior of the potential will arise by trying to push the cutoff scale of the standard model further to even higher scales but keeping the IR physics constant. While the bare as well as the effective potential are stable in a polynomial expansion of the potential, a second minimum occurs during the RG flow, rendering the effective average potential for some finite RG scales metastable. We introduced the term pseudostable for this special behavior in [128]. However, as long as the calculation is done in a polynomial expansion of the scalar potential, it is questionable, if the appearance or/and disappearance of the second minimum during the RG flow can take place or is only an intricate artifact of the polynomial truncation. Actually, a polynomial truncation is not sufficient to study the global behavior of the potential under the occurrence of two competing minima. In order to answer this question, an RG study of the entire scalar potential beyond a polynomial expansion is done. This investigation will demonstrate how restrictions to polynomial running couplings can produce misleading results for the effective potential.

However, note that if a second minimum develops during the RG flow, it arises in a different manner than the instability of the perturbative calculation. In the case studied in [128], the possible pseudo-stability is seeded in the bosonic bare potential already. Moreover, it could be the case that the underlying UV theory generates a bare Higgs potential with several minima. A specific example for this scenario can be obtained from string phenomenology [129]. The RG flow of such a potential would be highly nontrivial, depending on the position and precise shape of the minima and is clearly beyond the scope of polynomial expansions of the potential in field amplitudes around the Fermi scale.

This thesis is organized as follows: In Chap. 2 we recapitulate the theoretical foundations of this work. We introduce the Higgs sector of the standard model as well as list the one-loop β functions of the relevant couplings to discuss the vacuum stability problem. Further, we demonstrate how the metastability occurs within the perturbative treatment. Finally, we

give a short overview on the FRG to treat the RG flow of the entire scalar potential beyond perturbation theory. Chapter 3 deals with a thorough study of the simple Higgs Yukawa theory. We start the analysis in a (extended) mean-field approximation in which analytical solutions for the Higgs mass and the effective potential are accessible. These solutions demonstrate that no instability in the effective potential occurs if the potential in the UV is bounded from below within ϕ^4 bare potentials. These results are substantiated by investigating the properties of the fermion determinant for various regularization prescriptions. Further, the nonperturbative flow equations for the couplings are studied in a polynomial expansion of the potential. The validity of the polynomial truncation is tested against the flow of the full scalar potential in order to discuss the fate of pseudostable potentials. In addition, we investigate the influence of further higher dimensional operators on the mechanism of diminishing the lower bound. Corrections from strong interactions to the flow equation of the Yukawa coupling are taken into account in Chap. 4. In Chap. 5 we consider chiral invariant Higgs-Yukawa models which respect the chiral structure and the symmetry group of the standard model electroweak Higgs sector. We start with a comparison between the simple Higgs-Yukawa model and a chiral Higgs-top-bottom model with a global symmetry group. Then, we broaden the discussion by means of gauging the $SU(2)$ symmetry. These studies are done within R_ξ gauges which allow to interpolate smoothly between the Landau and the unitary gauge. Finally, we give an outlook on the RG flow equation for the full standard-model Higgs potential on a nonperturbative level.

The compilation of this thesis is solely due to the author. However, parts of this work were done in several collaborations with various authors and have been published in a number of articles. First investigations of Higgs mass bounds in simple Yukawa systems were published in [112] in collaboration with H. Gies and C. Gneiting. The investigation of the flow of the scalar potential beyond a polynomial truncation in Sect. 3.6 is based on a paper in preparation with J. Borchardt and H. Gies. The influence of further higher dimensional operators on Higgs mass bounds (Sect. 3.7) was studied with M. Warschinke and H. Gies and is based on unpublished material. The discussion about the scale of new physics within the Higgs-top-QCD model in Chap. 4 was done in collaboration with A. Eichhorn, H. Gies, J. Jäckel, T. Plehn, and M. Scherer [128]. The investigation of Chap. 5 was done in collaboration with H. Gies. The first section of this chapter is already published in [116].

2 Theoretical foundations

In the following chapter, we review the theoretical concepts and mathematical techniques to tackle the renormalization group flow of the standard model Higgs sector. A brief introduction to spontaneous symmetry breaking, the quantization of gauge theories, and the Higgs mechanism can be found in the appendix, App. A.1. We incorporate the Higgs mechanism with the local gauge symmetries of the electroweak sector and the matter content of the standard model to obtain massive gauge bosons as well as massive fermions. The inclusion of the strong force completes our summary of the standard model. Of course, the content of these sections is already presented in almost every textbook about quantum field theory and theoretical particle physics, e.g., see [130–132]. However, we rather use these sections to introduce our notation and conventions as well as for reasons of completeness. Afterward, we consider the RG flow of the standard model to discuss the vacuum metastability problem as it was done in the literature so far. Therefore, we list the perturbative β functions for the standard model running couplings. In the literature the usual approximation for the Higgs effective potential is obtained from these β functions. We carefully discuss the advantages and shortcomings of the perturbative approach and finally introduce the functional renormalization group as an alternative tool for the computation of the effective action which allows nonperturbative investigations.

2.1 Standard Model of particle physics

The standard model of particle physics describes the interactions between particles via gauge theories. It consists of the Glashow-Weinberg-Salam (GWS) theory and quantum chromodynamics (QCD) which explain the electroweak interactions as well as the strong force, respectively. The symmetry group of the latter is given by a $\mathrm{SU}(3)_\mathrm{c}$ gauge theory whereas the electroweak theory contains the weak isospin, $\mathrm{SU}(2)_\mathrm{L}$, as well as the weak hypercharge, $\mathrm{U}(1)_\mathrm{Y}$. Furthermore, the GWS theory explains the occurrence of three massive gauge bosons via the Higgs mechanism and a remaining massless gauge boson which is interpreted as the force carrier particle of the electromagnetic interaction. Thus, the standard model symmetry group $\mathrm{SU}(3)_\mathrm{c} \times \mathrm{SU}(2)_\mathrm{L} \times \mathrm{U}(1)_\mathrm{Y}$ is broken down to $\mathrm{SU}(3)_\mathrm{c} \times \mathrm{U}(1)_\mathrm{em}$ after electroweak symmetry breaking.

The matter particles are Dirac fermions and can be divided into two types, quarks and leptons. Quarks are charged under the strong force and each quark flavor transforms as a triplet under $\mathrm{SU}(3)_\mathrm{c}$. Leptons do not interact with gluons, the $\mathrm{SU}(3)_\mathrm{c}$ gauge bosons, and

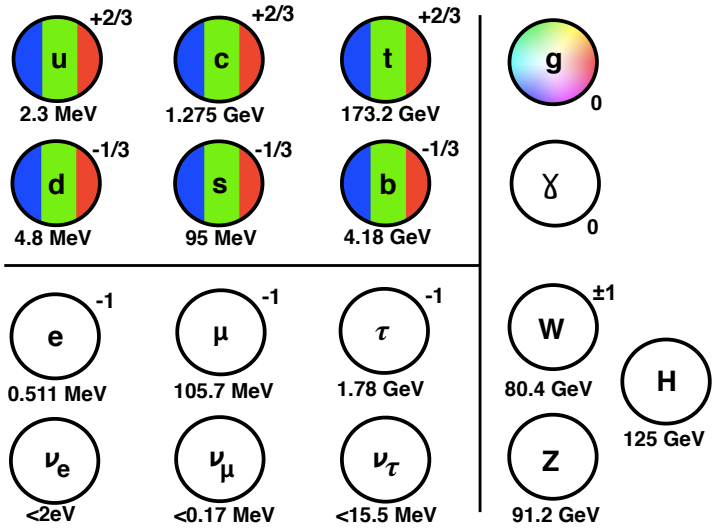

Figure 2.1: Sketch of the particle content of the standard model. The six quark flavors are gauged under $\mathrm{SU}(3)_\mathrm{c}$ and interact with the gluons, while the six leptons transform trivial under $\mathrm{SU}(3)_\mathrm{c}$. The photon γ as the gauge boson of the electromagnetic interaction couples to all charged particles. The massive gauge bosons, $W^\pm$ and Z, act on the isospin doublet structure, see main text. Finally, the Higgs field is responsible for the mass generation of the quarks, leptons, and weak gauge bosons. All masses and experimental data are obtained from the website of the Particle Data Group or its recent review [133].

transform trivially under $\mathrm{SU}(3)_\mathrm{c}$. Both fermion types are gauged regarding the electroweak interactions. Though, only left-handed components take part in the $\mathrm{SU}(2)_\mathrm{L}$ interaction and are assigned to doublets while the right-handed fermions are singlets. Moreover, left-handed and right-handed fermions are charged under $\mathrm{U}(1)_\mathrm{Y}$ but in different representations, i.e., they couple with different coupling strengths to the $\mathrm{U}(1)_\mathrm{Y}$ gauge boson. A sketch of the standard model particle content is given in Fig. 2.1.

The action of the standard model of particle physics can be split into four parts, a pure gauge part, the Higgs sector, a gauge invariant kinetic term for the fermions, and a term containing the Yukawa interactions between the Higgs field and the fermions,

$$S_\mathrm{SM} = \int d^4x \, (\mathcal{L}_\mathrm{g} + \mathcal{L}_\mathrm{H} + \mathcal{L}_\mathrm{f} + \mathcal{L}_\mathrm{Y}). \tag{2.1}$$

We discuss these sectors and how they describe the interactions between the different particles in the following.

Gauge Sector The pure gauge sector is given by the kinetic terms for the different types of gauge bosons as well as by the self-interactions for the nonabelian gauge fields. We denote the gauge fields of the weak isospin, the weak hypercharge, and the strong interaction with W_i^μ, B^μ, and G_I^μ, respectively. These gauge fields transform according to the adjoint representation

of their related gauge group. The Lagrangian reads,

$$\mathcal{L}_{\mathrm{g}} = \frac{1}{4} B_{\mu\nu} B^{\mu\nu} + \frac{1}{4} W_{i\,\mu\nu} W_i^{\mu\nu} + \frac{1}{4} G_{I\,\mu\nu} G_I^{\mu\nu},$$

where the field strength tensors are defined as,

$$\begin{aligned} B^{\mu\nu} &= \partial^\mu B^\nu - \partial^\nu B^\mu, \\ W_i^{\mu\nu} &= \partial^\mu W_i^\nu - \partial^\nu W_i^\mu - g\, f_{ijk} W_j^\mu W_k^\nu, \\ G_I^{\mu\nu} &= \partial^\mu G_I^\nu - \partial^\nu G_I^\mu - g_{\mathrm{s}}\, f_{IJK} G_J^\mu G_K^\nu. \end{aligned}$$

f_{ijk} and f_{IJK} are the structure constants of the nonabelian gauge groups $\mathrm{SU}(2)_{\mathrm{L}}$ and $\mathrm{SU}(3)_{\mathrm{c}}$, respectively. Note, that we use small letters to denote indices of the weak symmetry group while capital letters denote indices regarding the strong force. Analogously, the generators of the su(2) algebra are given by t_i, and the generators of su(3) by T_I. Further, lower indices, starting from $i, j, k, ...$, denote components from fields which are in the adjoint representation while upper indices, starting from $a, b, c, ...$, indicate components from fields in the fundamental representation. The gauge coupling constants are g_{s} for the strong force and g for the weak isospin. The gauge coupling of the weak hypercharge is denoted by g' and will appear only in the interaction terms between the abelian gauge boson B and the fermions as well as the Higgs field in the following. Note that we will formulate our theories in Euclidean spacetime throughout this thesis for convenience.

Higgs Sector of the GWS Theory We have to construct a model which contains two electrically charged gauge bosons ($W^\pm$) with a mass of $m_{\mathrm{W}} = 80.4\mathrm{GeV}$, a massive, electrically neutral Z-boson with $m_{\mathrm{Z}} = 91.2\mathrm{GeV}$, and a massless photon after electroweak symmetry breaking. In order to achieve these phenomenological constraints, we consider a complex scalar doublet, i.e., we investigate a Higgs field in the fundamental representation of $\mathrm{SU}(2)_{\mathrm{L}}$. In addition, we gauge the Higgs field under $\mathrm{U}(1)_{\mathrm{Y}}$ such that the complete gauge transformation reads

$$\phi \to e^{\mathrm{i}\alpha_i t_i} e^{\mathrm{i}\beta Y_\phi} \phi. \tag{2.2}$$

A convenient choice for the fundamental su(2) generators is $t_i = \frac{\sigma_i}{2}$, with Pauli matrices σ_i. In order to get a massless photon and the desired mass split between the W and Z bosons, the scalar hypercharge must be $Y_\phi = 1/2$. The Higgs field is coupled in a gauge invariant manner to the electroweak gauge bosons via the covariant derivative,

$$D_\mu \phi = \partial_\mu \phi + \mathrm{i} g\, W_{i\mu}\, t_i \phi + \mathrm{i} g' B_\mu Y_\phi \phi. \tag{2.3}$$

Scalar self-interactions can be obtained from the gauge invariant product $\phi^\dagger\phi$. Thus the classical Higgs Lagrangian is given by

$$\mathcal{L}_\mathrm{H} = (D_\mu\phi)^\dagger D^\mu\phi + U(\phi^\dagger\phi),$$

with a scalar potential that is quartic in the Higgs field, $U(\phi^\dagger\phi) = m^2\phi^\dagger\phi + \frac{\lambda_2}{2}(\phi^\dagger\phi)^2$. In case, that the scalar field acquires a vacuum expectation value (vev), a particular combination of gauge transformation leaves the vacuum state invariant. Whiteout loss of generality, we chose a coordinate system in the internal field space such that the vev points into the real direction of the second component,

$$\phi^a = \frac{v}{\sqrt{2}}n^a + \varphi^a, \qquad n^a = \delta^{a2} \quad \text{and} \quad \langle\varphi\rangle = 0. \tag{2.4}$$

Then, a gauge transformation (2.2) with $\alpha_1 = \alpha_2 = 0$ and $\alpha_3 = \beta$ leaves the vacuum invariant. This remaining symmetry is associated with the electromagnetic interaction $\mathrm{U}(1)_\mathrm{em}$. Therefore, the physical spectrum of the theory contains a massless gauge boson, the photon, which corresponds to this particular combination of generators.

In order to work out the precise physical spectrum, let us investigate the gauge-invariant kinetic term of the scalar field in detail,

$$\begin{aligned}(D_\mu\phi)^\dagger D^\mu\phi \;=\; &\partial_\mu\phi^\dagger\partial^\mu\phi + \frac{g^2}{4}\phi^\dagger\phi W_{i\mu}W_i^\mu + \frac{g'^2}{4}\phi^\dagger\phi B_\mu B^\mu + gg'\phi^\dagger t_i\phi B_\mu W_i^\mu \\ &+ \mathrm{i}g\left[(\partial_\mu\phi^\dagger)t_i\phi - \phi^\dagger t_i\partial_\mu\phi\right]W_i^\mu + \mathrm{i}\frac{g'}{2}\left[(\partial_\mu\phi^\dagger)\phi - \phi^\dagger\partial_\mu\phi\right]B^\mu.\end{aligned}$$

Decomposing the scalar field into the vev and fluctuations around it, according to Eq. (2.4), yields mass-like terms for all four gauge bosons, a mixing term between B^μ and W_3^μ, and mixing terms between the three would-be Goldstone bosons and the longitudinal parts of the gauge bosons. The latter can be removed from the Lagrangian by an appropriate gauge choice, cf. Sect. A.1. Thus, the mass term for the gauge bosons in the gauge-fixed Lagrangian reads

$$\frac{1}{2}\frac{g^2v^2}{4}\left[(W_1^\mu)^2 + (W_2^\mu)^2\right] + \frac{1}{2}\frac{v^2}{4}\left[gW_3^\mu - g'B^\mu\right]^2.$$

To obtain the mass eigenstates of the theory, we perform a rotation in field space to achieve a propagator which is diagonal in the fields,

$$\begin{pmatrix}Z\\A\end{pmatrix} = \begin{pmatrix}\cos\theta_\mathrm{W} & -\sin\theta_\mathrm{W}\\ \sin\theta_\mathrm{W} & \cos\theta_\mathrm{W}\end{pmatrix}\begin{pmatrix}W_3\\B\end{pmatrix}, \qquad \cos\theta_\mathrm{W} = \frac{g}{\sqrt{g^2+g'^2}}, \quad \sin\theta_\mathrm{W} = \frac{g'}{\sqrt{g^2+g'^2}}.$$

θ_W is called the Weinberg angle or weak mixing angle. After this rotation, the theory contains two massive gauge bosons with mass $m_\mathrm{W} = \frac{1}{2}gv$ and a third massive gauge boson with mass $m_\mathrm{Z} = \frac{1}{2}\sqrt{g^2+g'^2}v$ while the fourth gauge boson remains massless. Furthermore, the physical

gauge bosons $W^\pm$ are a superposition of the fields W_1 and W_2, $W^\pm = \frac{1}{\sqrt{2}}(W_1 \mp \mathrm{i}W_2)$.

Rewriting the covariant derivative (2.3) in terms of the physical fields $W^\pm$, Z, and A, one can identify the electric charge as $e = gg'/\sqrt{g^2 + g'^2}$ and the corresponding generator of the remaining gauge symmetry $\mathrm{U}(1)_\mathrm{em}$ is given by,

$$\mathcal{Q} = t_3 + Y,$$

i.e., the electric charge quantum number is given by the Gell-Mann–Nishijima formula. Thus, the second component for the Higgs field is electrically neutral while the first component has charge +1. Accordingly, the gauge fields $W^\pm$ have electric charge ± 1 and the other two gauge bosons are electrically neutral.

Fermionic Sector The fermion content of the standard model consists of six quark flavors (up, down, strange, charm, bottom, top) and six lepton flavors (electron, muon, tauon, and the corresponding three neutrinos), see Fig. 2.1. These are classified in three generations which are given by $(u^{+\frac{2}{3}}, d^{-\frac{1}{3}}; e^{-1}, \nu_e)$, $(c^{+\frac{2}{3}}, s^{-\frac{1}{3}}; \mu^{-1}, \nu_\mu)$, and $(t^{+\frac{2}{3}}, b^{-\frac{1}{3}}; \tau^{-1}, \nu_\tau)$. The two quarks as well as the two leptons of each generation are combined as weak isospin doublets.

The electroweak interaction distinguishes between left-handed and right-handed chirality for the fermions which can be defined with the aid of the projection operators $\mathbb{P}_\mathrm{L}$ and $\mathbb{P}_\mathrm{R}$,

$$\psi_{\mathrm{L/R}} = \mathbb{P}_{\mathrm{L/R}}\psi, \qquad \text{where} \qquad \mathbb{P}_{\mathrm{L/R}} = \frac{1}{2}(\mathbb{1} \mp \gamma_*).$$

γ_* is proportional to the product of the Dirac matrices γ_μ and thus obeys $\{\gamma_*, \gamma_\mu\} = 0$. In contrast to a mass term, the kinetic term for a fermion decomposes into separate terms for the left-handed and right-handed component, $\bar{\psi}\mathrm{i}\partial\!\!\!/\psi = \bar{\psi}_\mathrm{L}\mathrm{i}\partial\!\!\!/\psi_\mathrm{L} + \bar{\psi}_\mathrm{R}\mathrm{i}\partial\!\!\!/\psi_\mathrm{R}$. Therefore, we can put the two components in different representations of a symmetry group. The $\mathrm{SU}(2)_\mathrm{L}$ gauge bosons couple solely to the left-handed fermions. These transform as the specified weak doublets, i.e., they are in the fundamental representation, while each right handed fermion is put into the trivial representation. Thus, the $\mathrm{SU}(2)_\mathrm{L}$ transformation for the third generation reads,

$$Q_\mathrm{L} = \begin{pmatrix} t_\mathrm{L} \\ b_\mathrm{L} \end{pmatrix} \to e^{\mathrm{i}\alpha_i t_i} Q_\mathrm{L}, \quad t_\mathrm{R} \to t_\mathrm{R}, \quad b_\mathrm{R} \to b_\mathrm{R},$$

and correspondingly for the leptons. Additionally, left-handed and right-handed components have different $\mathrm{U}(1)_\mathrm{Y}$ quantum numbers. This is necessary in order that the resulting electric charge for the Dirac fermions are consistent. Hence, the weak hypercharge of the right-handed quarks and leptons is identical with the electric quantum number. These are $+2/3$ for up-type quarks (up, charm, top), $-1/3$ for down-type quarks (down, strange, bottom), -1 for electrically charged leptons (electron, muon, tauon), and 0 for neutrinos. The hypercharge of left-handed quarks is assigned to be $+1/6$ while that of the left-handed leptons is $-1/2$.

The assignment of the hypercharges within a generation leads to another important property of the standard model. It is anomaly free. An anomaly is a breaking of a symmetry which is manifest at the classical level but is no longer realized in the quantum theory. On the level of the path integral an anomaly occurs, if the measure is not invariant under the desired symmetry transformation. Global anomalies are not a problem at all but gauge anomalies would imply that observables would depend on the chosen gauge. Thus, the occurrence of a gauge anomaly would immediately render a theory inconsistent. While there is no difficulty in coupling the fermions to the weak gauge bosons in a chiral manner at the classical level, it is not trivial to show that this symmetry persists at the quantum level. In fact, it is known that chiral gauge theories can be plagued by anomalies. Fortunately, the particular assignment of the quantum numbers leads to a cancellation of the anomalous terms within every generation of the standard model separately.

In contrast to leptons, each quark is charged under the strong force and transforms according to the fundamental representation. After these assignments, we are able to write down a gauge-invariant kinetic term for the quarks and leptons of one generation. Due to the fact that the covariant derivatives are diagonal with respect to the generation indices for the case that the fermions are eigenstates of the electroweak interaction (flavor eigenstates), the kinetic term for the standard model fermions is given by the sum over the kinetic terms for each generation. Note, that these eigenstates are not necessarily mass eigenstates. Thus, the gauge invariant kinetic term for the quarks and leptons finally reads:

$$\mathcal{L}_\mathrm{f} = \sum_{\tilde{a}=1}^{3} \left[\bar{Q}_{\tilde{a}} \mathrm{i} \not{\mathbf{D}} Q_{\tilde{a}} + \bar{L}_{\tilde{a}} \mathrm{i} \not{\mathtt{D}} L_{\tilde{a}} \right],$$

where $\tilde{a}$ runs over the three generations and $\mathbf{D}$ and $\mathtt{D}$ are the covariant derivatives for the quarks and leptons, respectively.

$$\begin{aligned}
(\mathbf{D}^\mu Q)^{aA} &= \partial^\mu Q^{aA} + \mathrm{i} g W_i^\mu t_i^{ab} \mathbb{P}_\mathrm{L} Q^{bA} + \mathrm{i} g' B^\mu Y_{Q_\mathrm{L}} \mathbb{P}_\mathrm{L} Q^{aA} + \mathrm{i} g' B^\mu Y_{Q_\mathrm{R}}^{ab} \mathbb{P}_\mathrm{R} Q^{bA} + \mathrm{i} g_\mathrm{s} G_I^\mu T_I^{AB} Q^{aB}, \\
(\mathtt{D}^\mu L)^a &= (\delta^{ab} \partial^\mu + \mathrm{i} g W_i^\mu t_i^{ab} \mathbb{P}_\mathrm{L} + \mathrm{i} g' B^\mu Y_{L_\mathrm{L}} \delta^{ab} \mathbb{P}_\mathrm{L} + \mathrm{i} g' B^\mu Y_{L_\mathrm{R}}^{ab} \mathbb{P}_\mathrm{R}) L^b,
\end{aligned}$$

with $Y_{Q_\mathrm{R}}^{ab} = \frac{2}{3}\delta^{a1}\delta^{1b} - \frac{1}{3}\delta^{a2}\delta^{2b}$ and $Y_{L_\mathrm{R}}^{ab} = -\delta^{a2}\delta^{2b}$.

Yukawa Sector Ordinary mass terms for the fermions violate gauge invariance due to the fact that left-handed and right-handed components transform under different representations of the electroweak gauge group. Thus, we are not able to add such a term to the Lagrangian, in contrast to experimental observations that fermions are massive. However, it is possible to construct gauge-invariant Yukawa interactions with the aid of the Higgs field. If the Higgs field forms a condensate, masses for the fermions are generated after electroweak symmetry breaking. For the sake of simplicity, we restrict the discussion of the occurring structures to one generation first. An example for a chiral Yukawa interaction term is given by, $\bar{Q}_\mathrm{L}^a \phi^a b_\mathrm{R}$ which

is obviously invariant under $\mathrm{SU}(2)_\mathrm{L}$ but also has a vanishing total hypercharge. Moreover, the Higgs field allows for interactions with both components of the $\mathrm{SU}(2)_\mathrm{L}$ doublet,

$$\mathrm{i}h_\mathrm{b}(\bar{Q}_\mathrm{L}\phi\, b_\mathrm{R} + \bar{b}_\mathrm{R}\,\phi^\dagger Q_\mathrm{L}) + \mathrm{i}h_\mathrm{t}(\bar{Q}_\mathrm{L}\phi_\mathrm{c}\, t_\mathrm{R} + \bar{t}_\mathrm{R}\,\phi_\mathrm{c}^\dagger Q_\mathrm{L}).$$

$\phi_\mathrm{c} = \mathrm{i}\sigma_2\phi^*$ is the charge-conjugated Higgs field and h_t as well as h_b are the top and bottom Yukawa couplings, respectively.

An analogous construction can be done for the leptons. It should be noted that the right-handed neutrinos have a special role. So far, a right-handed neutrino does not take part in any gauge interaction in the standard model. Thus, right-handed neutrinos are usually not included in the so-called minimal standard model which can be justified if neutrinos are massless. However, it is (nowadays) an experimental fact that at least two of the three neutrinos are massive due to the observed neutrino oscillations. Coupling the neutrinos to the Higgs field allows to incorporate masses for the neutrinos without affecting the basic structure of the standard model.

A further subtlety arises if more than one fermion generation is considered. Then, we are able to construct gauge-invariant Yukawa interaction terms which allow to couple quark (or lepton) species from different generations. These interactions can be parametrized by Yukawa coupling matrices which allow for transitions between different generations,

$$\mathcal{L}_\mathrm{Y} = \mathrm{i}\sum_{\tilde{a},\tilde{b}} \left(h^d_{\tilde{a}\tilde{b}}\bar{Q}_{\mathrm{L}\,\tilde{a}}\phi\, d_{\mathrm{R}\,\tilde{b}} + h^u_{\tilde{a}\tilde{b}}\bar{Q}_{\mathrm{L}\,\tilde{a}}\phi_\mathrm{c} u_{\mathrm{R}\,\tilde{b}} + h^e_{\tilde{a}\tilde{b}}\bar{L}_{\mathrm{L}\,\tilde{a}}\phi\, e_{\mathrm{R}\,\tilde{b}} + h^\nu_{\tilde{a}\tilde{b}}\bar{L}_{\mathrm{L}\,\tilde{a}}\phi\, \nu_{\mathrm{R}\,\tilde{b}} + \mathrm{h.c.}\right).$$

If the Higgs field acquires a vev, also the mass matrix for the fermions is off-diagonal. Thus, the Higgs mechanism provides mass terms for the fermions as well as a mixing between the flavor eigenstates of the electroweak interaction. By performing several rotations and phase redefinitions in field space, one is able to diagonalize the mass matrix by a bi-unitary transformation for the left-handed and right-handed fermion fields. As a consequence, the coupling of the Higgs particle to the fermions is diagonal too and the associated Yukawa couplings are proportional to the fermion masses. However, the fermion-gauge-boson interactions become off-diagonal in its generation indices in terms of the physical mass eigenstates of the particles due to the bi-unitary transformation. Interactions of neutral gauge bosons are only among fermions of the same flavor due to the unitarity of the transformation. Thus, there are no flavor-changing neutral currents at the classical level. Though, a nontrivial mixing matrix remains in the quark as well as in the lepton sector. The mixing between quark flavors is described by the unitary Cabbibo-Kobayashi-Maskawa (CKM) matrix [134, 135]. A mixing of lepton flavors appears only if right-handed neutrinos are added to the standard model. The corresponding PMNS matrix allows for a phenomenological description of neutrino oscillations [136, 137]. These matrices allow for transitions between fermions of different generations via charged W bosons.

2.2 Renormalization group and effective actions

Up to now, we analyzed the symmetries and interactions of the standard model on a classical level, i.e., the classical action (2.1) defines the theory of particle interactions on a microscopic scale. However, some properties of the full quantum theory will generically differ from those of the classical theory. For instance, the vacuum expectation value of the classical theory is given by the homogeneous field configuration that minimizes the classical potential of the microscopic theory. However, this value can be altered by quantum corrections. In order to predict macroscopic observables, that are measured in an experiment, one has to average over all possible microscopic quantum fluctuations.

The relevant information of a QFT is encoded in correlation functions. In case that all correlation functions of a theory are known, we are in principle able to compute every physical observable. The correlation functions can be obtained from a partition function, that integrates over all field configurations weighted with an exponential of the microscopic action,

$$\mathcal{Z}[J] = \int \mathcal{D}\Psi \, e^{-S[\Psi]+J\cdot\Psi}.$$

Here, the microscopic quantum fields of the theory are combined into a generalized field vector $\Psi = (\phi^a, \bar{\psi}^{a\,T}, \psi^a, A_i^\mu, \cdots)$ for compactness of notation. The scalar product of Ψ with the corresponding external source fields J implies a sum over all internal indices as well as an integration over all spacetime points, $J \cdot \Psi = \int_x J_a(x)\Psi_a(x)$. The desired correlation functions can be obtained from the partition function via functional differentiation with respect to the source fields.

Moreover, we can define a generating functional for the one-particle irreducible (1PI) correlation functions by a Legendre transform of the Schwinger functional, $\ln \mathcal{Z}[J]$,

$$\Gamma[\Phi] = \sup_J \left\{ J \cdot \Phi - \ln \mathcal{Z}[J] \right\}.$$

For $J = J_{\text{sup}}$, the generalized field vector Φ is the vacuum expectation value of the microscopic fields Ψ in presence of the external source. Finally, we can identify Γ as the effective action which governs the dynamics of the macroscopic fields Φ, i.e., it describes the evolution of the effective degrees of freedom of a theory at a macroscopic scale where all quantum fluctuations are integrated out.

In principle, the effective action can be obtained from the classical action, however, this is a highly nontrivial task and exact solutions are only known for a few toy models, e.g., see [138, 139]. Possible approximate solutions for the effective action can be classified as perturbative and nonperturbative techniques. Both approaches have their own advantages and disadvantages. Functional methods allow for nonperturbative solutions but the involved necessary truncations are difficult to control. A realization of such a method is given by a vertex expansion of the effective action. The expansion coefficients are the 1PI proper vertices that can be obtained from

Dyson-Schwinger equations [140–142] which are an infinite tower of coupled integral equations. Approximate solutions, e.g., for gauge theories in the nonperturbative regime, are constructed by finite truncations of the infinite tower of the Dyson-Schwinger equations [143–145].

In case of small couplings, the effective action can be expanded in a perturbation series. This series can be consistently defined order by order in terms of loop diagrams. For example, the functional integral can be reduced to a Gaußian type integral for the approximation of small field amplitudes and thus the 1-loop approximation is given by the well-known tr-log formula,

$$\Gamma^{1l} = S + \frac{1}{2}\,\mathrm{STr}\,\ln S^{(2)}. \tag{2.5}$$

Here, $S^{(2)}$ denotes the second functional derivative with respect to the fields and the supertrace STr implies traces over discrete as well as continuous indices and contains a negative sign for Graßmann-valued fields.

If quantum corrections to the classical action are taken into account, a generic problem will occur. The corresponding loop integrals are usually divergent. This fact is deeply connected to our formulation of QFT's in terms of local field theories. One reason for this is that the local structure automatically implies that the theory respects causality. Of course, nonlocal effects emerge in the full quantum theory once all quantum fluctuations are integrated out. Moreover, the microscopic action of gauge theories already contains nonlocal structures. However, these nonlocalities are of such a form that they can be localized by introducing additional degrees of freedom such that causality is preserved. Due to the local structure of the interactions, we consider field amplitudes at different spacetime points as independent degrees of freedom with their own quantum fluctuations. Therefore, fluctuations at arbitrarily short distances appear as virtual quanta with arbitrarily large momenta in Feynman diagrams and the corresponding loop integrals are divergent. However, it turns out that these divergences can be removed for theories with certain interaction terms in perturbation theory by the procedures of regularization and renormalization.

The first step is to regularize the divergent integrals, i.e., they are mapped on a finite value by introducing at least one additional parameter. The original divergence can be recovered by taking a particular limit of this parameter. In a next step, a prescription is given how to redefine the theory in order that observables do not depend on the arbitrarily introduced parameter. Furthermore, this redefinition has to be done in such a way that the original divergence does not emerge anymore. This procedure is called renormalization. Operators with a nonnegative mass dimension are renormalizable in perturbation theory which can be obtained by simple dimensional analysis. Note, that all interaction terms of the standard model (2.1) are of that type. The way how to regularize and renormalize is not unique but a measurable quantity does not depend on the used renormalization scheme. As a result of the renormalization procedure, a mass scale is introduced into the theory and the former coupling constants of the classical theory become scale dependent, i.e., the variation of the renormalization point μ implies a change in

the couplings. This is necessary for physical observables, for instance, a cross-section, to become independent of the renormalization point. The scale dependence is described in terms of a β function for the considered coupling constants λ_i,

$$\mu \frac{d\lambda_i}{d\mu} = \beta_{\lambda_i}(\lambda_j),$$

where the β function can depend on all couplings which are involved in a theory in general.

Initially, renormalization was a pure mathematical tool to avoid that loop calculations are plagued by infinities and was used as a recipe to give a QFT a well-defined meaning. However, it turned out, that the renormalization group provides a connection between physics across different scales via effective descriptions and allows for some formal analogies to statistical systems and the physics of phase transitions [146]. Especially, the resulting picture of effective field theories governs our present-day viewpoint in high energy physics.

Effective theories serve as an efficient description of nature in modern theoretical physics. These are able to explain physical laws on a quantitative level over a certain range of validity but lose their predictive power beyond this scope and have to be replaced by a more fundamental theory. In addition, physics can look very different at different energy or length scales even though one and the same physical system is considered. A macroscopic effective theory can often be characterized by a few parameters and it is not necessary to know the precise underlying microscopic theory in many cases. For example, let us consider a system of a flowing liquid. On a macroscopic scale, a sufficient description is given by fluid dynamics and we do not have to know that the liquid is made of molecules and atoms. On the other hand, the properties of atoms are independent of the details of the strong interactions inside its nucleus. Furthermore, the nuclear forces can be understood as an effective theory, where pions mediate between the constituents of an atomic nucleus, the protons and neutrons. This phenomenological model is quite efficient in describing the binding inside an atomic nucleus but does not care about the microscopic structure of the hadrons which is governed by completely different degrees of freedom, quarks and gluons.

In principle, it is possible to investigate the complex properties at macroscopic scales with the fundamental interactions and symmetries provided by a microscopic theory, for instance, to describe the behavior of an atom or its nucleus by the standard model action, without the need for an effective description. However, the complexity of this task is on such a high level, that it is far beyond any realistic scenario. As mentioned before, there is also no need for this because the effective theory is sufficient in predicting quantitative results within their range of validity. Thus, one of the aims of modern theoretical physics is to predict the remaining symmetries and effective couplings on macroscopic scales from the underlying microscopic theory.

The connection between physics at different energy or length scales is provided by the renormalization group. If the underlying microscopic action S of a theory is given, we are able to derive the effective couplings and remaining symmetries on larger scales by averaging over

fluctuations at high energy scales. An intuitive picture is given by Kadanoff's block-spin model [147]. Quantum fluctuations from high energy scales do not explicitly show up in the dynamics of the effective theory but are rather integrated in the effective couplings which become scale dependent. For instance, the weak interaction describes the beta decay via the exchange of a W-boson between an electron, a neutrino, an up-quark, and a down-quark. However, at energy scales much smaller than the W mass, the beta decay is well described by an effective four-fermion interaction where the underlying dynamics of the gauge boson is integrated in the effective dynamics of the four-fermion coupling.

Due to the RG we are able to uniquely determine the macroscopic physics from the underlying microscopic one. The reverse statement is rather intricate. Information of the microscopic details get lost due to the coarse graining of the RG with the result that different microscopic theories can lead to the same effective action. In order to determine a unique RG trajectory, we have to know the values of all running couplings to arbitrary precision. In this rather theoretical case, the flow towards the UV could be investigated. However, in some cases, we do not have access to the microscopic theory and only know the effective dynamics. The prime example is gravity but also the underlying theory of the standard model of particle physics is yet unknown. At least, the RG can be used to study bounds on parameters of a theory resulting from the underlying dynamics. Accordingly, the scale of maximal UV extension might be calculable and thus the RG could be used as a tool to constrain the underlying dynamics as we will show during the course of this work.

2.3 Perturbative effective Higgs potential and vacuum stability problem

Bounds on the Higgs mass can be obtained by investigating the RG flow of the standard model Higgs potential. Within a perturbative calculation, the bare Higgs potential is assumed to be of ϕ^4-type in order to allow for perturbative renormalizability. The effective Higgs potential is obtained by taking radiative corrections into account which may alter the shape of the classical Higgs potential. First, Coleman and Weinberg studied the occurrence of spontaneous symmetry breaking from radiative corrections in gauged Higgs models without a scalar mass parameter [148]. Then the investigation of radiative corrections to the scalar potential was generalized to various other models, see [71] for a review on the Higgs effective potenial. Clearly, the effective potential has to have a minimum at the Fermi scale to allow for electroweak symmetry breaking in order to be compatible with the observed experimental data. This can be achieved by imposing suitable renormalization conditions on the scalar mass parameter. Based on the work of Coleman and Weinberg, the RG-improved, perturbative effective potential for large

field values, $\phi \gg v$, is usually constructed in the following way,

$$U_{\text{eff}} = \frac{\lambda_2(\mu = \phi)}{8}\phi^4, \tag{2.6}$$

where μ is the renormalization scale. Relating the shape of the effective potential to the running of the ϕ^4 coupling is the great advantage of the perturbative approach because the perturbative running of the standard model couplings is known to high precision. The dependence of the standard model couplings on the renormalization scale is governed by the RG β functions. Current state of the art are three-loop computations, see [83].

However, the main qualitative properties are already visible at the one-loop level, in order to investigate the occurrence of bounds on the Higgs mass. Within a one-loop approximation, the relevant perturbative β functions read,

$$\beta_{g_s^2} = -\frac{g_s^4}{8\pi^2}7, \qquad \beta_{g^2} = -\frac{g^4}{8\pi^2}\frac{19}{6}, \qquad \beta_{g'^2} = \frac{g'^4}{8\pi^2}\frac{41}{6}, \tag{2.7}$$

$$\begin{aligned}\beta_{\lambda_2} = \frac{1}{16\pi^2}\Big[&12\lambda_2^2 + 4\lambda_2(3h_t^2 + 3h_b^2 + h_\tau) - 4(3h_t^4 + 3h_b^4 + h_\tau^4) - 3\lambda_2(3g^2 + g'^2) \\ &+ \frac{9}{4}g^4 + \frac{3}{4}g'^4 + \frac{3}{2}g^2g'^2\Big],\end{aligned} \tag{2.8}$$

$$\beta_{h_t^2} = \frac{h_t^2}{8\pi^2}\left[\frac{9}{2}h_t^2 + \frac{3}{2}h_b^2 + h_\tau^2 - 8g_s^2 - \frac{9}{4}g^2 - \frac{17}{12}g'^2\right], \tag{2.9}$$

$$\beta_{h_b^2} = \frac{h_b^2}{8\pi^2}\left[\frac{3}{2}h_t^2 + \frac{9}{2}h_b^2 + h_\tau^2 - 8g_s^2 - \frac{9}{4}g^2 - \frac{5}{12}g'^2\right], \tag{2.10}$$

$$\beta_{h_\tau^2} = \frac{h_\tau^2}{8\pi^2}\left[3h_t^2 + 3h_b^2 + \frac{5}{2}h_\tau^2 - \frac{9}{4}g^2 - \frac{45}{12}g'^2\right]. \tag{2.11}$$

Here, only the Yukawa couplings of the third generation are taken into account due to the negligible size of the Yukawa couplings of the other two generations. We also dropped the influence of the tau neutrino Yukawa coupling for the same reason. Of course, the mass of the charm quark is of the order of the bottom quark and the tau lepton, however, also these two could be neglected due to the large value of the top quark as we will see in Chap. 5 and are mere listed for reasons of completeness. Furthermore, we will use these β functions as a cross check for our nonperturbative flow equations which include the perturbative running as a particular limit. Note that we do not use the SU(5) normalization of the hypercharge $g_1 = \sqrt{5/3}g'$ and a normalization of $\frac{\lambda_2}{8}\phi^4$ in Eq.(2.6) instead of $\frac{\lambda_2}{4}\phi^4$ for convenience in contrast to most articles in the literature, cf. [83].

An upper bound on the Higgs mass is obtained by investigating β_{λ_2} for large quartic couplings. In this case, $\beta_{\lambda_2} \simeq \lambda_2^2$ can be integrated straightforwardly. The occurrence of the perturbative Landau pole automatically sets a scale of maximal UV extension. Strictly speaking, the Landau pole indicates rather a breakdown of perturbation theory, however, nonperturbative calculations support the statement of an upper triviality bound on the Higgs mass [46–51].

For light Higgs masses, i.e., small quartic couplings, the β function for λ_2 is essentially

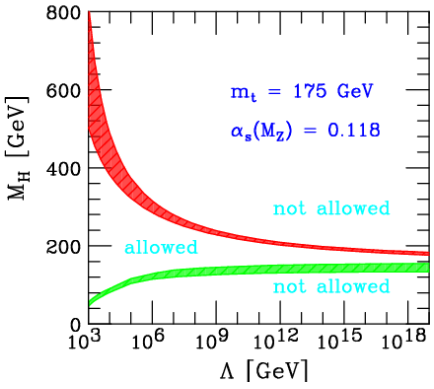

Figure 2.2: Sketch of possible mass bounds for the Higgs obtained from the vacuum stability problem as well as from the triviality problem for a top mass of 175GeV. The source of this plot is [149].

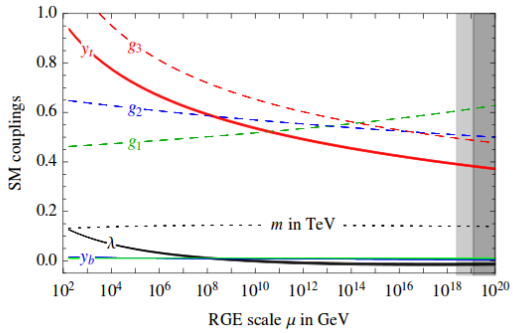

Figure 2.3: In [83] the RG running of the SM gauge couplings $g_1 = \sqrt{5/3}g'$, $g_2 = g$, $g_3 = g_s$, the Yukawa couplings for the top $y_t = h_t$, bottom $y_b = h_b$, and tau $y_\tau = h_\tau$, as well as for the quartic coupling $\lambda = \frac{\lambda_2}{2}$ are extrapolated from the electroweak scale up to the Planck scale. These computations are done with three-loop RG equations and two-loop matching conditions at the electroweak scale.

dominated by the large top Yukawa coupling. Obviously, the pure fermion-loop contribution $\sim h_t^4$ comes with a negative sign, implying that it tends to diminish λ_2 towards the UV. Thus, the integrated quartic coupling $\lambda_2(\mu)$ can drop below zero at high energy scales depending on the ratio of λ_2 and h_t. Inserting this result into Eq. (2.6) with the identification $\mu = \phi$, the effective potential develops an instability. However, the influence of electroweak gauge boson fluctuations can stabilize the effective potential at large energy scales. The reason is that the electroweak gauge couplings become predominant at these scales such that λ_2 can turn positive again, yielding a potential with a second minimum. In case that the value of the potential at the second minimum is smaller than the value at the electroweak minimum the potential is metastable with rather dramatic consequences for our existence. Of course, new physics at some high cutoff scale of the standard model may modify the running such that no in-/metastability emerges. Quantitative bounds on the mass of the Higgs can be received from these considerations and are depicted in Fig. 2.2, cf. [63, 149]. For a given UV cutoff scale, the Higgs mass has to be in a finite IR window of allowed Higgs masses in order that the standard model is not affected by a vacuum stability problem or a triviality problem.

Currently, the lower bound is in tension with the measured value for the Higgs mass. In case the Higgs potential does not suffer from a stability problem up to the Planck scale, the Higgs mass has to be heavier than 129.6 ± 1.5GeV with the error arising form theoretical uncertainties and experimental errors. The RG running of the relevant standard model couplings for the Higgs effective potential are depicted in Fig. 2.3. For the measured values of the particle masses and

gauge couplings, the scalar quartic coupling turns negative at approximately 10^{10}GeV and the effective Higgs potential receives a second minimum [83]. In fact, the second minimum emerge as the true ground state, yielding a metastable effective potential, but appears at a trans-Planckian scale of 10^{26}GeV, see [84]. Due to the fact that the inverse decay rate of the false vacuum decay exceeds the lifetime of our universe, it is considered that we live in a metastable scenario [98].

However, these conclusions are based on various assumptions. First of all, it is assumed that the standard model degrees of freedom are valid up to the Planck scale, i.e., that the running of the couplings can be extrapolated from the Fermi to the Planck scale or even higher. Further, the effective potential shall be well approximated by Eq. (2.6) and thus is only given in terms of the running $\lambda_2(\mu)$ for large field values, $\phi \gg v$. Though, precisely the assumption, that the field amplitude ϕ is the only relevant scale at large values, fails in the presence of new physics emerging at a finite UV cutoff. Moreover, higher-dimensional operators, like $\lambda_3\phi^6$, as well as threshold effects are not considered within the usual perturbative framework but these effects may stabilize the scalar potential in the UV. Additionally, it is assumed that the calculations of tunnel rates can be done within the metastable potential obtained from the pure standard model calculation, i.e., new physics will not effect this result. Recently, this fact was also questioned in the literature with the outcome that higher-order operators, initialized by the underlying theory, can change the decay rates drastically [150–152].

In order to circumvent these assumptions, we would like to impose a conceptually slightly different and more conservative viewpoint on the effective Higgs potential and the occurrence of Higgs mass bounds throughout this thesis. This point of view relies more on the spirit of the Wilsonian RG and in terms of effective field theories. As far as we know, the standard model is not a fundamental theory of nature and therefore should be defined with an intrinsic cutoff which signals the breakdown of the theory beyond this scale. This might be at the Planck scale or even on scales far below. Within the Wilsonian spirit, we aim at solving the so-defined quantum theory by integrating out fluctuations from the UV cutoff Λ towards the observable long-range physics.

2.4 Functional renormalization group

The functional renormalization group (FRG) is a mathematical implementation of the Wilsonian idea of integrating out quantum fluctuations momentum shell by momentum shell [153, 154]. First exact flow equations were provided by Wegner and Houghton [155], Wilson [44], as well as Polchinski [156]. Its modern formulation is in terms of a scale dependent action functional Γ_k, the effective average action [157]. The effective average action smoothly interpolates between the microscopic action at some UV cutoff scale Λ, $\Gamma_{k\to\Lambda} \to S$, and the effective action, $\Gamma_{k\to 0} \to \Gamma$, where all quantum fluctuations are integrated out, defining the generator of the fully dressed proper vertices. At intermediate scales k, Γ_k is an effective description which

takes the high energy fluctuations into account but fluctuations at scales smaller than k are suppressed.

Such a concept can be implemented on the functional integral level by studying a scale dependent generating functional where the classical action is modified by a momentum dependent mass term for the fields,

$$\mathcal{Z}_k[J] = \int \mathcal{D}\Psi \, e^{-S[\Psi]-\Delta S_k+J\cdot\Psi}, \qquad \Delta S_k = \int_p \Psi^T(-p)R_k(p)\Psi(p).$$

The regulator function $R_k(p)$, which is matrix valued in field space, shall fulfill the following constraints in order to implement the desired scale-dependent averaging procedure. To implement the correct IR limit, $R_k(p)$ has to vanish for $k \to 0$ to recover the standard generating functional and thus the effective action. Furthermore, $\lim_{k\to\Lambda\to\infty} R_k(p) \to \infty$ ensures that the effective average action, defined in Eq. (2.12), becomes the classical action S in the deep UV due to a justified saddle-point approximation in this limit which filters out the classical field configuration. Additionally, the constraint $R_k(p) > 0$ for $\frac{p^2}{k^2} \to 0$ establishes that R_k acts as an IR regulator and suppresses fluctuations below the RG scale k in a mass-like fashion. The effective average action is defined via a modified Legendre transform,

$$\Gamma_k[\Phi] = \sup_J \{J\cdot\Phi - \ln \mathcal{Z}_k[J]\} - \Delta S_k. \tag{2.12}$$

Note that for finite k the effective average action can contain a nonconvexity due to the regulator term.

The variation of the flowing effective average action Γ_k with respect to the RG scale k is governed by the Wetterich equation [157],

$$\partial_t\Gamma_k \equiv k\partial_k\Gamma_k = \frac{1}{2}\,\mathrm{STr}\left[(\Gamma_k^{(2)} + R_k)^{-1}\partial_t R_k\right], \tag{2.13}$$

where $t = \ln\frac{k}{\Lambda}$ and Λ the UV cutoff scale. For detailed reviews see [158–166]. $\Gamma_k^{(2)}$ denotes the Hessian of Γ_k with respect to the fluctuating fields. The solution of the Wetterich equation defines an RG trajectory in theory space. This space of action functionals is spanned by all possible field operators which are invariant under the considered symmetries. The endpoints of each trajectory are fixed by the classical action as well as the effective action by construction. Thus, the microscopic bare action can be used as an initial condition for the functional differential equation (2.13). Then, integrating out quantum fluctuations in an infinitesimal thin momentum shell dk results in a change of the action, i.e., a change of the couplings, governed by the Wetterich equation. The occurrence of the regulator in the regularized propagator suppresses IR modes with momenta smaller than k by construction, while $\partial_t R_k$, which is peaked around $p^2 \approx k^2$ and vanishes for $p^2 \gg k^2$, establishes UV finiteness. As a consequence, the effective average action Γ_k is dominated by fluctuations with momenta $p^2 \simeq k^2$, which imple-

ments the concept of a smooth momentum-shell integration and contains all the information of high-energy quantum fluctuations. Investigating the flow of Γ_k down to $k = 0$, finally results in the full effective action.

However, even if the endpoints of an RG trajectory are fixed, the precise form of the trajectory depends on the chosen regulator R_k. Choosing a certain regulator corresponds to specifying the details of the momentum shell regularization. Thus, different regulator functions correspond to different regularization schemes and a variation of the RG trajectory with respect to the regulator represents the RG scheme dependence from nonuniversal quantities.

The Wetterich equation has a simple one-loop structure. Nevertheless, it is an exact RG equation due to the exact propagator in the loop as well as the occurrence of fully dressed vertices at the considered RG scale, leading to particular resummation effects. For instance, perturbation theory can be recovered to any order from the exact nonperturbative flow equation by taking certain limits, e.g., see [167, 168]. The one-loop structure has the benefit, that no overlapping loop calculations have to be done as they occur in two or higher loop calculations, for instance, in perturbation theory or Dyson-Schwinger equations. Moreover, an exact equivalence to the full functional integral formulation can be established, e.g., see [164]. In contrast to the functional integral formalism, the Wetterich equation is a differential equation and no functional integral has to be performed whose rigorous mathematical definition is difficult.

The flow equation will generically create all symmetry-compatible operators during the RG flow even though these operators are not present in the microscopic action. Thus, only the consideration of all these (infinitely many) operators leads to an exact result for the effective action and an infinite tower of coupled differential equations has to be studied in analogy to the Dyson-Schwinger equations. Therefore, one has to choose a suitable truncation for the given physical problem. In addition to perturbative expansions, nonperturbative approximation schemes can be devised for the flow equation. Systematic and consistent expansion schemes, which do not rely on a perturbative coupling ordering, are, for instance, the vertex expansion or the derivative expansion. In contrast to perturbation theory, higher-order terms of a nonperturbative expansion are not necessarily smaller than lower-order terms. The expansion rather refers to an systematic and consistent ordering scheme of all possible operators.

In absence of a small expansion parameter, the reliability of an approximative solution to the flow equation due to a truncation has to be checked carefully. One way to examine the convergence of a systematic expansion is to investigate the impact of higher-order terms. However, such computations can become very extensive. Furthermore, such studies have to be treated with some caution. In principle it is possible that a result appears to converge under a systematic enhancement of a truncation, however, an operator outside the considered truncation could spoil the result completely. Thus, cross checks with other complementary methods or in the best case with experimental data should be performed. In addition, the choice of the regulator function influences the reliability of the approximative solution. Of course, physical observables resulting from the full solution of the Wetterich equation are independent of the regulator choice

by construction. Unfortunately, exact solutions for realistic applications are not accessible and the necessity to truncate the flow induces spurious regulator dependencies. The amount of this dependence is a measure for the importance of neglected higher-order operators outside a given truncation.

Nonetheless, the freedom to choose R_k arbitrarily, besides the three conditions as mentioned before, can be used for an optimization of the flow. In this context, a flow is optimized if the results obtained from a truncated flow are, in some sense, as close as possible to the exact solution. In this case, the error induced by terms outside a given truncation is minimized. Based on the investigations in [169, 170], we will use a linear regulator which is optimized regarding the derivative expansion at next-to-leading order that we use in this thesis. For detailed discussions on optimization schemes for different physical applications we refer to the literature [163, 171–174].

Being not restricted to an expansion in small couplings, the FRG has various applications for nonperturbative phenomena. These range from the asymptotic safety scenario for quantum gravity [41, 175–179], nonperturbative studies of Yang-Mills theory [180–183], QCD and the QCD phase diagramm [184–191], supersymmetry [192–194], the description of bound states [195–197], BCS-BEC crossover in ultracold atoms [198–200], to solid-state physics and low-dimensional fermionic systems [201–203], and high energy particle physics [53, 56, 204, 205]. Moreover, asymptotically safe gravity interactions are likely to put the Higgs mass onto its "conventional" lower bound, yielding a prediction for the Higgs mass before its discovery [206], also see [101].

In the following chapters, we revisit Higgs mass bounds by analytic means using the FRG. Within a consistent systematic derivative expansion, the FRG provides for a tool to analyze the problem nonperturbatively and allows to estimate errors of the approximation scheme. This allows us to investigate lower as well as upper Higgs mass bounds in a unified setting. Though, the parameter region near the conventional lower bound appears perturbatively accessible, the nonperturbative functional RG has better access to and control of threshold effects and can treat arbitrary bare potentials. The latter turns out to be essential for the lower bound. Moreover, standard perturbative meta-stability analyses of the effective potential indicate that a second lower minimum might occur at nonpertubatively large values of the Higgs field, also calling for a nonperturbative tool. In a Wilsonian spirit, the microscopic bare action at Λ, corresponds to an UV initial condition for the long-range physics extracted at IR scales. The resulting solution provides for a mapping from the microscopic bare parameters to the set of physical parameters, which are given by the masses of the Higgs, the fermions, the weak gauge bosons, the strong coupling, and the vacuum expectation value. These physical parameters can be related to renormalized couplings in the quantum effective action, such as the renormalized Yukawa couplings and the effective potential U_{eff} as well as the renormalized gauge couplings.

Furthermore, we are not restricted to polynomial expansions of the scalar potential, cf. Eq. (2.6) where only the running of the quartic coupling is taken into account which determines

the precise shape of the bare potential in the UV and the effective potential in the IR by identifying the renormalization scale with the field amplitude. The FRG allows to investigate the full multiscale problem by means of a scale dependent effective average potential as a local term of Γ_k, which depends on both scales $U_k(\phi)$. Thus, we are able to follow the RG flow for the full potential at every field value in order to discuss the properties of the resulting effective potential in the IR.

3 Simple Higgs-Yukawa model

The entire standard model is a quite intricate theory and hard to tackle on a nonperturbative level. However, many of the fluctuation-induced features of Higgs mass bounds in the standard model can already be studied in a greatly simplified toy model. Basically, we utilize the fact that the top has the most dominant influence on the running of the scalar potential at not too large scales (more precisely on scales below a possible GUT scale), see Sect. 2.3. Therefore, we investigate a simple Yukawa toy model in detail within this chapter before we proceed to more realistic approximations. This allows us to concentrate on the basic mechanisms for the mass bounds and we avoid intricate questions arising from the gauge-Higgs interplay in the full standard model [207, 208].

The considered model involves a Dirac fermion flavor ψ and a real scalar boson ϕ representing the top quark and the Higgs, respectively, and is defined by the Euclidean classical action

$$S = \int d^4x \left[\frac{1}{2}(\partial_\mu \phi)^2 + U_\Lambda(\phi^2) + \bar{\psi}\, \mathrm{i}\not{\partial}\psi + \mathrm{i}\frac{\bar{h}}{\sqrt{2}}\,\phi\bar{\psi}\psi \right]. \tag{3.1}$$

Restricting to the class of perturbatively renormalizable scalar self-interactions, the bare potential is given by $U_\Lambda = \frac{\bar{m}^2}{2}\phi^2 + \frac{\bar{\lambda}_2}{8}\phi^4$. The normalization of the Yukawa coupling is implemented consistently with that of the standard model Higgs-Yukawa coupling where the complex Higgs field contains a factor $1/\sqrt{2}$ (see Chap. 5). From now on, we denote unrenormalized couplings and masses with a bar.

This model is invariant under a discrete chiral symmetry,

$$\psi \to e^{\mathrm{i}\frac{\pi}{2}\gamma_5}\psi, \qquad \bar{\psi} \to \bar{\psi}\, e^{\mathrm{i}\frac{\pi}{2}\gamma_5}, \qquad \phi \to -\phi, \tag{3.2}$$

which protects the fermions against acquiring a direct mass term. Since the symmetry is only discrete, its spontaneous breaking owing to a nonzero expectation value for the scalar field $\langle\phi\rangle \neq 0$ does not give rise to massless Goldstone bosons. This feature mimics the property of the standard model that the Goldstone modes are eaten by the massive electroweak gauge bosons.

For the following discussion it is important to note that the standard model in its conventional form may not be extendible to arbitrarily high momentum scales. The problem of triviality – where substantial evidence has been accumulated for ϕ^4-type theories – is likely to extend to the Higgs-Yukawa sector as well, see [52]. If so, the definition of our toy model unavoidably requires

a UV cutoff Λ which physically plays the role of the scale of a maximum UV extension up to which a quantum field theory description is appropriate. In this sense, the cutoff, together with a specified regularization prescription, remains an implicit physical parameter of the theory. If the cutoff scale is sufficiently large, Wilsonian renormalization guarantees that the IR physics essentially depends only on a finite number of relevant and marginal parameters, rendering the theory predictive (in spite of our ignorance about the physics beyond Λ).

In fact, the strategy of perturbative renormalization manifestly allows to take the limit $\Lambda \to \infty$ once physical observables are expressed in terms of renormalized quantities. Some schemes such as dimensional regularization can even be applied without any explicit appearance of a UV cutoff scale. For the general definition of the theory, it is however important to accept the fact that the cutoff Λ may unavoidably have to be kept finite. In principle, perturbative predictions for $\Lambda \to \infty$ may differ from those with a finite cutoff. However, let m_{Obs} denote the scale of a typical IR observable; then this difference is typically of order $(m_{\mathrm{Obs}}/\Lambda)^p$, where p is some appropriate power. For sufficiently large Λ, this difference hence becomes insignificant.

In this setting, we aim at solving the so defined quantum theory by integrating out fluctuations from the UV cutoff Λ towards the observable long-range physics as aforementioned. Within our toy model, the RG flow provides for a mapping from the microscopic bare parameters of the potential, which are the bare mass $\bar{m}^2$ and the bare quartic coupling $\bar{\lambda}_2$ for ϕ^4-type potentials, as well as $\bar{h}$ and Λ and possibly further RG irrelevant bare couplings, to the set of physical parameters which are given by the top mass m_{t}, the Higgs mass m_{H}, the vacuum expectation value v and still the cutoff Λ. These physical observables are related to renormalized couplings in the quantum effective action such as the renormalized Yukawa coupling h and the effective potential U, see below. The precise relation is fixed by imposing a renormalization condition at an a priori arbitrary renormalization point. As we require to end up in the SSB regime in order to obtain the desired phenomenology, the long-range physics of the present model is characterized by massive degrees of freedom. Therefore, we can choose the renormalization point to be a deep IR scale μ_0 being much smaller than all mass scales. In this way, the physical parameters can directly be read off from the values of the renormalized couplings in the deep IR. Denoting the minimum of the effective potential by ϕ_0, we identify

$$v = Z_\phi^{1/2}\langle\phi\rangle = Z_\phi^{1/2}\phi_0, \qquad m_{\mathrm{t}}^2 = v^2h^2, \qquad m_{\mathrm{H}}^2 = \frac{1}{Z_\phi}\frac{\partial^2 U}{\partial\phi^2}\Big|_{\phi_0}, \tag{3.3}$$

where all renormalized couplings are considered in the deep IR. This also holds for the wave function renormalization Z_ϕ, which is introduced below. For the derivative expansion, which we use throughout this thesis, these mass definitions already agree with the pole masses.

Beside fixing the renormalization condition in the deep IR, it is equally well possible to impose suitable renormalization conditions at the UV cutoff Λ, conceptually. A perturbative study of possible Higgs mass values for partly randomized UV initial conditions at the Planck scale has, for instance, been performed for the standard model in [81]. Thus, we can fix h

and the scalar potential U in terms of their bare quantities at the cutoff, $h_\Lambda = \bar{h}$ and U_Λ. In practice, the fixing can be done such that the constraints set by the physical values of v and m_t are satisfied.

In order to come in contact with the standard model, we fix the vacuum expectation value to be at $v \simeq 246\mathrm{GeV}$ and the top mass at $m_\mathrm{t} \simeq 173\mathrm{GeV}$. We use here the value for the top mass measured by kinematically reconstructing its decay products and comparing these to Monte Carlo simulations. For Higgs mass bounds, actually the pole mass is considered to be the appropriate quantity, which could significantly differ from the experimentally quoted value [82]. In any case, quantitative results of the present toy model should anyway only be considered as an illustrative example. Furthermore, choosing a fixed cutoff Λ leaves only m_H as a free parameter which becomes a function of the whole set of microscopic bare parameters. We stress that it is meaningless to quantitatively compare the Higgs mass bounds obtained below with the measured Higgs mass of $m_\mathrm{H} \simeq 125\mathrm{GeV}$, as the toy model considered here differs in many quantitative aspects from the top-Higgs sector of the standard model.

Constraints on the Higgs mass are now obtained if the region of attainable Higgs masses is bounded for any given combination of bare parameters. These bare parameters are essentially unconstrained, as they are provided by a yet unknown underlying microscopic theory. Only a stable bare scalar potential bounded from below is required in order to facilitate a meaningful definition of the quantum theory. In the present section, we start with the standard class of initial bare $\bar{\lambda}_2\phi^4$ potentials. UV stability then implies that $\bar{\lambda}_2 \geq 0$ for this class of potentials. We then extend our considerations to more general potentials. For instance, also a negative $\bar{\lambda}_2$ is permitted if the potential is stabilized for large ϕ, e.g., by positive $\phi^6, \phi^8, \ldots$ terms in the bare potential. We emphasize that these higher-order terms cannot be excluded by referring to renormalizability criteria within the spirit that the standard model is only an effective field theory only valid below a certain UV cutoff. This is because we consider them to be present in the microscopic UV potential at a fixed (possibly physical) UV cutoff Λ. Presently no experiment can impose relevant constraints on such terms which could arise from an underlying UV completion of the standard model. Renormalizability rather tells us that the IR is dominated by the power-counting "renormalizable" operators in the standard model, provided that the UV theory starts near the perturbative Gaußian fixed point.

Before we start to investigate the nonperturbative flow equations and the computation of Higgs mass bounds within the present model, we analyze the properties of the effective potential by means of a simple one-loop approximation in analogy to Sect. 2.3 of the full standard model calculation. By doing this, we point out the qualitative and quantitative differences between the present toy model and the standard model. Taking only top fluctuations into account, yields full analytic solutions. We demonstrate how a seeming instability occurs in the renormalized effective potential, however, the analytical study of the fermion determinant sheds a different light on the stability issue. We already presented the discussion of the fermion determinant in one of our publications [116]. The investigation of the nonperturbative flow is based on [112]

and on yet unpublished material in preparation with H. Gies and J. Borchardt as well as M. Warschinke.

3.1 Renormalized one-loop effective potential

It is a straightforward task to derive the one-loop β functions for the involved couplings in the model defined in Eq. (3.1). They read for the renormalized quartic coupling λ_2 and the squared Yukawa coupling h^2,

$$\beta_{\lambda_2} = \frac{1}{16\pi^2}(9\lambda_2^2 + 4h^2\lambda_2 - 4h^4), \qquad \beta_{h^2} = \frac{1}{8\pi^2}\frac{5}{2}h^4. \tag{3.4}$$

Obviously, the coefficients in front of the couplings do not agree with those in Eqn. (2.8)-(2.9) due to the different field content of the models. For instance, the additional factor of 3 in front of the terms proportional to the top Yukawa coupling in Eq. (2.8) is due to the fact that there are three colored copies of the top in the standard model while the different coefficient for λ_2^2 is due to the additional scalar degrees of freedom of the Higgs field which is a complex $\mathrm{SU}(2)_\mathrm{L}$ doublet in the standard model.

In analogy to the considerations in Sect. 2.3, the dependence of the ϕ^4 coupling on the scale μ can be computed by integrating its β function from the IR, where the boundary condition is fixed in terms of the Higgs mass, upwards to higher scales. Restricting to the pure fermion contribution of the one-loop flow equation and neglecting the running of the Yukawa coupling is justifiable for our current purpose. The pure fermion contribution to the running of λ_2 is the driving force in the vacuum stability discussion, that leads to negative quartic couplings towards the UV. This goes along with the fact, that the considered term is the dominating contribution to the flow of λ_2. Furthermore, the restriction of a nonrunning $h(\mu) = h_{\mu_0} = h_\Lambda$ can be motivated by the fact that h flows logarithmically and thus changes only slightly as long as we do not consider too large scales where, similar to the pure ϕ^4 theory, a Landau pole emerges. Taking the neglected two types of diagrams and a running h into account would only lead to minor different quantitative values but does not change the qualitative picture.

Within these simplifications the 1-loop β function for the quartic coupling can be integrated straightforwardly,

$$\frac{\partial\lambda_2}{\partial \ln\mu} = -\frac{h_\Lambda^4}{4\pi^2} \qquad \Rightarrow \qquad \lambda_2(\mu) = \lambda_{2,\mu_0} - \frac{h_\Lambda^4}{8\pi^2}\ln\frac{\mu^2}{\mu_0^2}, \tag{3.5}$$

where μ_0 is some arbitrary typically low-energy renormalization scale where the renormalization condition on λ_2 is imposed.

Imposing a suitable renormalization condition on the mass term and assuming that the effective potential is well approximated by a ϕ^4-type potential with $\lambda_2(\mu = \phi)$ for large field values $\phi \gg v$ according to Eq. (2.6), the renormalized effective (single-scale) potential reads

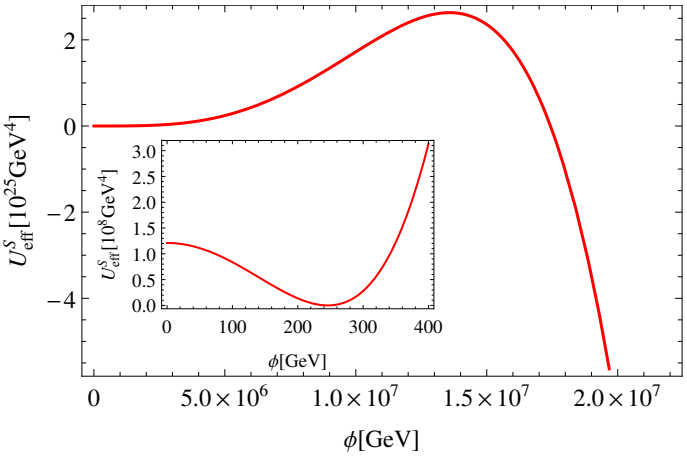

Figure 3.1: Conventional effective single-scale potential $U^{\rm S}_{\rm eff}$ as a function of the field amplitude ϕ. While the potential looks stable around the electroweak minimum, it develops a seeming instability at large field values within our toy model. This instability is driven by top fluctuations which turn the scalar self-coupling negative at large scales.

within our simple approximation for the running of the quartic coupling:

$$U^{\rm S}_{\rm eff}(\phi) = \frac{m^2_{\mu_0}}{2}\phi^2 + \frac{\lambda_2(\mu=\phi)}{8}\phi^4 = \frac{m^2_{\mu_0}}{2}\phi^2 + \frac{\lambda_{2,\mu_0}}{8}\phi^4 - \frac{h^4_\Lambda\phi^4}{64\pi^2}\ln\frac{\phi^2}{\mu_0^2}. \tag{3.6}$$

We emphasize, that the identification $\mu = \phi$ mixes momentum scale information μ with the field amplitude. In general, the full effective action in field theory would provide separate information about the two scales which need not be the same. Further note, that we do not distinguish between bare and renormalized scalar fields in the present as well as in the next section, as this is not relevant at this order.

Following the standard procedure, we impose the renormalization conditions in such a way that the minimum $\phi_0 = v$ as well as the curvature at the minimum stay at its classical values at $\mu = v$, e.g., see [110]. To be more precise:

$$0 = U^{\rm S}_{\rm eff}{}'(v) \;\Rightarrow\; m^2_v = \frac{h^4_\Lambda v^2}{32\pi^2} - \frac{\lambda_{2,v}v^2}{2}, \qquad m^2_{\rm H} = U^{\rm S}_{\rm eff}{}''(v) \;\Rightarrow\; \lambda_{2,v} = \frac{m^2_{\rm H}}{v^2} + \frac{3h^4_\Lambda}{16\pi^2}. \tag{3.7}$$

Thus the renormalized effective single-scale potential reads finally:

$$U^{\rm S}_{\rm eff}(\phi) = -\left[\frac{m^2_{\rm H}}{2} + \frac{m^4_{\rm t}}{4\pi^2v^2}\right]\frac{\phi^2}{2} + \left[\frac{m^2_{\rm H}}{v^2} + \frac{3m^4_{\rm t}}{4\pi^2v^4}\right]\frac{\phi^4}{8} - \frac{m^4_{\rm t}\,\phi^4}{16\pi^2v^4}\ln\frac{\phi^2}{v^2}, \tag{3.8}$$

where the top mass is given by $m^2_{\rm t} = \frac{1}{2}h^2_\Lambda v^2$. Clearly, the potential develops an instability for large Yukawa couplings, correspondingly large $m_{\rm t}$. For the values of $m_{\rm H} = 125{\rm GeV}$, $m_{\rm t} = 173{\rm GeV}$ and $v = 246{\rm GeV}$, the shape of the potential is given in Fig. 3.1. The instability occurs at a scale of $\sim 10^7{\rm GeV}$ for the Higgs-Yukawa toy model and taking only the pure fermion loop into account.

While the Higgs-Yukawa model seems to exhibit an vacuum instability, the situation in the

standard model is slightly different. In the latter the electroweak fluctuations become large at high energy scales, which turns the quartic coupling positive again. As discussed in Sect. 2.3, the potential will be bounded from below and a second minimum arises beyond the Planck scale which turns out to be the global one. Therefore, it is a particularity of our toy model that the effective potential becomes entirely unstable. Nevertheless, the mechanisms that lead to the in-/metastability are the same and can be investigated in the present model.

3.2 Fermion determinant and (in-)stability

With hindsight, the arguments underlying Eq. (2.6) rely on the assumption that the field amplitude ϕ provides for the only relevant scale at large values. It is precisely this assumption that fails in the presence of a finite cutoff independently of the size of the cutoff. In order to see this, let us start from the Euclidean generating functional for the scalar correlation functions of the model

$$Z[J] = \int_\Lambda \mathcal{D}\phi\mathcal{D}\bar{\psi}\mathcal{D}\psi e^{-S[\phi,\bar{\psi},\psi]+\int J\phi}, \tag{3.9}$$

where the appearance of Λ at the functional integral shall remind us of the fact that the theory requires a regularization procedure as part of its definition. As the action is a quadratic form in the fermion fields, the corresponding fermionic integral can be carried out and yields

$$Z[J] = \int_\Lambda \mathcal{D}\phi \det{}_\Lambda[\mathfrak{D}(\phi)] e^{-S_\mathrm{B}[\phi]+\int J\phi} = \int_\Lambda \mathcal{D}\phi\, e^{-S_\mathrm{B}[\phi]-S_{\mathrm{F},\Lambda}[\phi]+\int J\phi}, \tag{3.10}$$

where S_B is the purely bosonic part of the action and $\mathfrak{D}(\phi)$ denotes the Dirac operator in the presence of the scalar field. In the second step of Eq. (3.10), we have introduced the effective action $S_{\mathrm{F},\Lambda}[\phi]$ arising from integrating out the fermion fluctuations. As the fermion determinant and thus also $S_{\mathrm{F},\Lambda}$ corresponds already to a loop-integration, it suffices for the present purpose to investigate its properties for a homogeneous mean field ϕ. Deviations from this mean field contribute to the full effective potential only in terms of fluctuations at higher-loop order. Therefore, we concentrate on the fermion-fluctuation induced contribution to the effective potential

$$U_\mathrm{F}(\rho) = -\frac{1}{\Omega}\ln\det{}_\Lambda[\mathfrak{D}(\phi)], \tag{3.11}$$

where $\Omega = \int d^4x$ denotes the spacetime volume, and we have used the fact that the dependence on ϕ must occur in terms of the $\mathbb{Z}_2$ invariant variable $\rho = \frac{1}{2}\phi^2$. Incidentally, Eq. (3.11) corresponds to the leading contribution to the effective potential in a large-N_f expansion.

The Dirac operator reads $\mathfrak{D}(\phi) = i\partial\!\!\!/ + i\frac{1}{\sqrt{2}}h_\Lambda\phi$. Because of γ_5 hermiticity, $i\partial\!\!\!/$ is isospectral

to $-i\partial\!\!\!/$ which allows us to write

$$U_{\mathrm{F}}(\rho) = -\frac{1}{2\Omega} \ln \frac{\det_\Lambda(-\partial^2 + h_\Lambda^2 \rho)}{\det_\Lambda(-\partial^2)}. \tag{3.12}$$

In proceeding from Eq. (3.11) to Eq. (3.12), we also used the freedom of choosing the normalization of the generating functional such that the fermion-induced effective potential is normalized to the zero-field limit, i.e., $U_{\mathrm{F}}(\rho = 0) = 0$. This resulting ratio of determinants can be evaluated straightforwardly, once a regularization procedure has been chosen. The final result will of course depend on the regularization for any finite value of the cutoff Λ. As argued above, we should not expect that the cutoff can be sent to infinity, since our model is likely to have a scale of maximum UV extent. In order to understand this regulator dependence, it is therefore instructive to compute Eq. (3.12) for different choices of the regularization.

A straightforward regularization is provided by a sharp cutoff in momentum space, such that Eq. (3.12) translates into

$$U_{\mathrm{F}}(\rho) = -2 \int_\Lambda \frac{d^4 p}{(2\pi)^4} \ln \left(1 + \frac{h_\Lambda^2 \rho}{p^2}\right), \tag{3.13}$$

where we have used that we work here with 4-component Dirac spinors. As expected, the integral contains quadratic and logarithmic "divergencies", which can be made explicit by writing the analytic exact result of the integral as

$$U_{\mathrm{F}}(\rho) = -\frac{\Lambda^2}{8\pi^2} h_\Lambda^2 \rho + \frac{1}{16\pi^2} \left[h_\Lambda^4 \rho^2 \ln \left(1 + \frac{\Lambda^2}{h_\Lambda^2 \rho}\right) + \Lambda^4 \left\{ \frac{h_\Lambda^2 \rho}{\Lambda^2} - \ln \left(1 + \frac{h_\Lambda^2 \rho}{\Lambda^2}\right) \right\} \right]. \tag{3.14}$$

Here observe that the quadratic divergence $\sim \Lambda^2$ has been isolated in the first term. The remaining term in square brackets contains only logarithmic divergencies $\sim \ln \Lambda$. It is however more important to note that the first term also isolates the only term proportional to $\rho \sim \phi^2$ and thus contributes to the mass parameter of the scalar field. The remaining terms represent the interacting part of the fermion-induced effective potential.

Most importantly: whereas the contribution to the mass term is negative, as it should be, since fermion fluctuations tend to induce chiral symmetry breaking, the whole interaction part in square brackets is strictly positive for all $\rho > 0$. This follows immediately from the inequality $\ln(1 + x) < x$ (for $x > 0$) applied to the last term. Similarly, it can be shown that also the derivative of the interacting part with respect to ρ is strictly positive for any finite value of ρ, h_Λ and Λ.

We conclude that the fermion determinant – apart from its contribution to the scalar mass term – is strictly positive and monotonically increasing in its interacting part. Therefore, once the scalar mass term has been fixed by a renormalization condition, the remaining contributions from the top fluctuations to the interacting part of the bosonic potential are strictly positive. This excludes the possibility that an instability beyond the electroweak vacuum is induced by

fermionic fluctuations. This can also be phrased in terms of a more rigorous statement: if the potential of the purely bosonic part S_B of the action in Eq. (3.10) is bounded from below by a function of the form $U_\mathrm{B}(\rho) > c_1 + c_2\rho^{1+\epsilon}$ with an arbitrary finite constant c_1 and finite positive constants $c_2, \epsilon > 0$, then also the full potential including the fermionic fluctuations is bounded from below.

This result is in obvious direct disagreement with the standard perturbative reasoning outlined above, cf. Eqn. (2.6) and (3.4). Nevertheless, it is in fact possible to "rediscover" this seeming instability of the standard reasoning from the stable contribution (3.14) by trying to take the limit $\Lambda \to \infty$. The leading-order terms in this limit read,

$$U_\mathrm{F}(\rho) = -\frac{\Lambda^2}{8\pi^2} h_\Lambda^2 \rho + \frac{1}{16\pi^2}\left[h_\Lambda^4 \rho^2 \ln\frac{\Lambda^2}{h_\Lambda^2\rho} + \frac{h_\Lambda^4\rho^2}{2} + \mathcal{O}\left(\frac{(h_\Lambda^2\rho)^3}{\Lambda^2}\right)\right]. \tag{3.15}$$

From here, it is tempting to isolate the divergencies $\sim \Lambda^2$ and $\ln\Lambda$, combine them with the bare scalar mass and ϕ^4 coupling parameters, and trade them for renormalized parameters $m_\mathrm{H}^2(\mu_0)$ and $\lambda_2(\mu_0)$. Ignoring the mass term for a moment, the renormalized interaction contribution to the effective potential would then read

$$U_\mathrm{F}(\rho) \stackrel{?}{\to} -\frac{1}{16\pi^2} h_\Lambda^4 \rho^2 \left(\ln\frac{h_\Lambda^2\rho}{\mu_0^2} + \text{const.}\right), \tag{3.16}$$

where the constant depends on the details of the renormalization scheme. This is precisely the fermion-loop contribution to the effective action, which we obtained from integrating the term $\sim h_\Lambda^4$ of the β_{λ_2} function (3.4) from μ_0 to μ and identifying $\mu^2 \sim \rho$ in the previous Sect. 3.1. Hence, we have "rederived" the contribution with the characteristic minus sign that seems to indicate the presence of an instability at large values of ρ, while the cutoff Λ seems to have disappeared completely.

The problem of this line of argument becomes obvious, once we go back to the cutoff-dependent leading order terms in Eq. (3.15). It is straightforward to work out that also these leading-order terms seem to have an instability: the interaction part of the potential in square brackets first develops a maximum and then eventually turns negative for large fields ρ. However, the location of the maximum is in fact at $h_\Lambda^2\rho = \Lambda^2$. In other words, these seeming instability features appear precisely at those field values, where the expansion in terms of the parameter $\frac{h_\Lambda^2\rho}{\Lambda^2} \ll 1$ breaks down. We conclude that the instability "discovered" in Eq. (3.16) is an artifact of having tried to send the cutoff to infinity $\Lambda \to \infty$ together with a problematic choice of renormalization conditions. In fact, it has been shown in [110, 111] for the present $\mathbb{Z}_2$-Yukawa model that the renormalization conditions needed to arrive at Eq. (3.16) require an unstable bare bosonic potential with negative bare ϕ^4 coupling, $\lambda_2(\Lambda) < 0$.

Some additional comments are in order:

(1) Our conclusions are identical to those of [107, 108], where essentially the same results have been found for the $\mathbb{Z}_2$-Yukawa model. In these works, lattice simulations have been compared

with the one-loop effective potential with a cutoff kept finite, matching the lattice data almost perfectly. By contrast, the effective potential with the cutoff removed à la Eq. (3.16) shows an artificial instability in strong disagreement with the nonperturbative simulation. This work has been criticized [79, 109] also because it is generically difficult on the lattice to bridge wide ranges of scales, in particular to separate the cutoff from the long-range mass scales by many orders of magnitude. As is clear from the above discussion, this problem does not exist for the present line of argument; the cutoff can be arbitrarily large in the above discussion of the fermion determinant. As long as it is finite, the interaction part of the determinant does not induce any instability.

(2) For the above discussion and the comparison to the standard line of arguments at one-loop order, it has been sufficient to evaluate the determinant for a homogeneous mean field. Though this does not interfere with our argument, one might ask whether the determinant behaves qualitatively differently for non-homogeneous fields. Some exact results are known for $d = 1 + 1$ dimensional determinants, where the Peierls instability at a finite chemical potential can lead to inhomogeneous ground states with lower free energy [209]. However, the vacuum ground state is generically homogeneous as no mechanism is known that can "pay" for the higher cost in kinetic energy. Absolute lower and upper bounds for fermion determinants have been found, e.g., for QED [210].

(3) The fact that the interaction part of the fermion contribution to the scalar potential is positive does not imply that the full theory cannot have further potentially (meta-)stable vacua. The conclusion rather is that such further vacua have to be provided by the bosonic sector. In particular, the bare bosonic potential U_{B} can in principle be chosen such that it has several vacua. As a special case, it is even possible to construct examples such that the bare bosonic potential has one minimum, but the sum of U_{B} and U_{F} has two minima. This is still very different from the perturbative reasoning which for the present model seems to suggest a global instability due to the fermionic fluctuations, whereas a global instability of $U_{\mathrm{B}} + U_{\mathrm{F}}$ in our analysis would have to be seeded from the choice of U_{B}. In other words, our arguments do not exclude that our electroweak vacuum is unstable, but they suggest that such an in-/metastability would have to be provided by the microscopic underlying theory, see [129]. In this case, however, the Higgs mass bounds from metastability as well as the life-time estimates of the electroweak vacuum would be very different from the conventional estimates, see, e.g., [150].

(4) As mentioned above, the result for the fermion determinant is regulator dependent, as long as the cutoff is kept finite. The preceding results have been derived for a sharp cutoff in momentum space. These results in fact generalize to arbitrary smooth cutoff shape functions in momentum space as they can be implemented straightforwardly within the functional RG framework, see Sect. 3.4. Though this is not an issue for the present model, one might be concerned about the fact that such regularizations are not gauge invariant. Hence a gauge-invariant regularization is studied in App. A.2, yielding the same conclusions as for the sharp

cutoff given above.

3.3 Nonperturbative RG flow equations

In this work, we study the nonperturbative renormalization flow of the Yukawa system within the following truncation based on the derivative expansion:

$$\Gamma_k = \int_x \left[\frac{Z_{\phi,k}}{2} (\partial_\mu \phi)^2 + U_k(\rho) + Z_{\psi,k}\, \bar{\psi}\, \mathrm{i} \partial\!\!\!/ \psi + \mathrm{i}\, \frac{\bar{h}_k}{\sqrt{2}}\, \phi \bar{\psi} \psi \right], \tag{3.17}$$

where the field invariant ρ is again given by $\rho = \frac{1}{2}\phi^2$, and the effective average potential U_k generally includes arbitrary powers of the field as they will be generated during the RG flow. In fact, the accuracy of the derivative expansion for Yukawa theories has been verified quantitatively in many contexts [211–216]. Here, we actively study its convergence by comparing leading-order (LO) results (obtained for $Z_{\phi,k} = 1, Z_{\psi,k} = 1$) to next-to-leading order (NLO) results. We find no signatures of a failure of this expansion even at comparatively strong coupling, see Sect. 3.5.

Inserting this ansatz (3.17) into the flow equation (2.13) provides us with the RG flows of $\bar{h}_k$, U_k and the wave function renormalizations $Z_{\phi,k}$ and $Z_{\psi,k}$; the latter flows will be followed in terms of the anomalous dimensions

$$\eta_\phi = -\partial_t \ln Z_{\phi,k}, \qquad \eta_\psi = -\partial_t \ln Z_{\psi,k}. \tag{3.18}$$

Details on the computation of these flow equations can be found in the appendix, see App. A.4.

The flow equation for the effective potential reads

$$\partial_t U_k = 2\, v_d\, k^d \left[l_0^{(\mathrm{B})d} \left(k^{-2}\, Z_{\phi,k}^{-1}\, [U_k' + 2\,\rho\, U_k''] \,; \eta_\phi \right) - d_\gamma\, l_0^{(\mathrm{F})d} \left(2\, k^{-2}\, Z_{\psi,k}^{-2}\, \bar{h}_k^2\, \rho; \eta_\psi \right) \right], \tag{3.19}$$

where primes denote derivatives with respect to the field invariant ρ, and $v_d^{-1} := 2^{d+1}\, \pi^{d/2}\, \Gamma(d/2)$. For generality, we work in d dimensions and with a d_γ dimensional representation of the Dirac algebra. We will later specialize to $d = 4$ and $d_\gamma = 4$. The threshold functions $l_0^{(\mathrm{B})d}$ and $l_0^{(\mathrm{F})d}$ arise from the integration over the loop momentum and carry the non-universal regulator dependence. For any physically admissible regulator, they approach finite constants for vanishing argument and decrease to zero for large first argument, describing the decoupling of massive modes. A list of threshold functions can be found in App. A.3. A diagrammatic representation of the contributions to the flow equation for the scalar potential is given in Fig. 3.2.

It is useful and convenient to introduce renormalized fields in order to fix the usual RG invariance of field rescalings,

$$\tilde{\phi} = Z_{\phi,k}^{1/2} \phi, \qquad \tilde{\psi} = Z_{\psi,k}^{1/2} \psi.$$

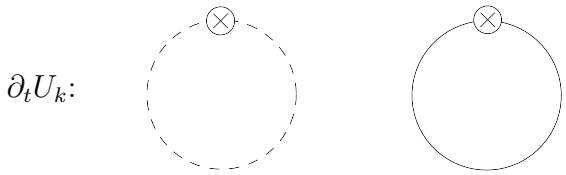

Figure 3.2: Diagrammatic representation for the contributions to the flow equation of the scalar potential. Dashed and solid lines denote scalar and fermion fields respectively. All internal propagators are considered as fully dressed at the scale k as implied by the Wetterich equation. Circles with a cross denote a regulator insertion $\partial_t R_k$.

Thus, we are able to rewrite the flow equations in terms of dimensionless renormalized quantities, such as

$$\tilde{\rho} = Z_{\phi,k}\, k^{2-d} \rho, \qquad u_k(\tilde{\rho}) = k^{-d} U_k(\rho)|_{\rho = k^{d-2} Z_\phi^{-1} \tilde{\rho}}, \qquad h_k^2 = Z_{\phi,k}^{-1}\, Z_{\psi,k}^{-2}\, k^{d-4}\, \bar{h}_k^2. \tag{3.20}$$

The flow of u_k for fixed $\tilde{\rho}$ is given by

$$\partial_t\, u_k = -d\, u_k + (d - 2 + \eta_\phi)\tilde{\rho} u_k' + 2 v_d \Big[l_0^{(\mathrm{B})d}\,(u_k' + 2\,\tilde{\rho}\, u_k''; \eta_\phi) - d_\gamma\, l_0^{(\mathrm{F})d}\left(\tilde{\rho}\, h_k^2; \eta_\psi\right) \Big], \tag{3.21}$$

where primes now denote derivatives with respect to $\tilde{\rho}$. The flow of the renormalized Yukawa coupling is of the form

$$\begin{aligned} \partial_t h_k^2 = &(d - 4 + \eta_\phi + 2\eta_\psi)\, h_k^2 + 4 v_d\, h_k^4 \Big[l_{1,1}^{(\mathrm{FB})d}(\mu_\mathrm{t}^2, \mu_\phi^2; \eta_\psi, \eta_\phi) - 2 h_k^2 \kappa_k\, l_{2,1}^{(\mathrm{FB})d}(\mu_\mathrm{t}^2, \mu_\phi^2; \eta_\psi, \eta_\phi) \\ &- \left(6\kappa_k u_k''(\kappa_k) + 4\kappa_k^2 u_k'''(\kappa_k)\right) l_{1,2}^{(\mathrm{FB})d}(\mu_\mathrm{t}^2, \mu_\phi^2; \eta_\psi, \eta_\phi) \Big], \end{aligned} \tag{3.22}$$

and $\kappa_k = \tilde{\rho}_0$ denotes the minimum of the potential u_k; i.e., if $\kappa_k \neq 0$ then $u_k'(\kappa_k) = 0$. Further, we have used the abbreviations $\mu_\phi^2 = u_k'(\kappa_k) + 2\kappa_k u_k''(\kappa_k)$ and $\mu_\mathrm{t}^2 = h_k^2 \kappa_k$ which are the flowing renormalized dimensionless mass of the Higgs and top field respectively. Finally, the anomalous dimensions are determined by

$$\begin{aligned} \eta_\phi = &\frac{8 v_d}{d} \kappa_k \Big[3u_k''(\kappa_k) + 2\kappa_k u_k'''(\kappa_k)\Big]^2 m_2^{(\mathrm{B})d}(\mu_\phi^2; \eta_\phi) \\ &+ \frac{4 v_d d_\gamma}{d} h_k^2 \Big[m_4^{(\mathrm{F})d}(\mu_\mathrm{t}^2; \eta_\psi) - \kappa_k h_k^2\; m_2^{(\mathrm{F})d}(\mu_\mathrm{t}^2; \eta_\psi) \Big], \end{aligned} \tag{3.23}$$

$$\eta_\psi = \frac{4 v_d}{d} h_k^2\; m_{1,2}^{(\mathrm{FB})d}(\mu_\mathrm{t}^2, \mu_\phi^2; \eta_\psi, \eta_\phi), \tag{3.24}$$

where the threshold functions are again discussed in App. A.3. A diagrammatic interpretation of the contributions to the Yukawa coupling as well as the anomalous dimensions is depicted in Fig. 3.3. These flow equations can be compared to those of similar investigations in the literature [52, 213, 217] within different physical contexts. Once the flow equations have been solved for suitable initial UV conditions, we can read off the fully renormalized long-range quantities in the limit $k \to 0$. For instance, the physical quantities defined in Eq. (3.3) require the

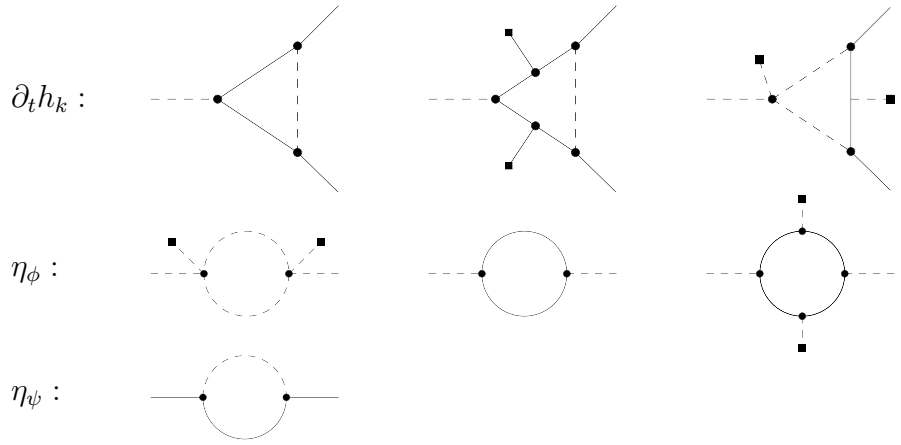

Figure 3.3: Diagrammatic contributions to the running of the Yukawa coupling as well as the anomalous dimensions of the fields. All internal propagators and vertices are considered as fully dressed at the scale k. For compactness, we suppressed the regulator insertions. Each diagram is implicitly understood as a sum over regulator insertions at one of the internal lines in each diagram. Filled squares denote couplings to the condensate $\sim \sqrt{2\kappa_k}$, cf App. A.4.

renormalized Yukawa coupling $h = h_{k\to 0}$ and the wave function renormalization $Z_\phi = Z_{\phi,k\to 0}$. The renormalized vacuum expectation value is obtained from $v^2 = \lim_{k\to 0} 2k^{d-2}\kappa_k$.

Moreover, we are able to extract the perturbative one-loop β functions for λ_2 and h^2, see Eq. (3.4), from these nonperturbative flow equations. Therefore, we neglect resummation effects and go to the deep Euclidean region where all momenta are considered to be much larger than the involved masses. Technically speaking, we set all anomalous dimensions occurring in the threshold functions to zero because these correspond to higher loop corrections but keeping the anomalous dimensions occurring from the dimensional scaling of the renormalized couplings which contribute to the perturbative one-loop flow equation via one-particle reducible graphs. In addition, we take the limits, $\kappa \to 0$, $\tilde{\rho} \to 0$, to consider the deep Euclidean region. Within this limit, the flow equations for the anomalous dimensions read,

$$\eta_\phi = \frac{4v_d d_\gamma}{d} h_k^2\, m_4^{(\mathrm{F})d}(0;0) \overset{d=4}{=} \frac{h_k^2}{8\pi^2}, \qquad \eta_\psi = \frac{4v_d}{d} h_k^2\, m_{1,2}^{(\mathrm{FB})d}(0,0;0,0) \overset{d=4}{=} \frac{h_k^2}{32\pi^2}. \tag{3.25}$$

Thus, the flow equation for h^2 in this limit reads,

$$\partial_t h_k^2 = (d-4+\eta_\phi+2\eta_\psi)\, h_k^2 + 4v_d\, h_k^4\, l_{1,1}^{(\mathrm{FB})d}(0,0;0,0) = (d-4+\eta_\phi+2\eta_\psi)h_k^2 + \frac{16v_d}{d}h_k^4 \overset{\substack{d=4 \\ \text{Eq.(3.25)}}}{=} \frac{5}{16\pi^2}h_k^4 \tag{3.26}$$

For the flow equation of λ_2, we expand the potential in powers of the field invariant $\tilde{\rho}$ up to the second order, $u_k = \lambda_{1,k}\tilde{\rho} + \frac{\lambda_{2,k}}{2}\tilde{\rho}$, where $\lambda_{1,k}$ corresponds to the renormalized mass term which will be neglected as we consider the deep Euclidean region. Then, the β function is given by,

$\partial_t \lambda_{2,k} = \partial_t(\partial_{\tilde{\rho}}^2 u_k)|_{\tilde{\rho}=0}$, and we finally obtain,

$$\begin{aligned}\partial_t \lambda_{2,k} &= (d-4+2\eta_\phi)u_k''(0) + 2v_d\partial_{\tilde{\rho}}^2\Big[l_0^{(\mathrm{B})d}\,(u_k' + 2\,\tilde{\rho}\,u_k'';0) - d_\gamma\, l_0^{(\mathrm{F})d}\left(\tilde{\rho}\,h_k^2;0\right)\Big]_{\tilde{\rho}=0,\lambda_{1,k}=0} \\ &= (d-4+2\eta_\phi)\lambda_{2,k} + \frac{8v_d}{d}(9\lambda_{2,k} - d_\gamma h_k^4) \end{aligned} \tag{3.27}$$

Considering $d = 4$ and approximating the anomalous dimensions with Eq. (3.25), the flow equation for the quartic coupling (Eq. (3.27)) and for the Yukawa coupling (Eq. (3.26)) are identical to Eq. (3.4). Thus, we obtained the universal one-loop coefficients of the β functions in a particular limit of the nonperturbative flow equations as we should.

However, we would like to point out that there is a conceptual difference between Eq. (3.4) and the flow equations given in (3.26) and (3.27). In the standard perturbative setup, the β functions (3.4) describe the variation of the coupling with respect to the renormalization scale μ which is an arbitrary scale in practice related to a measurement scale. By contrast, the one-loop β functions resulting from the FRG describe the variation of a coupling with respect to the IR cutoff scale k introduced by R_k. Both scales are introduced as arbitrary auxiliary scales which can be chosen independently. Nonetheless, changing from the different meanings of the energy scales k and μ corresponds to a change of the renormalization scheme. Due to the universality of the one-loop coefficients (and also of the two-loop coefficients in a mass-independent scheme), we obtain the correct perturbative limit. FRG results in the context of universality are further discussed in [166, 218–220].

3.4 Mean-field analysis

Before we tackle the full set of nonperturbative flow equations (3.21)-(3.24), let us first perform a mean-field analysis. The purpose of this is twofold: first, we are able to generalize our results for the fermion determinant obtained for a sharp cutoff to a wider class of regulator shape functions and rephrase the results of Sect. 3.2 in the language of the flow equation. Second, the mean-field approximation allows for an analytical treatment of Higgs mass bounds and the effective action. Thus, we are able to give a first impression on the reliability of approximations, which we use to analyze the nonperturbative flow equations, by comparing the analytical results against truncated solutions of the potential, e.g., in a polynomial approximation.

The mean-field analysis corresponds to a one-loop approximation of the effective potential including fermion fluctuations (as well as boson fluctuations in an extended mean-field setup), while keeping the wave function renormalizations and the Yukawa coupling fixed,

$$Z_{\phi,k}, Z_{\psi,k} \to 1, \quad h_k \to h_\Lambda. \tag{3.28}$$

The mean-field effective potential U^{MF} could, of course, be calculated directly from a Gaußian approximation of the generating functional, yielding the standard $\log\det$-formula (2.5) or ac-

cordingly (3.11). Nevertheless, we derive it from the flow equation, since it provides direct access to the use of an arbitrarily shaped regulator function, which can be used to model the physical UV cutoff mechanism.

The standard mean-field (MF) approximation is equivalent to the large-N_f approximation, taking only fermionic fluctuations into account. The corresponding mean-field effective potential is obtained from the flow equation (3.19) by integrating the fermion contributions $\sim l_0^{(\mathrm{F})d}$ from $k = \Lambda$ to $k = 0$, while keeping the Yukawa coupling on the right-hand side fixed at $h_k \to h_\Lambda$. In addition, we neglect the term coming from the scalar fluctuations $\sim l_0^{(\mathrm{B})d}$. We obtain for the mean-field effective average potential for finite k in $d = 4$ dimensions

$$U_k^{\mathrm{MF}}(\rho) = U_\Lambda(\rho) + \frac{d_\gamma}{2}\int_p \ln\left(\frac{p^2\Big(1+r_\mathrm{F}(p^2/\Lambda^2)\Big)^2 + h_\Lambda^2\rho}{p^2\Big(1+r_\mathrm{F}(p^2/k^2)\Big)^2 + h_\Lambda^2\rho}\right), \tag{3.29}$$

where $\int_p = \int \frac{d^dp}{(2\pi)^d}$ and r_F is the regulator shape function which depends on the ratio of the momentum and the RG scale k. In order to provide for a regularization, $r_\mathrm{F}(x)$ should vanish for large argument and diverge sufficiently fast to positive infinity for $x \to 0$. Apart from analyticity for all finite $x > 0$, no further requirements on r_F are needed; however, for the interpretation of a physical regularization, we assume r_F to be nonnegative for finite x. The second derivative of the mean-field effective potential ($k = 0$) with respect to ρ encodes the fermionic contributions to the interacting part of the effective potential:

$$U_{k=0}^{\mathrm{MF}\,\prime\prime} = U_\Lambda'' + \frac{d_\gamma h_\Lambda^4}{64\pi^2}\int_0^\infty dp\, p^3 \frac{\Big[p^2\Big(1+r_\mathrm{F}(p^2/\Lambda^2)\Big)^2 - p^2\Big]\Big[p^2\Big(1+r_{\mathrm{F},\Lambda}(p^2/\Lambda^2)\Big)^2 + p^2 + h_\Lambda^2\rho\Big]}{\Big[p^2\Big(1+r_{\mathrm{F},\Lambda}(p^2/\Lambda^2)\Big)^2 + h_\Lambda^2\rho\Big]^2\Big[p^2+h_\Lambda^2\rho\Big]^2}.$$

The integrand is strictly nonnegative for $r_\mathrm{F} \geq 0$ and so is the integral. This corroborates the conclusion from Sect. 3.2 that the interaction part of the fermion determinant is strictly positive for a general class of arbitrary smooth cutoff shape functions in momentum space.

The extended mean-field (EMF) approximation is obtained by including also the scalar fluctuations on the same Gaußian level. Introducing the abbreviation $M_\Lambda^2(\rho) = U_\Lambda'(\rho) + 2\rho U_\Lambda''(\rho)$, we find,

$$U_k^{\mathrm{EMF}}(\rho) = U_k^{\mathrm{MF}}(\rho) - \frac{1}{2}\int_p \ln\left(\frac{p^2\Big(1+r_\mathrm{B}(p^2/\Lambda^2)\Big) + M_\Lambda^2(\rho)}{p^2\Big(1+r_\mathrm{B}(p^2/k^2)\Big) + M_\Lambda^2(\rho)}\right). \tag{3.30}$$

While the mean-field approximation becomes exact in the strict large-N_f limit, the extended-mean-field approximation takes $1/N_\mathrm{f}$ corrections into account. However, further subtleties arise in the extended-mean-field case from convexity violations and complex solutions for the potential as discussed in [221]. These subtleties of the extended mean-field approximation are however irrelevant for the nonperturbative functional RG solution discussed in the following sections. Hence, we will mainly stay within the standard mean-field approximation in the

following for the purpose of illustration.

For both approximations, the momentum integration can be done analytically for a suitable choice of the regulator shape functions $r_{\mathrm{B}}(x)$, $r_{\mathrm{F}}(x)$. For instance, for the linear regulator (cf. App. A.3) we obtain for the scale dependent mean-field effective average potential

$$U_k^{\mathrm{MF}}(\rho) = U_\Lambda(\rho) - \frac{h_\Lambda^2(\Lambda^2 - k^2)\rho}{16\pi^2} + \frac{h^4\rho^2}{16\pi^2}\ln\frac{\Lambda^2 + h_\Lambda^2\rho}{k^2 + h_\Lambda^2\rho}. \tag{3.31}$$

By varying the RG scale k, we are able to study how the mean-field effective potential, $U^{\mathrm{MF}}(\rho) = U_{k=0}^{\mathrm{MF}}(\rho)$, is build up by fermionic fluctuations added to the bare potential U_Λ. In a similar manner the flow of the extended mean-field potential can be studied. This reads in the limit $k \to 0$,

$$\begin{aligned} U^{\mathrm{EMF}}(\rho) = U^{\mathrm{MF}}(\rho) + \frac{1}{64\pi^2}\Bigg[&\Big(M_\Lambda^2(\rho) - M_\Lambda^2(0)\Big)\Lambda^2 \\ &- M_\Lambda^4(\rho)\ln\frac{\Lambda^2 + M_\Lambda^2(\rho)}{M_\Lambda^2(\rho)} + M_\Lambda^4(0)\ln\frac{\Lambda^2 + M_\Lambda^2(0)}{M_\Lambda^2(0)}\Bigg], \end{aligned} \tag{3.32}$$

where we have normalized $U^{\mathrm{EMF}}(\rho)$ such that $U^{\mathrm{EMF}}(0) = 0$. In the following we will show that Eq. (3.32) can be used to illustrate the appearance of a lower bound for the Higgs mass.

3.4.1 Bare potentials of ϕ^4-type

First, let us confine to bare potentials of ϕ^4-type,

$$U_\Lambda(\rho) = m_\Lambda^2\rho + \frac{\lambda_{2,\Lambda}}{2}\rho^2, \tag{3.33}$$

with $\lambda_{2,\Lambda} \geq 0$ in order to start with a physical meaningful bare potential which is bounded from below. For a given UV cutoff Λ, two out of the three bare parameters $m_\Lambda^2, \lambda_{2,\Lambda}, h_\Lambda$ can be fixed by fixing the top mass and the vacuum expectation value; more precisely, fixing $h_\Lambda = \frac{\sqrt{2}m_{\mathrm{t}}}{v}$ and determining m_Λ^2 from the transcendental equation

$$U^{\mathrm{EMF}\prime}(\rho_0 = v^2/2) = 0, \tag{3.34}$$

leaves us with the Higgs mass as a function of the bare scalar coupling, $m_{\mathrm{H}} = m_{\mathrm{H}}(\lambda_{2,\Lambda})$. In the standard mean-field approximation, it is easy to see that $m_{\mathrm{H}} = m_{\mathrm{H}}(\lambda_{2,\Lambda})$ increases monotonically with $\lambda_{2,\Lambda}$, therefore a lower bound on the Higgs mass is obtained from the lowest possible value of $\lambda_{2,\Lambda}$, which is $\lambda_{2,\Lambda}^{\min} = 0$ for potentials of the form of Eq. (3.33). (In the extended mean-field approximation, the same conclusion holds unless $\lambda_{2,\Lambda}$ approaches the strong-coupling value $\lambda_{2,\Lambda} \to \frac{4}{3}h_\Lambda^2$ where an EMF-artifact induces singular behavior).

Equation (3.34) can easily be solved numerically. For an analytical estimate, let us stay within the mean-field approximation. Determining m_Λ^2 from the condition $U^{\mathrm{MF}\prime}(\rho_0 = v^2/2) = 0$ for

fixed values of m_t and v such that a minimum occurs at the electroweak scale, we find ($d_\gamma = 4$)

$$m_\Lambda^2(\Lambda, \lambda_{2,\Lambda}) = \frac{h_\Lambda^2}{8\pi^2}\Lambda^2 - \frac{\lambda_{2,\Lambda}}{2}v^2 - \frac{h_\Lambda^4 v^2}{8\pi^2}\left[2\ln\left(1+\frac{\Lambda^2}{m_\mathrm{t}^2}\right) - \frac{\Lambda^2}{\Lambda^2+m_\mathrm{t}^2}\right]. \tag{3.35}$$

Note that the first term on the right-hand side is of order Λ^2 while the remaining terms are of order v^2. This is necessary to allow for a potentially large scale separation between the electroweak minimum and the cutoff scale. The first term precisely cancels the fermionic induced mass term $\sim \rho$ in the mean-field potential (3.31) by construction. The other terms achieve that a nontrivial minimum occurs at the Fermi scale. While this can be accomplished in terms of an analytical expression within the mean-field approximation, it will become a rather substantial issue for the numerical analysis of the flow equations on a nonperturbative level because a large amount of fine-tuning for the initial mass parameter is required.

Relation (3.35) fixes the effective mean-field potential as a function of $\lambda_{2,\Lambda}$ and Λ. Within these analytical expressions obtained from the linear regulator, it is straightforward to convince oneself again that no further extrema will be generated by fermion fluctuations for any finite but arbitrary value for Λ and ρ, similar to the sharp cutoff, cf. Eq. (3.14). The Higgs mass finally reads,

$$m_\mathrm{H}^2(\Lambda, \lambda_{2,\Lambda}) = v^2 U^{\mathrm{MF}\prime\prime}(v^2/2) = \frac{m_\mathrm{t}^4}{4\pi^2 v^2}\left[2\ln\left(1+\frac{\Lambda^2}{m_\mathrm{t}^2}\right) - \frac{3\Lambda^4 + 2m_\mathrm{t}^2\Lambda^2}{(\Lambda^2+m_\mathrm{t}^2)^2}\right] + v^2\lambda_{2,\Lambda}. \tag{3.36}$$

This renders explicit that the lower bound for UV potentials of quartic type (3.33) is given by $m_\mathrm{H}(\Lambda, \lambda_{2,\Lambda} = 0)$.

The mean-field analysis performed here gives a first insight into how lower bounds for the Higgs mass follow from the mapping from bare to renormalized quantities. It also exemplifies that the mere existence of a lower bound on the Higgs mass for bare potentials of ϕ^4-type is essentially a consequence of top fluctuations that drive the curvature of the effective potential at its nontrivial minimum to finite values. This statement will also hold on the nonperturbative level. We plot the mean-field results for the Higgs mass as a function of Λ for various values of $\lambda_{2,\Lambda}$ in Fig. 3.4 as solid lines.

The plot also shows corrections from bosonic fluctuations as described by extended mean-field theory $U^{\mathrm{EMF}}(\rho)$ as dashed lines for the same values of $\lambda_{2,\Lambda}$. We observe that scalar fluctuations tend to decrease the Higgs mass values. This agrees with the fact that scalar fluctuations drive the effective potential towards the symmetric regime, thus flattening the curvature at the minimum. However, the lower bound of the Higgs mass remains unaffected by the scalar fluctuations, because the scalar field is non-interacting for $\lambda_{2,\Lambda} = 0$ in the EMF approximation.

As we are working with an explicit finite cutoff Λ, these results are regulator depended. Therefore, let us study the influence of this scheme dependence specified in terms of the regulator shape functions $r_\mathrm{B}(p^2/k^2)$, $r_\mathrm{F}(p^2/k^2)$. The Higgs mass in Eq. (3.36) is obtained for the linear regulator, which fulfills optimization criteria for the used derivative expansion (3.17).

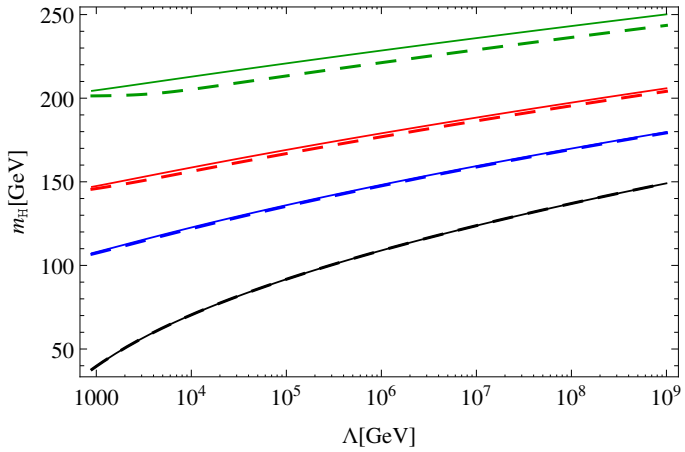

Figure 3.4: Extended mean-field analysis of the lower bound for the Higgs mass m_{H} versus the UV cutoff Λ, based on a bare potential U_Λ of ϕ^4-type. For an initial UV potential which is flat apart from a mass term $U_\Lambda = \frac{1}{2}m_\Lambda^2\phi^2$, the fermionic fluctuations drive the Higgs mass to a finite minimal value. The solid lines correspond to standard mean-field theory accounting only for top fluctuations, cf. Eq. (3.36), whereas the dashed lines also include scalar fluctuations on the Gaußian level (extended mean-field). The four different line sets correspond to increasing values of the initial ϕ^4 coupling of $\lambda_{2,\Lambda} = 0, \frac{1}{6}, \frac{1}{3}, \frac{2}{3}$ from bottom to top.

Roughly speaking it leads to the shortest RG trajectory in theory space. On the other hand, the sharp cutoff leads to the longest RG trajectory and is in some sense the opposite of the linear regulator in terms of optimization. Using the results of the fermion determinant for the sharp cutoff (3.14), the Higgs mass reads,

$$m^2_{\mathrm{H,sharp}}(\Lambda,\lambda_{2,\Lambda}) = \frac{m_{\mathrm{t}}^4}{4\pi^2 v^2}\left[2\ln\left(1+\frac{\Lambda^2}{m_{\mathrm{t}}^2}\right)-\frac{2\Lambda^2}{\Lambda^2+m_{\mathrm{t}}^2}\right]+v^2\lambda_{2,\Lambda}. \tag{3.37}$$

For $\Lambda^2 \gg m_{\mathrm{t}}^2$, the difference between the sharp cutoff and the linear regulator is given by $m^2_{\mathrm{H,sharp}} - m^2_{\mathrm{H,lin}} = \frac{m_{\mathrm{t}}^4}{4\pi^2 v^2}$. For $m_{\mathrm{H}} > 100\mathrm{GeV}$, the regulator dependence is only at the percent level for the Higgs mass between these two extreme choices for the regulator. Moreover, a change of the regularization scheme such as a change of the shape functions can be mapped onto a change of the initial conditions for the bare couplings (i.e., a change of the renormalization constants) which is $\lambda_{2,\Lambda}$ in this example. Thus, we keep the regulator fixed in the following and solely vary the bare couplings.

As a consequence, the occurrence of a lower Higgs mass bound implies that for a given Higgs mass, say $m_{\mathrm{H}} = 125\mathrm{GeV}$, a maximal scale can be read off, up to which the model can be extended. Assuming that $\lambda_{2,\Lambda} = 0$, we find that for a cutoff of $\Lambda_{\mathrm{cr}} = 1.22 \cdot 10^7\mathrm{GeV}$ we get the desired Higgs mass within our toy model. For larger values of the UV cutoff no physical RG trajectory can be found, connecting a physically meaningful bare potential to an IR Higgs mass of 125GeV.

By ignoring this fact, however, the seeming instability of the renormalized one-loop effective potential occurs again by trying to send the cutoff to larger scales but keeping the IR physics

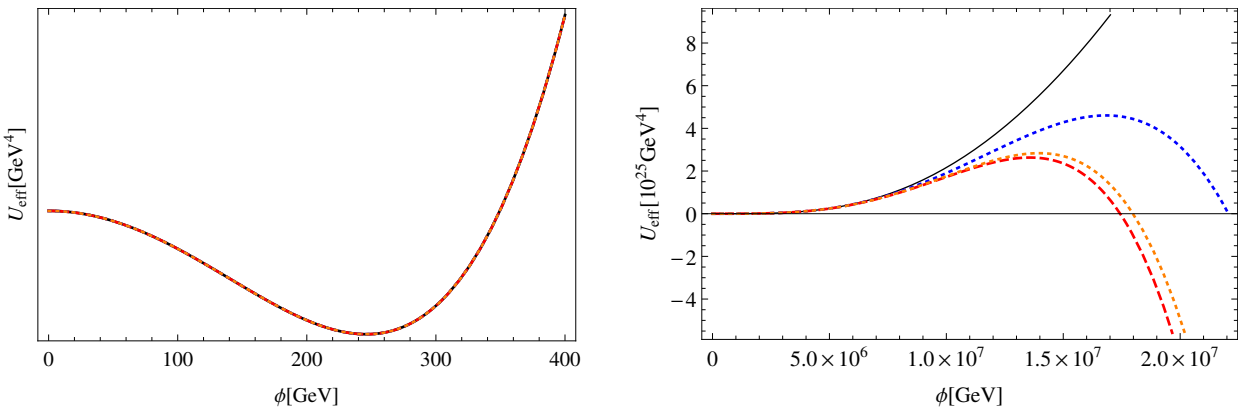

Figure 3.5: Approach of the mean-field potential to the perturbative effective single-scale potential if we blindly allow for larger cutoffs than the critical value of $\Lambda_{\text{cr}} = 1.22 \cdot 10^7\text{GeV}$ (black solid line). The blue dotted line is obtained for $\Lambda = 2 \cdot 10^7\text{GeV}$ and the orange dotted line for $\Lambda = 5 \cdot 10^7\text{GeV}$. For $\Lambda > 10^8\text{GeV}$, there is no visible difference between the mean-field potential and the single-scale potential where $\Lambda \to \infty$ (red dashed) in this plot. For all potentials we fix the IR physics such that the minimum is at the Fermi scale and the curvature at the minimum gives a Higgs mass of 125GeV (left panel). The right panel shows the behavior of the effective potential for large field values.

fixed. Precisely this strategy was implicitly done in the computation of the renormalized effective single-scale potential (3.8) as we have already pointed out in Sect. 3.2 for the sharp cutoff as well as ζ-function regularization in App. A.2. This important statement is once more highlighted in Fig. 3.5 for the mean-field potential obtained from the linear regulator. Therefore, we choose the bare quartic coupling $\lambda_{2,\Lambda}$ such that the curvature at the electroweak minimum is consistent with a mass of 125GeV. For a cutoff much larger than the electroweak scale, this expression reads:

$$\lambda_{2,\Lambda} = \frac{m_{\text{H}}^2}{v^2} - \frac{h_\Lambda^4}{2\pi^2}\left[\ln\frac{\Lambda^2}{m_{\text{t}}^2} - \frac{3}{2}\right] + \mathcal{O}\left(\frac{1}{\Lambda^2}\right). \tag{3.38}$$

Inserting Eq. (3.38) and Eq. (3.35), which tell us how to choose the counter terms for the mass parameter and the quartic coupling, into the mean-field effective potential finally leads to a potential with a minimum at 246GeV and a Higgs mass of 125GeV by construction,

$$U^{\text{MF}} = -\left[\frac{m_{\text{H}}^2}{2} + \frac{m_{\text{t}}^4}{4\pi^2 v^2}\right]\rho + \left[\frac{m_{\text{H}}^2}{v^2} + \frac{3m_{\text{t}}^4}{4\pi^2 v^4}\right]\frac{1}{2}\rho^2 - \frac{m_{\text{t}}^4\,\rho^2}{4\pi^2 v^4}\ln\left(\frac{\Lambda^2}{\Lambda^2 + h_\Lambda^2\rho}\frac{2\rho}{v^2}\right) + \mathcal{O}\left(\frac{1}{\Lambda^2}\right).$$

However, the value of the cutoff is still a free parameter. If we chose a cutoff larger than the critical value Λ_{cr}, the potential develops an instability and converges rapidly to the single-scale potential. For $\Lambda > 10^8\text{GeV}$ there is no notable difference between the shape of the mean-field effective potential with a finite cutoff and the renormalized effective single-scale potential (3.8) which is obtained by taking the limit $\Lambda \to \infty$.

However, in all cases where the cutoff is larger than Λ_{cr}, the consistency condition that the

bare potential should be bounded from below in order to start with a well defined generating functional is no longer fulfilled. This can be directly read off from expression (3.38). The bare quartic coupling has to be chosen negative by trying to send the cutoff to infinity which is not an appropriate physical choice. Therefore, the seeming instability appears due to a problematic UV boundary condition on the theory. As long as the consistency condition $\lambda_{2,\Lambda} \geq 0$ is fulfilled, no instability can be found within the class of quartic bare potentials. A similar conclusion has been drawn in [110, 111] for the sharp cutoff as already pointed out.

Let us finally remark that upper bounds cannot meaningfully be studied in the mean-field approximation; this is because "RG improvement" is necessary to observe the nonperturbative approach to triviality (reflected by the Landau-pole behavior within RG-improved perturbation theory).

3.4.2 Generalized bare potentials

The lower Higgs mass bound determined above arises from the fact that the values for the bare quartic coupling $\lambda_{2,\Lambda}$ are bounded from below. This is necessary in order to start with a well-defined theory in the UV for our confined bare potentials (3.33) of ϕ^4-type. Such a restriction on the bare potential is typically also required in perturbation theory because higher-order operators are perturbatively nonrenormalizable. By contrast, the Wetterich equation provides us with a nonperturbative tool, so we can easily investigate the influence of RG irrelevant higher-order operators on the flow of the effective average action. Alternatively, this could also be studied with perturbative methods in an effective-field-theory approach.

In the following, we address the question how modifications $\Delta U_\Lambda(\rho)$ of the quartic bare potential can exert an influence on the phenomenologically relevant lower Higgs mass bound. In general, the underlying theory of the standard model will generate all possible operators allowed by the symmetry at the UV cutoff scale. Thus, the bare potential can in principle be an arbitrary function of the scalar field and is not necessarily restricted to the class of perturbatively renormalizable operators. The only constraint which we impose is that the potential is bounded from below in order to start with a well-defined quantum field theory at the cutoff. We emphasize that no further experimental constraints exist. The simplest extension of the standard potential has an additional operator of the form ϕ^6,

$$U_\Lambda(\rho) = m_\Lambda^2 \rho + \frac{\lambda_{2,\Lambda}}{2}\rho^2 + \Delta U_\Lambda(\rho) = m_\Lambda^2 \rho + \frac{\lambda_{2,\Lambda}}{2}\rho^2 + \frac{\lambda_{3,\Lambda}}{6\Lambda^2}\rho^3. \tag{3.39}$$

In this case, negative values for the bare quartic coupling $\lambda_{2,\Lambda}$ are permissible if the potential is stabilized by a positive $\lambda_{3,\Lambda}$. Again, Eq. (3.34) can be solved explicitly for m_Λ^2 in the mean-field approximation, yielding the Higgs mass as a function of $\lambda_{2,\Lambda}$ and $\lambda_{3,\Lambda}$ for a given cutoff. The

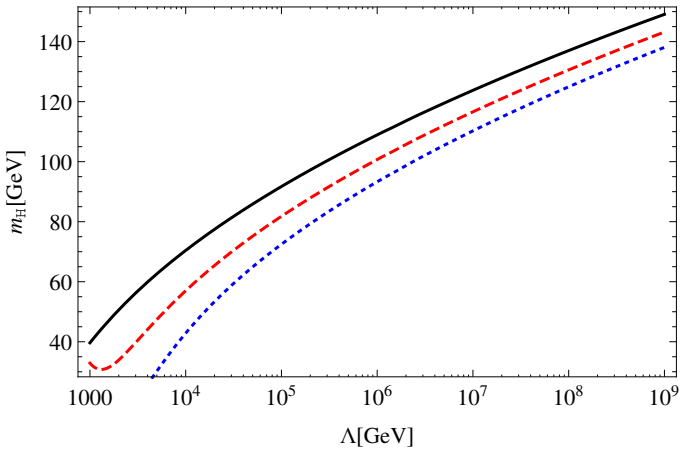

Figure 3.6: Extended mean-field analysis of the lower bound for the Higgs mass m_{H} versus the UV cutoff Λ, based on a bare potential U_Λ of ϕ^6-type. We have plotted the lower bound in the ϕ^4 theory ($\lambda_{2,\Lambda} = \lambda_{3,\Lambda} = 0$) as solid black line. Results for theories with bare couplings $\lambda_{2,\Lambda} = -\frac{1}{30}$ and $\lambda_{3,\Lambda} = \frac{2}{3}$ are depicted as red dashed line, and $\lambda_{2,\Lambda} = -\frac{1}{15}$ and $\lambda_{3,\Lambda} = 2$ as blue dotted line.

Higgs mass reads

$$m_{\mathrm{H}}^2(\Lambda, \lambda_{2,\Lambda}, \lambda_{3,\Lambda}) = \frac{m_{\mathrm{top}}^4}{4\pi^2 v^2}\left[2\ln\left(1+\frac{\Lambda^2}{m_{\mathrm{top}}^2}\right) - \frac{3\Lambda^4 + 2m_{\mathrm{top}}^2\Lambda^2}{(\Lambda^2 + m_{\mathrm{top}}^2)^2}\right] + v^2\lambda_{2,\Lambda} + \frac{v^4}{2\Lambda^2}\lambda_{3,\Lambda}. \quad (3.40)$$

Obviously, we are able to construct a theory with a Higgs mass below the previous lower bound if the contribution of the term $\sim \lambda_{2,\Lambda}$, for $\lambda_{2,\Lambda} < 0$, exceeds that of the positive term $\sim \lambda_{3,\Lambda}$.

The same mechanism works in the extended mean-field analysis but there it requires a solution to the transcendental Eq. (3.34) in order to determine m_Λ^2. A numerical solution is plotted in Fig. 3.6 for different values of $\lambda_{2,\Lambda}$ and $\lambda_{3,\Lambda}$. Furthermore, we have checked that for the given masses no additional minimum appears in the effective potential besides the one at $v = 246\,\mathrm{GeV}$.

In conclusion, we find a rather substantial influence of the precise form of the bare scalar potential on the lower bound of the Higgs boson mass. At first sight, this seems to be at odds with common wisdom of renormalizable field theories that IR observables should be independent of the details of the microscopic UV theory. This statement (formulated under suitable mild assumptions) is, of course, left untouched here. However, the main point is that the notion of a Higgs mass bound is strictly speaking not a pure IR observable. Higgs mass bounds are typically formulated as a function of the UV cutoff Λ, i.e., $m_{\mathrm{H,bound}} = m_{\mathrm{H,bound}}(\Lambda)$. Hence, in order to quantify this dependence, we have to make certain assumptions about the system at and near the cutoff. This includes the choice of a regularization scheme, specifying the details of the UV regularization at the cutoff and this incorporates dynamical properties of the flow near the cutoff which can be rather strongly influenced by the bare theory. Quantitatively, we find that rather mild modifications of the bare potential can have a significant impact on the lower Higgs mass bound.

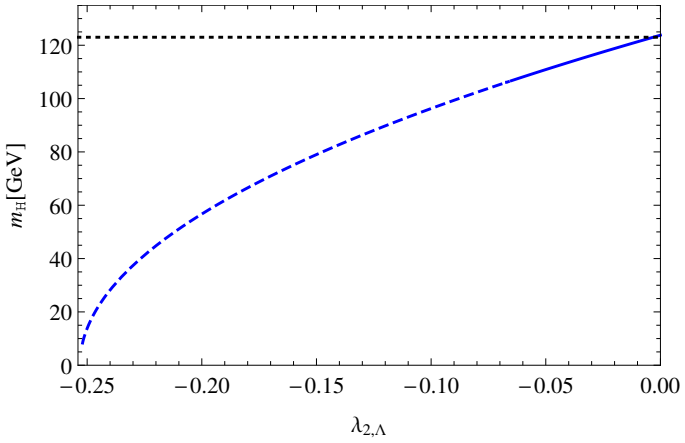

Figure 3.7: Higgs masses for the class of generalized bare potentials for $\Lambda = 10^7$GeV. The bare potential is stabilized by $\lambda_{3,\Lambda} = 3$. The horizontal black dotted line marks the lower Higgs mass consistency bound within quartic bare potentials. The blue solid line indicates values for $\lambda_{2,\Lambda}$ where the IR potential is stable while for the blue dashed line a metastability occurs.

Moreover, it seems that there is no longer a lower bound at all. Taking a fixed positive $\lambda_{3,\Lambda}$ to stabilize the bare potential, in principle all Higgs masses down to zero can be obtained by choosing a negative $\lambda_{2,\Lambda}$ and increasing its absolute value. Though, we have to discuss some particularities, if we follow this strategy to diminish the lower bound. First of all, it is no longer guaranteed that the class of bare potentials given by Eq. (3.39) has only a unique minimum. For a negative $\lambda_{2,\Lambda}$ with large enough absolute value and positive m_Λ^2 and $\lambda_{3,\Lambda}$, the bare potential can exhibit a nontrivial minimum beside the symmetric one at vanishing field amplitude, such that the bare potential may already be metastable. The RG evolution of potentials with several minima is interesting on its own, e.g., for the investigation of first order phase transitions where two competing minima occur [222–225], but beyond the scope of this work. Since we are able to push the Higgs mass to zero for generalized bare potentials which are stable, we do not consider this case in the following. Thus, we impose the unique-minimum condition

$$\lambda_{2,\Lambda}^2 < \frac{2\lambda_{3,\Lambda} m_\Lambda^2}{\Lambda^2} \tag{3.41}$$

on the bare parameters.

The remaining class of stable generalized bare potentials, which fulfill condition (3.41), can be subdivided into two types. For small absolute values of $\lambda_{2,\Lambda}$ (and $\lambda_{2,\Lambda}$ being negative), we are able to find Higgs masses below the lower ϕ^4 consistency bound ($\lambda_{2,\Lambda} = 0$) and the bare potential, the effective potential as well as the potential at intermediate scales is stable. Nevertheless, this stability property of the effective potential has to be studied very carefully. If the absolute value of the negative quartic coupling exceeds a certain value, the effective average action develops a further minimum during the RG flow such that the effective potential becomes metastable within the Higgs-Yukawa model, while the bare potential is stable.

Let us illustrate these cases by calculating a short example. For this, we assume that the

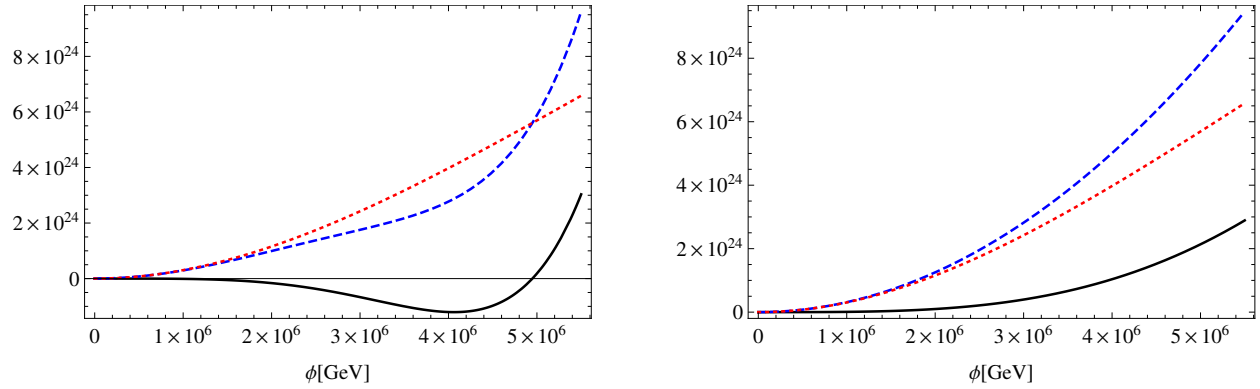

Figure 3.8: Mean-field potential as the difference between the bare potential and the absolute value of the fermion determinant according to Eq. (3.31) for $k = 0$. For the class of generalized bare potentials the capability to develop a metastability is already seeded in the bare potential (left panel) while for a quartic bare potential the potential in the UV always exceeds the contribution from the fermion loop for field values above the Fermi scale such that the effective potential is stable (right panel).

cutoff is at $\Lambda = 10^7$GeV. The lower Higgs mass bound within the quartic class of bare potentials is given by $m_{\mathrm{H}} = 123.8$GeV. Smaller masses cannot be obtained on physical RG trajectories due to the consistency condition $\lambda_{2,\Lambda} \geq 0$ within this restricted class of bare potentials. Allowing for generalized bare potentials, e.g., Eq. (3.39), we can chose $\lambda_{2,\Lambda}<0$ and stabilize the bare potential by a fixed positive value for the $\lambda_{3,\Lambda}$ coupling, e.g., $\lambda_{3,\Lambda} = 3$. The dependency of the Higgs mass on the bare quartic coupling can be found in Fig. 3.7. Obviously, we are able to obtain Higgs masses below $m_{\mathrm{H}} = 123.8$GeV. The scalar potentials are stable during the RG flow until we reach a value for the bare quartic coupling of $\lambda_{2,\Lambda} = -0.065$ (blue solid line). Beyond this value a second minimum arise. In principle both possibilities, either the second minimum is the global one or a local one, can be observed. We found a smooth transition between these options by increasing the absolute value of $\lambda_{2,\Lambda}$. However, the case that the second minimum is a local one appears only for a small range of $\lambda_{2,\Lambda}$ values. In our example, this is the case for $-0.065 > \lambda_{2,\Lambda} > -0.0671$. Thus, for $\lambda_{2,\Lambda} < -0.0671$ (blue dashed line) the second minimum is the true ground state, which renders the effective potential metastable. Hence, we are not necessarily able to push the Higgs mass to arbitrarily small values for any Λ if absolute stability for the flowing potential U_k^{MF} within the ϕ^6-class is required. Similar statements probably hold for any polynomial bare potential but the situation might be different for potentials beyond the polynomial type. This property will be further commented in the next sections.

We would like to emphasize that the behavior of the scalar potential to develop a second minimum during the RG flow has a completely different reason than the metastability of the renormalized effective potential in the standard model. Here, the metastability is a particularity of the class of generalized bare potentials. It is already seeded in the, still stable, bare potential which is illustrated in Fig. 3.8. There, we depict the effective mean-field potential (black solid line) as the difference between the bare potential (blue dashed line) and the absolute value of

the fermion determinant (red dotted line). The left figure shows the case of initial parameters where a second minimum arises in the effective potential at large values for the cutoff while the right figure depicts the case where the bare as well as the effective potential is stable. It becomes obvious how the modified structure of the generalized bare potential with a negative $\lambda_{2,\Lambda}$ is responsible for the second minimum at large scales besides the electroweak one. By contrast, the bare potential always exceeds the fermion determinant for quartic bare potentials such that the mean-field potential is stable.

The statement of diminishing the lower bound can also be rephrased, keeping the IR Higgs mass fixed but pushing the UV cutoff Λ towards larger scales. This automatically implies that the bare quartic coupling has to be chosen negative and the bare potential should be stabilized by at least a positive $\lambda_{3,\Lambda}$. We are able to find initial conditions such that the scale of maximal UV extension within our toy model can be shifted to $\Lambda = 1.3 \cdot 10^8$GeV while having completely stable potentials during the entire RG flow and a Higgs mass of 125GeV for the case of $\lambda_{3,\Lambda} = 3$. Therefore, we are able to enlarge the critical UV cutoff Λ_{cr} by an order of magnitude compared to the quartic bare potentials. For larger Λ a second minimum appears which renders the effective potential metastable within the generalized class of ϕ^6 bare potentials.

3.4.3 Polynomial expansion and its validity

In closing, let us discuss the validity of polynomial expansions of the mean-field effective potential before we start to investigate the computation of Higgs mass bounds and the properties of the effective potential on a nonperturbative level for the following reason: the set of flow equations (3.21)-(3.24) is a system of nonlinear coupled partial differential equations (PDE's). However, a simplification can be performed by expanding the scalar potential in a Taylor series, $\sum \lambda_{n,k}\rho^n$, and investigating the flow of the coefficients $\lambda_{n,k}$ instead of the running of the full potential. Thus, the system of coupled PDE's reduces to a system of coupled ordinary differential equations, which minimizes the numerical effort drastically. In order to get a first impression on the reliability of such an approximation, we expand the analytic solution of the mean-field potential in a polynomial expansion and compare the polynomial results against the "exact" mean-field results.

For the computation of Higgs masses, we are interested in the curvature around the electroweak minimum. Therefore, we expand the (extended) mean-field effective potential at $k = 0$ around the Fermi scale. While this approximation is efficient to describe the properties of the effective potential at the ground state, it fails to describe the global behavior of the effective potential. The asymptotic behavior of the full mean-field solution is governed by the asymptotic behavior of the bare potential as can be seen in Eq. (3.30). By contrast, the asymptotic behavior of the polynomial expansion is given by the highest power of the field which is taken into account in the truncation. Moreover, the coefficients of the resulting polynomial series have alternating sign, $\lambda_{2n} > 0$, $\lambda_{2n+1} < 0$. Thus, studying only the flow of the coefficients could

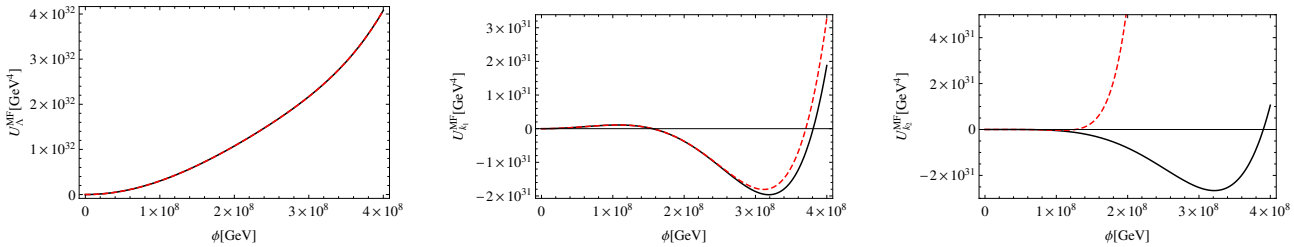

Figure 3.9: Full mean-field potential (black solid line) and the potential approximated by a Taylor expansion (red dashed line) around the origin up to ϕ^8 for different values of the RG scale k. The left panel shows the bare potential for $\Lambda = 10^9$GeV ($\lambda_{3,\Lambda} = 3$, and $\lambda_{2,\Lambda}$ is chosen such that $m_{\mathrm{H}} = 125$GeV), where the Taylor approximation fits the full potential as it should. The middle plot shows the scalar potential slightly below the UV cutoff, $k_1 = 2.5 \cdot 108$ GeV $< \Lambda$, where the second minimum is built up. Toward the IR, $k_2 = 5 \cdot 107$GeV, the second minimum settles while it disappears within the Taylor expansion (right plot).

lead to the conclusion that the potential has an instability if a truncation up to an odd power in ρ is considered. However, this is merely an artifact of the polynomial truncation because we know that the mean-field potential does not develop an instability if a physically meaningful bare potential is chosen. Further, this seeming instability only appears at very large scales far beyond the radius of convergence of the polynomial expansion. In order to get an estimate for this radius of convergence, we expand the potential to high powers of the scalar field. Expanding up to $n = 200$ and comparing the ratio of consecutive coefficient for large n, we find that this ratio settles around $\frac{v^2}{2}$.

Another particularity occurs in case of generalized bare potentials which lead to metastable effective potentials. Therefore, let us investigate the flowing effective average potential (3.31) by expanding it around the minimum near the origin even if a second competing minimum at large field values occurs. In Fig. 3.9 we depict the flow of this polynomial expansion and compare it to the full solution of the flow of the mean-field effective potential. First, the potential approximated by a polynomial expansion develops a second minimum during the RG flow similar to the closed-form mean-field potential. However, it turns out that the second minimum also disappears before the electroweak minimum is built by fermion fluctuations. Thus, the UV scalar potential as well as the effective potential in the IR seems to be absolutely stable but the effective average potential at intermediate scales is metastable within the polynomial expansion. For such a behavior we introduced the term pseudostable in [128]. Anyhow, the appearance or the disappearance of a second minimum at large field values is questionable due to the limited radius of convergence of the polynomial expansion. In contrast to the polynomial case, the second minimum survives the RG flow of the untruncated potential. Thus, the pseudostable case seems rather to be an artifact of the polynomial expansion which fails to describe the potential at scales beyond its validity. However, the polynomial expansion already gives a hint for the metastable scenario. In all cases where the effective potential exhibits a second minimum, the polynomial expansion also develops a minimum for large RG scales k close to Λ. Additionally, no second minimum occurs in the polynomial truncation during the RG flow

if the closed-form result is stable.

This fact can be circumstantiated by investigating the radius of convergence of the flowing mean-field potential in a polynomial approximation. Expanding Eq. (3.31) around $\rho = 0$ yields,

$$U_k^{\mathrm{MF}} = \left[m_\Lambda^2 - \frac{h_\Lambda^2(\Lambda^2 - k^2)}{16\pi^2}\right]\rho + \left[\frac{\lambda_{2,\Lambda}}{2} + \frac{h_\Lambda^4}{16\pi^2}\ln\frac{\Lambda^2}{k^2}\right]\rho^2 + \left[\frac{\lambda_{3,\Lambda}}{6\Lambda^2} + \frac{h_\Lambda^6}{16\pi^2}\left(\frac{1}{\Lambda^2} - \frac{1}{k^2}\right)\right]\rho^3 + \frac{1}{16\pi^2}\sum_{n=2}^{\infty}\frac{(-1)^n}{n}h_\Lambda^{2(n+2)}\frac{\Lambda^{2n} - k^{2n}}{(k^n\Lambda^n)^2}\rho^{n+2} \quad \equiv m_k^2\rho + \sum_{n=2}^{\infty}\frac{\lambda_{n,k}}{n!k^{2n}}\rho^n.$$

This series converges for

$$\rho < \frac{k^2}{h_\Lambda^2}\frac{n+1}{n}\frac{1 - \left[\frac{k}{\Lambda}\right]^{2n}}{1 - \left[\frac{k}{\Lambda}\right]^{2n+2}} \overset{n\to\infty}{=} \begin{cases}\infty & \text{for } k^2 = \Lambda^2 \\ \frac{k^2}{h_\Lambda^2} & \text{for } k^2 < \Lambda^2\end{cases}.$$

While the radius of convergence is infinity for $k = \Lambda$ as it should because the bare potential is a polynomial, it is proportional to the RG scale k^2, $\rho_{\max} = \frac{k^2}{h_\Lambda^2}$ for $k^2 < \Lambda^2$. Ignoring for a moment higher powers than ρ^3 for not to small RG scales $k \lesssim \Lambda$ the mean-field potential is well approximated by the first line of the power series over a wide range of scales. Thus, the pseudostability can be qualitatively understood from the unique-minimum condition in Eq. (3.41), which can be applied to any scale k if we truncate the potential to a polynomial up to ρ^3. While the negative $\lambda_{2,k}$ grows and becomes positive during the RG flow, $\lambda_{3,k}$ rapidly decreases. If $\lambda_{2,k}$ turns positive before the decreasing of $\lambda_{3,k}$ violates the unique-minimum condition, then the scale-dependent potential is always stable during the RG evolution in this approximation. On the other hand, a second minimum occurs roughly at the order of the RG scale $k^2 \lesssim \Lambda^2$, $\rho_0 = \frac{|\lambda_{2,k}|}{\lambda_{3,k}}\left(1 + \sqrt{1 - \frac{2m_k^2\lambda_{3,k}}{\lambda_{2,k}^2 k^2}}\right)k^2$, if the unique minimum condition is violated. Due to the fact that the second minimum occurs at the order of k which is of the same order as the radius of convergence, the polynomial expansion displays this property of the closed-form U_k^{MF} that a second minimum may emerge during the RG flow in the class of generalized bare potentials. This minimum freezes out within the closed-form solution at a fixed scale after the RG flow passes the characteristic scale of this minimum. At the same time the radius of convergence of the polynomial expansion shrinks by decreasing k such that the minimum lies beyond the radius of convergence. Therefore, the polynomial expansion is not able to account the evolution of the second minimum properly and the disappearance of the second minimum is an artifact of the polynomial expansion, see Fig. 3.9. Of course, switching from an expansion around the minimum at vanishing field to a Taylor series around the minimum at large field values would account for a proper description of this minimum. However, we would lose a precise description of the emergence of the Fermi minimum which is of our primary interest in order to describe electroweak physics.

3.5 Nonperturbative Higgs mass bounds

The mean-field approximation has turned out to be remarkably accurate by direct comparison with nonperturbative lattice simulations for the present model [107, 108]. As lattice simulations are typically limited as far as the separation of the UV scale from the physical scales is concerned, a nonperturbative continuum analysis of beyond mean-field theory seems indispensable in order to appropriately account for scalar fluctuations and the mutual back-reactions between fermionic and scalar fluctuations on a wide range of scales.

For the solution of the flow equations, we use the formulation in terms of dimensionless renormalized quantities as introduced in Sect. 3.3. To leading-order in the derivative expansion, we solve the flow equations for the effective potential u_k and for the Yukawa coupling h_k. At next-to-leading order, we include the wave-function renormalizations η_ϕ and η_ψ.

Since we are mainly interested in the properties of the effective potential near its minimum, we use a polynomial expansion of the potential. The stability and convergence of this expansion will be checked explicitly. Furthermore we will compare the results of the polynomial expansion against the full potential flow in the next section. In the symmetric regime (SYM) where the minimum of the potential occurs at $\kappa_k = 0$, we expand around vanishing field amplitude. In the symmetry-broken regime (SSB), we instead expand around the nonvanishing vev,

$$u_k = \sum_{n=1}^{N_\mathrm{p}} \frac{\lambda_{n,k}}{n!}\,\tilde{\rho}^n \quad \text{(SYM)}, \qquad\qquad u_k = \sum_{n=2}^{N_\mathrm{p}} \frac{\lambda_{n,k}}{n!}\,(\tilde{\rho}-\kappa_k)^n \quad \text{(SSB)}, \tag{3.42}$$

such that the potential is parameterized by N_p couplings λ_n (the mass term is related to $\lambda_{1,k}$ in the SYM regime and vanishes at the transition to the SSB regime where the nonvanishing order parameter is related to κ_k). The flows of $\lambda_1, \ldots, \lambda_{N_\mathrm{p}}$ (SYM), or $\kappa, \lambda_2, \ldots \lambda_{N_\mathrm{p}}$ (SSB), can directly be derived from Eq. (3.21).

For small bare scalar coupling $\lambda_{2,\Lambda}$, a physical flow typically starts in the SYM regime. Near the electroweak scale, fermionic fluctuations drive the system into the SSB regime at a scale k_SSB, where we have to switch from the SYM flow to the SSB flow. Here, a nonzero minimum builds up, inducing masses for the fermions and the Higgs scalar. This leads to a decoupling of the modes, and the flow freezes out completely; i.e., all right-hand sides of the dimensionful flow equations go to zero for $k \to 0$. For large bare scalar coupling $\lambda_{2,\Lambda}$, the physical flow starts already in the SSB regime with a small value for κ_Λ. The flow can still run over many scales until κ_k grows large near the electroweak scale, implying again the decoupling of all modes.

3.5.1 ϕ^4-type bare potentials

Let us again start with the restricted class of bare potentials of ϕ^4-type,

$$u_\Lambda = \lambda_{1,\Lambda}\tilde{\rho} + \frac{\lambda_{2,\Lambda}}{2}\tilde{\rho}^2, \tag{3.43}$$

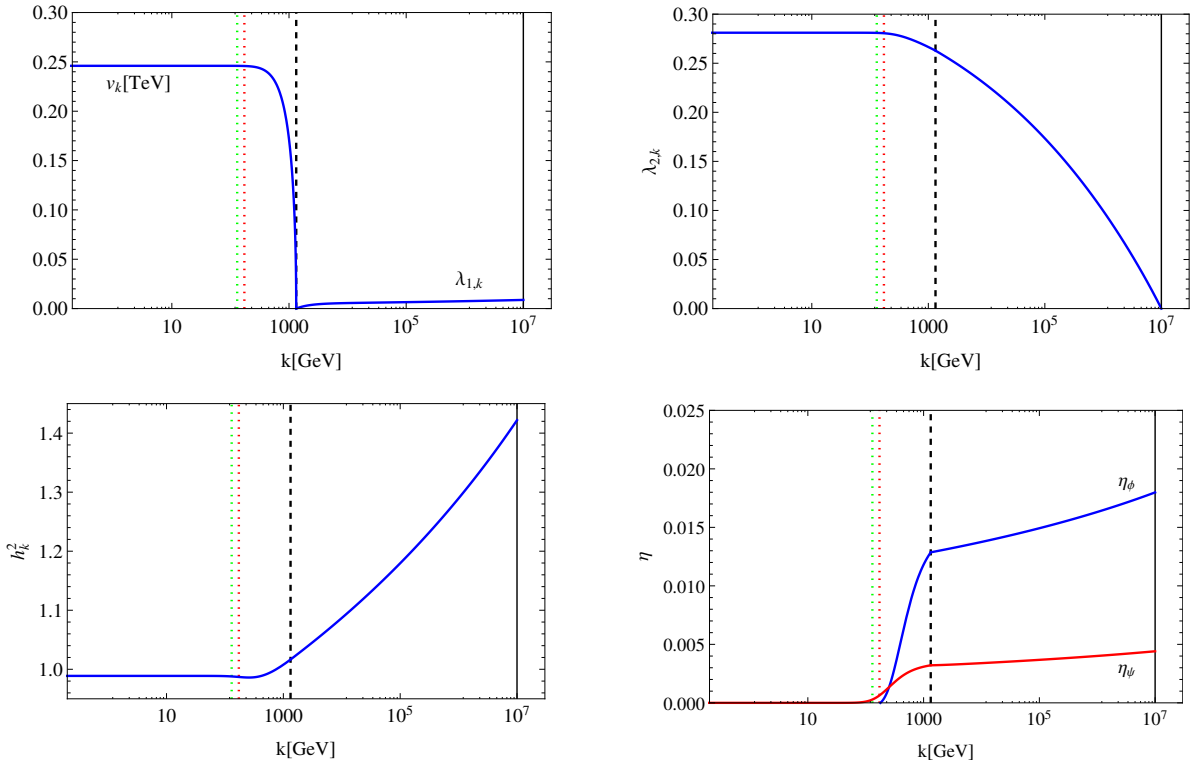

Figure 3.10: Example flow for $\Lambda = 10^7$GeV and $\lambda_{2,\Lambda} = 0$. $\lambda_{1,\Lambda}$ and h_Λ are adjusted such that the flow ends in the SSB regime with a vev of 246GeV and $m_\mathrm{t} = 173$GeV. The transition from the SYM regime to the SSB regime driven by top fluctuations is of the order of 1 TeV (black dashed line) where we switch from the expansion around vanishing field to the expansion around κ_k. The flow of the dimensionful vev shown in the upper left panel is given by $v_k = \sqrt{2k^2\kappa_k}$. At the mass scales of m_t (red dotted) and m_H (green dotted) threshold effects set in and thus the flow equations freeze out.

where $\lambda_{1,\Lambda} \equiv m_\Lambda^2/\Lambda^2$ for a wave function renormalization $Z_{\phi,\Lambda} = 1$. For a given cutoff Λ, the flow equations map the bare parameters m_Λ^2, $\lambda_{2,\Lambda}$, h_Λ onto the physical parameters v, m_t, m_H. In practice, we tune m_Λ^2 to establish the correct vacuum expectation value $v \simeq 246$GeV for a given cutoff Λ. This is, in fact, a numerical tuning problem, corresponding to the problem of separating the scale hierarchies in the standard model [226]. At the same time, h_Λ is varied until the flow ends at the right value of m_t. This leaves us with the Higgs mass as a function of $\lambda_{2,\Lambda}$ for a given cutoff Λ, $m_\mathrm{H} = m_\mathrm{H}(\Lambda, \lambda_{2,\Lambda})$, where $\lambda_{2,\Lambda}$ is allowed to be an a priori arbitrary non-negative real number for the class of bare potentials (3.43). An example flow for the mass parameter, the quartic coupling, the Yukawa coupling, as well as the anomalous dimensions is shown in Fig. 3.10.

In Fig. 3.11, we depict the function $m_\mathrm{H}(\lambda_{2,\Lambda})$ for a cutoff $\Lambda = 10^7$GeV for various approximations. For $\lambda_{2,\Lambda} \lesssim 0.01$, the Higgs mass becomes rather independent of $\lambda_{2,\Lambda}$ approaching its lower bound. This observation is in perfect agreement with lattice simulations [107, 108, 117, 122, 123]. For larger bare coupling $\lambda_{2,\Lambda}$, the Higgs mass increases and approaches a regime of saturation for $\lambda_{2,\Lambda} \gg 1$. This is reminiscent of RG-improved perturbation theory, where the

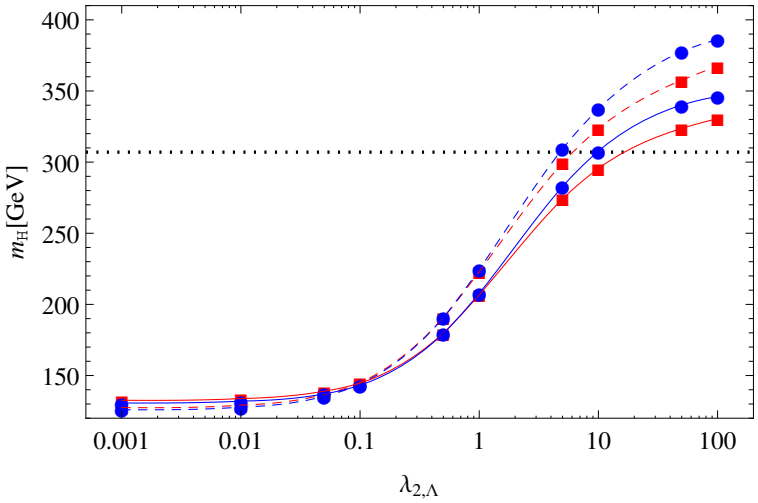

Figure 3.11: Higgs mass values versus the bare scalar coupling $\lambda_{2,\Lambda}$ for a cutoff $\Lambda = 10^7$GeV. The dashed lines denote the results within LO derivative expansion; the NLO deviates from the LO result by at most 10 % for large coupling, demonstrating the satisfactory convergence of the derivative expansion. Also the convergence of the polynomial expansion is shown: red lines with squares are obtained within the lowest nontrivial order with $N_\mathrm{p} = 2$, blue lines with circles denote the $N_\mathrm{p} = 4$ result; even higher orders $N_P = 5, 6, \ldots$ show no further deviation from the $N_\mathrm{p} = 4$ curves. The horizontal black dotted line depicts the upper bound arising from the Landau pole in the perturbative calculation.

bare coupling hits the Landau pole $\lambda_{2,\Lambda} \to \infty$ already at a finite cutoff Λ.

Whereas the Landau pole in perturbation theory in the first place signals the breakdown of the perturbative expansion, our truncation of the RG flow does neither rely on perturbative ordering nor require a weak coupling. Instead, our derivative expansion is organized in terms of field operators with increasing number of derivatives. In order to check the convergence of this expansion, we can compare the results for the Higgs mass to leading order (LO) and next-to-leading order (NLO) in this expansion. To leading order, we drop the running of the kinetic terms in Eq. (3.17) by setting the anomalous dimensions to zero, $\eta_{\psi,\phi} \to 0$. The resulting Higgs masses are plotted as dashed lines in Fig. 3.11. We observe that the difference to the NLO result (solid lines) is rather small for the lower Higgs mass bound for $\lambda_{2,\Lambda} \to 0$; even for the largest accessible couplings, we observe a maximum deviation of 10%, confirming that the derivative expansion constitutes a satisfactory approximation for our purpose for the whole range from weak to strong coupling.

Furthermore, we study the convergence of the polynomial expansion of the scalar potential in Fig. 3.11. For this purpose, we successively take higher powers of the scalar field into account, as they are generated during the RG flow, but put their initial values to zero such that we are still in the class of quartic bare potentials. To lowest nontrivial order $N_\mathrm{p} = 2$ (red lines with squares), we obtain already a complete picture of the physics of Higgs mass bounds. For $N_\mathrm{p} = 4$ (blue lines with circles), though the upper Higgs mass bound is already approached for smaller bare couplings $\lambda_{2,\Lambda}$, the value of the upper bound changes by at most 5%. For even

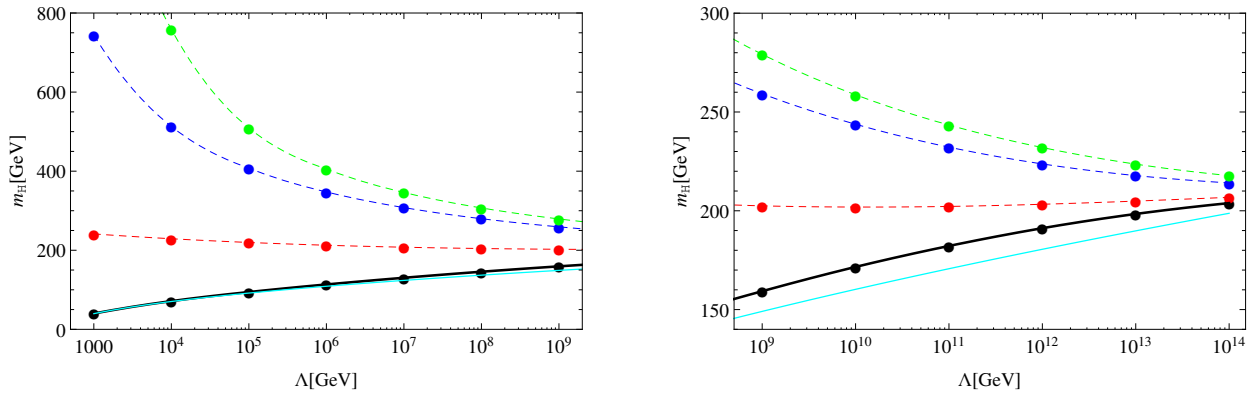

Figure 3.12: Higgs mass bounds versus cutoff Λ. The black solid line denotes the lower bound for the Higgs mass derived within the class of bare ϕ^4 potentials. The thin cyan line shows the lower bound as derived within mean-field approximation. The dashed lines mark upper bounds if the bare scalar coupling is allowed to start maximally from $\lambda_{2,\Lambda} = 1, 10, 100$ from bottom to top, respectively. An artificial restriction to the perturbative domain $\lambda_{2,\Lambda} \lesssim 1$ underestimates the upper bound by a factor $\gtrsim \mathcal{O}(1)$.

higher orders, the corresponding results lie on top of the $N_\mathrm{p} = 4$ curves. Within our numerical accuracy we find no significant difference for $N_\mathrm{p} = 4, 5, 6, \ldots, 20$.

In Fig. 3.12, we show the resulting Higgs mass bounds, arising within the class of ϕ^4 bare potentials. The solid black line characterizes the lower bound resulting from the RG flow for a wide range of cutoffs $\Lambda = 10^3 \ldots 10^{14}$GeV. Also shown is the lower bound as derived within the mean-field approximation in the previous section (thin cyan line), which neglects the running of the Yukawa coupling, of the anomalous dimension, and RG improvement of the scalar potential. In the full flow, we observe nontrivial cancellations among these terms, such that the mean-field result represents a surprisingly good approximation over a wide range of cutoff scales. The agreement between mean-field and nonperturbative RG results for the lower bound also indicates that threshold effects may play a quantitative, but not a qualitatively substantial role for the lower bound. This confirms the observation that threshold corrections can reliably be dealt with also in a perturbative context[98, 99, 227].

The dashed lines depict upper bounds for the Higgs mass for bare couplings $\lambda_{2,\Lambda} = 1, 10, 100$ from bottom to top. In particular, we find that if we limited ourselves to a perturbative domain, choosing $\lambda_{2,\Lambda} \leq 1$, we would artificially underestimate the upper bound by a factor $\gtrsim \mathcal{O}(1)$.

Further, we are not able to study Higgs mass bounds up to the Planck scale within this toy model if we would like to keep the IR top mass fixed at 173GeV. This is due to the fact that a pole in the running of the Yukawa coupling emerges around $10^{16} \ldots 10^{18}$GeV. Studying the perturbative running of the Yukawa coupling, a Landau pole arises at roughly 10^{16}GeV if a top mass of 173GeV is required. In fact, this pole also persists in the nonperturbative calculation at slightly higher scales, see Fig. 3.13. However, this is a particularity of the present toy model where the Yukawa coupling increases towards higher scales. The situation in the standard model is different because gauge boson fluctuations drive the Yukawa coupling to

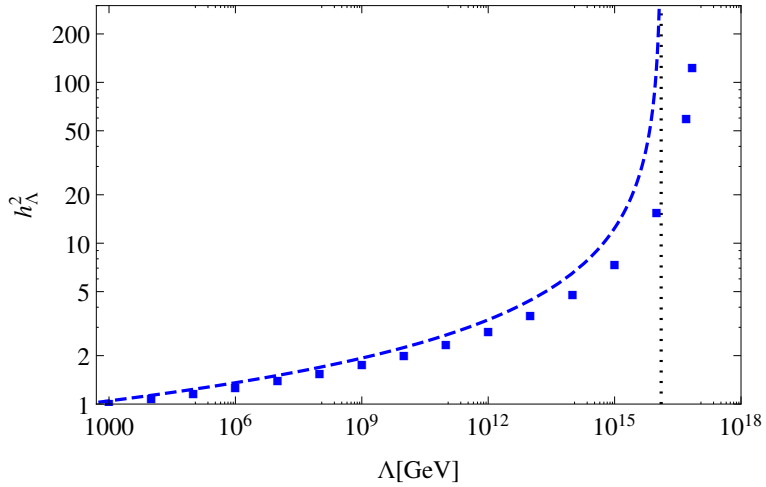

Figure 3.13: Bare Yukawa couplings versus the cutoff scale Λ. Filled squares mark h_Λ^2 for the nonperturbative flow equations for a given cutoff such that the IR top mass is given by 173GeV for the lower Higgs mass bound ($\lambda_{2,\Lambda} = 0$) and fine-tuned $\lambda_{1,\Lambda}$. The dashed line depict corresponding bare values for the perturbative β function (3.4) which develops a Landau pole (black dashed line).

smaller values, see Fig. 2.3.

Incidentally, the fact that the upper and lower bound approach each other for increasing UV cutoff Λ can be traced back to the existence of an RG fixed point in the flow of the ratio λ/h_k^2 [228, 229]. In the limit of large cutoff, this IR window actually shrinks to a point implying a tight relation between Higgs and top mass.

3.5.2 Generalized bare potentials

Let us now study extensions of the initial bare potential beyond the ϕ^4-type. Motivated by the results of the mean-field approximation, we concentrate on potentials with a negative $\lambda_{2,\Lambda}$ where the UV stability is guaranteed by a positive $\lambda_3\phi^6$. It is possible to construct bare potentials which give rise to Higgs masses below the lower bound within the class of ϕ^4 bare potentials, similar to the mean-field approach. Fig. 3.14 shows the lower bound within ϕ^4 theory (black solid line) in comparison to Higgs mass values for example flows which start with $\lambda_{2,\Lambda} = -0.05$ (orange dotted) as well as $\lambda_{2,\Lambda} = -0.08$ (orange dashed) in the UV where the bare potential is stabilized by $\lambda_{3,\Lambda} = 3$. These examples clearly illustrate that the lower bound within ϕ^4-like initial UV potentials does no longer hold, if higher dimensional operators are also permitted.

Moreover, this phenomenon can be understood from the RG flow itself: first we note that in both cases (ϕ^4-like as well as the beyond-ϕ^4 examples above) the flow starts in the symmetric regime and fulfills the unique-minimum condition (3.41) for the bare potential. In the beyond-ϕ^4 examples, the quartic coupling λ_2 runs quickly to positive values, whereas λ_3 becomes very small as is expected in the vicinity of the Gaußian fixed point. As a consequence, this particular system flows back into the class of ϕ^4-type potentials. The decisive difference, however, is that

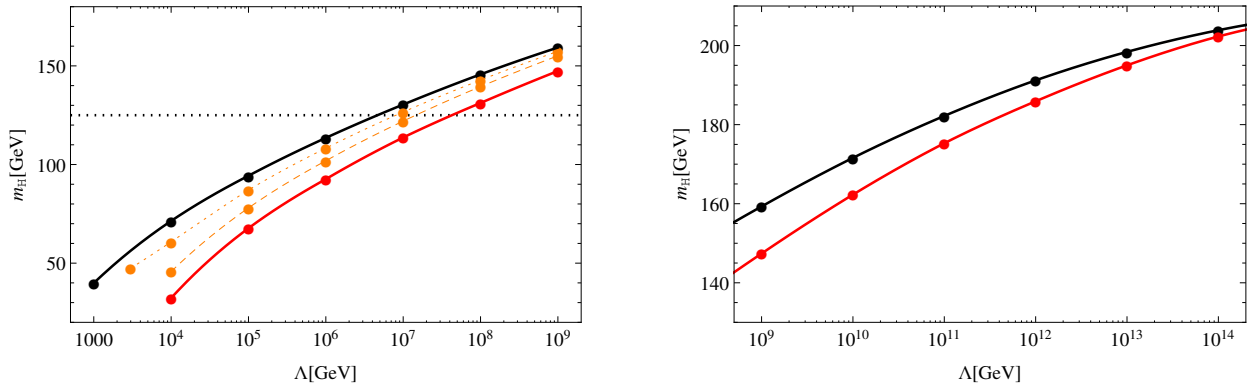

Figure 3.14: Higgs mass versus cutoff Λ. The black line denotes the lower bound for the Higgs mass derived within the class of bare ϕ^4 potentials. The orange lines show Higgs masses below the ϕ^4 consistency bound by allowing for generalized bare potentials. The masses are derived for $\lambda_{3,\Lambda} = 3$ and $\lambda_{2,\Lambda} = -0.05$ (dotted) as well as $\lambda_{2,\Lambda} = -0.08$ (dashed). The red line denotes the lowest possible Higgs masses within the ϕ^6-class with $\lambda_{3,\Lambda} = 3$ where the scalar potential is stable during the entire RG evolution. The black dotted line marks a Higgs mass of 125GeV, demonstrating that the scale of new physics can be shifted by an order of magnitude by dropping the restriction to quartic bare potentials within the present toy model.

the scale k_{GFP} where the system is again near the Gaußian fixed point is now lower than the initial UV scale Λ. Loosely speaking, some "RG time" is required to run from the beyond-ϕ^4 form of the potential back to the ϕ^4 Gaußian type, see Fig. 3.16 and the discussion below.

From another viewpoint, the RG flow can map an initial bare action with $\lambda_2 < 0$ and $\lambda_3 > 0$ at an initial UV scale Λ to a theory with $\lambda_2 \geq 0$ and $\lambda_3 \approx 0$ at a smaller scale $k_{\mathrm{GFP}} < \Lambda$. Therefore, the orange curves (beyond-ϕ^4) in Fig. 3.14 can also be viewed as a horizontally displaced version of the black curve (ϕ^4-like) to effectively larger cutoff values. We emphasize that the present example has neither been specifically designed or fine-tuned, nor does it represent an exhaustive study of admissible initial potentials. A wide range of beyond-ϕ^4 potentials initiating the flow at Λ leads to Higgs masses below the bound of the ϕ^4-type class. Still, the mechanism observed above starting from stable potentials with $\lambda_2 < 0$ and globally stabilizing higher-order terms appears rather generic. We have also checked for more involved initial conditions that the results for the Higgs masses do not change for higher-order $N_P \geq 4$ polynomial expansions of the scalar potential.

In fact, the influence of higher dimensional operators has also been studied in lattice simulations in a chiral Higgs-Yukawa model [123], by adding a positive $\lambda_3\phi^6$ term to the bare potential. No lowering of the Higgs mass bound has been observed in this study. This is indeed in agreement with our observations, because merely adding this term has barely any effect on the Higgs mass bound and rather leads to an increase of the Higgs mass. Our mechanism for lowering the mass bound works particularly well for initial UV potentials with $\lambda_2 < 0$. In other words, the $\lambda_2 < 0$ deformation requires a comparatively long RG time to run the potential back to the ϕ^4 Gaußian type. In fact, our mechanism of diminishing the lower bound was confirmed

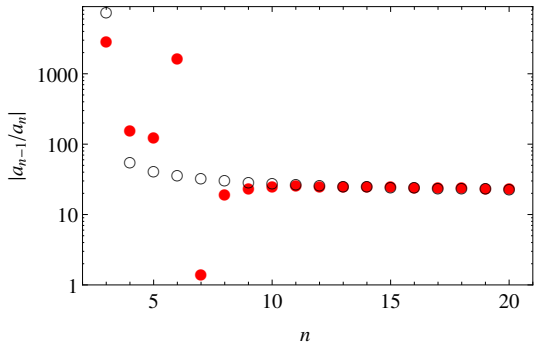

Figure 3.15: Estimate for the radius of convergence in units of 10^3GeV^2 of the polynomial expansion of the effective potentials in terms of the absolute values of the ratios of expansion coefficients. The red filled circles are derived for a theory which starts at $\Lambda = 10^7\,\text{GeV}$ with all couplings set to zero apart from the mass term. The black empty circles are for the case $\Lambda = 10^7\,\text{GeV}$ and $\lambda_2 = 1$ and $\lambda_n = 0$ $(n \geq 3)$.

by the lattice in a subsequent work by allowing for negative $\lambda_{2,\Lambda}$ [125].

Having put the significance of the lower bound of the Higgs mass derived for ϕ^4-type bare potentials into perspective, let us address the issue of stability: while the standard approach to vacuum stability in the present simple model based on RG-improved perturbation theory has been questioned by lattice simulations [107, 108] and functional RG methods [110] (in turn critically assessed by [79]), a full stability analysis would require to follow the RG flow of arbitrary physically admissible initial potentials. In particular, the RG evolution of potentials with multiple local minima would have to be dealt with quantitatively. While this is indeed possible with appropriate numerical solvers [213, 230–233], we confine ourselves to the validity region of the polynomial expansion of the effective potential about a local minimum in this section and investigate the flow of the entire scalar potential in the next section.

Since high-order polynomials typically have multiple local minima, we have to estimate the radius of convergence of our expansion in field space. A new local minimum showing up within this convergence region could then be interpreted as a signature of instability. If such minima only occur outside the convergence radius, we consider them as an artifact of the polynomial expansion.

As in the mean-field case, a rough estimate for the radius of convergence is given by comparing the quotients of successive couplings λ_n/λ_{n+1} for large n in the infrared. In practice we solve the system of coupled differential equations for $N_P = 20$, switching back to dimensionful quantities at a scale where the flows are frozen out, i.e., $U_k = u_k k^4 = \sum_n a_n(k^2\tilde{\rho} - v^2/2)^n$ with $a_n = \frac{\lambda_n}{n!}k^{4-2n}$, and computing the dimensionful radius of convergence by comparing $\frac{a_n(k)}{a_{n+1}(k)}$ for $k \to 0$. The results expressed in units of 10^3GeV for various initial conditions are plotted in Fig. 3.15.

Our primary observation is that this estimate for the radius of convergence appears to stabilize at a universal value rather independent of the chosen initial conditions. The resulting value near $\simeq 23000\text{GeV}^2$ is of the order of the vacuum expectation value $v^2/2 = 30258\,\text{GeV}^2$ for large n. We still observe a slight drift in our data even at high order, which might be due to the fact that the inner region of the effective potential owing to its convexity cannot be resolved within a polynomial expansion in the SSB regime as a matter of principle. Restricting the field amplitudes to values of the order of the ratio of the highest couplings in the truncation,

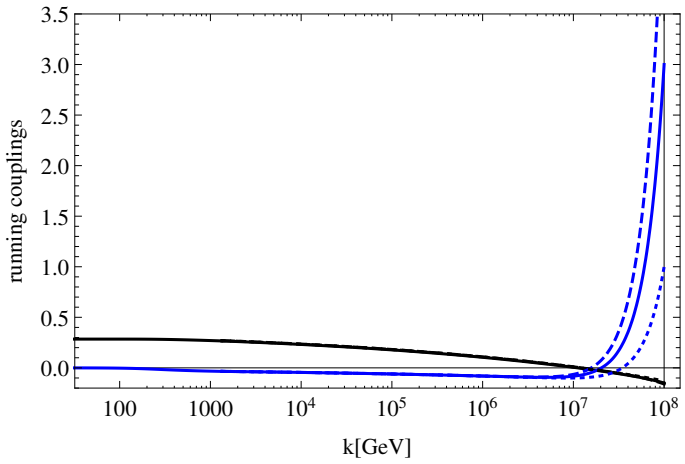

Figure 3.16: Example flow for λ_2 (black solid line) and λ_3 (blue lines) for generalized bare potentials. The cutoff can be enlarged by roughly an order of magnitude with completely stable potentials during the entire RG evolution by choosing $\lambda_{3,\Lambda} = 3$ and $\lambda_{2,\Lambda} = -0.15$ in contrast to the lower bound of quartic bare potentials $\lambda_{2,\Lambda} = \lambda_{3,\Lambda} = 0$. Choosing different values for $\lambda_{3,\Lambda}$ (dotted: $\lambda_{3,\Lambda} = 1$, dashed: $\lambda_{3,\Lambda} = 5$) with appropriate values of $\lambda_{2,\Lambda}$ does not lead to a sizeable shift in the Higgs mass due to the fact that the running of λ_3 is strongly attracted by its pseudo-fixed point value.

$k^2\tilde{\rho}_{\max} \simeq \frac{v^2}{2} + |\frac{a_{N_P-1}}{a_{N_P}}|$, we find in all studied cases that the effective potential is a convex monotonically rising function in the outer region ($\phi > v$). No evidence for an instability within this radius of convergence is found.

Further, we would like to emphasize that in all studied cases presented in Fig. 3.14 the scalar potential is also stable during the entire RG flow. However, we observe that a second minimum at comparatively large field values emerges if we try to further diminish the lower Higgs mass bound by decreasing $\lambda_{2,\Lambda}$, in complete analogy to the mean-field results. This further minimum disappears throughout the RG flow, rendering the potential pseudostable. Precisely this behavior was an artifact of the polynomial expansion within the mean-field approximation. In fact, we will demonstrate in the next section that this pseudostability becomes a real metastability also for the solution of the full nonperturbative flow equations. Thus, a new lower bound may be defined for the class of ϕ^6 bare potentials if we require absolute stability for the scalar potential at every scale $0 \leq k \leq \Lambda$. Such a lower bound is given by the red line in Fig. 3.14. These Higgs masses are obtained by fixing $\lambda_{3,\Lambda} = 3$ and increasing the absolute value of the negative bare quartic coupling $\lambda_{2,\Lambda}$ until a second minimum emerges during the flow. The red line depicts exactly those values for the Higgs mass at the transition before the potential becomes metastable (correspondingly pseudostable for the polynomial expansion). Thus, the scalar potential is stable for Higgs masses above the red line and metastable for masses below this transition.

Of course, this new lower bound is obtained for a particular class of generalized bare potentials, which are of ϕ^6 type with $\lambda_{3,\Lambda} = 3$. In order to investigate the dependence of the lower mass bound for entirely stable potentials at every RG scale, let us analyze the flow equations

in a little more detail. In Fig. 3.16 we depict an example running of λ_2 (black) and λ_3 (blue) by the solid lines. First of all, this plot illustrates the mapping from a theory which starts at Λ with $\lambda_{3,\Lambda} \approx 0$ and $\lambda_{2,\Lambda} \approx 0$ to a theory at an effectively enlarged cutoff with $\lambda_{3,\Lambda} > 0$ and $\lambda_{2,\Lambda} < 0$. However, the canonical dimension of λ_3 implies that it quickly decreases towards the infrared because the model is dominated by the Gaußian fixed point, while λ_2 increases. As we pointed out in the mean-field analysis, the scale dependent potential $u_k(\tilde{\rho})$ is always stable during the RG evolution, if λ_2 turns positive before the stabilizing effect of λ_3 dies out. By contrast, the potential becomes metastable if the zero of the function λ_2 is crossed after λ_3 becomes small and violates the unique-minimum condition.

Whether the potential develops a metastability or is entirely stable, depends on the initial value of $\lambda_{2,\Lambda}$ for fixed $\lambda_{3,\Lambda}$. Roughly speaking for larger values of $\lambda_{2,\Lambda}$ the running λ_2 curve (black) is shifted upward (besides small quantitative variations), implying that the potential is modified into the direction of stable potentials but at the same time larger Higgs masses. To obtain smaller masses, the black curve has to be shifted downwards such that $\lambda_2(k) = 0$ is fulfilled for smaller k and thus the potential develops a second minimum during the RG flow. By this variation of $\lambda_{2,\Lambda}$ the flow of λ_3 is insignificantly modified as one would expect from an irrelevant operator. These observations agree with solutions of the RG flow for the full effective potential beyond the polynomial expansion as worked out in using pseudo-spectral methods (Chebyshev expansion), see next section.

One could naively expect that the red curve in Fig. 3.14 can be further diminished by increasing $\lambda_{3,\Lambda}$, such that a greater absolute value of $\lambda_{2,\Lambda}$ can be chosen until the potential develops a second minimum. However, decreasing the Higgs mass but requiring stable potentials is difficult since there is a strongly infrared-attractive pseudo-fixed point for higher order couplings. Briefly, this can be verified by investigating the flow equations for higher order couplings which have the form

$$\partial_t \lambda_{n,k} = (2n-4)\lambda_{n,k} + \eta \lambda_{n,k} + f.$$

The first term reflects the canonical dimension of the operator. The second term is a generalized anomalous dimension term, i.e., η is independent of $\lambda_{n,k}$. We also include contributions which are strictly speaking not an anomalous dimension, but are nevertheless linear in the coupling. Finally, f is a function depending on other couplings ($h_k^{2n}, \lambda_{n+1,k}$, and $\lambda_{m,k}$ with $m < n$) and is independent of $\lambda_{n,k}$. For instance, $f = f(h_k^6, \lambda_{4,k}, \lambda_{2,k}, \lambda_{1,k})$ for $\lambda_{3,k}$. It is straightforward to find a pseudo-fixed point, $\lambda_{3\,*} = -\frac{f}{2+\eta}$, where the values for f and η can be derived by inserting Eq. (3.42) into Eq. (3.21). The pseudo-fixed point shows a remarkably small scale dependence, since the running of λ_2 and h is also comparatively small (the small contributions from threshold effects ($\lambda_{1,k}$) as well as from the irrelevant coupling $\lambda_{4,k}$ can be neglected). Additionally, the ratio $\frac{\lambda_2}{h^2}$ also approaches a fixed point [228, 229]. Because the anomalous dimension η is small, the canonical dimension renders the fixed point strongly infrared attractive. Arbitrary initial

values for $\lambda_{3,\Lambda}$ quickly converge toward the pseudo-fixed point. This fact is also illustrated in Fig. 3.16, where example runnings of λ_3 for different initial values are depicted as dashed and dotted lines. As a consequence, a further increasing of the cutoff scale for a fixed Higgs mass is almost impossible. The additional RG time, which we obtain from running back from the beyond ϕ^4 type potentials to the ϕ^4 Gaußian type, is limited to the interval until λ_3 is governed by its pseudo-fixed point behavior where it becomes small, implying that the stabilizing effects die out. Similar conclusions hold for higher order couplings. Of course, one could stabilize the bare potential by allowing for nonvanishing $\lambda_{4,\Lambda}, \lambda_{5,\Lambda}, \cdots$, but those couplings are even faster governed by their canonical scaling due to dimensional analysis. The fact that the scale of new physics can only be shifted by a few orders of magnitude for a fixed Higgs mass might be a particularity of the class of polynomial bare potentials. The investigation of bare potentials beyond this class and their RG evolution over a wide range of scales could clarify whether this is indeed the case or not. At least the mean-field approximation could give a hint how a bare potential beyond a polynomial type may look like in order to shift the scale of new physics to even higher scales. For instance, a bare potential which contains the negative fermion determinant and a conventional double-well potential,

$$U_\Lambda = \frac{\lambda_{2,\Lambda}}{2}\left(\rho - \frac{v^2}{2}\right)^2 + \frac{h_\Lambda^2 \Lambda^2 \rho}{16\pi^2} - \frac{h^4\rho^2}{16\pi^2}\ln\frac{\Lambda^2 + h_\Lambda^2\rho}{h_\Lambda^2\rho} \tag{3.44}$$

would lead to a potential in the IR, which is just given by a ϕ^4-type Higgs potential, $U^{\mathrm{MF}} = \frac{\lambda_{2,\Lambda}}{2}(\rho - \frac{v^2}{2})^2$ with an arbitrary $\lambda_{2,\Lambda}$ and thus an arbitrary Higgs mass. Whether such a line of argumentation also holds beyond the simple mean-field approximation is left open for further investigations.

3.6 Full potential flow

So far, we have discussed the occurrence of Higgs mass bounds in polynomial truncations of the scalar potential for the full nonperturbative RG running. This gives satisfactory results for the masses and couplings of the particles around the electroweak minimum but the global behavior of the scalar potential can be studied only in a small region around the Fermi scale. In order to investigate the global properties of the effective average potential, we investigate the full flow equations given by Eqn. (3.21)-(3.24). In contrast to the simple mean-field calculation this approach includes several improvements. First of all, the whole set of flow equations contains bosonic fluctuations as well, whereas we have concentrated on the fermion induced part of the effective potential for the most part in Sect. 3.4. Further, the nonperturbative flow equations automatically involve RG improvement such that the complex mutual back-reactions between bosonic and fermionic fluctuations are incorporated over a wide range of scales. Furthermore, we are able to study the onset of convexity of the effective potential which is beyond the scope of the simple mean-field approximation. At the end, the effective potential should be a convex

function after all fluctuations are integrated out due to the fact that the effective action is defined via a Legendre transform. However, rigorous proofs that the effective potential becomes convex are only known for pure scalar field theories [234]. Also, the mean-field approximation might not properly account for the evolution of a potential with two competing minima due to the fact that only the classical propagator is used to integrate out quantum fluctuations at any scale. While this might describe potentials well which do not exhibit a metastability and are convex in the outer region, this has to be thoroughly checked in a metastable scenario where the potential becomes nonconvex for $\phi > v$.

In Sect. 3.5, we were provided with a system of coupled ordinary differential equations which are comparatively easy to solve. Going beyond the polynomial expansion is more challenging. This is because the flow of the entire potential has to be traced over a wide range of scales. Our method of choice are pseudo-spectral methods to solve the set of partial differential equations. These methods were already successfully applied to various physical problems [193, 235–237]. For the present problem, we use a code developed and provided by the authors of [237].

The basis functions of pseudo-spectral methods are global and of high degree. Thus, one reaches high accuracy with a comparatively small amount of grid points [238]. In this sense, pseudo-spectral methods are memory minimizing. In principle, pseudo-spectral methods include any kind of function system. However, in most of the cases Chebyshev polynomials of the first kind are employed. Chebyshev polynomials originate from the family of orthogonal function systems and are closely related to the Fourier basis via a transformation in the argument. In contrast to Laguerre polynomials which change the asymptotic behavior of the solution if the order of truncation is modified, boundary effects are minimized since they are defined on a finite interval. On the other hand, in comparison to other bounded function systems, e.g. Legendre polynomials, they show the best convergence properties. For analytical functions the convergence is exponential. This guarantees high accuracy although only few coefficients are taken into account. Higher order coefficients provide an error estimate for the absolute remainder of the solution. A detailed description of the numerical techniques will be given in [239]. In summary, the pseudo-spectral method stays very stable over many scales of magnitude in k. Therefore, we are able to choose high UV cutoffs. This choice is solely restricted by the number of digits needed for tuning the IR quantities, i.e., realizing a large scale separation. All full potential computations have been done with `long double` in C. Thus, we restricted ourselves to a maximal UV cutoff of 10^9GeV for the full potential calculation. In principle, higher values for Λ are accessible by using a higher accuracy for the floating point.

As a first benchmark for the numerical solver, we compare the resulting Higgs masses for different initial values for the flow equations over a large range of cutoff values. In Fig. 3.17, we depict the Higgs mass over the UV cutoff Λ for example flows in the restricted class of ϕ^4 bare potentials (black) as well as for the class of generalized bare potentials (red and orange). The solid lines mark the Higgs masses computed within the polynomial truncation while filled circles indicate the Higgs masses resulting from the full potential computation. The full potential

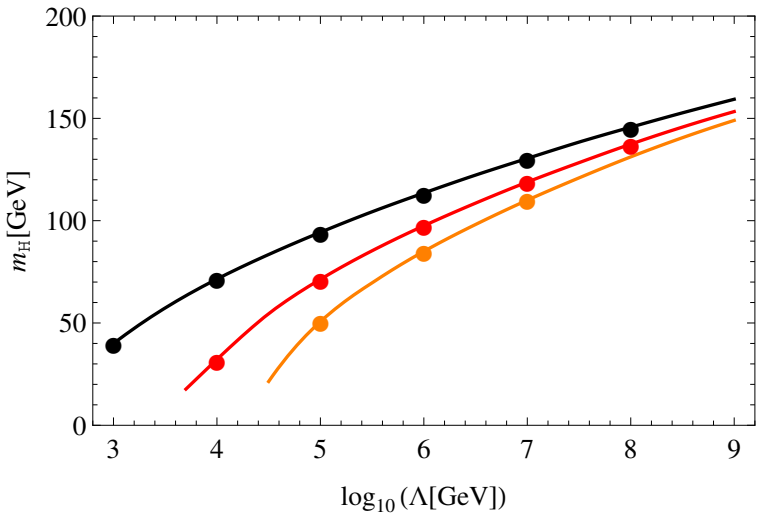

Figure 3.17: Higgs mass as a function of the UV cutoff. The filled circles are obtained by solving the full PDE system. These match perfectly with the Higgs masses computed within a polynomial expansion of the scalar potential for the class of ϕ^4-type bare potentials (black) as well as generalized bare potentials for both cases, either the effective potential is stable (red) or metastable (orange).

computations lay perfectly on top of the polynomial results.

After this successful test that the global solver properly reproduces the local behavior around the Fermi scale, let us start to compare the global behavior, at first for the class of ϕ^4 bare potentials. Basically, the polynomial truncation lacks a good description of the asymptotic behavior of the potential which can be seen in Fig. 3.18. This is not surprising since the flow equations suggest the asymptotic behavior to be that of the UV potential because fluctuations for large field values are suppressed. By contrast, the asymptotic behavior of the polynomial expansion goes like the highest power of the field which is taken into account in the truncation as we already discussed in the mean-field approximation.

Despite the fact that the polynomial truncation cannot describe the asymptotic behavior correctly, it still gives an indication for the behavior of the effective average potential. As long as the class of renormalizable bare potentials is considered, no hint for an in-/metastability can be found within the radius of convergence of the polynomial expansion. The full potential calculation supports the statement, that the fermion determinant cannot introduce any instability into the effective potential. As long as the UV potential is well defined within the ϕ^4-type potentials, the effective potential is stable. It is worth mentioning, that the mean-field potential agrees quite well with the results for the full potential, for small as well as for larger field values, see green dashed curve in Fig. 3.18. The fluctuations of the bosons seem to play a minor role whereas the fermionic contributions are predominant. Moreover, neglecting the anomalous dimensions and dynamics of the Yukawa-coupling does not have a significant effect. Thus, the simple mean-field effective potential is an effective tool to get first insights into the global behavior of the scalar potential.

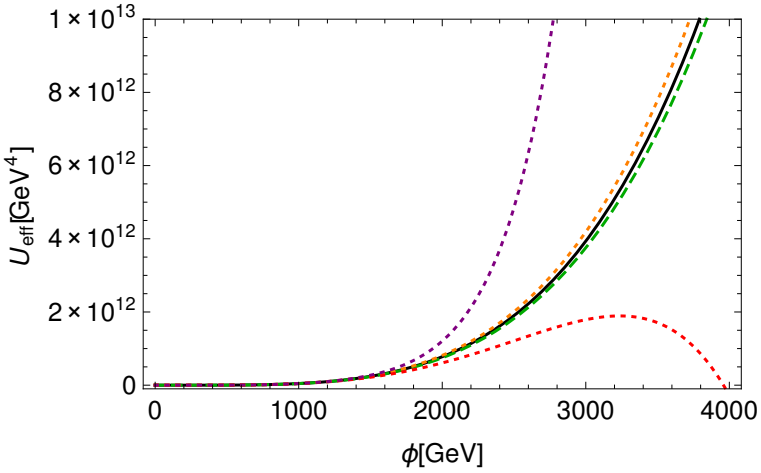

Figure 3.18: Comparison between the effective potential of the full calculation (black), the mean-field result (green dashed) and polynomial truncated potentials (dotted) up to fourth order (orange), sixth order (red) and eight order (purple) for the stable case.

Regarding the class of generalized bare potentials, the qualitative picture remains the same. Furthermore, if no second minimum emerges during the polynomial truncated flow, the full flow does not develop an outer minimum for field values larger than the Fermi scale as well. Thus, there indeed exists a class of stable bare potentials giving rise to Higss masses below the lower bound which is depicted by the red curve in Fig. 3.17. Therefore, the mechanism of diminishing the lower bound for completely stable potentials survives beyond the polynomial expansion and the simple mean-field calculation. Thus higher order operators can diminish the lower Higgs mass bound at the cutoff scale of the standard model.

In the case of stable potentials, the dynamics of the potential for comparatively large fields originates from dimensional scaling behavior which is displayed by the first two terms in Eq. (3.21). This is still true for field values larger than the cutoff scale within the class of potentials which develop a second minimum at scales comparable to the cutoff. In reminiscence of the discussion at the beginning of this section and of the mean-field discussion in Sect. 3.4, it is already clear that the polynomially expanded potential is not able to display the evolution of the outer minimum for large field values correctly. Thus, we concentrate on a comparison between mean-field and full potential calculations.

At the scale of the second minimum we observe slight quantitative differences between the mean-field potential and the effective potential computed from the full RG flow. Assuming the same bare potential, the resulting Higgs-mass differs by a few percent. This is not surprising having an additional look at the propagators in (3.21). As the curvature at the maximum of the potential is negative, the bosonic fluctuations become more important resulting in a large error of the mean-field results. In order to compare the same IR physics, we adjust the Higgs mass to be the same in the full potential calculation and the mean-field approximation rather than starting with the same bare quartic coupling $\lambda_{2,\Lambda}$ in the UV. The resulting potentials are depicted in Fig. 3.19. It is obvious that an additional effect causes a remaining deviation of

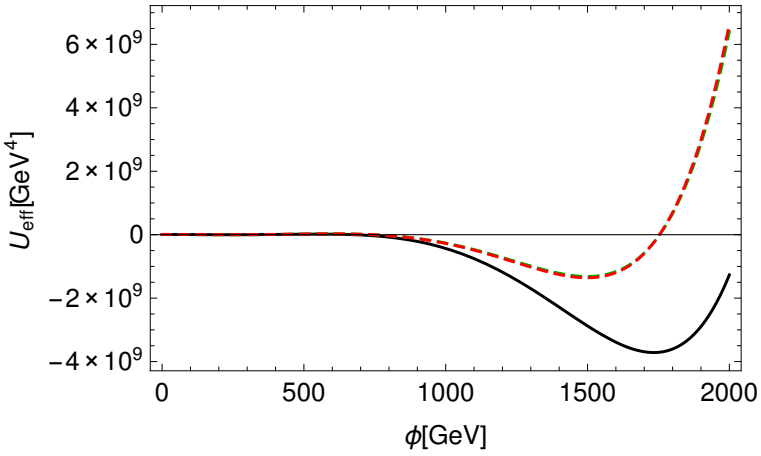

Figure 3.19: Comparison between the effective potential of the full calculation (black), the mean-field result (red dashed) and the full calculation neglecting the anomalous dimensions (green dashed line, which almost overlaps with the red dashed line) for the metastable case. Note that the resolution of this plot is not high enough to show electroweak minimum at 246GeV.

both IR-potentials. This effect can be traced back to the anomalous dimensions of the fields. Due to the rescaling of the fields and the additional interactions, a deviation around the second minimum is observed. If the anomalous dimensions are ignored in the full nonperturbative potential calculation as in the mean-field approximation, mean-field and full potential results match well, see Fig. 3.19.

The good agreement between mean-field result and the full potential, especially in the last case, is astonishing because the mean-field approximation is not able to describe convexity mechanisms. Naively one would expect that convexity already plays an important role during the freeze-out of the masses and the vev in the full potential computation. We comment on this properties in App. A.5.

Again, we would like to emphasize that we are already able to decide whether the effective potential is metastable or stable from the polynomial expansion. Of course, the polynomial expansion is not able to precisely describe the evolution of the second minimum. However, it can be used to depict the emergence of a second minimum on a quantitative level in the considered class of generalized bare potentials. Thus, we will restrict ourselves to the polynomial expansion for the following investigations. If a pseudostability occurs in the evolution of $u_k(\tilde{\rho})$ it is likely that the full effective potential beyond the polynomial expansion is metastable.

3.7 Generalized Yukawa interaction

Finally, let us investigate an enlargement of our truncation by means of a generalized Yukawa interaction term, $\bar{h} \to \bar{H}(\rho)$. The purpose of this is twofold: first, we can check whether these additional operators, which we neglected up to now, strongly affect the flow of the previous truncation (3.17) or play only a minor role. Second, we are able to investigate further generalized

bare actions and their influence on Higgs mass bounds.

So far, we observed that modifications of the bare scalar potential can have a significant impact on the lower Higgs mass bound. However, restricting to ϕ^6-type bare potentials (or probably to any class of stable bare potentials of a polynomial type) which have a unique minimum, the Higgs mass cannot be arbitrarily decreased by requiring stable scalar potentials during the entire RG flow. In addition to modifying the running of the scalar sector by deforming the bare potential, we can also pursue another direction. The lower Higgs mass bound within ϕ^4 bare potentials is mainly dominated by the Yukawa sector, i.e., the large top Yukawa coupling. Thus, the lower bound is approached for lighter Higgs masses if the values of the Yukawa coupling are smaller during the RG flow. For instance, the lower bound in the standard model is given by $\sim 130\text{GeV}$ in contrast to $m_\text{H} > 200\text{GeV}$ in the Higgs-Yukawa model for large cutoff scales due to the presence of gauge bosons. Gauge boson contributions to the running of h lead to a decrease of the running Yukawa coupling towards the UV in contrast to the simple Higgs Yukawa toy model where the Yukawa coupling runs into a pole for large RG scales. Thus, the contribution of h to the running scalar mass is weakened. The phenomenological implications of the gauge sectors will be discussed in detail in the next chapters. Any other mechanism that lowers the values of h would also lower the resulting Higgs masses. As generalized bare potentials u_Λ allow to choose smaller values for $\lambda_{2,\Lambda}$ in order to lower the bound, a generalized bare Yukawa potential $H_\Lambda(\rho)$ could lead to smaller values of the bare Yukawa coupling $y_{0,\Lambda} \equiv H_\Lambda(0)$ which still lead to a phenomenologically correct IR description of the top mass.

In order to illustrate our main points in a transparent fashion, we consider the truncation

$$\Gamma_k = \int_x \left[\frac{Z_\phi}{2} (\partial_\mu \phi)^2 + U(\rho) + Z_\psi \, \bar{\psi} \, \mathrm{i} \partial\!\!\!/ \psi + \mathrm{i} \, \frac{1}{\sqrt{2}} \bar{H}(\rho) \phi \bar{\psi} \psi \right]. \tag{3.45}$$

Note that we suppress the k dependence for compactness of notation from now on. This dependence is implicitly understood ($U = U_k$, $\bar{H} = \bar{H}_k$, $Z_\phi = Z_{\phi,k}$, $Z_\psi = Z_{\psi,k}$). Due to the fact that the Yukawa functional only depends on the field invariant ρ, the model is still invariant under the discrete chiral symmetry defined in Eq. (3.2). This implies that a mass term for the fermion is still forbidden and has to be generated due to spontaneous symmetry breaking.

The flow equations can be obtained in a similar manner to the simple Yukawa model in Sect. 3.3, also see App. A.4. Only the projection rule on the Yukawa interaction has to be changed in an obvious manner in order to gain the full ρ dependence. Thus, the flow equations read

$$\begin{aligned}
\partial_t u =& - d\, u + (d - 2 + \eta_\phi) \tilde{\rho} u' + 2 v_d \Big[l_0^{(\text{B})d}(u' + 2\tilde{\rho} u''; \eta_\phi) - d_\gamma \, l_0^{(\text{F})d}(\tilde{\rho} H^2; \eta_\psi) \Big], \\
\partial_t H =& \frac{1}{2}(d - 4 + \eta_\phi + 2\eta_\psi) H + (d - 2 + \eta_\phi) \tilde{\rho} H' \\
& + 2 v_d \left[H (H + 2\tilde{\rho} H')^2 l_{1,1}^{(\text{FB})d}(\tilde{\rho} H^2, u' + 2\tilde{\rho} u''; \eta_\psi, \eta_\phi) - (3H' + 2\tilde{\rho} H'') l_1^{(\text{B})d}(u' + 2\tilde{\rho} u''; \eta_\phi) \right],
\end{aligned}$$

$$\begin{aligned}\eta_\phi =& \frac{4v_d}{d}\Big[2\kappa\Big(3u''(\kappa)+2\kappa u'''(\kappa)\Big)^2 m_2^{(\mathrm{B})d}(\mu_\phi^2;\eta_\phi)\\ &+ d_\gamma\Big(H(\kappa)+2\kappa H'(\kappa)\Big)^2\Big(m_4^{(\mathrm{F})d}(\mu_\mathrm{t}^2;\eta_\psi)-\kappa H^2(\kappa)\, m_2^{(\mathrm{F})d}(\mu_\mathrm{t}^2;\eta_\psi)\Big)\Big],\\ \eta_\psi =& \frac{4v_d}{d}(H(\kappa)+2\kappa H'(\kappa))^2 m_{1,2}^{(\mathrm{FB})d}(\mu_\mathrm{t}^2,\mu_\phi^2;\eta_\psi,\eta_\phi),\end{aligned}$$

in terms of dimensionless renormalized couplings and fields, where $H(\tilde{\rho})$ is given by

$$H(\tilde{\rho}) = Z_\phi^{-\frac{1}{2}} Z_\psi^{-1} k^{\frac{d-4}{2}}\, \bar{H}(\rho)\Big|_{\rho=k^{d-2}Z_\phi^{-1}\tilde{\rho}}.$$

The flow equations for the scalar potential as well as the Yukawa potential maintain the full $\tilde{\rho}$ dependence. The equations for the anomalous dimensions are evaluated at the minimum κ of the scalar potential and we have used the abbreviations $\mu_\mathrm{t}^2 = \kappa\, H^2(\kappa)$ and $\mu_\phi^2 = u'(\kappa) + 2\kappa\, u''(\kappa)$. These flow equations for a Yukawa model with generalized Yukawa coupling were already investigated in different physical contexts such as the chiral phase structure of QCD [240, 241], a Yukawa theory coupled to gravity [242, 243], as well as studies of global fixed-point solutions and criticality in low dimensions [54].

As we are mainly interested in the computation of Higgs masses and thus the properties of the scalar potential at the Fermi scale, we again perform a polynomial expansion of the coupling functional u and this time also of H such that the system of coupled PDE's simplifies to a system of coupled ODE's for the expansion coefficients. For the scalar potential, we use Eq. (3.42). The Yukawa functional H is expanded in a power series around vanishing field values in the SYM regime and the nonvanishing minimum κ of the scalar potential in the SSB regime as well,

$$H(\tilde{\rho}) = \sum_{n=0}^{N_\mathrm{H}} \frac{y_n}{n!}\,\tilde{\rho}^n \quad (\mathrm{SYM}), \qquad H(\tilde{\rho}) = \sum_{n=0}^{N_\mathrm{H}} \frac{y_n}{n!}\,(\tilde{\rho}-\kappa)^n \quad (\mathrm{SSB}), \tag{3.46}$$

where we identify the "usual" Yukawa coupling as $h = y_0$. We test the convergence of this polynomial expansion by successively increasing N_H. The initial value of the Yukawa coupling $y_{0,\Lambda}$ is used to tune the top mass to its IR value while we set $y_{n,\Lambda} = 0$ for $n = 1, \ldots, N_\mathrm{H}$ first. Similar to the convergence of the potential, see Fig. 3.11, we observe a fast convergence for the resulting Higgs masses. Changing from $N_\mathrm{H} = 0$ up to $N_\mathrm{H} = 2$ leads to a negligible change in the obtained Higgs masses of ~ 0.5GeV for small cutoffs but a few GeV for large Λ. For $N_\mathrm{H} > 2$, we find no significant deviations within our numerical accuracy from the $N_\mathrm{H} = 2$ results.

Moreover, we would like to mention, that the results obtained for $N_\mathrm{H} = 0$, which corresponds to a restriction to the previous truncation (3.17), are not identical to the Higgs masses obtained in the previous sections. This is simply because the flow equations for h and y_0 do not coincide in the SSB regime. For $N_\mathrm{H} = 0$, the flow equation for y_0 is given by $\partial_t y_0 = \partial_t H(\kappa)$ which corresponds to the first triangle diagram in Fig. 3.3. However, for the flow equation of h we projected onto the coupling between the scalar fluctuations around the vev to the fermions

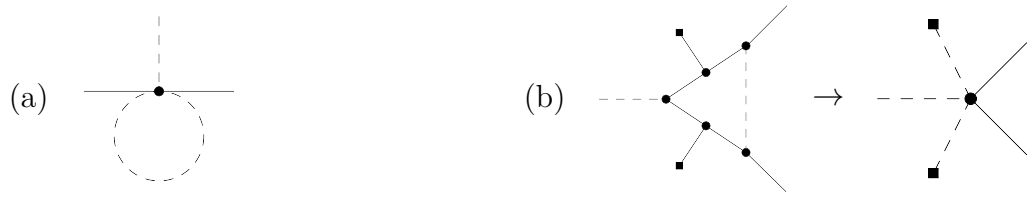

Figure 3.20: (a) Example for an additional contribution, which is proportional to y_1, to the flow of the Yukawa coupling y_0, if higher-order operators of the form $\rho^n \phi\bar{\psi}\psi$ are taken into account. (b) Parts of these higher order couplings were already considered in the flow equation of h in Eq. (3.22). The triangle diagrams with external vev insertions (filled squares) in Fig. 3.3 are now included in the running of the three-scalar-two-fermion vertex by restricting two of the scalar legs to the vev. A similar translation holds for the third triangle diagram which has two scalar lines in the loop in Fig. 3.3.

$\varphi\bar{\psi}\psi$ rather than to the operator $\phi\bar{\psi}\psi$, see the discussion in App. A.4. This leads to additional contributions which effectively take contributions from higher-order couplings already into account. In other words, taking higher truncations into account, the running of y_0 gets corrections from the y_1 coupling, for instance. In the flow equation of h, cf. Eq. (3.22), we encoded parts of these higher order corrections in the two additional triangle diagrams which are proportional to the condensate, see Fig. 3.20. This leads to slightly improved results compared to the naive truncation $N_{\mathrm{H}} = 0$. In fact, the Higgs mass obtained in the previous sections are quite close to the results for truncations with $N_{\mathrm{H}} \geq 2$ for generalized Yukawa interactions. In all studied cases, the deviation between these two truncations is less than 1%. For small cutoffs the deviation is a few 0.1GeV and thus comparable to the error obtained for $N_{\mathrm{H}} = 0$. For large cutoffs we observe a maximal variation in the Higgs mass of 1GeV in the strong scalar coupling regime and negligible deviations for the lower Higgs mass bound.

The fact that we only observe small deviations for the obtained Higgs masses between the simple truncation (3.17) and taking a generalized Yukawa functional of the scalar fields into account(3.45) is not astonishing. The main deviation between the running couplings in the different truncations is in the SSB regime. However, the system flows only for a short RG time in the SSB regime before a decoupling of the massive modes set in, in case we are close to the lower bound. In case $\lambda_{2,\Lambda}$ is large (upper bound), we already start in the SSB regime. However, due to the dominance of the scalar fluctuations, the fermion sector plays a less important role and we also observe only slight changes.

The situation becomes more interesting if we already allow for a generalized Yukawa potential in the bare action $H_\Lambda(\tilde{\rho})$ and investigate its influence on the conventional lower Higgs mass bound ($H_\Lambda(\tilde{\rho}) = y_{0,\Lambda}$, and $\lambda_{2,\Lambda} = \lambda_{3,\Lambda} = \cdots = 0$). Indeed, we find Higgs masses below the lower bound by the rather mild modification of choosing $y_{1,\Lambda} > 0$. The size of this shift is roughly of the same order of magnitude as we already observed by allowing for generalized scalar bare potentials u_Λ. As we already pointed out, a modification of the running of y_0, which builds up the lower Higgs mass bound, could lead to such a diminishment. Comparing the resulting flows of y_0 for $y_{1,\Lambda} = 0$ and $y_{1,\Lambda} > 0$ shows an insignificant shift for the values of $y_0(k)$

such that this mechanism is not able to explain the observed shift in the Higgs mass.

However, the modification of the bare Yukawa functional also influences the flow of the scalar potential in a direct manner and not only indirectly via the running of y_0. This effect can be investigated on the mean-field level again. The mean-field effective scalar potential can be straightforwardly generalized and reads for the linear regulator,

$$U^{\mathrm{MF}}(\rho) = U_\Lambda(\rho) - \frac{\Big[H_\Lambda(0)\Big]^2 \Lambda^2 \rho}{16\pi^2} + \frac{1}{16\pi^2}\left[-\Big[H_\Lambda(\rho) - H_\Lambda(0)\Big]^2 \Lambda^2 \rho + \Big[H_\Lambda(\rho)\Big]^4 \rho^2 \ln\left(1 + \frac{\Lambda^2}{\Big[H_\Lambda(\rho)\Big]^2 \rho}\right)\right],$$

where we separated the interaction part of the Fermion determinant in the second line. This is a positive monotonically increasing function for $H_\Lambda(\rho) = y_{0,\Lambda}$. Obviously, this function can lose its positivity property if we allow for generalized Yukawa interactions beyond $H_\Lambda = y_{0,\Lambda}$, depending on the precise shape of the in principal arbitrary $H_\Lambda(\rho)$. Hence, the fermion interaction can induce a metastability even in the class of ϕ^4 bare potentials.

Also, this fact can be seen from the flow equation of λ_2. While the usual Yukawa coupling contributes according to $-y_0^4$ and thus leads to an increase of the quartic coupling towards the IR, an additional contribution coming from y_1 contributes according to $+y_1 y_0$. Thus a sufficiently large value for $y_{1,\Lambda}$ can lead to a decrease of λ_2 near the cutoff scale. Starting with a vanishing interacting scalar bare potential ($\lambda_{2,\Lambda} = \lambda_{3,\Lambda} = \cdots = 0$), λ_2 runs to negative values while λ_3 becomes positive (and similar for the higher order scalar couplings) driven by y_1. Due to the fact, that y_1 quickly becomes small during the RG flow as is expected in the vicinity of the Gaußian fixed-point by reason of power-counting arguments, the flow equations become dominated by the contributions arising from the pure Yukawa interaction term $\sim -y_0^{2n}$. Roughly speaking, we flow into the class of generalized bare potentials with $\lambda_{2,\Lambda} < 0$ and $\lambda_{3,\Lambda} > 0$ after a short RG time in some sense. In complete analogy to the generalized bare potentials with $\lambda_{2,\Lambda} < 0$ and stabilized by $\lambda_{3,\Lambda}$, a metastability occurs during the RG flow if $y_{1,\Lambda}$ exceeds a critical value driving λ_2 to too small values.

Following the same strategy as in the case of generalized bare potentials, we trust the polynomial expansion as long as no second minimum deeper than the minimum at the electroweak scale emerges during the RG flow. Fixing $\lambda_{2,\Lambda} = \lambda_{3,\Lambda} = \cdots = 0$ and increasing $y_{1,\Lambda}$ until a potential second minimum becomes the global one, we obtain Higgs masses which we already cover in the class of generalized bare potentials. The naive expectation, that a combination of both mechanisms (generalized u_Λ and H_Λ) leads to a further decrease of the lower Higgs mass bound, is investigated in the following. Basically one can use, that the vanishing of λ_3 can be delayed for a small RG time by choosing, for instance, $\lambda_{3\Lambda} = 3$ in addition to $y_{1,\Lambda} > 0$. Hence, lower values for λ_2 during the flow are accessible and the Higgs mass decreases. However, this further diminishing is rather small which is due to the fact that the running of the higher-order

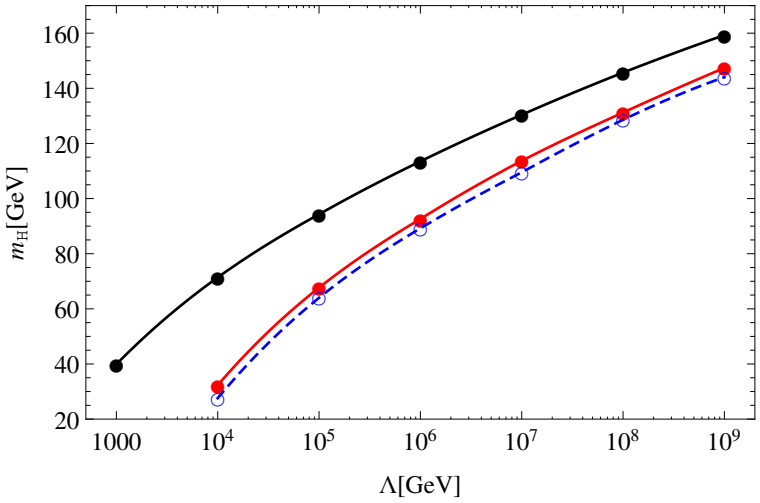

Figure 3.21: Higgs mass versus cutoff. The black curve denotes the conventional lower Higgs mass bound obtained from a theory which only include perturbatively renormalizable operators at the UV cutoff scale. The red curve gives a lower bound in the class of generalized scalar bare potentials of ϕ^6 type with the requirement that no metastability occurs during the RG flow. The Higgs masses given by the blue dashed line are obtained from a further generalization to Yukawa potentials of the form $y_{0,\Lambda} + y_{1,\Lambda}\tilde{\rho}$.

couplings is strongly affected by their infrared attractive pseudo-fixed points which cannot be circumvented by this strategy. In order to illustrate this fact, we depict the lowest accessible Higgs masses from the different generalizations of the bare action in Fig. 3.21. We compare the Higgs masses obtained for the conventional lower Higgs mass bound ($\lambda_{2,\Lambda} = \lambda_{3,\Lambda} = \cdots = 0$ and $y_{1,\Lambda} = y_{2,\Lambda} = \cdots = 0$), for the lower bound obtained from the class of ϕ^6 bare potentials with the requirement of the stable scalar potentials during the entire RG flow and a similar lower bound but for the parameters $\lambda_{2,\Lambda} = 0$, $\lambda_{3,\Lambda} = 3$, and the value of $y_{1,\Lambda}$ put to the transition where the scalar effective potential becomes metastable.

As the benefit in diminishing the lower consistency Higgs mass bound is rather small, we only consider "simple" Yukawa interaction terms in the following again.

4 Higgs-top-QCD model

Before we proceed to chiral Higgs-Yukawa models, which take the chiral structure of the standard model into account, we will present here a first impact how gauge bosons modify the running of the matter sector. Parts of this chapter, especially Sect. 4.3 is based on [128]. Obviously, we are not able to test the influence of the electroweak gauge bosons in a consistent manner within the simple Higgs-Yukawa toy model because these are directly related to the chiral structure of the fermions. Nevertheless, the contribution of the strong interaction on the running of the top Yukawa coupling can be investigated in a self-contained manner. Moreover, this investigation can be motivated by the fact that the strong coupling constant g_{s} dominates the β functions of the Yukawa couplings of the quarks, see Eqn.(2.9)-(2.10). Due to the strong influence on the running of the Yukawa coupling, also the running of the Higgs sector, which does not directly couple to the gluons, will be indirectly modified.

The model is given by the following gauge-fixed, classical (Euclidean) action:

$$\begin{aligned} S = \int d^4x \Bigg[& \frac{1}{2}(\partial_\mu \phi)^2 + U_\Lambda(\phi^2) + \bar{\psi}^A \, \mathrm{i}\not{\mathbf{D}}^{AB} \psi^B + \mathrm{i}\frac{\bar{h}}{\sqrt{2}} \, \phi \, \bar{\psi}^A \psi^A + \frac{1}{4} G_{I\mu\nu} G_I^{\mu\nu} \\ & + \frac{1}{2\xi_{\mathrm{s}}} \left(\partial_\mu G_I^\mu\right)^2 + u_I \mathcal{M}_{IJ} u_J \Bigg], \end{aligned} \tag{4.1}$$

where $\mathbf{D}_\mu^{AB} = \delta^{AB}\partial_\mu + i\bar{g}_{\mathrm{s}} G_I^\mu T_I^{AB}$ is the covariant derivative acting on the color structure of the top quark ψ^A. The Faddeev-Popov determinant is given by $\mathcal{M}_{IJ} = \partial_\mu \mathbf{D}_{IJ}^\mu$ with the covariant derivative in the adjoint representation, and $G_I^{\mu\nu}$ is the field strength tensor for the $\mathrm{SU}(3)_{\mathrm{c}}$ gauge bosons G_I^μ. The classical scalar potential U_Λ depends on the $\mathbb{Z}_2$-invariant $\rho = \frac{1}{2}\phi^2$ and thus the model has still a discrete chiral symmetry, Eq. (3.2).

4.1 Flow equations

At next-to-leading order in the derivative expansion, the truncation of the Higgs-top-QCD model defined in Eq. (4.1) reads,

$$\begin{aligned} \Gamma_k = \int_x \Bigg[& \frac{Z_\phi}{2}(\partial_\mu \phi)^2 + U(\rho) + Z_\psi \bar{\psi}^A \, \mathrm{i}\not{\mathbf{D}}^{AB} \psi^B + \mathrm{i}\frac{\bar{h}}{\sqrt{2}} \, \phi \bar{\psi}^A \psi^A + \frac{Z_{\mathrm{G}}}{4} G_{I\mu\nu} G_I^{\mu\nu} \\ & + \frac{Z_{\mathrm{G}}}{2\xi_{\mathrm{s}}} \left(\partial_\mu G_I^\mu\right)^2 + Z_{\mathrm{u}} u_I \mathcal{M}_{IJ} u_J \Bigg]. \end{aligned} \tag{4.2}$$

The dependence on the RG scale k is omitted for convenience. Note, that we already have chosen a gauge-fixed truncation accordingly to the gauge-fixed action (4.1). However, there is a choice between two strategies how to deal with a gauge theory. Either one chooses a gauge-fixed formulation or constructs gauge-invariant flow equations [244–247]. While the latter seems to provide a conceptually clean set up, the former is more convenient for practical calculations. For any quantitative statement, we will evaluate the following flow equations in the Landau gauge $\xi_\mathrm{s} = 0$. Note, that this gauge choice is also a fixed point of the RG flow due to the fact that the gauge-fixing parameter renormalizes multiplicatively [248].

Inserting the truncation into the Wetterich equation (2.13) leads to the nonperturbative flow equations for the various operators by appropriate projection rules. In comparison to the simple Higgs-Yukawa model, the flow equations for the scalar quantities are only modified by the fact, that each pure fermion loop gets an additional combinatorial factor $N_\mathrm{c} = 3$ due to the fact, that the model now contains N_c copies of the top quark.

$$\partial_t u_k = -d\, u_k + (d - 2 + \eta_\phi)\tilde{\rho} u_k' + 2v_d\Big[l_0^{(\mathrm{B})d}\,(u_k' + 2\,\tilde{\rho}\, u_k''; \eta_\phi) - d_\gamma N_\mathrm{c}\, l_0^{(\mathrm{F})d}\left(\tilde{\rho}\, h_k^2; \eta_\psi\right)\Big], \tag{4.3}$$

$$\begin{aligned}\eta_\phi = {}& \frac{8v_d}{d}\kappa_k\Big[3u''(\kappa) + 2\kappa u'''(\kappa)\Big]^2 m_2^{(\mathrm{B})d}(\mu_\phi^2; \eta_\phi) \\ & + \frac{4v_d d_\gamma N_\mathrm{c}}{d} h^2\Big[m_4^{(\mathrm{F})d}(\mu_\mathrm{t}^2; \eta_\psi) - \kappa h^2 m_2^{(\mathrm{F})d}(\mu_\mathrm{t}^2; \eta_\psi)\Big].\end{aligned} \tag{4.4}$$

Note that also a field-independent contribution from a gluon $\sim l_0^{(\mathrm{B})d}(0; \eta_\mathrm{G})$ as well as a ghost loop $\sim l_0^{(\mathrm{B})d}(0; \eta_\mathrm{u})$ contribute to the running of the scalar potential which we have omitted as they do only contribute to an unobservable (as long as gravity is not considered) vacuum shift. The flow equation for the Yukawa coupling gets additional contributions from the interactions between the quarks and gluons. It reads,

$$\begin{aligned}\partial_t h^2 = {}& (d - 4 + \eta_\phi + 2\eta_\psi)\, h^2 + 4v_d\, h^4\Big[l_{1,1}^{(\mathrm{FB})d}(\mu_\mathrm{t}^2, \mu_\phi^2; \eta_\psi, \eta_\phi) - 2h^2\kappa\, l_{2,1}^{(\mathrm{FB})d}(\mu_\mathrm{t}^2, \mu_\phi^2; \eta_\psi, \eta_\phi) \\ & - \Big(6\kappa u''(\kappa) + 4\kappa^2 u'''(\kappa)\Big)\, l_{1,2}^{(\mathrm{FB})d}(\mu_\mathrm{t}^2, \mu_\phi^2; \eta_\psi, \eta_\phi)\Big] \\ & + 4v_d\frac{N_\mathrm{c}^2 - 1}{2N_\mathrm{c}} h^2 g_\mathrm{s}^2 (d - 1 + \xi_\mathrm{s})\Big[- l_{1,1}^{(\mathrm{FB})d}(\mu_\mathrm{t}^2, 0; \eta_\psi, \eta_\mathrm{G}) + 2h^2\kappa\, l_{2,1}^{(\mathrm{FB})d}(\mu_\mathrm{t}^2, 0; \eta_\psi, \eta_\mathrm{G})\Big],\end{aligned} \tag{4.5}$$

where κ is the minimum of the scalar potential, i.e., $\kappa = 0$ in the SYM regime and $u'(\kappa) = 0$ in the SSB regime. The renormalized dimensionless strong coupling is given by $g_\mathrm{s}^2 = Z_\mathrm{G}^{-1} k^{d-4} \bar{g}_\mathrm{s}^2$. The anomalous dimension of the fermion reads,

$$\begin{aligned}\eta_\psi = {}& \frac{4v_d}{d} h^2\Big[m_{1,2}^{(\mathrm{FB})d}(\mu_\mathrm{t}^2, \mu_\phi^2; \eta_\psi, \eta_\phi) \\ & + 2\frac{N_\mathrm{c}^2 - 1}{2N_\mathrm{c}} g_\mathrm{s}^2\Big((d - 1 - \xi_\mathrm{s}) m_{1,2}^{(\mathrm{FB})d}(\mu_\mathrm{t}^2, 0; \eta_\psi, \eta_G) - (d - 1)(1 - \xi_\mathrm{s})\tilde{m}_{1,1}^{(\mathrm{FB})d}(\mu_\mathrm{t}^2, 0; \eta_\psi, \eta_G)\Big)\Big].\end{aligned} \tag{4.6}$$

The threshold functions can be found in App. A.3. A diagrammatic interpretation of the

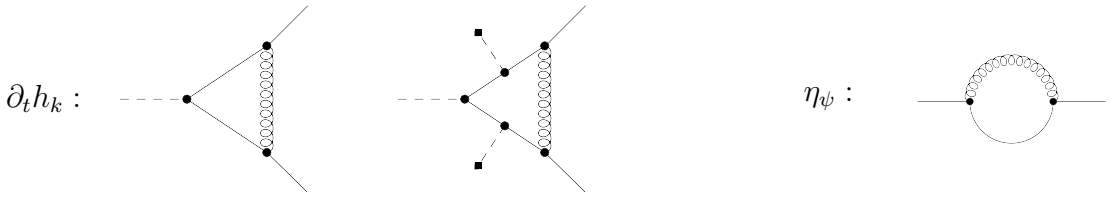

Figure 4.1: Additional diagrammatic contributions to the running of the Yukawa coupling as well as the anomalous dimension of the fermion. Curly lines depict gluons. For compactness, we suppress the regulator insertions.

additional contributions arising from the quark-gluon interplay are depicted in Fig. 4.1. While we will use these flow equations in order to investigate the indirect contributions of the strong interaction to the Higgs mass via the Yukawa couplings, similar models are studied to investigate low energy properties of QCD, for instance, see [249].

To complete the set of flow equations within this model, we have to investigate the flow equations of the gauge sector as well, i.e., of the strong coupling g_s and the anomalous dimension of the gluon η_G. The running of the Yang-Mills coupling can be investigated on a nonperturbative level as well [180], however, we will only take it on a perturbative level into account. This approximation is justified because we are only interested in the properties of the flow equations far above the QCD scale. Near the electroweak scale threshold effects set in which imply that the scalar potential, the Yukawa coupling as well as the anomalous dimensions of the scalar and fermion field freeze out before g_s grows to large values near the typical energy scale of QCD which is of order 1GeV. The perturbative one-loop computation for the beta function for g_s, e.g., within the background field formalism, can be found in almost every textbook on particle physics, cf. [130, 131]. It reads,

$$\partial_t g_\mathrm{s}^2 = g_\mathrm{s}^2 \eta_\mathrm{G}, \qquad \eta_\mathrm{G} = -\frac{g_\mathrm{s}^2}{8\pi^2}\left(\frac{11}{3}N_\mathrm{c} - \frac{2}{3}n_\mathrm{f}\right), \tag{4.7}$$

where n_f is the number of different quark flavors in the model. In order to describe a standard model like behavior, we choose $n_\mathrm{f} = 6$ although we have only considered the top quark in our truncation (4.2). Strictly speaking, we consider a model which includes additional $\mathrm{SU}(3)_\mathrm{c}$-invariant kinetic terms for the five other standard model quark flavors but their Yukawa couplings to the Higgs field are set to zero. Thus, we consider the correct running of the pure strong sector while the flow equations for the Higgs-top sector are not affect by this modification. Due to the negligible size of the Yukawa couplings of the other fermions compared to the top quark Yukawa coupling, this is a rather good approximation for the pure Higgs-top-QCD sector of the standard model, even if we do not consider the correct chiral structure of the Higgs-Yukawa sector. In order to solve the flow equation $\partial_t g_\mathrm{s}^2$, we choose an initial value at the UV cutoff scale Λ such that we obtain an IR value at the mass scale of the Z boson of $g_\mathrm{s}^2(k = m_\mathrm{Z}) = 4\pi\alpha_\mathrm{s}(k = m_\mathrm{Z}) = 4\pi \cdot 0.118$.

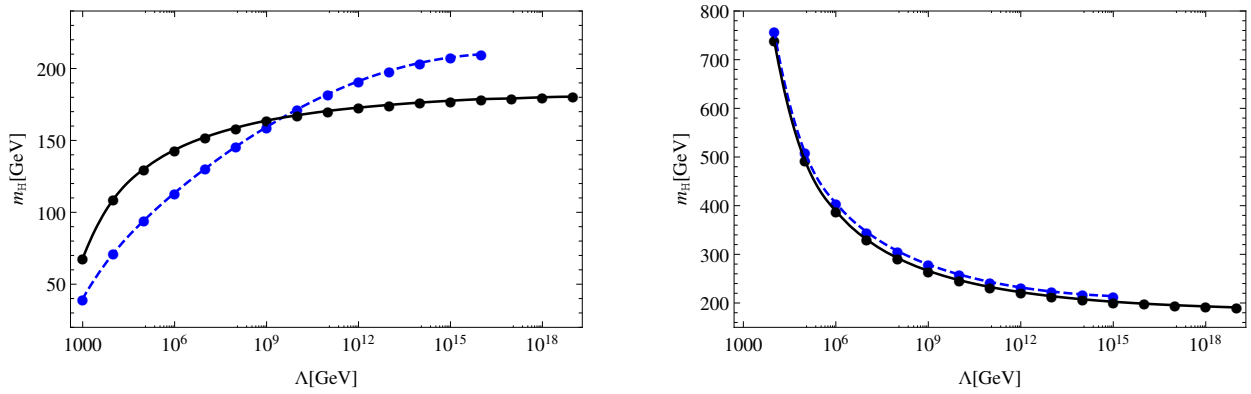

Figure 4.2: Comparison between the simple Higgs-Yukawa model (blue dashed) and the Higgs-top-QCD model (black solid). The left panel shows the lower Higgs mass consistency bound within the class of ϕ^4 potentials. The right panel depicts Higgs masses for a strongly coupled scalar sector $\lambda_{2,\Lambda} = 100$. Within the simple Yukawa model, Higgs mass bounds cannot be investigated at the Planck scale due to singular behavior of the running Yukawa coupling at scales $k > 10^{16}$GeV.

4.2 Higgs mass bounds

Let us proceed with our by now well familiar investigation of Higgs mass bounds, first within the class of ϕ^4 bare potentials and afterwards for the generalized class of ϕ^6 potentials. Therefore, we again expand the potential in a power series at vanishing field amplitude in the SYM regime as well as the nontrivial vev in the SSB regime, see Eq. (3.42). Restricting to quartic bare potentials, we observe the same qualitative behavior as in the simple Higgs-Yukawa model. The Higgs mass is an increasing function with respect to the bare quartic coupling and thus a lower mass bound arises from the consistency condition $\lambda_{2,\Lambda} \geq 0$. Within the polynomial truncation the resulting Higgs masses converge fast for increasing N_p. Again, we find no deviations within our numerical accuracy for truncations with $N_\mathrm{p} \geq 4$. Changing from leading order ($\eta_\phi = \eta_\psi = \eta_\mathrm{G} = 0$) to next to leading order in the derivative expansion, we find small deviations of a few percent for small $\lambda_{2,\Lambda}$. For larger $\lambda_{2,\Lambda}$, the deviations increase to $\sim 15\%$.

In Fig. 4.2, we compare the resulting Higgs masses of the present Higgs-top-QCD model to the masses obtained within the simple Higgs-Yukawa model. The left figure shows the lower bound ($\lambda_{2,\Lambda} = 0$) arising in both models. The large quantitative differences between these two curves demonstrate the strong (indirect) influence of the QCD sector on the Higgs mass via the Yukawa coupling. First of all note, that now $N_\mathrm{c} = 3$ copies of the top quark contribute to the running of the scalar potential. Thus, the mass bound obtained in the simple model (blue dashed line) would be shifted by roughly a factor of $\sqrt{3}$ if one would neglect the influence of the strong coupling constant on the running Yukawa coupling. However, the behavior of the running Yukawa coupling changes qualitatively due to the additional contributions from the gluons. In contrast to the simple model, where the Yukawa coupling grows towards the UV and finally runs into a pole at $k > 10^{16}$GeV (see Fig. 3.13), it becomes smaller at high scales

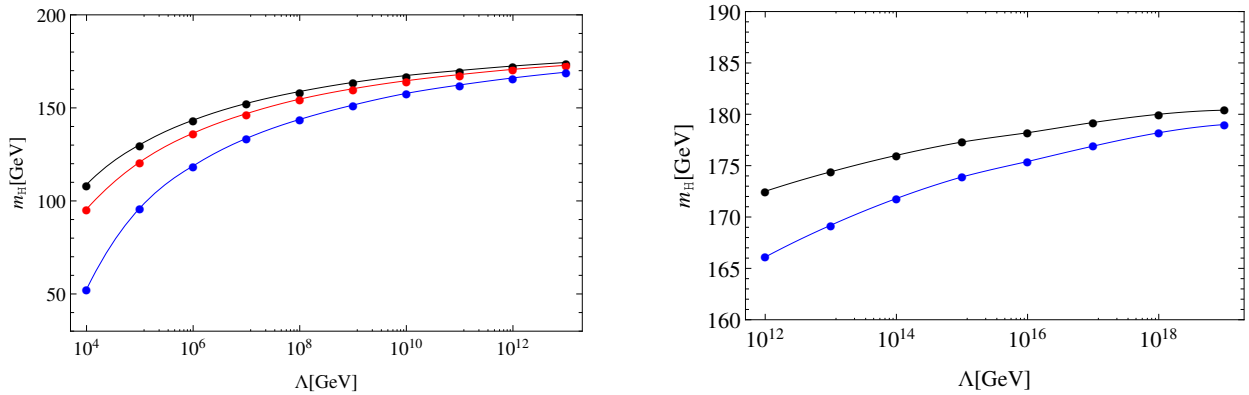

Figure 4.3: Higgs mass versus cutoff Λ. The black line denotes the lower bound for the Higgs mass derived within the class of bare ϕ^4 potentials. The red and blue lines show Higgs masses below the ϕ^4 consistency bound by allowing for generalized bare potentials. The masses are derived for $\lambda_{3,\Lambda} = 3$ and $\lambda_{2,\Lambda} = -0.08$ (red) as well as $\lambda_{3,\Lambda} = 10$ $\lambda_{2,\Lambda} = -0.15$ (blue). In all cases no second minimum occurs during the entire RG flow such that the potentials are stable at every RG scale k.

within the present model. Therefore, the Yukawa coupling contributes with a lower strength to the running of the scalar sector which results in smaller Higgs masses. This effect becomes significant for large UV cutoffs where these effects accumulate over a long RG flow. Thus, the lower Higgs mass bound is even below the lower bound of the simple Yukawa model despite the larger fermion content. By contrast, Higgs masses close to the upper bound are less affected. In this case, the theory is rather dominated by scalar self-interactions such that a change in the running Yukawa coupling or the additional field content plays a minor role.

By allowing for generalized bare potentials, we are able to test if the mechanism of diminishing the lower bound also holds within the Higgs-top-QCD model. In principle, there is the possibility that this mechanism gets washed out due to the new degrees of freedom. As we pointed out in Subsect. 3.5.2, the lowering can be viewed as a shift from initial conditions of the quartic-type bare potentials at a certain cutoff scale to a theory with $\lambda_{2,\Lambda} < 0$ but the bare potential stabilized by a positive $\lambda_{3,\Lambda}$ at an effectively larger cutoff value. However, such a shift seems to be less effective for large cutoff values due to the flatten of the lower bound at large Λ. This flatten is even stronger in the Higgs-top-QCD model such that such a shift may only lead to an unimportant shift of the Higgs mass. However, careful investigations show, that it is still possible to construct example flows which are entirely stable and diminish the ϕ^4 consistency bound significantly over a wide range of cutoff values, see Fig. 4.3. Indeed, this diminishing is less effective at the Planck scale, where the Higgs mass bound can be relaxed be roughly 1GeV before a metastability occurs during the RG flow even if the bare potential is stable.

4.3 The Higgs phase diagram and the scale of new physics

As we pointed out at the beginning of this chapter, the present model with its simple Yukawa structure does not reflect the weak gauge structure of the standard model. However, the electroweak gauge couplings have significant effects. First, the gauge couplings give an important positive contribution to the flow equation of the scalar quartic coupling, balancing the negative top Yukawa terms for small values of λ_2. Second, they decrease the Yukawa coupling in the UV, and thus also increase λ_2 towards large scales. In order to come in contact with standard model phenomenology at a quantitative level for the first time, we effectively model their contributions to the running of the scalar potential as well as the Yukawa coupling by a fiducial coupling g_{F}. The contribution to the potential in $d = 4$ reads,

$$\partial_t u = (\text{rhs. of Eq. (4.3)}) + \frac{1}{32\pi^2}\frac{c_u}{1+\frac{1}{2}g_{\mathrm{F}}\tilde{\rho}}. \tag{4.8}$$

We further modify the running of the Yukawa coupling by a term $-\frac{c_h}{8\pi^2}h^2 g_{\mathrm{F}}^2$ in the SYM regime. We choose the additional constants and the fiducial gauge coupling in such a way that the resulting running of the quartic coupling λ_2 and the Yukawa coupling h^2 in the perturbative limit is quantitatively similar to the running of the standard model Higgs quartic coupling and the standard model top Yukawa coupling. Therefore, we choose $c_u = 16$, $c_h = \frac{97}{30}$ and $g_{\mathrm{F}} = 0.57$.

In order to investigate the RG evolution of the standard model, its physical masses and couplings have to be related to the fundamental parameters appearing in the β functions. So far, we identified, for instance, the top or the Higgs mass with their pole masses of their propagators which have a rather simple structure owing our derivative expansion. In general, the full propagator of a particle will be an intricate function of the momentum such that the simple identification, for instance, for the top mass $m_{\mathrm{t}} = \frac{1}{\sqrt{2}}h_{\mathrm{t}}v$ should be only viewed as a first approximation. In principle a thorough study of the relation between the masses within our FRG scheme and the physical masses measured in an experiment have to be performed. However, this is beyond the scope of this work. In order to get a first insight into this dependency, we investigate the dependence of the lower Higgs mass bound on the value of the top mass within the derivative expansion in App. A.7 for a chiral Higgs-Yukawa theory.

Nevertheless, within the perturbative setting this procedure is well-established up to NNLO [83]. In order to compare to the perturbative results and extract universal physical results, we can establish a matching procedure. We choose to match the flows at the TeV scale. This scale is sufficiently deep inside the Euclidean region but not yet affected by possible higher-dimensional operators. Our procedure equates the running couplings in the perturbative $\overline{MS}$ scheme and the FRG scheme at the matching scale. These read at $k = 1\mathrm{TeV}$: $\lambda_2 = 0.202$, $h = 0.867$, $g_{\mathrm{s}} = 1.060$. Approaching that scale from the ultraviolet, typical FRG trajectories are still in the symmetric regime, an electroweak minimum of the potential has not been generated yet, and the threshold effects in the FRG flow equations are subleading. As the values for the

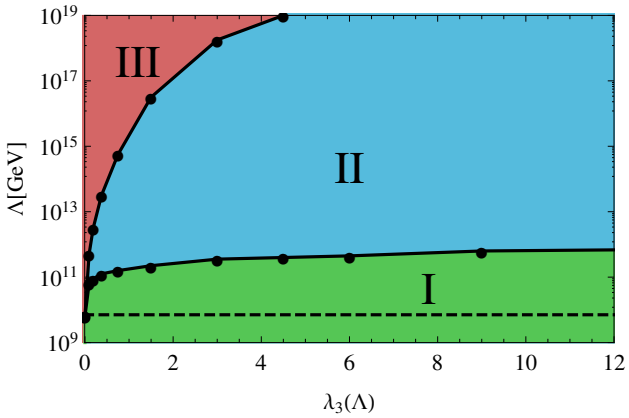

Figure 4.4: Different stability regions as a function of Λ and $\lambda_{3,\Lambda}$. In region I (green) the potential is stable everywhere. In region II (blue) the UV- potential is stable, while the potential is only pseudostable for intermediate scales in a polynomial truncation. Based on our investigations in Sect.3.4 and Sect.3.6 it is likely that this entire region results in a metastable potential. In region III (red) the UV-potential violates the unique-minimum condition. The black dashed line denotes the UV cutoff resulting from the consistency bound within the ϕ^4 bare potentials.

couplings agree with those of the $\overline{MS}$ scheme at the matching scale, our matching scheme guarantees that UV-initial conditions for the FRG flow are mapped to physical values in the infrared with high accuracy. For further details of this mapping see [128]. As aforementioned, in a more elaborate FRG setup, using a more sophisticated truncation of the operator space, our mapping using $\overline{MS}$ parameters will become obsolete and quantitatively precise values for physical observables can be read off from the FRG flow trajectories at $k = 0$ directly.

While we basically concentrated on the diminishing of the lower Higgs mass bound within the class of ϕ^6-type bare potentials, let us rephrase this statement by investigating how many orders of magnitude the UV cutoff scale can be shifted by allowing for generalized bare potentials. Therefore, we fix $\lambda_{2,\Lambda}$ such that the resulting Higgs mass in the IR approaches $m_{\mathrm{H}} = 125\mathrm{GeV}$ and we scan for different values of $\lambda_{3,\Lambda}$ at which cutoff value the polynomial expansion becomes pseudostable at a finite RG scale k which will probably lead to a metastable effective potential.

Within this standard-model like theory, we are able to increase the cutoff scale by at least two orders of magnitude while retaining the full stability of the electroweak vacuum. This result is depicted in Fig. 4.4 where the green region I corresponds to completely stable scalar potentials during the entire RG flow. Increasing the possible cutoff scales by further orders of magnitude is difficult since there is a strongly infrared-attractive pseudo-fixed point at $\lambda_3 \approx 0$, see Subsect. 3.5.2. The large blue region II depicts initial conditions where the UV potential is stable, but our polynomially expanded potentials exhibit further minima at intermediate scales, which will render the potential metastable. Finally, in the red region III the UV potential is already metastable, as might be the effective potential.

5 Chiral Higgs-Yukawa models

Within Chap. 3 we have analyzed the occurrence of Higgs mass bounds in a toy model which simplifies the interaction between the fermions, especially the top quark, and the Higgs field to a simple Yukawa interaction. In this chapter, we generalize our results to the chiral structure of the standard model Higgs-Yukawa sector which is also used in lattice simulations [117–123]. Additionally, we gauge the $\mathrm{SU}(2)_\mathrm{L}$ structure in order to take contributions from the weak gauge bosons into account. The results obtained in Sect. 5.1 are based on our work in [116].

5.1 Chiral Higgs-top-bottom model

We start our investigations of the chiral Yukawa structure in a chiral Higgs-Yukawa model with a global $\mathrm{SU}(2)_\mathrm{L} \times \mathrm{U}(1)_\mathrm{Y}$ symmetry forming a self-contained subset of the standard-model. The field content consists of a scalar field which is a complex SU(2)-doublet

$$\phi = \frac{1}{\sqrt{2}} \begin{pmatrix} \phi_2 + \mathrm{i}\phi_1 \\ \phi_4 + \mathrm{i}\phi_3 \end{pmatrix}, \tag{5.1}$$

and two Dirac fermions which represent the top and bottom quark. The left-handed components of the bottom and top transform as a doublet under $\mathrm{SU}(2)_\mathrm{L}$ while the right-handed components are singlets.

$$\psi_\mathrm{L} = \begin{pmatrix} t_\mathrm{L} \\ b_\mathrm{L} \end{pmatrix}, \quad t_\mathrm{R}, \quad b_\mathrm{R}.$$

The classical Euclidean action of the model is given by

$$\begin{aligned} S = \int d^4x \Big[& \partial_\mu \phi^\dagger \partial^\mu \phi + U_\Lambda(\rho) + \mathrm{i}\bar{\psi}_\mathrm{L} \not{\partial} \psi_\mathrm{L} + \mathrm{i}\bar{t}_\mathrm{R} \not{\partial} t_\mathrm{R} + \mathrm{i}\bar{b}_\mathrm{R} \not{\partial} b_\mathrm{R} \\ & + \mathrm{i}\bar{h}_\mathrm{b}(\bar{\psi}_\mathrm{L} \phi b_\mathrm{R} + \bar{b}_\mathrm{R} \phi^\dagger \psi_\mathrm{L}) + \mathrm{i}\bar{h}_\mathrm{t}(\bar{\psi}_\mathrm{L} \phi_\mathrm{c} t_\mathrm{R} + \bar{t}_\mathrm{R} \phi_\mathrm{c}^\dagger \psi_\mathrm{L}) \Big]. \end{aligned} \tag{5.2}$$

where $\phi_\mathrm{c} = \mathrm{i}\sigma_2 \phi^*$ denotes the charge conjugated scalar. The scalar field couples to the fermions via a chiral Yukawa interaction where $\bar{h}_\mathrm{t}$ and $\bar{h}_\mathrm{b}$ are the (bare) Yukawa couplings for the top and bottom respectively. Furthermore, we include scalar self-interactions encoded in the scalar potential which depends on the field invariant $\rho = \phi^\dagger \phi$.

The action (5.2) is invariant under the following global symmetry transformations

$$\phi \to e^{\mathrm{i}\alpha^i \frac{\sigma^i}{2}}\phi, \qquad \psi_\mathrm{L} \to e^{\mathrm{i}\alpha^i \frac{\sigma^i}{2}}\psi_\mathrm{L}, \qquad t_\mathrm{R} \to t_\mathrm{R}, \qquad b_\mathrm{R} \to b_\mathrm{R},$$

where σ^i are the Pauli matrices acting on the $\mathrm{SU}(2)_\mathrm{L}$ doublet structure and

$$\phi \to e^{\mathrm{i}\beta_\mathrm{s}}\phi, \qquad \psi_\mathrm{L} \to e^{\mathrm{i}\beta_\mathrm{L}}\psi_\mathrm{L}, \qquad t_\mathrm{R} \to e^{\mathrm{i}\beta_\mathrm{R}^\mathrm{t}}t_\mathrm{R}, \qquad b_\mathrm{R} \to e^{\mathrm{i}\beta_\mathrm{R}^\mathrm{b}}b_\mathrm{R}.$$

Here, the β angles are related to a single angle by the usual hypercharge assignments, $\beta_\mathrm{s} = \frac{1}{2}\beta$, $\beta_\mathrm{L} = \frac{1}{6}\beta$, $\beta_\mathrm{R}^\mathrm{t} = \frac{2}{3}\beta$, and $\beta_\mathrm{R}^\mathrm{b} = -\frac{1}{3}\beta$. Thus, the model has a global $\mathrm{SU}(2)_\mathrm{L} \times \mathrm{U}(1)_\mathrm{Y}$ symmetry. The symmetry can be spontaneously broken down to a global $\mathrm{U}(1)_\mathrm{em}$ by a nonzero vacuum expectation value of the scalar field $\phi \to v$, giving rise to Dirac masses for the fermions and the Higgs boson mass.

The classical action is already equipped with a potential for the scalar field $U_\Lambda(\rho)$. Symmetry breaking in the quantum theory occurs, if the corresponding renormalized potential U develops a nonvanishing minimum ρ_0. In this case, we can again write the masses in terms of this minimum and the renormalized Yukawa couplings h_t and h_b,

$$v = \sqrt{2}Z_\phi^{\frac{1}{2}}\langle\phi\rangle = \sqrt{2Z_\phi\rho_0}, \qquad m_\mathrm{H}^2 = v^2\frac{U''(\rho_0)}{Z_\phi^2}, \qquad m_\mathrm{t}^2 = \frac{1}{2}v^2h_\mathrm{t}^2, \qquad m_\mathrm{b}^2 = \frac{1}{2}v^2h_\mathrm{b}^2,$$

where we accounted for a wave function renormalization Z_ϕ defined in conjunction with the other renormalized quantities in analogy to Chap. 3.

Apart from the missing further matter and flavor content, we also ignore the gauge sectors of the standard model first to concentrate on the chiral structure of the matter sector. In order to make closer contact with the standard model language, we fix $v = 246\mathrm{GeV}$, $m_\mathrm{t} = 173\mathrm{GeV}$ and $m_\mathrm{b} = 4.2\mathrm{GeV}$ for illustrative purposes, but leave the Higgs mass as a free parameter.

Analogously to the simple Higgs-Yukawa model, the present chiral Higgs-Yukawa model may not be extendible to arbitrarily high momentum scales, also see the discussion on potential non-Gaußian fixed-points in App. A.8. Thus, we are working in an effective-field-theory picture once more where the cutoff plays the physical scale at which new degrees of freedom occur. Also, we impose suitable renormalization conditions at the UV cutoff Λ in complete analogy to the simple Higgs-Yukawa model. For the present model, we can fix h_t, h_b, and the scalar potential U in terms of their bare quantities at the cutoff, $h_{\mathrm{t}\Lambda} = \bar{h}_\mathrm{t}$, $h_{\mathrm{b}\Lambda} = \bar{h}_\mathrm{b}$, and U_Λ. In practice, the fixing can be done such that the constraints set by the physical values of v, m_t, and m_b are satisfied. From this viewpoint, the Higgs boson mass as the remaining free parameter becomes a function of the unconstrained combinations of the UV couplings. Now, bounds on the Higgs boson mass arise, if all permissible choices of UV couplings result in a finite range of Higgs boson masses.

The effective average action at next-to-leading order (NLO) in a derivative expansion corre-

sponds to the following truncation:

$$\begin{aligned}\Gamma_k = \int_x \Big[& Z_\phi |\partial_\mu \phi|^2 + U(\rho) + Z_{\mathrm{L}} \bar{\psi}_{\mathrm{L}} \mathrm{i}\partial\!\!\!/ \psi_{\mathrm{L}} + Z_{\mathrm{R_t}} \bar{t}_{\mathrm{R}} \mathrm{i}\partial\!\!\!/ t_{\mathrm{R}} + Z_{\mathrm{R_t}} \bar{b}_{\mathrm{R}} \mathrm{i}\partial\!\!\!/ b_{\mathrm{R}} \\ & + \mathrm{i}\bar{h}_{\mathrm{b}} (\bar{\psi}_{\mathrm{L}} \phi b_{\mathrm{R}} + \bar{b}_{\mathrm{R}} \phi^\dagger \psi_{\mathrm{L}}) + \mathrm{i}\bar{h}_{\mathrm{t}} (\bar{\psi}_{\mathrm{L}} \phi_{\mathrm{c}} t_{\mathrm{R}} + \bar{t}_{\mathrm{R}} \phi_{\mathrm{c}}^\dagger \psi_{\mathrm{L}}) \Big].\end{aligned} \tag{5.3}$$

Here the scalar potential, both Yukawa couplings and the wave function renormalizations for the different fields Z_ϕ, Z_{L}, $Z_{\mathrm{R_t}}$, and $Z_{\mathrm{R_b}}$ depend on the RG scale k ($U = U_k$, $h_{\mathrm{t}} = h_{\mathrm{t},k}$, $\cdots$). As a remainder, this dependence is suppressed for compactness of notation.

Inserting this truncation into the Wetterich equation leads to the β functions, i.e., the flow equations for the effective potential, the Yukawa couplings as well as for the wave function renormalizations. Again, we encoded the latter in the anomalous dimensions of the fields, $\eta_i = -\partial_t \ln Z_i$, where i labels the different fields.

Dimensionless renormalized quantities are defined accordingly to Eq. (3.20) as

$$\tilde{\rho} = Z_\phi k^{2-d} \phi^\dagger \phi, \qquad h_{\mathrm{t}}^2 = Z_\phi^{-1} Z_{\mathrm{L}}^{-1} Z_{\mathrm{R_t}}^{-1} k^{d-4} \bar{h}_{\mathrm{t}}^2, \qquad h_{\mathrm{b}}^2 = Z_\phi^{-1} Z_{\mathrm{L}}^{-1} Z_{\mathrm{R_b}}^{-1} k^{d-4} \bar{h}_{\mathrm{b}}^2.$$

and the dimensionless potential simply reads, $u = k^{-d} U$. In the following, we list the flow equations for the various quantities, as they follow from the Wetterich equation, using standard calculation techniques. The flow equation for the potential can be written as:

$$\begin{aligned}\partial_t u = & -du + (d - 2 + \eta_\phi)\tilde{\rho} u' + 2v_d \Big[3\, l_0^{(\mathrm{B})d}(u'; \eta_\phi) + l_0^{(\mathrm{B})d}(u' + 2\tilde{\rho} u''; \eta_\phi) \\ & - \frac{d_\gamma}{2} \Big(l_0^{(\mathrm{F})d}(h_{\mathrm{t}}^2 \tilde{\rho}; \eta_{\mathrm{L}}) + l_0^{(\mathrm{F})d}(h_{\mathrm{b}}^2 \tilde{\rho}; \eta_{\mathrm{L}}) + l_0^{(\mathrm{F})d}(h_{\mathrm{t}}^2 \tilde{\rho}; \eta_{\mathrm{R_t}}) + l_0^{(\mathrm{F})d}(h_{\mathrm{b}}^2 \tilde{\rho}; \eta_{\mathrm{R_b}}) \Big) \Big],\end{aligned} \tag{5.4}$$

where primes denote derivatives with respect to $\tilde{\rho}$ and the threshold functions are listed in App. A.3. The diagrammatic interpretation is again in terms of bosonic and fermionic loop diagrams, see Fig. 3.2. This time, we have three scalar loops for the three Goldstone bosons $\sim 3 l_0^{(\mathrm{B})d}(u'; \eta_\phi)$ and one scalar loop $\sim l_0^{(\mathrm{B})d}(u' + 2\tilde{\rho} u''; \eta_\phi)$ for the radial mode as well as four fermion loops, one for each of the four chiral fermions. Using the same regulator shape functions for the two chiral fermions of the same flavor and introducing anomalous dimensions for the corresponding Dirac fermions,

$$\eta_{\mathrm{t}} = \frac{1}{2}(\eta_{\mathrm{L}} + \eta_{\mathrm{R_t}}), \qquad \eta_{\mathrm{b}} = \frac{1}{2}(\eta_{\mathrm{L}} + \eta_{\mathrm{R_b}}), \tag{5.5}$$

the fermionic contribution to the flow equation for the scalar potential can also be written in terms of Dirac fermions

$$\begin{aligned}\partial_t u = & -du + (d - 2 + \eta_\phi)\tilde{\rho} u' \\ & + 2v_d \Big[3\, l_0^{(\mathrm{B})d}(u'; \eta_\phi) + l_0^{(\mathrm{B})d}(u' + 2\tilde{\rho} u''; \eta_\phi) - d_\gamma \Big(l_0^{(\mathrm{F})d}(h_{\mathrm{t}}^2 \tilde{\rho}; \eta_{\mathrm{t}}) + l_0^{(\mathrm{F})d}(h_{\mathrm{b}}^2 \tilde{\rho}; \eta_{\mathrm{b}}) \Big) \Big].\end{aligned}$$

The flow equations for the Yukawa couplings are

$$\begin{aligned}
\partial_t h_{\mathrm{t}}^2 &= (d-4+\eta_\phi+2\eta_{\mathrm{t}})h_{\mathrm{t}}^2 \\
&\quad + 4v_d h_{\mathrm{t}}^4\Big[l_{1,1}^{(\mathrm{FB})d}(\mu_{\mathrm{t}}^2,\mu_{\phi_{\mathrm{R}}}^2;\eta_{\mathrm{t}},\eta_\phi) - l_{1,1}^{(\mathrm{FB})d}(\mu_{\mathrm{t}}^2,\mu_{\phi_{\mathrm{G}}}^2;\eta_{\mathrm{t}},\eta_\phi) \\
&\qquad - 2h_{\mathrm{t}}^2\kappa\Big(l_{2,1}^{(\mathrm{FB})d}(\mu_{\mathrm{t}}^2,\mu_{\phi_{\mathrm{R}}}^2;\eta_{\mathrm{t}},\eta_\phi) - l_{2,1}^{(\mathrm{FB})d}(\mu_{\mathrm{t}}^2,\mu_{\phi_{\mathrm{G}}}^2;\eta_{\mathrm{t}},\eta_\phi)\Big) \\
&\qquad - \Big(6\kappa\, u''(\kappa)+4\kappa^2 u'''(\kappa)\Big)l_{1,2}^{(\mathrm{FB})d}(\mu_{\mathrm{t}}^2,\mu_{\phi_{\mathrm{R}}}^2;\eta_{\mathrm{t}},\eta_\phi) + 2\kappa\, u''(\kappa) l_{1,2}^{(\mathrm{FB})d}(\mu_{\mathrm{t}}^2,\mu_{\phi_{\mathrm{G}}}^2;\eta_{\mathrm{t}},\eta_\phi)\Big] \\
&\quad + 8v_d h_{\mathrm{t}}^2 h_{\mathrm{b}}^2\Big[- l_{1,1}^{(\mathrm{FB})d}(\mu_{\mathrm{b}}^2,\mu_{\phi_{\mathrm{G}}}^2;\eta_{\mathrm{b}},\eta_\phi) + 2h_{\mathrm{b}}^2\kappa l_{2,1}^{(\mathrm{FB})d}(\mu_{\mathrm{b}}^2,\mu_{\phi_{\mathrm{G}}}^2;\eta_{\mathrm{b}},\eta_\phi) \\
&\qquad\qquad + 2\kappa\, u''(\kappa)\, l_{1,2}^{(\mathrm{FB})d}(\mu_{\mathrm{b}}^2,\mu_{\phi_{\mathrm{G}}}^2;\eta_{\mathrm{b}},\eta_\phi)\Big]\Big|_{\tilde\rho=\kappa},
\end{aligned} \tag{5.6}$$

$$\begin{aligned}
\partial_t h_{\mathrm{b}}^2 &= (d-4+\eta_\phi+2\eta_{\mathrm{b}})h_{\mathrm{b}}^2 \\
&\quad + 4v_d h_{\mathrm{b}}^4\Big[l_{1,1}^{(\mathrm{FB})d}(\mu_{\mathrm{b}}^2,\mu_{\phi_{\mathrm{R}}}^2;\eta_{\mathrm{b}},\eta_\phi) - l_{1,1}^{(\mathrm{FB})d}(\mu_{\mathrm{b}}^2,\mu_{\phi_{\mathrm{G}}}^2;\eta_{\mathrm{b}},\eta_\phi) \\
&\qquad - 2h_{\mathrm{b}}^2\kappa\Big(l_{2,1}^{(\mathrm{FB})d}(\mu_{\mathrm{b}}^2,\mu_{\phi_{\mathrm{R}}}^2;\eta_{\mathrm{b}},\eta_\phi) - l_{2,1}^{(\mathrm{FB})d}(\mu_{\mathrm{b}}^2,\mu_{\phi_{\mathrm{G}}}^2;\eta_{\mathrm{b}},\eta_\phi)\Big) \\
&\qquad - \Big(6\kappa\, u''(\kappa)+4\kappa^2 u'''(\kappa)\Big)l_{1,2}^{(\mathrm{FB})d}(\mu_{\mathrm{b}}^2,\mu_{\phi_{\mathrm{R}}}^2;\eta_{\mathrm{b}},\eta_\phi) + 2\kappa\, u''(\kappa) l_{1,2}^{(\mathrm{FB})d}(\mu_{\mathrm{b}}^2,\mu_{\phi_{\mathrm{G}}}^2;\eta_{\mathrm{b}},\eta_\phi)\Big] \\
&\quad + 8v_d h_{\mathrm{t}}^2 h_{\mathrm{b}}^2\Big[- l_{1,1}^{(\mathrm{FB})d}(\mu_{\mathrm{t}}^2,\mu_{\phi_{\mathrm{G}}}^2;\eta_{\mathrm{t}},\eta_\phi) + 2h_{\mathrm{t}}^2\kappa l_{2,1}^{(\mathrm{FB})d}(\mu_{\mathrm{t}}^2,\mu_{\phi_{\mathrm{G}}}^2;\eta_{\mathrm{t}},\eta_\phi) \\
&\qquad\qquad + 2\kappa\, u''(\kappa)\, l_{1,2}^{(\mathrm{FB})d}(\mu_{\mathrm{t}}^2,\mu_{\phi_{\mathrm{G}}}^2;\eta_{\mathrm{t}},\eta_\phi)\Big]\Big|_{\tilde\rho=\kappa},
\end{aligned} \tag{5.7}$$

where κ denotes the minimum of the potential. $\mu_{\phi_{\mathrm{R}}}^2 = u'(\kappa)+2\kappa\, u''(\kappa)$, $\mu_{\phi_{\mathrm{G}}}^2 = u'(\kappa)$, $\mu_{\mathrm{t}}^2 = h_{\mathrm{t}}^2\kappa$, and $\mu_{\mathrm{b}}^2 = h_{\mathrm{b}}^2\kappa$ are the dimensionless renormalized masses of the radial mode, the Goldstone mode, the top quark and the bottom quark, respectively. While the masses of the radial excitation and the Goldstone mode coincide in the SYM regime $\kappa = 0$, the Goldstone mass vanishes in the SSB regime ($u'(\kappa) = 0$) according to the Goldstone theorem. Finally, the anomalous dimensions are given by

$$\begin{aligned}
\eta_\phi &= \frac{8v_d}{d}\kappa\Big[3u''(\kappa)\, m_2^{(\mathrm{B})d}(\mu_{\phi_{\mathrm{G}}}^2;\eta_\phi) + (3u''(\kappa)+2\kappa u'''(\kappa))^2 m_2^{(\mathrm{B})d}(\mu_{\phi_{\mathrm{R}}}^2;\eta_\phi)\Big] \\
&\quad - \frac{4v_d d_\gamma}{d}\Big[\kappa h_{\mathrm{t}}^4 m_2^{(\mathrm{F})d}(\mu_{\mathrm{t}}^2;\eta_{\mathrm{t}}) - h_{\mathrm{t}}^2 m_4^{(\mathrm{F})d}(\mu_{\mathrm{t}}^2;\eta_{\mathrm{t}}) + \kappa h_{\mathrm{b}}^4 m_2^{(\mathrm{F})d}(\mu_{\mathrm{b}}^2;\eta_{\mathrm{b}}) - h_{\mathrm{b}}^2 m_4^{(\mathrm{F})d}(\mu_{\mathrm{b}}^2;\eta_{\mathrm{b}})\Big],
\end{aligned} \tag{5.8}$$

$$\begin{aligned}
\eta_{\mathrm{L}} &= \frac{4v_d}{d}\Big[h_{\mathrm{t}}^2\, m_{1,2}^{(\mathrm{FB})d}(\mu_{\mathrm{t}}^2,\mu_{\phi_{\mathrm{R}}}^2;\eta_{\mathrm{R_t}},\eta_\phi) + h_{\mathrm{t}}^2\, m_{1,2}^{(\mathrm{FB})d}(\mu_{\mathrm{t}}^2,\mu_{\phi_{\mathrm{G}}}^2;\eta_{\mathrm{R_t}},\eta_\phi)\Big) \\
&\qquad + 2h_{\mathrm{b}}^2\, m_{1,2}^{(\mathrm{FB})d}(\mu_{\mathrm{b}}^2,\mu_{\phi_{\mathrm{G}}}^2;\eta_{\mathrm{R_b}},\eta_\phi)\Big],
\end{aligned} \tag{5.9}$$

$$\eta_{\mathrm{R}}^{\mathrm{t}} = \frac{4v_d}{d}h_{\mathrm{t}}^2\Big[m_{1,2}^{(\mathrm{FB})d}(\mu_{\mathrm{t}}^2,\mu_{\phi_{\mathrm{R}}}^2;\eta_{\mathrm{L}},\eta_\phi) + m_{1,2}^{(\mathrm{FB})d}(\mu_{\mathrm{t}}^2,\mu_{\phi_{\mathrm{G}}}^2;\eta_{\mathrm{L}},\eta_\phi) + 2m_{1,2}^{(\mathrm{FB})d}(\mu_{\mathrm{b}}^2,\mu_{\phi_{\mathrm{G}}}^2;\eta_{\mathrm{L}},\eta_\phi)\Big], \tag{5.10}$$

$$\eta_{\mathrm{R}}^{\mathrm{b}} = \frac{4v_d}{d}h_{\mathrm{b}}^2\Big[m_{1,2}^{(\mathrm{FB})d}(\mu_{\mathrm{b}}^2,\mu_{\phi_{\mathrm{R}}}^2;\eta_{\mathrm{L}},\eta_\phi) + m_{1,2}^{(\mathrm{FB})d}(\mu_{\mathrm{b}}^2,\mu_{\phi_{\mathrm{G}}}^2;\eta_{\mathrm{L}},\eta_\phi) + 2m_{1,2}^{(\mathrm{FB})d}(\mu_{\mathrm{t}}^2,\mu_{\phi_{\mathrm{G}}}^2;\eta_{\mathrm{L}},\eta_\phi)\Big]. \tag{5.11}$$

Note that at the present level of our truncation there is an ambiguity in the projection rule

on the scalar anomalous dimension as well as on the anomalous dimension for the left-handed quark. For the anomalous dimension of the scalar field, we could either project on the kinetic operator of the radial or the Goldstone mode. In a similar manner a projection on the kinetic operator of the left-handed top quark or the left-handed bottom quark lead to different flow equations. In this work, we project on the anomalous dimension of the Higgs excitation as well as the top quark due to the fact that these two degrees of freedom are of our primary interest. This ambiguity will be resolved beyond NLO in the derivative expansion. For a sketch of the diagrammatic contributions to these flow equations see Fig. 3.3, with appropriate identifications of the fermionic and bosonic lines with the various particles. The flow equations agree with those for the $\mathbb{Z}_2$-symmetric simple Yukawa model, Sect. 3.3, in the limit of a vanishing bottom sector, $h_\mathrm{b} = 0$, and ignoring the terms arising from the additional scalar contributions. As a further cross-check, we note that our flows also agree with those of [56] for $h_\mathrm{b} = 0$ and upon dropping the gauge sector in that work. The reliability of the derivative expansion is again monitored with the aid of the anomalous dimension, providing a rough measure for the importance of the higher-derivative terms. As in the simple model, we study the convergence of the derivative expansion by comparing leading-order results ($\eta_i = 0$) to the full NLO calculation.

Quantitative results for the Higgs mass bounds in the present chiral Higgs-Yukawa model have been investigated in extensive lattice simulations [117–123] up to cutoff scales of the order of several TeV. The present flow equation study can elucidate the underlying RG mechanisms in more detail and can bridge a wide range of scales. Furthermore, it is straightforward to deal with two distinct quark masses, $h_\mathrm{t} \neq h_\mathrm{b}$, in our functional approach, whereas simulations with the physical ratio $m_\mathrm{t}/m_\mathrm{b} \simeq 40$ are rather expensive on the lattice.

Before we turn to a quantitative analysis of the RG flow, we have to cure a deficiency of the chiral Yukawa model in comparison with the full standard model top-bottom-Higgs sector. Since chiral symmetry breaking in the present model breaks a global symmetry, our present model has massless Goldstone bosons in the physical spectrum. This is different from the standard model where the would-be Goldstone bosons due to their interplay with the gauge sector are ultimately absent from the physical spectrum, the latter finally containing massive vector excitations. In order to make contact with the standard model physics, we therefore have to modify our chiral Yukawa model, otherwise the massless Goldstone modes have the potential to induce an IR behavior which is very different from that of the standard model. This modification of the model is not unique and could be done in various ways. For instance on the lattice, the influence of the unwanted Goldstone bosons is identified by their strong finite volume effects and subtracted accordingly [117, 122]. Similarly, we could study the onset of Goldstone dynamics in the limit $k \to 0$ and perform a similar subtraction.

In the present work, we model the decoupling of Goldstone bosons more physically as inspired by the Higgs mechanism in the fully gauged version of the theory: generically all dependencies on the particle masses and their decoupling is contained in the threshold functions of the flow

equations. For the linear regulators used below, this dependence occurs in the form

$$\frac{k^2}{k^2+m^2} \tag{5.12}$$

to some power. For $k \to 0$, all these functions vanish for finite particle masses m, whereas massless modes such as Goldstone modes with $m = m_{\mathrm{G}} = 0$ contribute equally on all scales k. (For other regulators, the functional dependence on k and m may look differently, but behaves analogously in the various limits.) The Goldstone modes can therefore directly be identified in our flow equations. They contribute to those threshold functions that contain an argument $\sim u'(\rho)$ in the SSB regime. As soon as we enter the broken regime, the corresponding mass argument $m_{\mathrm{G}}^2/k^2 \sim u'(\kappa) = \mu_{\phi_{\mathrm{G}}}^2$ vanishes at the running minimum κ of the potential. We thus can dynamically remove the Goldstone modes by the replacement

$$\frac{k^2}{k^2+m_{\mathrm{G}}^2} \to \frac{k^2}{k^2+m_{\mathrm{G}}^2+\zeta\frac{v_k^2}{2}} \overset{m_{\mathrm{G}}=0}{=} \frac{k^2}{k^2+\zeta\frac{v_k^2}{2}},$$

in the broken regime. Here, v_k is the running vacuum expectation value approaching $v_k \to v$ in the long range limit $k \to 0$, and ζ is an a priori free parameter. Inspired by the decoupling of massive vector bosons in the full standard model, we choose ζ in such a way that the resulting masses for the Goldstone bosons have the same order of magnitude as the W boson mass scale, e.g. $\zeta = 2(80/246)^2$. It turns out that the results for the lower Higgs mass bound is only slightly affected by different choices of ζ, as well as different choices of removing the Goldstone mode contributions, cf. App. A.6.

As a result, all fluctuations acquire a mass in the regime of spontaneous symmetry breaking (SSB) and the whole flow freezes out, similarly to the $\mathbb{Z}_2$ Yukawa model and as expected in the full standard model.

Now that we have amended our model with a dynamical removal of the unwanted Goldstone bosons, the RG flow of the model is technically similar to the simpler $\mathbb{Z}_2$ invariant Yukawa model extensively studied in Chap. 3. In the following, we therefore focus on the new features induced by the additional degrees of freedom of the chiral model such as the bottom quark and the three additional real scalar fields. Further technical details follow those in Chap. 3.

We extract the relevant information to compute Higgs mass bounds from a power series expansion of the potential about its flowing minimum. In the SYM regime, we expand about zero field-amplitude and the expansion point in the SSB regime is set by the nonvanishing vev, see Eq. (3.42). In practice, all results studied in this work converge rather rapidly in this expansion.

5.1.1 Bare potentials of ϕ^4 type

First, we determine mass bounds for the Higgs boson arising from microscopic bare potentials of ϕ^4 type,

$$u_\Lambda = \lambda_{1,\Lambda}\rho + \frac{\lambda_{2,\Lambda}}{2}\rho^2 \quad \text{(SYM)}, \qquad u_\Lambda = \frac{\lambda_{2,\Lambda}}{2}(\rho - \kappa_\Lambda)^2 \quad \text{(SSB)}. \tag{5.13}$$

As a reminder, for small $\lambda_{2,\Lambda}$ a physical flow typically starts in the SYM regime. Near the electroweak scale the system is driven into the SSB regime by fermionic fluctuations. Mathematically speaking, we switch from the flow equations for the SYM to the SSB couplings at the scale, where λ_1 crosses zero. In the SSB regime a nonzero vev builds up, inducing masses for all particles in the theory including the would-be Goldstone bosons as discussed above. This results in a decoupling of all modes in the IR and therefore all dimensionful quantities freeze out.

By contrast: for large $\lambda_{2,\Lambda}$, the theory already starts in the SSB regime with a small value for κ_Λ. The flow still runs over many scales, depending on the initial conditions, until κ eventually grows large near the electroweak scale. As a result, all modes decouple and we can read off the long-range observables.

The flow equations provide us with a map of the UV parameters to physical parameters such as the mass of the Higgs, the top or the bottom quark. In the following, we fine tune either $\lambda_{1,\Lambda}$ if we start in the SYM regime or κ_Λ in the SSB regime, in order to arrive at a vev of $v_{k\to 0} = 246\text{GeV}$ in the IR. Further, we vary the bare top $h_{t,\Lambda}$ and bottom $h_{b,\Lambda}$ Yukawa coupling such that we obtain the desired top and bottom quark mass, $m_\text{t} \simeq 173\text{GeV}$ and $m_\text{b} \simeq 4.2\text{GeV}$. For this reduced class of bare ϕ^4 potentials, the Higgs mass is only a function of the bare quartic coupling $\lambda_{2,\Lambda}$ for a fixed cutoff. In order to start with a well defined theory in the UV, $\lambda_{2,\Lambda}$ must be strictly nonnegative.

Also in the present chiral model, we find that the Higgs mass is a monotonically increasing function of the bare quartic coupling, which can be seen in Fig. 5.1. Here, the Higgs mass m_H is plotted as a function of the bare quartic coupling $\lambda_{2,\Lambda}$ for a fixed cutoff $\Lambda = 10^7\text{GeV}$. The lower bound is approached for $\lambda_{2,\Lambda} \to 0$, where the Higgs mass becomes rather independent of $\lambda_{2,\Lambda}$. This was also shown in lattice simulations [117]. For large bare quartic couplings the Higgs mass reaches a region of saturation. To test the convergence of our expansion and truncation, we plotted the Higgs mass in various approximations in Fig. 5.1. The derivative expansion is tested by comparing leading-order (LO) (dashed lines) to NLO results (solid lines). At LO, we drop the running of the kinetic terms in Eq. (5.3), achieved by setting the anomalous dimensions to zero in the flow equations (5.4) and (5.6)-(5.11). These differ by at most 12% for small as well as for large couplings. The difference for small couplings is somewhat larger than in the $\mathbb{Z}_2$-symmetric Yukawa model due to the additional scalar degrees of freedom.

Furthermore, we varied N_p to check the convergence of the polynomial expansion of the potential. The simplest nontrivial order is given by $N_\text{p} = 2$ and plotted as red lines with

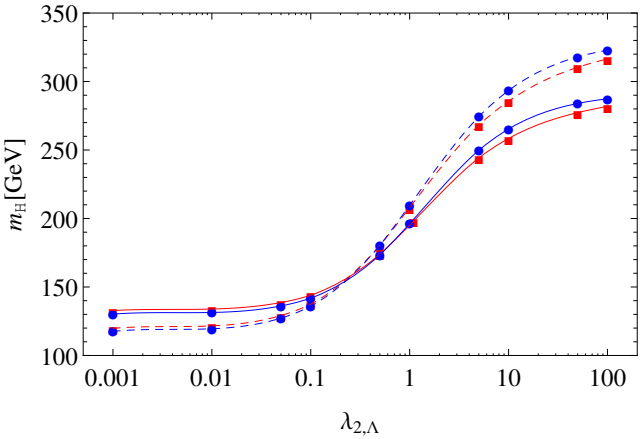

Figure 5.1: Higgs mass $m_{\rm H}$ as a function of the bare quartic coupling $\lambda_{2,\Lambda}$ for fixed cutoff $\Lambda = 10^7$GeV for various approximations. Dashed lines depict leading order results in the derivative expansion while solid lines show the next-to-leading order. Also the convergence of the polynomial truncation of the scalar potential is illustrated. Red lines with squares arise from $N_{\rm p} = 2$ whereas blue lines with circles are derived for $N_{\rm p} = 4$.

squares in Fig. 5.1. For $N_{\rm p} = 4$ (blue lines with circles) there are only small deviations for small $\lambda_{2,\Lambda}$ ($\sim$ 2GeV) and deviations of 5% for large $\lambda_{2,\Lambda}$ compared to $N_{\rm p} = 2$. Beyond this, we find no deviations between the Higgs masses for $N_{\rm p} = 4, 5, 6, 8, 10$ within our numerical accuracy, again demonstrating the remarkable convergence of the polynomial truncation for the present purpose.

In Fig. 5.2, resulting Higgs masses are plotted as a function of the UV cutoff for different bare quartic couplings for a wide range of cutoff values $\Lambda = 10^3, \cdots, 10^9$GeV. The lower black line is derived for $\lambda_{2,\Lambda} = 0$ and indicates a lower bound for $m_{\rm H}$ within the ϕ^4 type bare potentials. Dashed lines depict upper Higgs mass bounds if one restricts the bare quartic coupling to $\lambda_{2,\Lambda} \leq 1, 10, 100$ (from bottom to top). Artificially restricting the coupling $\lambda_{2,\Lambda}$ to the perturbatively accessible domain, say, $\lambda_{2,\Lambda} \lesssim 1$, the upper bound is obviously significantly underestimated.

By comparing the chiral Yukawa model to the simple Yukawa model, we are able to study the influence of the additional standard model degrees of freedom on the Higgs mass bounds. As expected, the bottom quark has no significant influence on the Higgs mass values, due to its substantially smaller Yukawa coupling. Higgs mass values only differ by less than 1 GeV if one neglects the coupling of the bottom to the Higgs. The main new contributions to the scalar potential and thus to the Higgs mass are induced by the additional scalar degrees of freedom. For the lower bound $\lambda_{2,\Lambda} = 0$ the scalar sector is weakly coupled, hence the Higgs mass is mainly built up by top fluctuations (apart from mutual RG backreactions). Therefore, the deviations between the two models are small for the lower Higgs mass bounds. For a strongly coupled scalar sector in the UV, $\lambda_{2,\Lambda} > 1$, the situation is different. There, the additional scalar degrees of freedom have a significantly larger impact. This results in smaller Higgs masses, since scalar fluctuations generically tend to drive the system into the SYM regime. The consequence of this

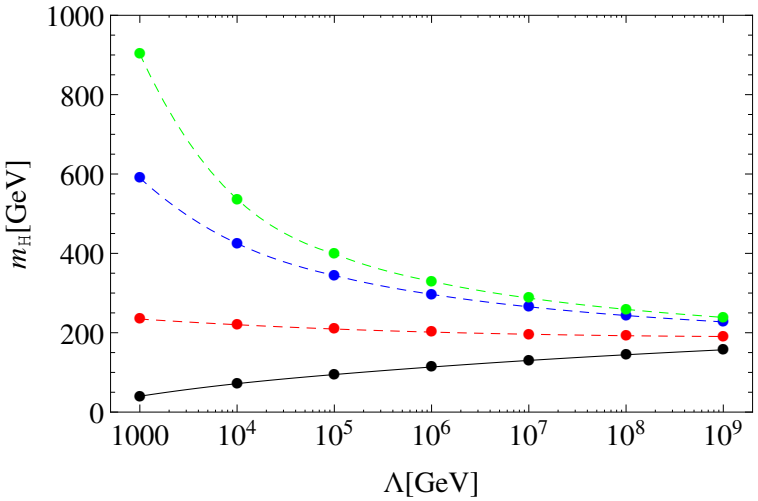

Figure 5.2: Higgs mass m_H as a function of the cutoff Λ for various bare quartic couplings. The black solid line represents a lower mass bound ($\lambda_{2,\Lambda} = 0$) within ϕ^4 theory. Dashed lines depict Higgs masses for $\lambda_{2,\Lambda} = 1, 10, 100$ from bottom to top.

is a flattening of the scalar potential near its minimum and hence a smaller value for the Higgs mass which is visualized in Fig. 5.3.

Finally, we should emphasize once more that the use of standard-model-like parameters is only for the purpose of illustration. The quantitative difference becomes obvious, e.g., from Fig. 5.2 where the "channel" of Higgs mass values that allow for a large cutoff is centered near $m_H \simeq 200$GeV. The same channel-like behavior in the full standard model occurs near $m_H \simeq 130$GeV. This quantitative difference is mainly due to the influence of the gauge sectors. In addition, the electroweak gauge sector can take a conceptually important influence on mass bounds: e.g., recent nonperturbative lattice simulations of the Yang-Mills-Higgs system suggest that the Higgs mass has to be larger than the weak gauge boson masses in certain parameter regimes, otherwise the electroweak sector would rather be in a QCD-like domain [250].

5.1.2 Generalized bare potentials

Motivated by previous continuum calculations in the simple Yukawa model and by lattice studies in the chiral version [125, 126], we study whether more general bare potentials can modify the phenomenologically relevant lower Higgs mass bound. The main purpose of this study is to demonstrate that the mechanism to diminish the lower bound without the occurrence of an in- or metastability of the potential also persists in a model with chiral Higgs-Yukawa structure.

As the RG flow of the parameters and the occurrence of the Higgs mass bounds within the class of ϕ^4 potentials works qualitatively similar to the simple Yukawa model, it is not a big

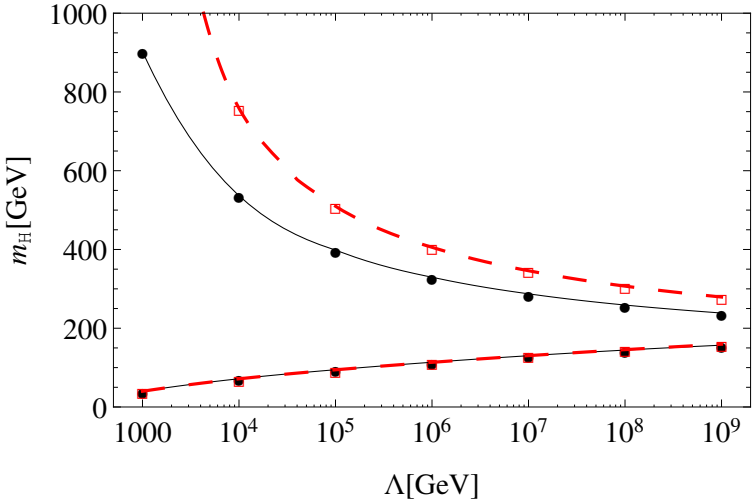

Figure 5.3: Higgs mass m_H as a function of the cutoff Λ for the chiral Higgs-Yukawa model (black solid lines) as well as for the simple $\mathbb{Z}_2$-symmetric Higgs-Yukawa theory (red dashed lines) as studied in [112]. For the lower mass bound no significant difference is observed between the two models. By contrast, a strongly coupled scalar sector ($\lambda_\Lambda = 100$) leads to significantly lower masses in the present model which is a consequence of the additional scalar degrees of freedom in the chiral model, see main text.

surprise that the simplest extension including a ϕ^6 term in the bare potential,

$$u_\Lambda = \lambda_{1,\Lambda}\rho + \frac{\lambda_{2,\Lambda}}{2}\rho^2 + \frac{\lambda_{3,\Lambda}}{6}\rho^3, \tag{5.14}$$

suffices to diminish the lower bound. Negative values for the bare quartic coupling $\lambda_{2,\Lambda}$ are permissible if the potential is stabilized by a positive $\lambda_{3,\Lambda}$. Basically, all mechanisms observed in Chap.3 translate in a direct manner to chiral Higgs-top-bottom model.

In Fig. 5.4 we illustrate this generic feature of generalized bare potentials by a simple example. The black dashed line depicts the lower bound within ϕ^4 theory ($\lambda_{2,\Lambda} = \lambda_{3,\Lambda} = 0$), whereas the red solid line shows Higgs masses for the initial data $\lambda_{2,\Lambda} = -0.1$ and $\lambda_{3,\Lambda} = 3$. This example flow shows that the lower Higgs-mass bound can be significantly relaxed if the restriction to bare potentials of ϕ^4 type is dropped. We emphasize once more that a restriction to renormalizable operators is meaningless for the bare action as Wilsonian renormalizability arguments do not apply to the bare field theory action that might be generated from an unknown underlying UV complete theory.

Analogously to the simple model with a discrete chiral symmetry, this phenomenon of a relaxed bound as a consequence of a modified bare theory can be understood by the RG flow itself, see the discussion in Subsect. 3.5.2. We emphasize that the effective potential is stable at all scales with one well defined minimum for the present choice of parameters. Of course, a further decrease of $\lambda_{2,\Lambda}$ leads to lower Higgs masses than the masses depicted for the example flow in Fig. 5.4 but at the same time a second minimum occurs in the scalar potential during the RG flow, which may render the potential metastable.

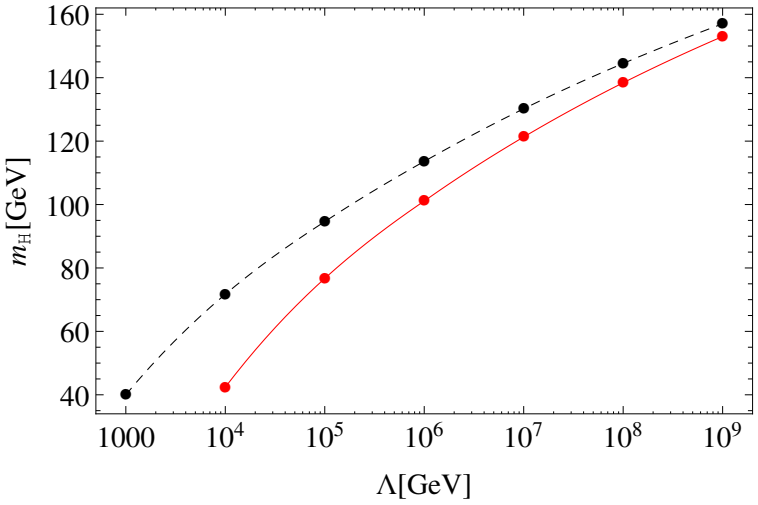

Figure 5.4: Higgs mass m_{H} as a function of the cutoff Λ. The black dashed curve again corresponds to the lower bound derived within the class of ϕ^4-type bare potentials. The red solid line shows an example of Higgs boson mass values derived from a more general class of bare potentials of Eq. (5.14) with the initial UV values $\lambda_{2,\Lambda} = -0.1$ and $\lambda_{3,\Lambda} = 3$. This demonstrates both that the lower bound can be significantly relaxed as well as that no in- or metastability is required for Higgs masses to occur below the conventional lower bound.

5.2 Gauged chiral Higgs-Yukawa model

Along our route to take all standard model degrees of freedom into account, the next step would be to gauge the previous chiral Higgs-top-bottom model under the $\mathrm{SU}(2)_{\mathrm{L}}$ symmetry group. Therefore, we choose the following truncation,

$$\begin{aligned}\Gamma_k = \int_x \Bigg[& \frac{Z_W}{4} W_{i\,\mu\nu} W_i^{\mu\nu} + Z_\phi (D_\mu \phi)^\dagger D^\mu \phi + Z_{\mathrm{L}} \bar{\psi}_{\mathrm{L}} \mathrm{i}\partial\!\!\!/ \psi_{\mathrm{L}} + Z_{\mathrm{R_t}} \bar{t}_{\mathrm{R}} \mathrm{i}\partial\!\!\!/ t_{\mathrm{R}} + Z_{\mathrm{R_t}} \bar{b}_{\mathrm{R}} \mathrm{i}\partial\!\!\!/ b_{\mathrm{R}} \\ & + U(\rho_1, \rho_2) + \mathrm{i}\bar{h}_{\mathrm{b}} (\bar{\psi}_{\mathrm{L}} \phi b_{\mathrm{R}} + \bar{b}_{\mathrm{R}} \phi^\dagger \psi_{\mathrm{L}}) + \mathrm{i}\bar{h}_{\mathrm{t}} (\bar{\psi}_{\mathrm{L}} \phi_{\mathrm{c}} t_{\mathrm{R}} + \bar{t}_{\mathrm{R}} \phi_{\mathrm{c}}^\dagger \psi_{\mathrm{L}}) \\ & + \frac{Z_W}{2\xi} C_i^\dagger C_i + Z_c \bar{c}_i \mathcal{M}_{ij} c_j \Bigg],\end{aligned} \tag{5.15}$$

where the gauge-fixing condition is constructed such that the mixing terms between the longitudinal gauge bosons and the would-be Goldstone bosons cancel, see App. A.1,

$$C_i = \partial_\mu W_i^\mu - \frac{i\xi g v}{\sqrt{2}} (n^\dagger t_i \varphi - \varphi^\dagger t_i n), \tag{5.16}$$

where n is a unit vector ($n^\dagger n = 1$) pointing into the direction of the vev and φ are the scalar excitations around the vev, $\phi = \frac{v}{\sqrt{2}} n + \varphi$. Note, that this gauge-fixing condition also explicitly breaks the global O(4) symmetry of the pure scalar part of the action (5.15) due to the fact that the Goldstone modes acquire a nonvanishing mass in the SSB regime which is proportional to the gauge-fixing parameter ξ. Thus, the potential will depend on two field invariants in general, $U = U(\rho_1, \rho_2)$. These invariants may be given by the square of the scalar

field in radial direction and the sum of the squared Goldstone modes. For instance, for a parametrization according to Eq. (5.1) and a vev pointing into the real direction of the second component of the scalar doublet, $n^a = \delta^{a2}$, we have $\rho_1 \equiv \frac{1}{4}(n^\dagger\phi + \phi^\dagger n)^2 = \frac{1}{2}\phi_4^2 = \frac{1}{2}(v+\varphi_4)^2$ and $\rho_2 = \phi^\dagger\phi - \rho_1 = \frac{1}{2}(\phi_1^2 + \phi_2^2 + \phi_3^2) = \frac{1}{2}(\varphi_1^2 + \varphi_2^2 + \varphi_3^2)$. However, the original symmetry will be restored either in the SYM regime or in case of the Landau gauge where the Goldstone bosons remain massless.

Similar to our studies of the Higgs-top-QCD model, we will consider the running of the renormalized dimensionless $\mathrm{SU}(2)_\mathrm{L}$ gauge coupling g on a perturbative level,

$$\partial_t g^2 = -\frac{g^4}{8\pi^2}\frac{19}{6} \equiv g^2\eta_\mathrm{W}. \tag{5.17}$$

Note, that we also take contributions from all fermions into account in order to get a standard model like phenomenology. We ignored the gauge-invariant kinetic terms of these particles in our present truncation (5.15) as their contributions to the running scalar sector can be neglected. As we do not include threshold effects in the flow equation of g, its running value will not freeze out in the IR. We fix its initial value by the standard requirement $m_\mathrm{W} = \frac{1}{2}g(k = m_\mathrm{W})v$. In principle, it is also possible to investigate the running of g on a nonperturbative level in order to include threshold effects as it was discussed in [56]. Indeed, it turns out that this improvement has a negligible quantitative influence. Note that all three weak gauge bosons in this model acquire the same mass as we do not consider the the $\mathrm{U}(1)_\mathrm{Y}$ gauge group which is responsible for the mass shift between the W and Z boson.

Nonetheless, we will treat the flow equations for the matter contend on a nonperturbative level and derive the flow equations for the scalar potential, the Yukawa couplings as well as the anomalous dimensions of the scalar and fermion fields for arbitrary gauge-fixing parameter ξ. Although, ξ will be a scale dependent parameter, we only consider a truncation in which ξ is independent of the RG scale k for simplicity.

The flow equation for the scalar potential within arbitrary R_ξ gauge is a rather intricate object due to the complex interplay between the Higgs field, the Goldstone modes, weak gauge bosons, and the ghost fields. However it turns out, that the flow equation simplifies enormously by considering one of two different limits. In the limit of the Landau gauge ($\xi \to 0$), the longitudinal parts of the gauge bosons will be removed, the Goldstone bosons are massless and thus the potential can be written in terms of a single invariant $\rho = \rho_1 + \rho_2 = \phi^\dagger\phi$ and the ghost fields do not couple to the scalar field as the ghost-scalar vertex is $\sim \xi$. Hence, the flow equation for the potential in Landau gauge reads,

$$\partial_t u = (\text{rhs. of Eq.(5.3)}) + (d-1)3\, l_0^{(\mathrm{B})d}\Big(\frac{g^2}{2}\tilde{\rho}; \eta_\mathrm{W}\Big) \tag{5.18}$$

where an additional term describing the contribution from a pure (transversal) gauge boson loop occurs. We have again omitted unimportant constant contributions to this flow equation.

On the other hand it is even more surprising, that we are also able to take the limit $\xi \to \infty$ in the SSB regime, which corresponds to the unitary gauge. While there is a prove of concept that it is in principle possible to perform perturbative calculations on a quantum level within the unitary gauge [251–254], the computations are rather intricate and are plagued by a multitude of infinities in intermediate steps such that it is even more convenient to choose a manifestly renormalizable gauge [255, 256]. However, the unitary gauge has the main advantage that it projects onto the physical degrees of freedom in a theory with hidden gauge symmetries. The fact that we are able to properly take the limit $\xi \to \infty$ is connected to the fact that the FRG also takes care of threshold effects. Taking first the limit to the deep Euclidean region and afterwards the limit to the unitary gauge leads in fact to ill-defined quantities within our truncation, for instance, the anomalous dimension of the scalar field diverges. However, taking first the limit $\xi \to \infty$, with the full threshold information provided by the FRG, everything remains finite. Thus we can finally write the following expression for the flow equation of the scalar potential in the unitary gauge,

$$\begin{aligned}\partial_t u = -du + (d-2+\eta_\phi)\tilde{\rho}_1 u' + 2v_d\Big[&l_0^{(\mathrm{B})d}(u' + 2\tilde{\rho}_1 u''; \eta_\phi) + (d-1)3\, l_0^{(\mathrm{B})d}\Big(\frac{g^2}{2}\tilde{\rho}_1; \eta_\mathrm{W}\Big) \\ &- \frac{d_\gamma}{2}\Big(l_0^{(\mathrm{F})d}(h_\mathrm{t}^2\tilde{\rho}_1; \eta_\mathrm{L}) + l_0^{(\mathrm{F})d}(h_\mathrm{b}^2\tilde{\rho}_1; \eta_\mathrm{L}) + l_0^{(\mathrm{F})d}(h_\mathrm{t}^2\tilde{\rho}_1; \eta_{\mathrm{R}_\mathrm{t}}) + l_0^{(\mathrm{F})d}(h_\mathrm{b}^2\tilde{\rho}_1; \eta_{\mathrm{R}_\mathrm{b}})\Big)\Big].\end{aligned} \tag{5.19}$$

Note that, for instance, the contribution from the Goldstone bosons in Eq. (5.18) (correspondingly Eq. (5.4)) is removed due to the fact that the Goldstone modes acquire an infinitely large mass in this limit and therefore decouple from the spectrum. This also explains the fact, that the arguments of the threshold functions only include the radial direction which points along the direction of the vev.

The flow equations for the Yukawa couplings are given by,

$$\begin{aligned}\partial_t h_\mathrm{t}^2 = (\text{rhs. of Eq.(5.5)}) - 2v_d h_\mathrm{t}^2 g^2 \xi\Big[&m_{1,1,1}^{(\mathrm{FBB})d}(\mu_\mathrm{t}^2, \mu_\phi^2, \xi\mu_\mathrm{W}^2; \eta_\mathrm{L}, \eta_\phi, \eta_\mathrm{W}) \\ &+ 2m_{1,1,1}^{(\mathrm{FBB})d}(\mu_\mathrm{b}^2, \mu_\phi^2, \xi\mu_\mathrm{W}^2; \eta_\mathrm{L}, \eta_\phi, \eta_\mathrm{W})\Big],\end{aligned} \tag{5.20}$$

$$\begin{aligned}\partial_t h_\mathrm{b}^2 = (\text{rhs. of Eq.(5.6)}) - 2v_d h_\mathrm{b}^2 g^2 \xi\Big[&m_{1,1,1}^{(\mathrm{FBB})d}(\mu_\mathrm{b}^2, \mu_\phi^2, \xi\mu_\mathrm{W}^2; \eta_\mathrm{L}, \eta_\phi, \eta_\mathrm{W}) \\ &+ 2m_{1,1,1}^{(\mathrm{FBB})d}(\mu_\mathrm{t}^2, \mu_\phi^2, \xi\mu_\mathrm{W}^2; \eta_\mathrm{L}, \eta_\phi, \eta_\mathrm{W})\Big].\end{aligned} \tag{5.21}$$

Note that the additional contributions here vanish either in the limit of the Landau gauge or the unitary gauge. This is because in the corresponding triangle diagrams a Goldstone boson as well as a longitudinal gauge boson occurs due to the vertex structure of the theory. In the Landau gauge the longitudinal gauge boson is removed while in the unitary gauge the Goldstone boson decouples. In a similar manner the flow equations of the anomalous dimensions for the

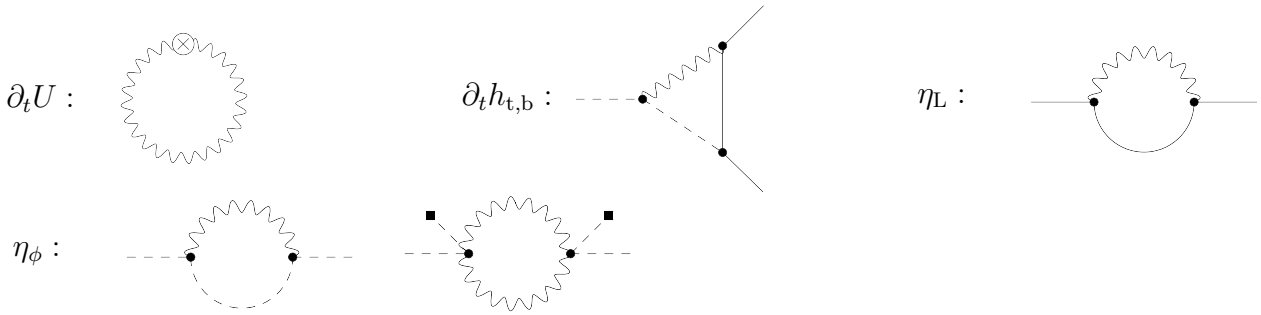

Figure 5.5: Additional diagrammatic contributions to the running of the scalar potential, the Yukawa couplings as well as the anomalous dimension of the fermion and the scalar field. Wiggled lines depict weak gauge bosons. For compactness, we again suppress the regulator insertions for the loop diagrams of $h_{\mathrm{t,b}}$, η_ϕ and η_{L}.

scalar field as well as for the left-handed chiral fermions can be considered. They read,

$$\begin{aligned}
\eta_\phi = (\text{rhs. of Eq.(5.7)}) &+ \frac{6v_d}{d} g^4 \kappa \Big[(d-1) m_2^{(\mathrm{B})d}(\mu_{\mathrm{W}}^2; \eta_{\mathrm{W}}) + \xi m_2^{(\mathrm{B})d}(\xi\mu_{\mathrm{W}}^2; \eta_{\mathrm{W}}) \\
&+ 4(d-1)\tilde{m}_2^{(\mathrm{B})d}(\mu_{\mathrm{W}}^2; \eta_{\mathrm{W}}) + 4(d-1)\xi^2 \tilde{m}_2^{(\mathrm{B})d}(\xi\mu_{\mathrm{W}}^2; \eta_{\mathrm{W}}) \Big] \\
&+ \frac{6v_d}{d} g^2 \Big[-2(d-1) l_{1,1}^{(\mathrm{BB})d}(\mu_{\phi_{\mathrm{G}}}^2, \mu_{\mathrm{W}}^2; \eta_\phi, \eta_{\mathrm{W}}) - 2\xi l_{1,1}^{(\mathrm{BB})d}(\mu_{\phi_{\mathrm{G}}}^2, \xi\mu_{\mathrm{W}}^2; \eta_\phi, \eta_{\mathrm{W}}) \\
&+ \xi m_{4,4}^{(\mathrm{BB})d}(\mu_{\phi_{\mathrm{G}}}^2, \xi\mu_{\mathrm{W}}^2; \eta_\phi, \eta_{\mathrm{W}}) - 3\xi m_{2,1}^{(\mathrm{BB})d}(\mu_{\phi_{\mathrm{G}}}^2, \xi\mu_{\mathrm{W}}^2; \eta_\phi, \eta_{\mathrm{W}}) \Big] \\
&- \frac{3v_d}{d} g^4 \kappa \xi^2 \, m_2^{(\mathrm{B})d}(\xi\mu_{\mathrm{W}}^2; \eta_c),
\end{aligned} \tag{5.22}$$

and

$$\begin{aligned}
\eta_{\mathrm{L}} = (\text{rhs. of Eq.(5.8)}) &+ \frac{2v_d}{d} g^2 \Big[(d-1) \Big(m_{1,2}^{(\mathrm{FB})d}(\mu_{\mathrm{t}}^2, \mu_{\mathrm{W}}^2; \eta_{\mathrm{L}}, \eta_{\mathrm{W}}) - \tilde{m}_{1,1}^{(\mathrm{FB})d}(\mu_{\mathrm{t}}^2, \mu_{\mathrm{W}}^2; \eta_{\mathrm{L}}, \eta_{\mathrm{W}}) \\
&\quad + 2m_{1,2}^{(\mathrm{FB})d}(\mu_{\mathrm{b}}^2, \mu_{\mathrm{W}}^2; \eta_{\mathrm{L}}, \eta_{\mathrm{W}}) - 2\tilde{m}_{1,1}^{(\mathrm{FB})d}(\mu_{\mathrm{b}}^2, \mu_{\mathrm{W}}^2; \eta_{\mathrm{L}}, \eta_{\mathrm{W}}) \Big) \\
&\quad - \xi \Big(m_{1,2}^{(\mathrm{FB})d}(\mu_{\mathrm{t}}^2, \mu_{\mathrm{W}}^2; \eta_{\mathrm{L}}, \eta_{\mathrm{W}}) - (d-1)\tilde{m}_{1,1}^{(\mathrm{FB})d}(\mu_{\mathrm{t}}^2, \mu_{\mathrm{W}}^2; \eta_{\mathrm{L}}, \eta_{\mathrm{W}}) \\
&\quad + 2m_{1,2}^{(\mathrm{FB})d}(\mu_{\mathrm{b}}^2, \mu_{\mathrm{W}}^2; \eta_{\mathrm{L}}, \eta_{\mathrm{W}}) - 2(d-1)\tilde{m}_{1,1}^{(\mathrm{FB})d}(\mu_{\mathrm{b}}^2, \mu_{\mathrm{W}}^2; \eta_{\mathrm{L}}, \eta_{\mathrm{W}}) \Big) \Big].
\end{aligned} \tag{5.23}$$

Note that the anomalous dimensions of the right-handed fermions do not change because they transform trivially under $\mathrm{SU}(2)_{\mathrm{L}}$ and thus are not affected by additional contributions. They are given in Eq. (5.10) and Eq (5.11).

As we have argued in the previous section, massless Goldstone bosons lead to an artificial log-like running in the deep IR. This problem can be avoided within the class of R_ξ gauges by choosing a finite ξ such that the Goldstone fluctuations become massive and freeze out. In addition, our FRG calculation also allows to choose the unitary gauge in the SSB regime such

that all unphysical degrees of freedom are removed from the theory. In order to investigate Higgs masses in the present gauged chiral Higgs-Yukawa theory we proceed as follows: in the case that the theory is in the symmetric regime, we perform the calculations in the Landau gauge. If a nonzero vev builds up, we switch to the unitary gauge at a certain scale. This scale is chosen dynamically by the condition that the dimensionless flowing minima κ exceeds a certain value κ_{s}. Within the unitary gauge all particles in the theory become massive and thus the nonperturbative flow equations freeze out in the IR. Though, the Higgs mass depends on κ_{s} and is in that sense gauge dependent.

This is due to the fact that, the considered flow equations are gauge depend, as is not a big surprise because β functions are off-shell quantities and therefore can depend on the gauge-fixing parameter. However, the way how we extract "physical" quantities from these β functions within our truncations imply, that also our results will be gauge-dependent because we only consider gauge-dependent elementary degrees of freedom and do not determine gauge invariant bound states. Nonetheless, in perturbation theory the same strategy yields very convincing results. The FMS mechanism provides an explanation for this equivalence by relating the pole structure of a propagator of a gauge-invariant bound state to a corresponding gauge-dependent degree of freedom [207, 257]. Recent lattice simulations indicate that this mechanism also holds on a nonperturbative level [208, 250, 258], at least for Higgs masses larger than the mass of the W boson m_{W}. Moreover, this mechanism may be further used to constrain new theories beyond the standard model [259, 260].

In this sense, we test how gauge artifacts affect our results by varying κ_{s}. Choosing values for κ_{s} of $\mathcal{O}(1)$, the resulting Higgs masses are negligibly affected by this variation. Choosing rather extreme conditions, i.e. close to the SYM regime $\kappa < \frac{1}{10}$ or deep in the SSB regime $\kappa > 10$ where the Landau gauge does not describe the physical degrees of freedom in an appropriate manner, the change in the Higgs mass will be rather large. In practice, we apply a minimum sensitivity criterion. For given initial conditions at a given cutoff, we choose κ_{s} such that the variation in the Higgs mass is minimized by varying κ_{s}.

As a result, the theory behaves like all other toy models before. We find a finite IR window of allowed Higgs masses within the class of ϕ^4 bare potentials where the lower bound is given by the consistency condition $\lambda_{2,\Lambda} \geq 0$. Moreover, we are able to get Higgs masses below this lower consistency bound by allowing for generalized bare potentials without necessarily introducing a metastable minimum. Such an example is depicted in Fig. 5.6. Note that it is straightforward to incorporate the flow equations derived within this section with the flow equations of Sect. 4.1 because the $\mathrm{SU}(3)_{\mathrm{c}}$ structure does not interfere with the elecroweak structure. Hence, the masses derived in Fig. 5.6 already contain the modifications of the QCD sector.

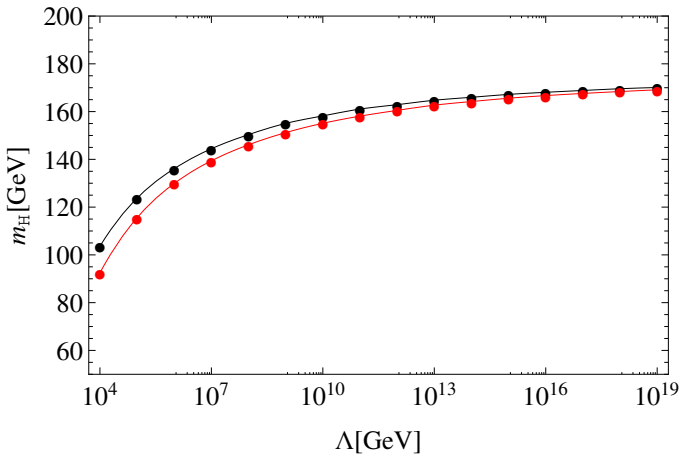

Figure 5.6: Higgs mass as a function of the cutoff. The black curve shows the lower Higgs mass bound within the ϕ^4-type bare potentials for the gauged chiral Higgs-Yukawa model which also includes $\mathrm{SU}(3)_\mathrm{c}$ corrections. The red curve depicts an example flow for Higgs masses with completely stable potentials during the entire RG flow by choosing $\lambda_{3,\Lambda} = 3$ and $\lambda_{2,\Lambda} = -0.1$.

5.3 Flow equation for the standard-model Higgs potential

Within all investigated toy models for the standard model Higgs sector, we observed a consistent picture on the occurrence of Higgs mass bounds resulting from the nonperturbative renormalization group flow. The remaining task is to generalize these considerations to the RG flow equations of the full standard model of particle physics. We use this final section to list the nonperturbative RG flow equations for the scalar sector of the standard model using a derivative expansion of the standard model action (2.1) but taking only the contributions of the two heaviest fermions on the running of the scalar sector into account.

The flow equation for the standard model Higgs potential in the Landau gauge reads,

$$\begin{aligned}\partial_t u = &-du + (d-2+\eta_\phi)\tilde{\rho}u' + 2v_d\Big[3\,l_0^{(\mathrm{B})d}(u';\eta_\phi) + l_0^{(\mathrm{B})d}(u'+2\tilde{\rho}u'';\eta_\phi)\\ &- \frac{d_\gamma}{2}N_\mathrm{c}\Big(l_0^{(\mathrm{F})d}(h_\mathrm{t}^2\tilde{\rho};\eta_\mathrm{L}) + l_0^{(\mathrm{F})d}(h_\mathrm{b}^2\tilde{\rho};\eta_\mathrm{L}) + l_0^{(\mathrm{F})d}(h_\mathrm{t}^2\tilde{\rho};\eta_{\mathrm{R_t}}) + l_0^{(\mathrm{F})d}(h_\mathrm{b}^2\tilde{\rho};\eta_{\mathrm{R_b}})\Big)\\ &+ (d-1)\Big(2l_0^{(\mathrm{B})d}\Big(\frac{g^2}{2}\tilde{\rho};\eta_\mathrm{W}\Big) + l_0^{(\mathrm{B})d}\Big(\frac{g^2+g'^2}{2}\tilde{\rho};\eta_\mathrm{Z}\Big) + l_0^{(\mathrm{B})d}(0;\eta_\mathrm{A})\Big)\Big]\end{aligned} \tag{5.24}$$

where we have used the convenient choice of using the same regulator functions for the degenerate W bosons as well as the B boson and that we can introduce the anomalous dimension of the Z boson η_Z and the anomalous dimension of the Photon η_A via the anomalous dimensions of the $\mathrm{SU}(2)_\mathrm{L}$ bosons η_W and $\mathrm{U}(1)_\mathrm{Y}$ boson η_B according to

$$\eta_\mathrm{Z} = \frac{g^2\eta_\mathrm{W} + g'^2\eta_\mathrm{B}}{g^2+g'^2}, \qquad \eta_\mathrm{A} = \frac{g'^2\eta_\mathrm{W} + g^2\eta_\mathrm{B}}{g^2+g'^2}. \tag{5.25}$$

The flow equation for the scalar anomalous dimension in the Landau gauge is given by

$$\begin{aligned}\eta_\phi = {}& \frac{8v_d}{d}\kappa\Big[3u''(\kappa)\, m_2^{(\mathrm{B})d}(\mu_{\phi_\mathrm{G}}^2;\eta_\phi) + (3u''(\kappa)+2\kappa u'''(\kappa))^2 m_2^{(\mathrm{B})d}(\mu_{\phi_\mathrm{R}}^2;\eta_\phi)\Big] \\ & - \frac{4v_d d_\gamma}{d} N_\mathrm{c}\Big[\kappa h_\mathrm{t}^4 m_2^{(\mathrm{F})d}(\mu_\mathrm{t}^2;\eta_\mathrm{t}) - h_\mathrm{t}^2 m_4^{(\mathrm{F})d}(\mu_\mathrm{t}^2;\eta_\mathrm{t}) + \kappa h_\mathrm{b}^4 m_2^{(\mathrm{F})d}(\mu_\mathrm{b}^2;\eta_\mathrm{b}) - h_\mathrm{b}^2 m_4^{(\mathrm{F})d}(\mu_\mathrm{b}^2;\eta_\mathrm{b})\Big] \\ & + \frac{2v_d(d-1)}{d}\kappa\Big[2g^4\Big(m_2^{(\mathrm{B})d}(\mu_\mathrm{W}^2;\eta_\mathrm{W}) + 4\tilde{m}_2^{(\mathrm{B})d}(\mu_\mathrm{W}^2;\eta_\mathrm{W})\Big) \\ & \qquad + (g^2+g'^2)^2\Big(m_2^{(\mathrm{B})d}(\mu_\mathrm{Z}^2;\eta_\mathrm{Z}) + 4\tilde{m}_2^{(\mathrm{B})d}(\mu_\mathrm{Z}^2;\eta_\mathrm{Z})\Big)\Big] \\ & - \frac{4v_d(d-1)}{d}\Big[2g^2 l_{1,1}^{(\mathrm{BB})d}(\mu_{\phi_\mathrm{G}}^2,\mu_\mathrm{W}^2;\eta_\phi,\eta_\mathrm{W}) + (g^2+g'^2) l_{1,1}^{(\mathrm{BB})d}(\mu_{\phi_\mathrm{G}}^2,\mu_\mathrm{Z}^2;\eta_\phi,\eta_\mathrm{Z})\Big],\end{aligned} \tag{5.26}$$

where $\mu_\mathrm{Z}^2 = \frac{1}{2}(g^2+g'^2)\kappa$. Note that the perturbative one-loop β function for the quartic self-coupling λ_2 (2.8) can be obtained from this flow equation by investigating the deep Euclidean region as well as neglecting resummation effects. In a similar manner to the previous section also these flow equations can be obtained in the unitary gauge in the SSB regime, which read

$$\begin{aligned}\partial_t u = {}& -du + (d-2+\eta_\phi)\tilde{\rho}_1 u' + 2v_d\Big[l_0^{(\mathrm{B})d}(u'+2\tilde{\rho}_1 u'';\eta_\phi) \\ & - \frac{d_\gamma}{2} N_\mathrm{c}\Big(l_0^{(\mathrm{F})d}(h_\mathrm{t}^2\tilde{\rho}_1;\eta_\mathrm{L}) + l_0^{(\mathrm{F})d}(h_\mathrm{b}^2\tilde{\rho}_1;\eta_\mathrm{L}) + l_0^{(\mathrm{F})d}(h_\mathrm{t}^2\tilde{\rho}_1;\eta_{\mathrm{R}_\mathrm{t}}) + l_0^{(\mathrm{F})d}(h_\mathrm{b}^2\tilde{\rho}_1;\eta_{\mathrm{R}_\mathrm{b}})\Big) \\ & + (d-1)\Big(2l_0^{(\mathrm{B})d}\Big(\frac{g^2}{2}\tilde{\rho}_1;\eta_\mathrm{W}\Big) + l_0^{(\mathrm{B})d}\Big(\frac{g^2+g'^2}{2}\tilde{\rho}_1;\eta_\mathrm{Z}\Big) + l_0^{(\mathrm{B})d}(0;\eta_\mathrm{A})\Big)\Big],\end{aligned} \tag{5.27}$$

and

$$\begin{aligned}\eta_\phi = {}& \frac{8v_d}{d}\kappa\Big[3u''(\kappa)\, m_2^{(\mathrm{B})d}(\mu_{\phi_\mathrm{G}}^2;\eta_\phi) + (3u''(\kappa)+2\kappa u'''(\kappa))^2 m_2^{(\mathrm{B})d}(\mu_{\phi_\mathrm{R}}^2;\eta_\phi)\Big] \\ & - \frac{4v_d d_\gamma}{d}\Big[\kappa h_\mathrm{t}^4 m_2^{(\mathrm{F})d}(\mu_\mathrm{t}^2;\eta_\mathrm{t}) - h_\mathrm{t}^2 m_4^{(\mathrm{F})d}(\mu_\mathrm{t}^2;\eta_\mathrm{t}) + \kappa h_\mathrm{b}^4 m_2^{(\mathrm{F})d}(\mu_\mathrm{b}^2;\eta_\mathrm{b}) - h_\mathrm{b}^2 m_4^{(\mathrm{F})d}(\mu_\mathrm{b}^2;\eta_\mathrm{b})\Big] \\ & + \frac{2v_d(d-1)}{d}\kappa\Big[2g^4\Big(m_2^{(\mathrm{B})d}(\mu_\mathrm{W}^2;\eta_\mathrm{W}) + 4\tilde{m}_2^{(\mathrm{B})d}(\mu_\mathrm{W}^2;\eta_\mathrm{W})\Big) \\ & \qquad + (g^2+g'^2)^2\Big(m_2^{(\mathrm{B})d}(\mu_\mathrm{Z}^2;\eta_\mathrm{Z}) + 4\tilde{m}_2^{(\mathrm{B})d}(\mu_\mathrm{Z}^2;\eta_\mathrm{Z})\Big)\Big].\end{aligned} \tag{5.28}$$

Together with flow equations for the Yukawa couplings, the anomalous dimensions of the fermion fields and the gauge bosons as well as the flow equations of the gauge couplings, these flow equations open the door to a nonperturbative study of the full standard model Higgs sector. As demonstrated in this thesis upper and lower mass bounds for the Higgs boson can be obtained within the standard class of ϕ^4-type bare potentials. Taking higher order operators on the standard model cutoff scale into account the lower bound can be diminished. An intensive study of these flow equations could tackle various problems beyond perturbation theory.

6 Conclusions and Outlook

In this thesis we have analyzed the properties of scalar effective potentials and determined Higgs mass bounds in various toy models which feature different aspects of the full standard model Higgs sector. Starting from a simple Yukawa model, sharing some similarities with the standard model Higgs–top-quark sector, we successively increased the field content by investigating corrections from the QCD-sector as well as an extension to the chiral structure of the Higgs-Yukawa sector. Finally, we presented a nonperturbative flow equation for the full standard model Higgs potential at next-to-leading order in a derivative expansion.

Our study is based on the functional renormalization group which can keep track of threshold phenomena, has better access to strong coupling regimes, and automatically accounts for "RG improvement". Most importantly for the present work, the functional RG can conveniently deal with arbitrary bare potentials. In agreement with the standard literature, the existence of an upper Higgs mass bound is a consequence of triviality of the scalar sector. As such, it is inherently non-universal.

We have critically re-examined conventional perturbative arguments that relate a lower bound for the Higgs mass with the stability of the effective potential. Based on exact results for the regularized fermion determinant, we have shown that the interacting part of the fermion determinant contributes strictly positively to the effective scalar potential for any finite field value, as long as the UV cutoff Λ is kept finite. We have shown that this result holds for a variety of regularization schemes including a general class of arbitrary smooth cutoff shape functions in momentum space as well as (gauge-invariant) ζ-function/proper-time regularization schemes.

Furthermore, we have shown that the conventional perturbative conclusion of a vacuum in-/metastability of the effective potential due to top-fluctuations can be rediscovered if the cutoff is forced to approach infinity together with standard ad hoc recipes to project onto the finite parts. For the example of the sharp cutoff, we have shown explicitly that this corresponds to an illegitimate order of limits, as the resulting instability occurs at scalar field values where the supposedly small expansion parameter of the $\Lambda \to \infty$ limit is actually of order one. A similar failure occurs for dimensional regularization where the standard procedures of projecting onto the finite parts violate the positivity properties of the interacting part of the effective potential. Our findings corroborate earlier results from nonperturbative lattice simulations [107, 108], but in addition allow for a large separation of the UV cutoff from the Fermi scale and an analytic control of the corresponding limits.

Because of the presumable triviality of the present model as well as the Higgs sector of the full

standard model, the cutoff most likely cannot be removed from the theory, at least not within a straightforward manner. The cutoff as well as a corresponding regularization scheme should rather be viewed as part of the definition of our particle physics models that parametrize the embedding of this field-theory description into a possibly UV complete theory. Still, as long as the cutoff is large compared to the Fermi scale, Wilsonian renormalization arguments guarantee that the low-energy observables are largely insensitive to the details of this embedding. We have demonstrated that a counter-example to this generic rule is given by bounds on the mass of the Higgs boson.

In this work, we have not performed an exhaustive analysis of different bare actions or potentials, but simply focused on a constructive example that leads to Higgs boson masses below the conventional lower bound and are not plagued by a vacuum in-/metastability problem. This together with our basic line of argument involving exact results for the fermion determinant demonstrate that there is no reason for concern arising from top-quark fluctuations as far as false vacuum decay in our universe is concerned, despite the comparatively light value of the measured Higgs mass. This does not mean that there might be no reason for concern at all. For instance, if the bare scalar potential itself features an instability induced by the underlying UV complete theory, our standard model could still live in an un- or metastable vacuum. Our arguments only exclude instabilities caused by the fluctuations of the fermionic matter fields within the standard model.

Our results suggest a revision of the standard picture of Higgs mass bounds as a function of the UV cutoff. Depending on the implicit assumptions made to derive mass bounds, this revision might be more or less significant. From our results on fermion determinants, it is clear that the conventional interpretation that top-quark fluctuations induce a vacuum instability is not tenable, but a result of taking an inconsistent $\Lambda \to \infty$ limit. Still, the top-quark fluctuations play, of course, a decisive role for the value of the Higgs mass. In order to reconcile these observations, we propose a UV-to-IR viewpoint: the Higgs mass bounds should be understood as a mapping from initial conditions set at the UV cutoff given in terms of a microscopic bare action S_Λ onto all IR values accessible by the RG flow of the system, $m_\mathrm{H} = m_\mathrm{H}[\Lambda; S_\Lambda]$. In this manner, Higgs mass bounds arise from consistency conditions imposed on the bare action. For instance, in order to start from a well-defined (Euclidean) partition function, the action needs to be bounded from below.

The conventional vacuum stability bounds then are approximately equivalent to such a consistency bound arising within a restricted class of bare actions, e.g., bare potentials of ϕ^4 type; here, the bare ϕ^4 coupling is required to be positive for consistency of the generating functional. However, as the bare action is not at our disposal but generally a result of the underlying UV embedding, there is no reason to make such restrictive assumptions. Already for slightly more general bare actions, we have been able to show that the conventional lower mass bounds can be substantially relaxed in all presented toy models. The reason is that a more general bare action can modify the RG flow near and below the cutoff. As a result, the consistency bound

of these generalized bare potentials lies below the vacuum stability bound. In particular, we have given an explicit example with a Higgs boson mass below the "stability bound" but an in fact stable effective potential on all scales; our results are in agreement with lattice simulations [125] and extend them to a much wider range of scales.

Determining the consistency bound remains an open problem, the solution of which requires further assumptions. One natural but not necessary assumption could be that the effective action should feature a unique minimum on all scales. The consistency bound then arise from a complicated extremization problem in the space of all consistent bare actions subject to the unique-minimum constraint (to be satisfied on all scales).

We demonstrated how such a consistency bound in the class of ϕ^6 bare potentials arises. Because of the canonical dimension the effects of this higher-dimensional operator will vanish quickly towards the infrared, but nevertheless can play a crucial role in the vicinity of the cutoff. We basically identify two scenarios. The UV-potential including higher-dimensional couplings with $\lambda_{2,\Lambda} < 0$ is stable, as is the effective potential. The electroweak minimum remains the global minimum throughout the entire RG evolution. In this case, already the ϕ^6 operator allows us to extend the UV-cutoff by a few orders of magnitude. On the other hand the scalar potential can develop a second minimum at large field values even if a stable UV-potential is required. Whether a second minimum emerges or not, depends on the price shape of the UV potential. Within the class of ϕ^6 bare potentials, we observe a smooth transition between these possibilities by decreasing $\lambda_{2,\Lambda}$ for fixed $\lambda_{3,\Lambda}$. Implementing the constraint that the electroweak minimum has to be sufficiently long-lived, this essentially reduces to the standard discussion of a viably long-lived meta-stable region.

Of course, we investigated only the simplest possible extension of bare potentials beyond the ϕ^4-type. Thus, it is still unclear whether the consistency bound remains finite. For future studies, it is one of the most pressing questions to quantitatively estimate the resulting consistency bound beyond the extensions considered in this thesis. Of course, it appears equally legitimate to give up the criterion of a unique minimum at all scales, but instead allow for further minima in the bare action. If the resulting IR effective action turns out to have one unique minimum again (to be identified with the electroweak minimum), such bare actions can lead to a further relaxation of the consistency bound described above. In the general case, it should be possible to construct bare actions with multiple local minima such that the full effective action has a global minimum different from the local electroweak minimum. Since such bare actions are less constrained than those of the preceding scenarios, we expect the resulting lower Higgs mass consistency bounds to be even more relaxed to smaller values. Again, a quantitative estimate of such consistency bounds including meta-stable scenarios remains an urgent question.

Comparing the conventional stability bounds with the present consistency bounds, the overall picture seems to be qualitatively similar. The primary main difference is of quantitative nature, since the unique-minimum consistency bound lies below the stability bound. Wilsonian RG arguments however suggest that this difference could become small for large UV cutoffs.

Nevertheless, the size of this quantitative difference substantially depends on the assumptions imposed on the size of the couplings in the bare action. Also, the consistency bound is necessarily regularization scheme dependent. As the regularization actually should model the details of the embedding into the underlying UV completion, this dependence has a physical meaning. Even larger differences are expected between the conventional meta-stability bound and the consistency bound including meta-stable scenarios. The reason is that the meta-stable features are expected to arise from the bare action and thus are largely unknown. The size of the meta-stable region and corresponding life-time estimates will be even more subject to assumptions on the bare action.

Independently of whether the measured value of the Higgs boson mass eventually turns out to lie slightly above or below the conventional lower bound, it is remarkable that the Higgs and top mass parameters appear to lie close to a region in the IR parameter space that can be connected to a bare UV effective potential that could exhibit almost vanishing scalar self-interactions. In this sense, a precise measurement of these mass parameters is relevant beyond the pure goal of precision data. These measurements can impose requirements that any UV embedding has to satisfy. The viewpoint of consistency bounds presented above provides a means to quantify these requirements. Therefore, a comprehensive quantitative exploration of these bounds appears most pressing.

One scenario appears particularly interesting: if the Higgs mass eventually turns out to be exactly compatible with a UV flat potential (apart from a possible mass term), a corresponding embedding would have to explain this rather particular feature. It is interesting to note that such scenarios exist even within purely quantum field theory approaches as, for instance, in models with asymptotically safe gravity [101, 206]. Recently, an asymptotically free scenario in a gauged chiral Yukawa model has been identified [56, 58], the UV limit of which corresponds to a flat scalar potential also allowing for comparatively light Higgs masses in the IR. An extension of these studies to the flow equation of the full standard model Higgs potential presented at the end of this thesis could shed light on the question as to whether this mechanism is also present in the full standard model.

Appendix

A.1 Higgs mechanism

Spontaneous symmetry breaking The discovery of the Higgs mechanism is closely related to the phenomenon of spontaneous symmetry breaking. A symmetry of a theory is called spontaneously broken, if the action is invariant under a given symmetry but the ground state of the theory does not respect this underlying symmetry. The simplest field theoretical realization of this phenomenon is given by a scalar field theory with a discrete $\mathbb{Z}_2$-symmetric potential, $U(\phi) = \frac{m^2}{2}\phi^2 + \frac{\lambda_2}{8}\phi^4$. The shape of the potential is determined by the parameters m^2 and λ_2. The quartic coupling λ_2 has to be positive in order to have a potential which is bounded from below. This requirement is necessary to have a well defined vacuum state which is the field configuration with lowest energy. Thus, a theory with an unbounded potential has no stable ground state and is considered as unphysical. By contrast, both possibilities for the sign of m^2 are allowed. For $m^2 > 0$, the potential has a unique minimum at vanishing field amplitude. Hence, the vacuum is still invariant under the symmetry of the theory. For $m^2 < 0$, the potential exhibits two equivalent minima at $\phi = \pm v = \pm\sqrt{-2m^2/\lambda_2}$ and a maximum at vanishing field amplitude. Of course, the potential is still $\mathbb{Z}_2$ symmetric but only one of the two minima can be the ground state of the theory. Hence, the vacuum expectation value (vev) v serves as an order parameter to decide whether the system is in the symmetric (SYM) regime for $v = 0$ or exhibits spontaneous symmetry breaking (SSB) for a nonvanishing v.

For an interpretation of the theory in the SSB regime and in order to study a perturbative analysis, it is convenient to split the scalar field into its vev and fluctuations around it, $\phi(x) = v + \varphi(x)$. Here, we have already chosen the positive minimum as the ground state which leads to the breakdown of the symmetry. Expanding the potential in terms of the fluctuating field φ, we obtain $U = -\frac{2m^2}{2}\varphi^2 + \sqrt{-\frac{m^2\lambda}{2}}\varphi^3 + \frac{\lambda}{8}\varphi^4$. Thus, the field φ has a real-valued mass $\sqrt{-2m^2}$. Further, the original $\mathbb{Z}_2$ symmetry is no longer apparent in terms of φ. However, the symmetry is just hidden. It manifests in the relation among the mass term, the cubic, and quartic coupling for the fluctuating field which only depends on two parameters.

A first application in particle physics of spontaneous symmetry breaking can be obtained by coupling the real valued scalar field to a Dirac fermion via a Yukawa interaction. In case that the scalar field forms a condensate, a mass term for the fermion is generated which is

proportional to the vev and the strength of the Yukawa interaction,

$$h\,\phi\bar{\psi}\psi = \underbrace{(hv)}_{m_\mathrm{f}}\,\bar{\psi}\psi + h\,\varphi\bar{\psi}\psi.$$

Theories with a continuous global symmetry show an even more interesting behavior. The simplest realization of such a symmetry is given by a complex scalar field. The potential,

$$U = m^2\phi^\dagger\phi + \frac{\lambda}{2}(\phi^\dagger\phi)^2 \tag{A.1}$$

is invariant under global phase transformations

$$\phi \to e^{\mathrm{i}\alpha}\phi, \qquad \phi^\dagger \to e^{-\mathrm{i}\alpha}\phi^\dagger, \qquad \alpha = \text{const.}$$

For $m^2 > 0$, the system is in the symmetric regime and the parameter m^2 describes the mass of the complex scalar field. Correspondingly the two independent real-valued scalar degrees of freedom have the same mass as they should due to the rotational invariance of the potential which is respected by the vacuum state.

In case of $m^2 < 0$, the potential has the well-known Mexican-hat profile. It is minimized for any ϕ which satisfies $\phi^\dagger\phi = \frac{1}{2}v^2 = -\frac{m^2}{\lambda}$ and hence has infinitely many degenerated minima along the trough of the potential. We choose a coordinate system in the internal field space such that the vacuum state is on the positive real axis,

$$\phi(x) = \frac{1}{\sqrt{2}}(\phi_1 + \mathrm{i}\phi_2) = \frac{1}{\sqrt{2}}(v + \varphi_1 + \mathrm{i}\varphi_2). \tag{A.2}$$

Any other choice would have been possible too and can be reached by a global phase transformation. Again, we expand the potential in terms of excitations around the ground state. Similar to the discrete case, the field φ_1 in radial direction becomes massive with a mass of $\sqrt{-2m^2}$ which is a result of the finite curvature of the potential in radial direction. In analogy to the standard model, excitations in radial directions are associated with the Higgs boson. By contrast, the field in the tangential direction φ_2 remains massless and is called a Goldstone field. It describes excitations along the bottom of the Mexican-hat potential and is massless due to the vanishing curvature along the minima of the potential.

These results can be generalized to larger symmetry groups straightforwardly. The occurrence of massless bosons is a generic property if a global continuous symmetry is spontaneously broken. This phenomenon is circumstantiated by the Goldstone theorem [261–263]. The Goldstone theorem predicts that the physical spectrum of the theory contains a massless particle for every spontaneously broken continuous global symmetry.

Basics of gauge theories The Goldstone theorem can be evaded by the mechanism introduced by Englert, Brout, Higgs, Guralnik, Hagen, and Kibble, which we will denote as Higgs

mechanism for short. Therefore, we have to impose local gauge symmetries rather than global ones. As a result of this, we have to introduce gauge bosons into the theory. Suppose a scalar field shall be invariant under a local nonabelian symmetry,

$$\phi \to e^{\mathrm{i}\,\alpha_i(x)t_i}\phi,$$

where t_i are the hermitian generators of a compact nonabelian Lie group. These generators form a Lie algebra and satisfy

$$[t_i, t_j] = \mathrm{i} f_{ijk} t_k$$

with the totally antisymmetric structure constants f_{ijk}. We will restrict ourselves to SU(N) theories in the following due to the fact that the symmetry group of the standard model is given by $\mathrm{SU(3)_c} \times \mathrm{SU(2)_L} \times \mathrm{U(1)_Y}$. Note, that also the Abelian group U(1) fits in this classification. The corresponding algebra is one-dimensional and hence the structure constants vanish. The potential (A.1) is still invariant under a local symmetry transformation but the standard kinetic term for the scalar field is not. However, replacing the partial derivative by the covariant derivative, $D_\mu = \partial_\mu + \mathrm{i}gW_{i\,\mu}t_i$, and demanding that the gauge field transforms according to

$$W_i^\mu t_i \to e^{\mathrm{i}\,\alpha_j(x)t_j}\left(W_i^\mu t_i - \frac{\mathrm{i}}{g}\partial^\mu\right)e^{\mathrm{i}\,\alpha_k(x)t_k}, \tag{A.3}$$

yields a gauge invariant kinetic term for the scalar field, $(D_\mu\phi)^\dagger D^\mu\phi$.

The dynamics of the gauge field is described by the Yang-Mills action

$$S = \int d^d x\, \frac{1}{4} F_{i\,\mu\nu} F_i^{\mu\nu}$$

with the field strength tensor

$$F_i^{\mu\nu} = \partial^\mu W_i^\nu - \partial^\nu W_i^\mu - g f_{ijk} W_j^\mu W_k^\nu.$$

Note that we formulate our theories in Euclidean spacetime throughout this thesis for convenience. The gauge invariant Yang-Mills action contains the kinetic term for the gauge fields as well as a three- and four-gauge-boson vertex. Though, a mass term, $m_W^2 W_{i\,\mu} W_i^\mu$, is explicitly prohibited due to gauge invariance.

The naive attempt to quantize a gauge theory fails. The functional integral with respect to the gauge fields is ill-defined since we integrate over infinitely many physically equivalent gauge field configurations. This gauge redundancy manifests in the gauge transformation (A.3) which continuously connects physical equivalent field configurations which are called a gauge orbit. Thus, we would like to constrain the functional measure to pick only one representative

of each gauge orbit. This is accomplished by a gauge-fixing condition, $C_i[W_i^\mu] = 0$, which cuts off the redundant field configurations. An example for a Lorentz invariant gauge fixing condition is given by the Lorenz gauge $C_i = \partial_\mu W_i^\mu$. To implement the gauge-fixing condition into the generating functional, we refer to the Faddeev-Popov quantization procedure [264]. Roughly, an identity of the form $\delta[C_i] \det \mathcal{M}_{ij}$ can be inserted in the generating functional in which $\mathcal{M}_{ij} = \frac{\delta C_i}{\delta \alpha_j}$ is the so-called Faddeev-Popov operator whose determinant is gauge invariant. Here, the delta functional ensures that only those field configurations contribute to the functional measure which obey the gauge fixing condition $C_i = 0$. In order to achieve a local theory, we rewrite the gauge-fixing delta functional via an Gaußian representation as well as the Faddeev-Popov determinant via an introduction of Graßmann valued scalar ghost fields into an exponential form. The gauge-fixed action finally reads,

$$S = \int d^d x \left[\frac{1}{4} F_{i\,\mu\nu} F_i^{\mu\nu} + \frac{1}{2\xi} (\partial_\mu W_i^\mu)(\partial_\nu W_i^\nu) + \bar{c}_i \mathcal{M}_{ij} c_j \right].$$

Common choices for the gauge-fixing parameter ξ are the Landau gauge ($\xi = 0$), Feynman gauge ($\xi = 1$) or Yennie gauge ($\xi = 3$). In case of the Landau gauge all of the weight is centered at the gauge copy which satisfies $\partial_\mu W_i^\mu = 0$.

The Faddeev-Popov procedure is based on the assumption that the gauge-fixing condition picks only one representative of a gauge orbit. In general, this assumption is not true. There are still gauge copies on the same gauge orbit which satisfy a given gauge-fixing condition due to the Gribov-Singer ambiguity [265, 266]. However, the Faddeev-Popov trick removes the gauge redundancy for perturbative amplitudes at least. Thus, $\mathcal{S}$-matrix elements are well defined and independent of the gauge-fixing condition in perturbation theory. Yet, a rigorous way to gauge fix a continuum Yang-Mills theory on a nonperturbative level lacks.

Hiding local gauge symmetries The situation is even more involved by including both spontaneous symmetry breaking and local gauge invariance into one and the same theory. For simplicity, let us start with the case of an U(1) theory and consider the kinetic operator of the scalar field

$$(D_\mu \phi)^\dagger D^\mu \phi = |\partial_\mu \phi|^2 + g^2 |\phi|^2 W_\mu W^\mu + \mathrm{i} g \left[(\partial_\mu \phi)^\dagger \phi - \phi^\dagger (\partial_\mu \phi) \right] W^\mu. \tag{A.4}$$

In case that the potential (A.1) is in the SSB regime, let us rewrite Eq. (A.4) in terms of the fluctuating fields φ_1 and φ_2 around the vev according to Eq. (A.2),

$$|D_\mu \phi|^2 = \frac{1}{2} (\partial_\mu \varphi_1)^2 + \frac{1}{2} (\partial_\mu \varphi_2)^2 + \frac{g^2 v^2}{2} W_\mu W^\mu + \frac{gv}{2} (\partial_\mu \varphi_2) W^\mu + \cdots . \tag{A.5}$$

where we have omitted terms that are cubic and quartic in the fields. The third term on the right hand side is a mass term for the gauge boson $m_\mathrm{W} = gv$ but we also get a mixing term

between the Goldstone boson φ_2 and the longitudinal part of the gauge boson. Due to this mixing, the Goldstone boson supplies the right pole in order to obtain a vacuum polarization amplitude which is properly transversal for the gauge boson. Furthermore, the Goldstone boson does not appear as an independent physical particle in the spectrum of the theory. The easiest way to verify this statement is to choose a fixed gauge. So far, we fixed the gauge by specifying the form of the gauge field, e.g., $\partial_\mu W^\mu = 0$, but also any other field that is charged under the considered gauge group (, i.e., it does not transform trivially) can be used. Due to the U(1) gauge symmetry $\phi \to e^{\mathrm{i}\alpha(x)}\phi$, we can choose a specific $\alpha(x)$ such that $\phi(x)$ becomes real valued everywhere. Due to this choice, the Goldstone field φ_2 is removed from the theory and the Lagrangian is given by

$$\mathcal{L} = \frac{1}{4} F_{i\,\mu\nu} F_i^{\mu\nu} + \frac{1}{2}(\partial_\mu \varphi_1)^2 + \frac{g^2}{2}(v+\varphi_1)^2 W_\mu W^\mu + U(\varphi_1^2),$$

which describes a real valued scalar field, the Higgs boson, interacting with a massive vector boson. This gauge choice is called unitary gauge because the unphysical degrees of freedom are removed from the Lagrangian and thus the unitarity of the $\mathcal{S}$-matrix is evident. One may wonder, that a mass term for the gauge boson explicitly appears in the Lagrangian which is obviously not gauge invariant. However, we already fixed a gauge in this formulation such that it is not a big surprise that the remaining Lagrangian is no longer invariant under gauge transformations.

In abuse of language, it is often said that the unphysical Goldstone bosons are eaten up by the gauge bosons by a simple count of degrees of freedom. We start with a formulation in terms of two real valued scalar degrees of freedom and two transversal degrees of freedom for the massless gauge boson. The massless Goldstone boson becomes the third component of the gauge boson via gauge rotation in the unitary gauge and vanishes from the spectrum which now contains a real valued scalar degree of freedom as well as a massive gauge boson with three polarization states. Thus, the number of degrees of freedom is preserved.

The situation becomes even more intricate, if a theory with hidden gauge symmetry shall be quantized. For the Faddeev-Popov method, we have to choose explicitly a suitable gauge-fixing condition. By using the naive attempt of choosing unitary gauge, it is possible to perform the quantization in terms of physical fields in principle but one quickly runs into difficult problems which one has to circumvent. This is due to the fact that certain divergencies do not cancel until the $\mathcal{S}$-matrix is calculated. At least there is a prove of concept that a quantization in unitary gauge can be performed [251–254]. However, for any practical calculation within the standard model it is more convenient to choose a so-called renormalizable R_ξ gauge [255, 256]. This gauges are constructed in such a way that all bilinear terms that involve a longitudinal gauge boson and a Goldstone mode are canceled in the gauge-fixed Lagrangian. For the case

of a U(1) gauge theory the gauge-fixing condition reads,

$$\mathcal{L}_{\rm gf} = \frac{1}{2\xi}\left(\partial_\mu W^\mu + \xi g v \varphi_2\right)^2 . \tag{A.6}$$

Note that this formalism also produces a mass term for the would-be Goldstone bosons, $m_{\rm G}^2 = \xi g^2 v^2 = \xi m_{\rm W}^2$. The fact that the Goldstone mass is proportional to the gauge fixing parameter already signals that it will be not produced in any physical process. We expect that all unphysical contributions will cancel out of all computations of gauge-invariant quantities. In fact this cancellation can be shown at least to all orders in perturbation theory [267]. A generalization from U(1) gauge theories to SU(N) gauge theories is straightforward. We discuss the case of a $\mathrm{SU}(2)_{\rm L} \times \mathrm{U}(1)_{\rm Y}$ gauge theory in Sect. 2.1.

A.2 ζ function regularization for the fermion determinant

It is illustrative to study the fermion determinant also using ζ function regularization which can be used to interpolate between propertime and dimensional regularization. For this, we write $U_{\rm F}$ of Eq. (3.12) as

$$U_{\rm F}(\rho) = \frac{1}{2\Omega}\int_{1/\Lambda^2}^{\infty}\frac{dT}{T}\left(e^{-h_\Lambda^2\rho T}-1\right)\,\mathrm{Tr}\,e^{\partial^2 T}, \tag{A.7}$$

where T is a propertime parameter, being introduced via Frullani's formula for a representation of the logarithm. Here the lower bound of the T integral serves as a (gauge-invariant) momentum cutoff. Furthermore, we now evaluate the momentum trace in d dimensions and introduce an arbitrary dimensionful scale μ_0 in order to implement the correct dimensionality of the potential, $\mathrm{Tr} \to \mathrm{tr}_\gamma \Omega \int \frac{d^4p}{(2\pi)^4} \to \mathrm{tr}_\gamma \frac{\Omega}{\mu_0^{d-4}} \int \frac{d^dp}{(2\pi)^d}$. We obtain,

$$U_{\rm F}(\rho) = \frac{2\mu_0^{4-d}}{(4\pi)^{\frac{d}{2}}}\int_{1/\Lambda^2}^{\infty}\frac{dT}{T^{1+\frac{d}{2}}}\left(e^{-h_\Lambda^2\rho T}-1\right). \tag{A.8}$$

In the limit $d \to 4$, we have the standard propertime regularization, whereas in the limit $\Lambda \to \infty$, we end up with dimensional regularization. Separating the mass term $\sim \rho$ as before, we get

$$U_{\rm F}(\rho) = -\frac{4\mu_0^{4-d}}{(d-2)(4\pi)^{\frac{d}{2}}}h^2\rho\Lambda^{d-2} + \frac{2\mu_0^{4-d}}{(4\pi)^{\frac{d}{2}}}\int_{1/\Lambda^2}^{\infty}\frac{dT}{T^{1+\frac{d}{2}}}\left(e^{-h_\Lambda^2\rho T}+h_\Lambda^2\rho T-1\right). \tag{A.9}$$

Again, we observe that the mass term (first term) contributes with the minus sign as expected, whereas the interaction part (second term) is a strictly positive function for all finite values of $\Lambda, h_\Lambda, \rho, d > 0$. The conclusions are therefore identical to the ones for the sharp cutoff. Incidentally, the propertime integration can be carried out analytically, the result can be written in

terms of an incomplete Γ function with the positivity properties of course remaining unchanged.

As the mass term will become part of the renormalized scalar mass term by means of a renormalization condition, let us now focus on the interaction part of Eq. (A.9). In order to take the limit towards dimensional regularization, we first take the limit $\Lambda \to \infty$, and then expand about $d = 4 - \epsilon$, as is standard. We then find for the interaction part

$$U_{\mathrm{F}}(\rho) \to \frac{2\mu_0^{4-d}}{(4\pi)^{\frac{d}{2}}}(h_\Lambda^2\rho)^{\frac{d}{2}}\Gamma(-d/2) = \frac{h_\Lambda^4\rho^2}{8\pi^2}\frac{1}{\epsilon} - \frac{h_\Lambda^4\rho^2}{16\pi^2}\left(\ln\frac{h_\Lambda^2\rho}{\mu_0^2} + \text{const.}\right) + \mathcal{O}(\epsilon). \tag{A.10}$$

Following the standard recipes, we would absorb the positive $1/\epsilon$ divergence in the bare ϕ^4 term by means of a renormalization condition. The finite part in Eq. (A.10) is identical to that of the sharp cutoff in Eq. (3.16) in the limit $\Lambda \to \infty$ (apart from the scheme-dependent constants), seemingly indicating an instability at large field values. With dimensional regularization, we would therefore arrive at the standard conclusion that fermionic fluctuations can induce an instability of the vacuum at large fields.

Whereas for the sharp cutoff, this was an obvious artifact of the $\Lambda \to \infty$ limit, the failure is less obvious here. Nevertheless, as we have derived this misleading result of a negative contribution from a strictly positive expression given in Eq. (A.9), it is clear that the standard strategies of dimensional regularization fail to describe the global behavior of the fermion determinant properly. The reason is that dimensional regularization is not only a regularization but at the same time a projection solely onto the logarithmic divergencies. It has in fact long been known that the use of dimensional regularization in the presence of large fields can become delicate; procedures to deal with this problem typically suggest to go back to the dimensionally continued propertime/ζ-function representation that we started out with [268, 269].

There is another perspective that explains why the standard perturbative argument of integrating the β function of the ϕ^4 theory is misleading as far as vacuum stability is concerned: the β functions are typically derived in mass-independent regularization schemes (though mass-dependent schemes have recently also been studied [270]), and it is implicitly assumed that the discussion can be performed in the deep Euclidean region where all mass scales are much smaller than any of the involved momentum scales of the fluctuations. The latter assumption is in fact not valid, as both scales the value of the field as well as the cutoff Λ can interfere non-trivially with each other. This is illustrated rather explicitly in the sharp-cutoff calculation given in Sect. 3.2.

A.3 Threshold functions

Here, we list the threshold functions that arise from the integration over loop momenta in the flow equations. The regulator functions for bosonic and fermionic fields can conveniently be written in terms of dimensionless regulator shape functions r_{B} and r_{F},

$$R_{\mathrm{B}}(p) = Z_{\mathrm{B}} p^2\, r_{\mathrm{B}}(p^2/k^2), \qquad R_{\mathrm{F}}(p) = -Z_{\mathrm{F}} \not{p}\, r_{\mathrm{F}}(p^2/k^2),$$

where $\mathrm{B} \in \{\phi, \mathrm{W_T}, \mathrm{W_L}, \cdots\}$ and $\mathrm{F} \in \{\mathrm{t}, \mathrm{b}, \mathrm{L}, \mathrm{R_t}, \cdots\}$. For a compact notation, we define the regularized kinetic term for the bosonic and fermionic fluctuations by $P_{\mathrm{B}} = p^2(1 + r_{\mathrm{B}})$ and $P_{\mathrm{F}} = p^2(1 + r_{\mathrm{F}})^2$. In case of chiral fermions, we have $P_{\mathrm{F}} = p^2(1 + r_{\mathrm{L}})(1 + r_{\mathrm{R}}))$ where r_{L} and r_{R} are the regulator shape functions for the left- and right-handed chiral fermion respectively. With the abbreviation $v_d^{-1} = 2^{d+1}\pi^{\frac{d}{2}}\Gamma\left(\frac{d}{2}\right)$, the threshold functions read,

$$\begin{aligned}
l_0^{(\mathrm{B})d}(\omega;\eta_{\mathrm{B}}) &= \frac{1}{4v_d} k^{-d} \int_p \frac{Z_{\mathrm{B}}^{-1}\partial_t R_{\mathrm{B}}}{P_{\mathrm{B}} + \omega k^2} \\
l_0^{(\mathrm{F})d}(\omega;\eta_{\mathrm{F}}) &= \frac{1}{2v_d} k^{-d} \int_p p^2(1 + r_{\mathrm{F}}) \frac{Z_{\mathrm{F}}^{-1}\partial_t (Z_{\mathrm{F}} r_{\mathrm{F}})}{P_{\mathrm{F}} + \omega k^2} \\
l_n^{(\mathrm{B})d}(\omega;\eta_{\mathrm{B}}) &= \frac{n}{4v_d} k^{2n-d} \int_p \frac{Z_{\mathrm{B}}^{-1}\partial_t R_{\mathrm{B}}}{(P_{\mathrm{B}} + \omega k^2)^{n+1}} \\
l_{n_1,n_2}^{(\mathrm{FB})d}(\omega_1,\omega_2;\eta_{\mathrm{F}},\eta_{\mathrm{B}}) &= -\frac{1}{4v_d} k^{2(n_1+n_2)-d} \int_p \tilde{\partial}_t \left[\frac{1}{(P_{\mathrm{F}} + \omega_1 k^2)^{n_1}} \frac{1}{(P_{\mathrm{B}} + \omega_2 k^2)^{n_2}}\right] \\
l_{n_1,n_2}^{(\mathrm{BB})d}(\omega_1,\omega_2;\eta_{\mathrm{B}_1},\eta_{\mathrm{B}_2}) &= -\frac{1}{4v_d} k^{2(n_1+n_2)-d} \int_p \tilde{\partial}_t \left[\frac{1}{(P_{\mathrm{B}_1} + \omega_1 k^2)^{n_1}} \frac{1}{(P_{\mathrm{B}_2} + \omega_2 k^2)^{n_2}}\right] \\
m_2^{(\mathrm{B})d}(\omega;\eta_{\mathrm{B}}) &= -\frac{1}{4v_d} k^{6-d} \int_p p^2 \tilde{\partial}_t \left[\frac{\partial_{p^2} P_{\mathrm{B}}}{(P_{\mathrm{B}} + \omega k^2)^2}\right]^2 \\
m_2^{(\mathrm{F})d}(\omega;\eta_{\mathrm{F}}) &= -\frac{1}{4v_d} k^{6-d} \int_p p^2 \tilde{\partial}_t \left[\frac{\partial_{p^2} P_{\mathrm{F}}}{(P_{\mathrm{F}} + \omega k^2)^2}\right]^2 \\
m_4^{(\mathrm{F})d}(\omega;\eta_{\mathrm{F}}) &= -\frac{1}{4v_d} k^{4-d} \int_p p^4 \tilde{\partial}_t \left[\partial_{p^2} \frac{1 + r_{\mathrm{F}}}{P_{\mathrm{F}} + \omega k^2}\right]^2 \\
m_{1,2}^{(\mathrm{FB})d}(\omega_1,\omega_2;\eta_{\mathrm{F}},\eta_{\mathrm{B}}) &= -\frac{1}{4v_d} k^{4-d} \int_p p^2 \tilde{\partial}_t \left[\frac{1 + r_{\mathrm{F}}}{P_{\mathrm{F}} + \omega_1 k^2} \frac{\partial_{p^2} P_{\mathrm{B}}}{(P_{\mathrm{B}} + \omega_2 k^2)^2}\right] \\
\tilde{m}_{1,1}^{(\mathrm{FB})d}(\omega_1,\omega_2;\eta_{\mathrm{F}},\eta_{\mathrm{B}}) &= -\frac{1}{4v_d} k^{4-d} \int_p \tilde{\partial}_t \left[\frac{1 + r_{\mathrm{F}}}{P_{\mathrm{F}} + \omega_1 k^2} \frac{1}{P_{\mathrm{B}} + \omega_2 k^2}\right] \\
\tilde{m}_2^{(\mathrm{B})d}(\omega;\eta_{\mathrm{B}}) &= -\frac{1}{16v_d} k^{6-d} \int_p \frac{1}{p^2} \tilde{\partial}_t \left[\frac{1}{P_{\mathrm{B}} + \omega k^2}\right]^2 \\
m_{4,4}^{(\mathrm{BB})d}(\omega_1,\omega_2;\eta_{\mathrm{B}_1},\eta_{\mathrm{B}_2}) &= -\frac{1}{4v_d} k^{4-d} \int_p p^4 \tilde{\partial}_t \left[\partial_{p^2} \frac{1}{P_{\mathrm{B}_1} + \omega_1 k^2}\right] \left[\partial_{p^2} \frac{1}{P_{\mathrm{B}_2} + \omega_2 k^2}\right] \\
m_{2,1}^{(\mathrm{BB})d}(\omega_1,\omega_2;\eta_{\mathrm{B}_1},\eta_{\mathrm{B}_2}) &= -\frac{1}{4v_d} k^{4-d} \int_p p^2 \tilde{\partial}_t \left[\frac{-\partial_{p^2} P_{\mathrm{B}_1}}{P_{\mathrm{B}_1} + \omega_1 k^2} \frac{1}{P_{\mathrm{B}_2} + \omega_2 k^2}\right] \\
m_{1,1,1}^{(\mathrm{FBB})d}(\omega_1,\omega_2,\omega_3;\eta_{\mathrm{F}},\eta_{\mathrm{B}_1},\eta_{\mathrm{B}_2}) &= -\frac{1}{4v_d} k^{4-d} \int_p \tilde{\partial}_t \left[\frac{(1 + r_{\mathrm{F}})p^2}{P_{\mathrm{F}} + \omega_1 k^2} \frac{1}{P_{\mathrm{B}_1} + \omega_2 k^2} \frac{1}{P_{\mathrm{B}_2} + \omega_3 k^2}\right].
\end{aligned}$$

$\tilde{\partial}_t$ is defined to act only on the scale dependence of the regulator function,

$$\tilde{\partial}_t = \int_x \sum_i \frac{\partial_t (Z_i r_i(x))}{Z_i} \frac{\delta}{\delta r_i(x)},$$

where i labels the different involved fields. The linear regulator which is used throughout this thesis reads,

$$r_{\mathrm{B}} = \left(\frac{k^2}{p^2} - 1 \right) \theta(k^2 - p^2).$$

The fermion shape function is chosen such that $(1 + r_{\mathrm{B}}) = (1 + r_{\mathrm{F}})^2$. For the linear regulator the momentum integrations can be performed analytically,

$$\begin{aligned}
l_0^{(\mathrm{B})d}(\omega; \eta_{\mathrm{B}}) &= \frac{2}{d} \frac{1 - \frac{\eta_{\mathrm{B}}}{d+2}}{1+\omega} \\
l_0^{(\mathrm{F})d}(\omega; \eta_{\mathrm{F}}) &= \frac{2}{d} \frac{1 - \frac{\eta_{\mathrm{F}}}{d+1}}{1+\omega} \\
l_n^{(\mathrm{B})d}(\omega; \eta_{\mathrm{B}}) &= \frac{2n}{d} \frac{1 - \frac{\eta_{\mathrm{B}}}{d+2}}{(1+\omega)^{n+1}} \\
l_{n_1,n_2}^{(\mathrm{FB})d}(\omega_1, \omega_2; \eta_{\mathrm{F}}, \eta_{\mathrm{B}}) &= \frac{2}{d} \frac{1}{(1+\omega_1)^{n_1}} \frac{1}{(1+\omega_2)^{n_2}} \left[\frac{n_1}{1+\omega_1} \left(1 - \frac{\eta_{\mathrm{F}}}{d+1} \right) + \frac{n_2}{1+\omega_2} \left(1 - \frac{\eta_{\mathrm{B}}}{d+2} \right) \right] \\
l_{n_1,n_2}^{(\mathrm{BB})d}(\omega_1, \omega_2; \eta_{\mathrm{B}_1}, \eta_{\mathrm{B}_2}) &= \frac{2}{d} \frac{1}{(1+\omega_1)^{n_1}} \frac{1}{(1+\omega_2)^{n_2}} \left[\frac{n_1}{1+\omega_1} \left(1 - \frac{\eta_{\mathrm{B}_1}}{d+1} \right) + \frac{n_2}{1+\omega_2} \left(1 - \frac{\eta_{\mathrm{B}_2}}{d+2} \right) \right] \\
m_2^{(\mathrm{B})d}(\omega; \eta_{\mathrm{B}}) &= \frac{1}{(1+\omega)^4} \\
m_2^{(\mathrm{F})d}(\omega; \eta_{\mathrm{F}}) &= \frac{1}{(1+\omega)^4} \\
m_4^{(\mathrm{F})d}(\omega; \eta_{\mathrm{F}}) &= \frac{1}{(1+\omega)^4} + \frac{1 - \eta_{\mathrm{F}}}{d-2} \frac{1}{(1+\omega)^3} - \left(\frac{1 - \eta_{\mathrm{F}}}{2(d-2)} + \frac{1}{4} \right) \frac{1}{(1+\omega)^2} \\
m_{12}^{(\mathrm{FB})d}(\omega_1, \omega_2; \eta_{\mathrm{F}}, \eta_{\mathrm{B}}) &= \frac{1 - \frac{\eta_{\mathrm{B}}}{d+1}}{(1+\omega_1)(1+\omega_2)^2} \\
\tilde{m}_{1,1}^{(\mathrm{FB})d}(\omega_1, \omega_2; \eta_{\mathrm{F}}, \eta_{\mathrm{B}}) &= \frac{2}{d-2} \frac{1}{(1+\omega_1)(1+\omega_2)} \left[\frac{1 - \frac{\eta_{\mathrm{B}}}{d+1}}{1+\omega_2} + \frac{1 - \frac{\eta_{\mathrm{F}}}{d}}{1+\omega_2} + \frac{1}{2} \left(1 + \frac{\eta_{\mathrm{F}}}{d} \right) \right] \\
\tilde{m}_2^{(\mathrm{B})d}(\omega; \eta_{\mathrm{B}}) &= \frac{1}{d-2} \frac{1 - \frac{\eta_{\mathrm{B}}}{d}}{(1+\omega)^3} \\
m_{4,4}^{(\mathrm{BB})d}(\omega_1, \omega_2; \eta_{\mathrm{B}_1}, \eta_{\mathrm{B}_2}) &= \frac{1}{(1+\omega_1)^2 (1+\omega_2)^2} \\
m_{2,1}^{(\mathrm{BB})d}(\omega_1, \omega_2; \eta_{\mathrm{B}_1}, \eta_{\mathrm{B}_2}) &= -\frac{1 - \frac{\eta_{\mathrm{B}_1}}{d+2}}{(1+\omega_1)^2 (1+\omega_2)}.
\end{aligned}$$

A.4 Flow equations for the simple Yukawa model

In order to evaluate the Wetterich equation, the Hessian of the effective average action is required,

$$\Gamma_k^{(2)} = \begin{pmatrix} \frac{\overrightarrow{\delta}}{\delta\phi(-p)} \\ \frac{\overrightarrow{\delta}}{\delta\psi(-p)} \\ \frac{\overrightarrow{\delta}}{\delta\bar{\psi}(p)} \end{pmatrix} \Gamma_k \left(\frac{\overleftarrow{\delta}}{\delta\phi(q)}, \frac{\overleftarrow{\delta}}{\delta\psi(q)}, \frac{\overleftarrow{\delta}}{\delta\bar{\psi}(-q)} \right) \equiv \begin{pmatrix} \Gamma_{\phi\phi} & \Gamma_{\phi\psi} & \Gamma_{\phi\bar{\psi}} \\ \Gamma_{\psi\phi} & 0 & \Gamma_{\psi\bar{\psi}} \\ \Gamma_{\bar{\psi}\phi} & \Gamma_{\bar{\psi}\psi} & 0 \end{pmatrix}.$$

The components of the fluctuation matrix can be calculated straightforwardly.

$$\begin{aligned} \Gamma_{\phi\phi} &= Z_\phi p^2 \delta_{p,q} + \int_x e^{\mathrm{i}(q-p)x} \Big[U'\Big(\rho(x)\Big) + 2\rho(x) U''\Big(\rho(x)\Big) \Big], \\ \Gamma_{\bar{\psi}\psi} &= -Z_\psi \not{p} \delta_{p,q} + \mathrm{i}\bar{h}\phi(p-q), \qquad \Gamma_{\psi\bar{\psi}} = -Z_\psi \not{p} \delta_{p,q} - \mathrm{i}\bar{h}\phi(p-q), \\ \Gamma_{\psi\phi} &= -\mathrm{i}\bar{h}\bar{\psi}^{\mathrm{T}}(q-p) = -\Gamma_{\phi\psi}^{\mathrm{T}}, \qquad \Gamma_{\bar{\psi}\phi} = \mathrm{i}\bar{h}\psi(p-q) = -\Gamma_{\phi\bar{\psi}}^{\mathrm{T}}. \end{aligned}$$

where $\delta_{p,q} \equiv (2\pi)^d \delta(p-q)$ and the transpose is regarding the Dirac structure. The regulator is given by,

$$R_k(p,q) = \begin{pmatrix} R_\phi(p) & 0 \\ 0 & R_{\mathrm{F}}(p) \end{pmatrix} \delta_{p,q}, \qquad R_\phi(p) = Z_\phi p^2 \, r_\phi, \quad R_{\mathrm{F}}(p) = \begin{pmatrix} 0 & -Z_\psi \not{p}^{\mathrm{T}} \, r_{\mathrm{F}} \\ -Z_\psi \not{p} \, r_{\mathrm{F}} & 0 \end{pmatrix}.$$

Scalar potential: The flow equation for the potential can be extracted from the projection onto constant scalar fields and vanishing fermions.

$$\partial_t U_k = \frac{1}{2\Omega} \mathrm{STr} \left[(\Gamma_k^{(2)} + R_k)^{-1} (\partial_t R_k) \right]_{\phi=\text{const.},\psi=0,\bar{\psi}=0}, \tag{A.11}$$

where $\Omega = \int_x$ is the spacetime volume. The regularized inverse propagator $(\Gamma_k^{(2)} + R_k)$ becomes block-diagonal in field space such that the bosonic and fermionic part can be calculated separately. After inverting the matrix $(\Gamma_k^{(2)} + R_k)$, multiplying it with $\partial_t R_k$ and taking the supertrace, the flow equation for the potential reads,

$$\partial_t U_k(\rho) = \frac{1}{2} \int_p \frac{\partial_t R_\phi}{Z_\phi P_\phi + U' + 2\rho U''} - \frac{d_\gamma}{2} \int_p \frac{Z_\psi p^2 (1 + r_{\mathrm{F}}) \partial_t (Z_\psi r_{\mathrm{F}})}{Z_\psi^2 P_{\mathrm{F}} + \bar{h}^2 \rho},$$

with $P_\phi = p^2(1 + r_\phi)$ and $P_{\mathrm{F}} = p^2(1 + r_{\mathrm{F}})^2$. Introducing dimensionless threshold functions (see App. A.3) which encode the details of the regularization scheme, this flow equation translates into Eq. (3.19) of the main text:

$$\partial_t U_k = 2 \, v_d \, k^d \left[l_0^{(\mathrm{B})d} \left(k^{-2} \, Z_{\phi,k}^{-1} \, [U_k' + 2 \, \rho \, U_k''] \, ; \eta_\phi \right) - d_\gamma \, l_0^{(\mathrm{F})d} \left(2 \, k^{-2} \, Z_{\psi,k}^{-2} \, \bar{h}_k^2 \, \rho ; \eta_\psi \right) \right]. \tag{A.12}$$

The first term $\sim l_0^{(\mathrm{B})d}$ corresponds to the boson loop in Fig. 3.2 and the second term $\sim l_0^{(\mathrm{F})d}$ corresponds to the fermion loop. In terms of dimensionless quantities, Eq. (3.20), the flow equation for the scalar potential translates to Eq. (3.21).

Yukawa coupling: First, we separate the bosonic field into its vev and deviations from the vev, $\phi(x) = v_k + \varphi(x)$ or in momentum space, $\phi(p) = v_k \delta_{p,0} + \varphi(p)$. For the Yukawa coupling, we project onto the operator $\varphi\bar{\psi}\psi$ and thus onto the coupling between the Higgs boson and the fermions rather than the Higgs field $\phi\bar{\psi}\psi$. While this distinction is irrelevant in the SYM regime, there is a difference in the SSB regime where the two operators flow differently. In general operators will contribute to the running of the Yukawa coupling which are beyond the chosen truncation, for instance, $\phi^{2n}\phi\bar{\psi}\psi$. Projecting with respect to the fluctuating field φ allows to include contributions of the form $v^{2n}\varphi\bar{\psi}\psi$. Thus, we effectively take an operator of the form $h(\kappa_k)\phi\bar{\psi}\psi$ into account where $h(\kappa_k)$ is a Yukawa functional evaluated at the minimum of the scalar potential. This is an improvement of the truncation in contrast to the simple projection onto $h(0)\phi\bar{\psi}\psi$ as we discuss in Sect. 3.7 due to the fact that the particles are interpreted as excitations around the ground state. Therefore, the projection rule for the Yukawa coupling reads,

$$\partial_t h = \frac{\sqrt{2}}{\mathrm{i}\Omega} \frac{\delta}{\delta\varphi(q)} \frac{\overrightarrow{\delta}}{\delta\bar{\psi}(q')} \partial_t \Gamma_k \frac{\overleftarrow{\delta}}{\delta\psi(q'')}\bigg|_0 , \tag{A.13}$$

where $|_0$ denotes that the equation is evaluated at vanishing fluctuating fields ($\varphi = 0$, $\psi = 0$, $\bar{\psi} = 0$) and momenta ($q = q' = q'' = 0$). In order to proceed, we decompose the matrix $(\Gamma_k^{(2)} + R_k)$ into a part which contains the vev and is independent of the fluctuating fields, $(\Gamma_{0,k}^{(2)} + R_k)$, and a remaining part including all fluctuations, $\Delta\Gamma_k^{(2)}$. The derivative $\tilde{\partial}_t$, which only acts on the momentum dependence of the regulator (cf. App. A.3), and an expansion of the logarithm by means of the Mercator series allows to write the flow equation as

$$\begin{aligned}\partial_t \Gamma_k &= \frac{1}{2}\,\mathrm{STr}\,\tilde{\partial}_t \ln(\Gamma_k^{(2)} + R_k) \\ &= \frac{1}{2}\,\mathrm{STr}\,\tilde{\partial}_t \ln(\Gamma_{0,k}^{(2)} + R_k) + \frac{1}{2}\,\mathrm{STr}\,\tilde{\partial}_t \sum_{n=1}^{\infty} \frac{(-1)^{n+1}}{n} \left[(\Gamma_{0,k}^{(2)} + R_k)^{-1} \Delta\Gamma_k^{(2)}\right]^n . \end{aligned} \tag{A.14}$$

Plugging Eq. (A.14) into Eq. (A.13), yields that only the term cubic in $\Delta\Gamma_k^{(2)}$ survives the projection. Performing the matrix calculations and the supertrace, the flow equation for the Yukawa coupling reads,

$$\begin{aligned}\partial_t \bar{h} = -\frac{\bar{h}^3}{2} \int_p \tilde{\partial}_t \Bigg[&\frac{1}{(Z_\psi^2 P_\mathrm{F} + \bar{h}^2\bar{\kappa})^2} \frac{1}{Z_\phi P_\phi + U' + 2\bar{\kappa}U''} - \frac{2\bar{\kappa}h^2}{(Z_\psi^2 P_\mathrm{F} + \bar{h}^2\bar{\kappa})^2} \frac{1}{Z_\phi P_\phi + U' + 2\bar{\kappa}U''} \\ &- \frac{1}{Z_\psi^2 P_\mathrm{F} + \bar{h}^2\rho} \frac{2\bar{\kappa}(3U'' + 2\bar{\kappa}U''')}{(Z_\phi P_\phi + U' + 2\bar{\kappa}U'')^2} \Bigg] ,\end{aligned}$$

where the scalar potential should be evaluated at the minimum of the potential $\rho = \bar{\kappa} = \frac{1}{2}\bar{v}^2$. In terms of threshold functions and dimensionless renormalized quantities, this expression translates into Eq. (3.22) given in the main text. Note, that the three contributions correspond to the three triangle diagrams given in Fig. 3.3. The filled squares in Fig. 3.3 are couplings to the condensate and correspond to the last two terms $\sim \bar{\kappa}$, which is a direct consequence of investigating the flow of the Yukawa coupling evaluated at the minimum of the scalar potential.

Anomalous dimension of the scalar field: Again, we start with a decomposition of the scalar field into its vev and fluctuations around the vev. The projection rule onto the kinetic term of the scalar field reads,

$$\partial_t Z_\phi = \frac{1}{\Omega}\partial_{p'^2}\frac{\delta}{\delta\varphi(p')}\frac{\delta}{\delta\varphi(-q')}\partial_t\Gamma_k\bigg|_0 . \tag{A.15}$$

The vertical line $|_0$ denotes again that the equation is evaluated at vanishing fluctuating fields and external momenta. Note, that this projection rule also implicitly includes $p' = q'$ before the momentum derivative is taken. Inserting Eq. (A.14) and performing the algebra leads to,

$$\partial_t Z_\phi = \frac{1}{d}\int_p \tilde{\partial}_t \Bigg\{ 2\bar{\kappa}(3U'' + 2\bar{\kappa}U''')^2\, p^2 \left[\partial_{p^2}\frac{1}{Z_\phi P_\phi + U' + 2\bar{\kappa}U''}\right]^2 + d_\gamma \bar{h}^2\, p^4 \left[\partial_{p^2}\frac{Z_\psi(1+r_{\mathrm{F}})}{Z_\psi^2 P_{\mathrm{F}} + \bar{h}^2\bar{\kappa}}\right]^2$$
$$\bar{h}^4\bar{\kappa}\, p^2 \left[\partial_{p^2}\frac{1}{Z_\psi^2 P_{\mathrm{F}} + \bar{h}^2\bar{\kappa}}\right]^2 \Bigg\} .$$

The scalar potential is evaluated at $\rho = \bar{\kappa}$. In terms of threshold functions and dimensionless renormalized quantities, this expression translates into Eq. (3.23). The diagrammatic interpretation is in terms of loop diagrams with two external scalar legs φ in Fig. 3.3.

Anomalous dimension of the fermion field: The projection on the wave function renormalization of the fermion field is given by,

$$\partial_t Z_\psi = -\frac{1}{d d_\gamma \Omega}\mathrm{tr}\,\gamma^\mu \partial_{q^\mu}\frac{\overrightarrow{\delta}}{\delta\bar{\psi}(q)}\partial_t\Gamma_k\frac{\overleftarrow{\delta}}{\delta\psi(q')}\bigg|_0 . \tag{A.16}$$

Again, the vertical line denotes that the external momenta have to be identify before the momentum derivative is taken and then are set to zero as well as vanishing fields. Only the term quadratic in the fluctuation fields $\Delta\Gamma_k^{(2)}$ from the expansion (A.14) survives the projection and the flow equation for the fermionic wave function renormalization finally reads,

$$\partial_t Z_\psi = \frac{\bar{h}^2}{d}\int_p p^2 \tilde{\partial}_t \left[\frac{Z_\psi(1+r_{\mathrm{F}})}{Z_\psi^2 P_{\mathrm{F}} + \bar{h}^2\bar{\kappa}}\frac{Z_\phi \partial_{p^2} P_\phi}{(Z_\phi P_\phi + U'(\bar{\kappa}) + 2\bar{\kappa}U''(\bar{\kappa}))^2}\right] .$$

In terms of threshold functions and dimensionless renormalized quantities, this expression translates into Eq. (3.24). The corresponding diagram has a loop with two external fermion legs and a scalar and fermion leg inside the loop.

A.5 Observations on convexity of the IR-potential

In case two minima are generated within the full potential flow with a global minimum for large field values beyond the Fermi scale, the question arises at which scale quantum fluctuations induce a tunneling process which drives the system to the real vacuum state. As tunneling probabilities depend on the height and width of the barrier between both minima, this question is linked to the onset of convexity after all characteristic mass scales are integrated out. Mean-field calculations are not able to display convexity processes. For this, the full RG improved information about bosonic fluctuations is needed, meaning the full potential flow has to be integrated out deep into the infrared. Unfortunately, this is quite challenging for any numerical method due to rising non-analyticities. Therefore, let us start with some discussions on the easier case with only the electroweak minimum where non-convexities appear only for small field values.

In comparison to pure bosonic models, fermionic fluctuations delay convexity processes since they enter the flow equation with opposite sign. Thus, bosonic fluctuations have to exceed these fluctuations first. As the onset of convexity is most distinct in derivatives of the potential, let us consider the first derivative of the potential in the following. For small field amplitudes, the first derivative of the potential converges, $u'(\tilde{\rho}) \to -1$. The dimensionless bosonic propagator approaches the singularity -1 and finally dominates the flow in the deep IR. The first derivative of the potential gets flat and approaches zero for fields smaller than $\tilde{\rho}_0$. According to our expectations, this mechanism is delayed if the Yukawa coupling is strong compared to the pure scalar self-couplings, see fig. A.1. The depicted potentials u' are taken at the same distance from the singularity of the bosonic propagator $1 - |u'(0)| = 0.01$. Note that the position of nonanalyticity ρ_{kink} moves outwards if $m_{\text{H}}/m_{\text{t}} \sim \lambda_2/h$ increases. However, if $m_{\text{H}}/m_{\text{t}}$ is small, convexity is hardly distinguishable before numerics break down due to the singular structure of the equations.

Let us now come back to the case of a metastable effective potential. It turned out that convexity is quite harder to detect in the range of numerically reasonable results. This is expected regarding the decreasing Higgs mass. In Fig. A.2, $\partial_k U'$ indicates how the potential U' develops during the flow in the IR where the minima are frozen out, implying that scalar mass, fermion mass and the vev have already approached their IR values. The considered scales k are slightly below the scalar mass. Therefore, it is not surprising that fermionic fluctuations still control the flow for small fields. Their influence decreases slowly and for small scales close to the scalar mass, the bosonic fluctuations win over the fermionic ones and a flattening of u' can again be observed. The behavior for larger fields, especially the oscillating structure

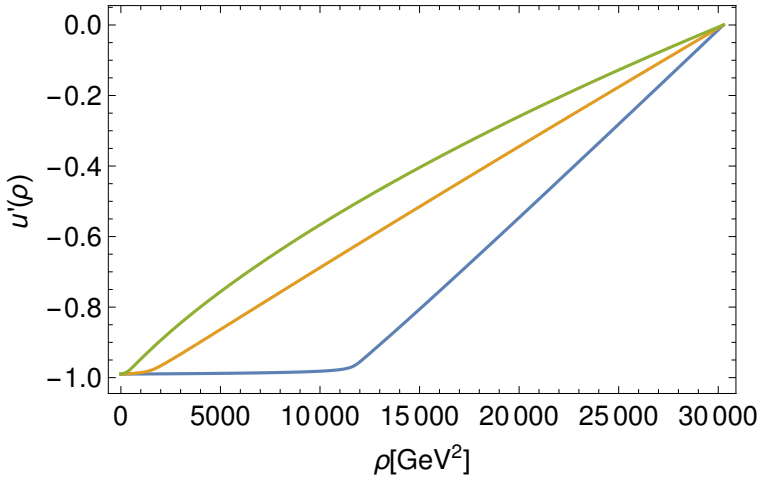

Figure A.1: The onset of convexity mechanisms is stronger if the relation between bosonic and fermionic coupling $m_{\mathrm{H}}/m_{\mathrm{t}}$ increases (from green to blue). Here, the first derivative of the potential is depicted. Convexity becomes manifest by flattening of the inner region, $0 \leq \rho \leq \rho_0 = \frac{246^2}{2}\mathrm{GeV}^2$.

which gets stronger towards the infrared originate from bosonic fluctuations. The zero of this oscillation is situated between the local maximum of the potential U and its inflection point. We suppose it to be an indication for the onset of convexity for large fields. Convexity seems to become first emergent at the potential barrier, leading to a slow decrease, before acting at the origin. However, it is not clear, which of both processes works faster. Following the line of argumentation above, we would expect to observe a manifestation of convexity in the structure of U' at only very small scales k.

In conclusion, this explains the similarity of both results from the mean-field approximation and the full RG improved potential calculation. Again, mean-field calculations do not display mechanisms of convexity. However, it represents the full potential very well up to scales far below the characteristic mass scales as these mechanisms appear to work very slowly.

A.6 Cut-Off mechanism for the Goldstone modes

In the main text, we have amended the chiral Yukawa model with a dynamical mechanism that effectively removes the Goldstone bosons from the low-energy spectrum by providing them with a mass of the order of the gauge-boson mass in the full standard model. Conceptually, this mechanism can be viewed as an IR deformation of our model and is neither universal nor unique. Here, we explore the sensitivity of our results for the Higgs boson mass on the details of this mechanism.

Within our deformation, let us vary the parameter ζ, which controls the size of the effective mass for the Goldstone bosons proportional to the vev, $m_{\mathrm{G}}^2 = \frac{1}{2}\zeta v_k^2$. Figure A.3 shows the Higgs mass depending on the effective Goldstone mass at $\Lambda = 10^7\mathrm{GeV}$. For a weakly coupled scalar sector, $\lambda_{2,\Lambda} = 0$ (blue squares), the impact of ζ on m_{H} is insignificant. Even if the Goldstone

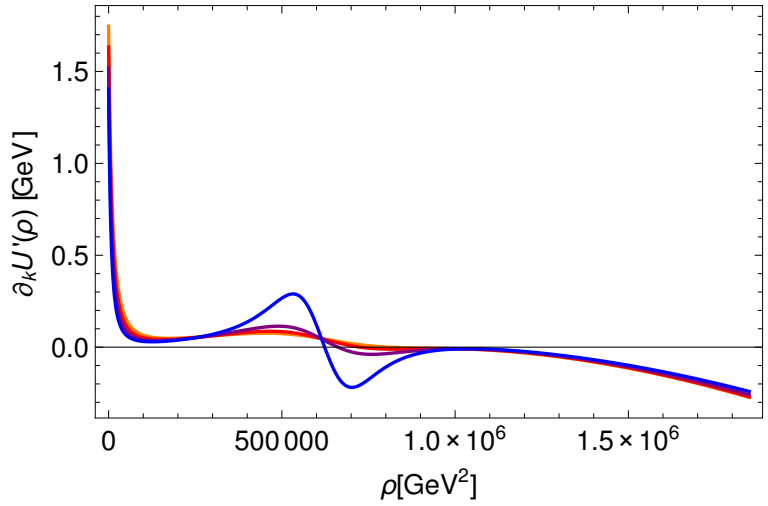

Figure A.2: The flow of the first derivative of the potential $\partial_k U'$ indicates the onset of convexity for large fields. Whereas the small field region is still dominated by fermionic fluctuations, the bosons control the flow for larger fields, especially the oscillation. Orange to blue depicts decreasing scale k.

mass changes by an order of magnitude the influence on the Higgs mass is less than 2 GeV. The situation is different for a strong scalar coupling, e.g., $\lambda_\Lambda = 10$ (red circles). For large effective Goldstone masses ($m_\mathrm{G} > m_\mathrm{H}$), we observe again only small deviations from the case $m_\mathrm{G} = 80\mathrm{GeV}$. This is because the Goldstone modes decouple roughly at the same scale as the top and the Higgs. However, if we choose smaller values of m_G the deviations become larger, e.g., we observe a deviation of 20% for $m_\mathrm{G} = 20\mathrm{GeV}$ compared to the case of $m_\mathrm{G} = 80\mathrm{GeV}$. The Goldstone modes contribute over a wider range of scales to the flow equations than the Higgs or the top quark. This finally results in a smaller Higgs mass. For vanishing m_G we observe a log-like running of λ_2. As a result, m_H approaches smaller and smaller values in the limit $\zeta \to 0$.

Of course, beyond the deformation of the model chosen in this work, other methods are conceivable to effectively remove the massless Goldstone bosons to mimic the physics of the fully gauged standard model. One option is to choose an arbitrary scale k_nG within the SSB regime at which we remove all Goldstone contributions to the flow equations by hand. This corresponds to switching on a source at k_nG which gives the Goldstone modes an infinitely large mass and leads to an ad hoc decoupling. Another possibility is to introduce a source term $J^a\phi^a$ on the level of the Lagrangian. This would leave the flow equations unchanged because only the Hessian of the effective average action $\Gamma_k^{(2)}$ contributes to the Wetterich equation. Still, the shape of the scalar potential would be changed by this explicit symmetry breaking term. As a result, source-dependent mass terms for all scalar degrees of freedom are induced, and also the vev as well as the couplings become source-dependent, $\kappa = \kappa(J)$, $\lambda_n = \lambda_n(J)$. In any case, each of these different IR deformations of the model leads to similar results. They parametrize a decoupling of the Goldstone modes which removes the contamination of the IR flow from degrees of freedom which are not present in the spectrum of the standard model.

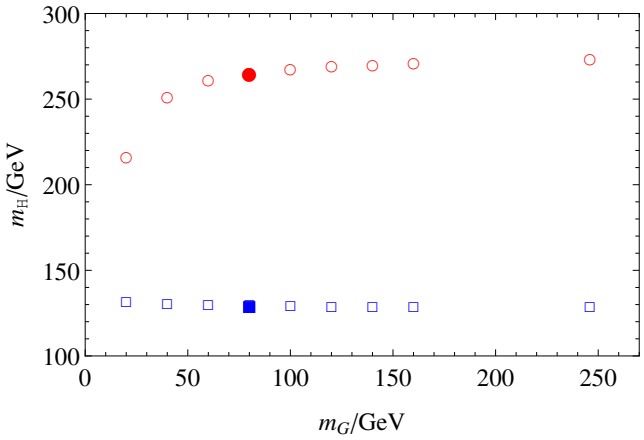

Figure A.3: Higgs mass m_H as a function of the modeled mass of the would-be Goldstone bosons for a weakly coupled ($\lambda_{2,\Lambda} = 0$, blue squares) as well as for a strongly coupled ($\lambda_{2,\Lambda} = 10$, red circles) scalar sector. The filled characters mark the Higgs masses computed for the value $m_G = 80$GeV which we have used in the main text to derive our quantitative results.

A.7 Impact of the top quark mass on Higgs mass values

The top mass plays an important role in the study of the lower Higgs mass bound within ϕ^4 theory. Within the perturbative line of reasoning, a change of the top mass by 1 GeV goes along with a change of the Higgs mass bound by approximately 2 GeV in standard model calculations. As the Higgs mass is near (or presumably below) the conventional lower bound, an accurate determination of the mass of the top quark in the appropriate renormalization scheme [82] is crucial for a discussion of the consequences of this "near criticality" [83].

In this appendix, we study the values for the Higgs boson mass for a given initial bare potential of ϕ^4 as a function of the top quark mass in order to analyze the top quark mass dependence in the present model. Within our truncation of the effective action, our top-mass IR parameter automatically coincides with the pole mass, the latter being the phenomenologically relevant quantity. (Straightforwardly computable) differences between these mass parameters only arise at next-to-next-to-leading order in the derivative expansion.

For the class of ϕ^4-type bare potentials, table A.1 summarizes our results for the Higgs mass for the lower mass bound ($\lambda_{2,\Lambda} = 0$) as well as for a strongly coupled scalar sector ($\lambda_{2,\Lambda} = 10$) as a function of the top quark mass for $\Lambda = 10^7$GeV. For the weakly coupled scalar sector, $\lambda_{2,\Lambda} = 0$, the Higgs mass is generated essentially through top quark fluctuations. Therefore, the resulting Higgs mass values are most sensitive to the precise mass of the top quark. In the present model, the Higgs mass is shifted by approximately 3 GeV for a change in the top mass by 2 GeV using a cutoff of $\Lambda = 10^7$GeV. With increasing cutoff the deviation of the Higgs mass is larger. This phenomenon is illustrated in Fig. A.4 where the spread of the lower bound for larger cutoff scales is shown.

By contrast, we find only a slight impact of the top mass on the Higgs mass for the case of a strongly coupled scalar sector. This illustrates that the Higgs mass is rather dominated by

m_{t}[GeV]	m_{H}[GeV] ($\lambda_{2,\Lambda} = 0$)	m_{H}[GeV] ($\lambda_{2,\Lambda} = 10$)
163	115.6	264.2
165	118.5	264.6
167	121.4	264.8
169	124.2	265.0
171	127.1	265.2
173	**130.1**	**265.4**
175	133.1	265.7
177	136.1	265.9
179	139.3	266.2
181	142.2	266.4
183	145.4	266.7

Table A.1: Higgs masses for the lower bound ($\lambda_{2,\Lambda} = 0$) and for a strongly interacting scalar sector ($\lambda_{2,\Lambda} = 10$) for a cutoff of $\Lambda = 10^7$GeV as a function of the top quark mass. Bold numbers indicate the standard top mass of 173GeV.

scalar fluctuations in this regime.

A.8 Fixed point structure

As the flow equation provides us with information about the system beyond perturbative limitations, we can explore the properties of the model also at stronger coupling. In particular, it is worthwhile to search for possible RG fixed points at finite values of the couplings (non-Gaußian fixed points), as these offer the chance to evade the triviality problem. Pure field-theory UV completions are possible within the asymptotic safety scenario, where the UV limit $\Lambda \to \infty$ can be taken safely by means of a UV stable RG fixed point [39], as is even explored for quantum gravity [41], see [217, 271] for reviews and examples. Provided such a fixed point exists and has suitable properties the theory remains interacting (non-trivial) in the long-range limit and has predictive power.

The search for such fixed points in Yukawa systems has recently been revived with systematic studies in the framework of the functional renormalization group. A general mechanism for inducing asymptotic safety in such systems has been identified in [52], relying on a dynamical balance between boson and fermion fluctuations. Chiral Yukawa models have successively been studied in this context [53] providing hints for the possible existence of such fixed points, but also indicating that fully gauged models may be required for a stable asymptotic safety scenario of standard-model like theories. Gauged models indeed appear to offer different routes to UV complete theories either in the weak-coupling asymptotically-free limit [56], at fully interacting fixed points (including the loss of asymptotic freedom) [55], or even in combination with quantum gravity [178, 242]. In fact, asymptotic safety has become a viable concept of consistently quantizing gravity in the recent years. Also nonlinear chiral models have been explored along this direction [272].

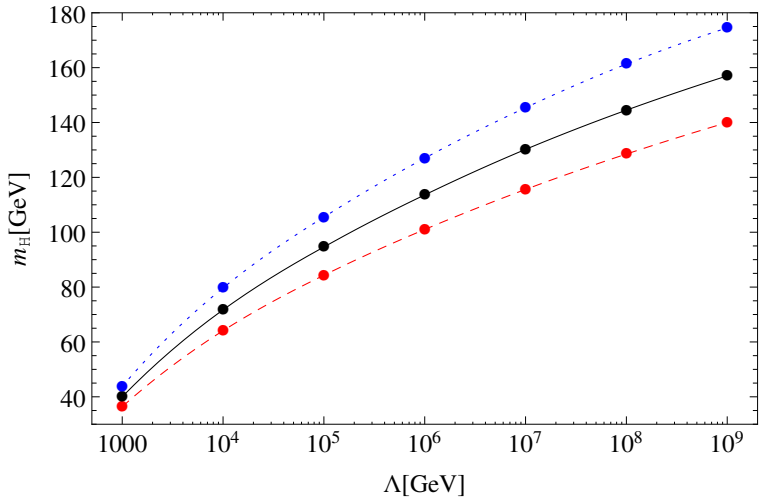

Figure A.4: Higgs mass m_{H} as a function of the cutoff Λ for different values of m_{t}. The black solid line is the lower bound for $m_{\mathrm{t}} = 173\mathrm{GeV}$ using $\lambda_{2,\Lambda} = 0$ for a ϕ^4-type bare potential. In addition lower Higgs mass bounds for $m_{\mathrm{t}} = 163\mathrm{GeV}$ (red dashed lower curve) and $m_{\mathrm{t}} = 183\mathrm{GeV}$ (blue dotted upper line) are plotted.

Here, we concentrate again on the pure chiral Yukawa sector, performing an analysis much in the spirit of [53], paying particular attention to the additional bottom quark degree of freedom.

A.8.1 Symmetric Regime

Whereas the mechanism identified in [52] operates in the regime of spontaneous symmetry breaking, it is instructive to start the fixed point search in the symmetric regime, where the flow equations are less complex. The flow equations for the Yukawa couplings using the linear regulator read in this regime:

$$\partial_t h_{\mathrm{t}}^2 = h_{\mathrm{t}}^2 \left[\eta_\phi + 2\eta_{\mathrm{t}} - h_{\mathrm{b}}^2 \frac{16 v_d}{d} \left(\frac{1 - \frac{\eta_{\mathrm{t}}}{d+1}}{1+\lambda_1} + \frac{1 - \frac{\eta_\phi}{d+2}}{(1+\lambda_1)^2} \right) \right],$$
$$\partial_t h_{\mathrm{b}}^2 = h_{\mathrm{b}}^2 \left[\eta_\phi + 2\eta_{\mathrm{b}} - h_{\mathrm{t}}^2 \frac{16 v_d}{d} \left(\frac{1 - \frac{\eta_{\mathrm{b}}}{d+1}}{1+\lambda_1} + \frac{1 - \frac{\eta_\phi}{d+2}}{(1+\lambda_1)^2} \right) \right],$$

where $\lambda_1 \geq 0$ corresponds to the mass-like term in the effective potential in the SYM regime. Let us start with resolving the fixed point conditions $\partial_t h_{\mathrm{t}}^2 = 0$ and $\partial_t h_{\mathrm{b}}^2 = 0$ in leading order in the derivative expansion: for $\eta_i = 0$, both conditions can be satisfied for either $h_{\mathrm{b}} = 0$ and h_{t} arbitrary or vice versa. Without loss of generality, let us assume that $h_{\mathrm{b}} = 0$, leaving us with a free parameter h_{t}^*, labeling a potential line of fixed points. Now it is easy also to solve the fixed-point condition for the effective potential, $\partial_t u = 0$, cf. Eq. (5.4), with an arbitrarily chosen value for h_{t}^* at least within a polynomial expansion of $u(\tilde{\rho})$. We do not pursue this any further, since this line of fixed points does not exist beyond leading order.

At next-to leading order it is necessary to include the equations for the anomalous dimensions,

which read for the linear regulator in the SYM regime

$$\begin{aligned}
\eta_\phi &= \frac{8v_d}{d}\Big[h_\mathrm{t}^2(4-\eta_\mathrm{t}) + h_\mathrm{b}^2(4-\eta_\mathrm{b})\Big],\\
\eta_\mathrm{t} &= \frac{4v_d}{d}\frac{3h_\mathrm{t}^2+h_\mathrm{b}^2}{(1+\lambda_1)^2}\Big(1-\frac{\eta_\phi}{d+1}\Big),\\
\eta_\mathrm{b} &= \frac{4v_d}{d}\frac{h_\mathrm{t}^2+3h_\mathrm{b}^2}{(1+\lambda_1)^2}\Big(1-\frac{\eta_\phi}{d+1}\Big).
\end{aligned}$$

It is useful to study a linear combination of the two fixed point conditions, $0 = \frac{1}{h_\mathrm{t}^2}\partial_t h_\mathrm{t}^2 - \frac{1}{h_\mathrm{b}^2}\partial_t h_\mathrm{b}^2$, assuming that $h_\mathrm{t} \neq 0 \neq h_\mathrm{b}$,

$$\begin{aligned}
0 &= \frac{1}{h_\mathrm{t}^2}\partial_t h_\mathrm{t}^2 - \frac{1}{h_\mathrm{b}^2}\partial_t h_\mathrm{b}^2\\
&= 2(\eta_\mathrm{t}+\eta_\mathrm{b}) - \frac{16v_d}{d}\left[\frac{1-\frac{\eta_\mathrm{b}}{d+1}}{1+\lambda_1} + \frac{1-\frac{\eta_\phi}{d+2}}{(1+\lambda_1)^2}\right](h_\mathrm{t}^2-h_\mathrm{b}^2)\\
&= -\frac{8v_d}{d}\left[2\frac{1-\frac{\eta_\mathrm{t}}{d+1}}{1+\lambda_1} + \frac{1-\frac{d\eta_\phi}{(d+2)(d+1)}}{(1+\lambda_1)^2}\right](h_\mathrm{t}^2-h_\mathrm{b}^2).
\end{aligned} \tag{A.17}$$

In order to justify the use of the derivative expansion of the effective action, we demand for the anomalous dimensions η_i to remain sufficiently small also at a possible fixed point, $\eta_i^* \lesssim 1$. As a consequence, the term in the square bracket of Eq. (A.17) is positive. This condition can only be solved by $h_\mathrm{t}^2 = h_\mathrm{b}^2$. Therefore the system of algebraic fixed-point equations reduces to

$$\begin{aligned}
0 &= \eta_\phi + 2\eta_\mathrm{t} - \frac{16v_d}{d}h_\mathrm{t}^2\Big[\frac{1-\frac{\eta_\mathrm{t}}{d+1}}{1+\lambda_1} + \frac{1-\frac{\eta_\phi}{d+2}}{(1+\lambda_1)^2}\Big],\\
\eta_\mathrm{t} &= \frac{16v_d}{d}h_\mathrm{t}^2\frac{1-\frac{\eta_\phi}{d+1}}{(1+\lambda_1)^2},\\
\eta_\phi &= \frac{16v_d}{d}h_\mathrm{t}^2(4-\eta_\mathrm{t}).
\end{aligned} \tag{A.18}$$

The constraints on the anomalous dimensions $\eta_i < 1$ imply that also $\eta_i > 0$ holds, as the negative terms linear in η_i on the right-hand sides of Eq. (A.18) remain subdominant compared with the positive terms. Expressing the constraints $0 < \eta_\phi < 1$ and $0 < \eta_t < 1$ through a constraint on the top Yukawa coupling via the last two lines of Eq. (A.18) leads to a constraint on h_t^2: $0 \leq h_\mathrm{t}^2 \leq 4\pi^2[5(1+\lambda_1)^2 - \sqrt{5}\sqrt{(1+\lambda_1)^4 - (1+\lambda_1)^2}]$ for $d = 4$. Within this constraint, a solution for the fixed point equation (first line of Eq. (A.18)) does not exist independently of any permissible value of λ_1. Hence, we do not find a nontrivial fixed point within our present truncation in the symmetric regime in four spacetime dimensions.

A.8.2 SSB regime

Because of the couplings of the fluctuating fields to the condensate the structure of the flow equations in the SSB regime is much richer than in the symmetric case. As a starting point we analyze the beta functions to leading order in the derivative expansion and expand the potential to the lowest nontrivial order in the field invariant, $u = \frac{\lambda_2}{2}(\rho - \kappa)^2$. Therefore, we have to solve the following nonlinear system of equations:

$$\begin{aligned}
\partial_t \kappa &= \beta_\kappa(\kappa^*, \lambda_2^*, h_\mathrm{t}^*, h_\mathrm{b}^*) &&= 0, \\
\partial_t \lambda_2 &= \beta_{\lambda_2}(\kappa^*, \lambda_2^*, h_\mathrm{t}^*, h_\mathrm{b}^*) &&= 0, \\
\partial_t h_\mathrm{t} &= \beta_{h_\mathrm{t}}(\kappa^*, \lambda_2^*, h_\mathrm{t}^*, h_\mathrm{b}^*) &&= 0, \\
\partial_t h_\mathrm{b} &= \beta_{h_\mathrm{b}}(\kappa^*, \lambda_2^*, h_\mathrm{t}^*, h_\mathrm{b}^*) &&= 0,
\end{aligned}$$

where the flow equations can be read off from Eqn. (5.4), (5.6) and (5.7). For the linear regulator, this system can be solved analytically resulting in two inequivalent fixed points for admissible physical parameters ($\kappa > 0$, $h_\mathrm{t}^2 \geq 0$, $h_\mathrm{b}^2 \geq 0$, $\lambda_2 > 0$). The values of the fixed point couplings are listed in Tab. A.2. First of all note that there are two additional fixed points by exchanging the numerical values for h_t^* and h_b^* due to the fact that the flow equations are symmetric under an exchange of the Yukawa couplings. Of course, these additional fixed points are physically equivalent to those given in Tab. A.2, corresponding to a mere renaming of the couplings.

κ^*	λ_2^*	h_t^{*2}	h_b^{*2}
0.006749086	14.6058	6942.84	0
0.000934843	270.652	661.201	0

Table A.2: Fixed point values for the various parameters in the SSB regime to leading order in the derivative expansion.

Furthermore, the flow equations of the Yukawa couplings are proportional to the Yukawa couplings themselves, $\partial_t h_a^2 \propto h_a^2$, which leads to a decoupling of the bottom quark at all scales. Therefore the system reduces to that studied in [53].

In order to check if these fixed points persist beyond the leading order, we have to include the anomalous dimensions of the fields. As long as these quantities, which measure the influence of higher derivative terms in our truncation, remain small, the derivative expansion appears legitimate. For a first impression of the size of the anomalous dimensions, we insert the leading order fixed point values listed in Tab. A.2 into the right-hand sides of Eqn. (5.8)-(5.11). Similar to the results of [53] the anomalous dimensions of the fields at the fixed points are large, especially η_t is much larger than one, ($\eta_\mathrm{t} \simeq 22$ for the first fixed point and $\eta_\mathrm{t} \simeq 4$ for the second one). This casts serious doubts on the existence of these fixed points in the full theory. In fact, it has been shown numerically in [53] that the fixed points do not persist as soon as

back-reactions of the anomalous dimensions are included. This can be traced back to large contributions of massless modes, such as the Goldstone and bottom quark modes near the would-be fixed point.

To summarize, we find no indications that the present chiral model in its pure form supports physically acceptable fixed points within the validity domain of the derivative expansion of the effective action.

Bibliography

[1] Georges Aad et al. 'Observation of a new particle in the search for the Standard Model Higgs boson with the ATLAS detector at the LHC'. In: *Phys. Lett.* B716 (2012), pp. 1–29. DOI: 10.1016/j.physletb.2012.08.020. arXiv: 1207.7214 [hep-ex].

[2] Serguei Chatrchyan et al. 'Observation of a new boson at a mass of 125 GeV with the CMS experiment at the LHC'. In: *Phys. Lett.* B716 (2012), pp. 30–61. DOI: 10.1016/j.physletb.2012.08.021. arXiv: 1207.7235 [hep-ex].

[3] S. L. Glashow. 'Partial Symmetries of Weak Interactions'. In: *Nucl. Phys.* 22 (1961), pp. 579–588. DOI: 10.1016/0029-5582(61)90469-2.

[4] F. Englert and R. Brout. 'Broken Symmetry and the Mass of Gauge Vector Mesons'. In: *Phys. Rev. Lett.* 13 (1964), pp. 321–323. DOI: 10.1103/PhysRevLett.13.321.

[5] Peter W. Higgs. 'Broken symmetries, massless particles and gauge fields'. In: *Phys. Lett.* 12 (1964), pp. 132–133. DOI: 10.1016/0031-9163(64)91136-9.

[6] Peter W. Higgs. 'Broken Symmetries and the Masses of Gauge Bosons'. In: *Phys. Rev. Lett.* 13 (1964), pp. 508–509. DOI: 10.1103/PhysRevLett.13.508.

[7] Peter W. Higgs. 'Spontaneous Symmetry Breakdown without Massless Bosons'. In: *Phys. Rev.* 145 (1966), pp. 1156–1163. DOI: 10.1103/PhysRev.145.1156.

[8] G. S. Guralnik, C. R. Hagen and T. W. B. Kibble. 'Global Conservation Laws and Massless Particles'. In: *Phys. Rev. Lett.* 13 (1964), pp. 585–587. DOI: 10.1103/PhysRevLett.13.585.

[9] Philip W. Anderson. 'Plasmons, Gauge Invariance, and Mass'. In: *Phys. Rev.* 130 (1963), pp. 439–442. DOI: 10.1103/PhysRev.130.439.

[10] Steven Weinberg. 'A Model of Leptons'. In: *Phys. Rev. Lett.* 19 (1967), pp. 1264–1266. DOI: 10.1103/PhysRevLett.19.1264.

[11] Abdus Salam. 'Weak and Electromagnetic Interactions'. In: *Conf. Proc.* C680519 (1968), pp. 367–377.

[12] S. L. Glashow, J. Iliopoulos and L. Maiani. 'Weak Interactions with Lepton-Hadron Symmetry'. In: *Phys. Rev.* D2 (1970), pp. 1285–1292. DOI: 10.1103/PhysRevD.2.1285.

[13] O. W. Greenberg. 'Spin and Unitary Spin Independence in a Paraquark Model of Baryons and Mesons'. In: *Phys. Rev. Lett.* 13 (1964), pp. 598–602. DOI: 10.1103/PhysRevLett.13.598.

[14] M. Y. Han and Yoichiro Nambu. 'Three Triplet Model with Double SU(3) Symmetry'. In: *Phys. Rev.* 139 (1965), B1006–B1010. DOI: 10.1103/PhysRev.139.B1006.

[15] M. Gell-Mann. 'Quarks'. In: *Acta Phys. Austriaca Suppl.* 9 (1972), pp. 733–761. DOI: 10.1007/978-3-7091-4034-5_20.

[16] G. Zweig. 'An SU(3) model for strong interaction symmetry and its breaking. Version 1'. In: (1964).

[17] G. Zweig. 'An SU(3) model for strong interaction symmetry and its breaking. Version 2'. In: *DEVELOPMENTS IN THE QUARK THEORY OF HADRONS. VOL. 1. 1964 - 1978*. Ed. by D.B. Lichtenberg and Simon Peter Rosen. 1964, pp. 22–101. URL: https://inspirehep.net/record/4674/files/cern-th-412.pdf.

[18] H. Fritzsch, Murray Gell-Mann and H. Leutwyler. 'Advantages of the Color Octet Gluon Picture'. In: *Phys. Lett.* B47 (1973), pp. 365–368. DOI: 10.1016/0370-2693(73)90625-4.

[19] F. J. Hasert et al. 'Observation of Neutrino Like Interactions Without Muon Or Electron in the Gargamelle Neutrino Experiment'. In: *Phys. Lett.* B46 (1973), pp. 138–140. DOI: 10.1016/0370-2693(73)90499-1.

[20] G. Arnison et al. 'Experimental Observation of Isolated Large Transverse Energy Electrons with Associated Missing Energy at s**(1/2) = 540-GeV'. In: *Phys. Lett.* B122 (1983), pp. 103–116. DOI: 10.1016/0370-2693(83)91177-2.

[21] G. Arnison et al. 'Experimental Observation of Lepton Pairs of Invariant Mass Around 95-GeV/c**2 at the CERN SPS Collider'. In: *Phys. Lett.* B126 (1983), pp. 398–410. DOI: 10.1016/0370-2693(83)90188-0.

[22] M. Banner et al. 'Observation of Single Isolated Electrons of High Transverse Momentum in Events with Missing Transverse Energy at the CERN anti-p p Collider'. In: *Phys. Lett.* B122 (1983), pp. 476–485. DOI: 10.1016/0370-2693(83)91605-2.

[23] F. Abe et al. 'Observation of top quark production in $\bar{p}p$ collisions'. In: *Phys. Rev. Lett.* 74 (1995), pp. 2626–2631. DOI: 10.1103/PhysRevLett.74.2626. arXiv: hep-ex/9503002 [hep-ex].

[24] S. Abachi et al. 'Observation of the top quark'. In: *Phys. Rev. Lett.* 74 (1995), pp. 2632–2637. DOI: 10.1103/PhysRevLett.74.2632. arXiv: hep-ex/9503003 [hep-ex].

[25] Georges Aad et al. 'Evidence for the spin-0 nature of the Higgs boson using ATLAS data'. In: *Phys. Lett.* B726 (2013), pp. 120–144. DOI: 10.1016/j.physletb.2013.08.026. arXiv: 1307.1432 [hep-ex].

[26] Serguei Chatrchyan et al. 'Study of the Mass and Spin-Parity of the Higgs Boson Candidate Via Its Decays to Z Boson Pairs'. In: *Phys. Rev. Lett.* 110.8 (2013), p. 081803. DOI: 10.1103/PhysRevLett.110.081803. arXiv: 1212.6639 [hep-ex].

[27] Vardan Khachatryan et al. 'Constraints on the spin-parity and anomalous HVV couplings of the Higgs boson in proton collisions at 7 and 8 TeV'. In: *Phys. Rev.* D92.1 (2015), p. 012004. DOI: 10.1103/PhysRevD.92.012004. arXiv: 1411.3441 [hep-ex].

[28] Serguei Chatrchyan et al. 'Observation of a new boson with mass near 125 GeV in pp collisions at $\sqrt{s} = 7$ and 8 TeV'. In: *JHEP* 06 (2013), p. 081. DOI: 10.1007/JHEP06(2013)081. arXiv: 1303.4571 [hep-ex].

[29] Georges Aad et al. 'Evidence for the Higgs-boson Yukawa coupling to tau leptons with the ATLAS detector'. In: *JHEP* 04 (2015), p. 117. DOI: 10.1007/JHEP04(2015)117. arXiv: 1501.04943 [hep-ex].

[30] Serguei Chatrchyan et al. 'Evidence for the direct decay of the 125 GeV Higgs boson to fermions'. In: *Nature Phys.* 10 (2014), pp. 557–560. DOI: 10.1038/nphys3005. arXiv: 1401.6527 [hep-ex].

[31] Roel Aaij et al. 'Angular analysis and differential branching fraction of the decay $B_s^0 \to \phi\mu^+\mu^-$'. In: *JHEP* 09 (2015), p. 179. DOI: 10.1007/JHEP09(2015)179. arXiv: 1506.08777 [hep-ex].

[32] Albert Einstein. 'The Foundation of the General Theory of Relativity'. In: *Annalen Phys.* 49 (1916). [Annalen Phys.14,517(2005)], pp. 769–822. DOI: 10.1002/andp.200590044.

[33] J. Polchinski. *String theory. Vol. 1: An introduction to the bosonic string*. Cambridge University Press, 2007. ISBN: 9780511252273, 9780521672276, 9780521633031.

[34] J. Polchinski. *String theory. Vol. 2: Superstring theory and beyond*. Cambridge University Press, 2007. ISBN: 9780511252280, 9780521633048, 9780521672283.

[35] Michael B. Green, J. H. Schwarz and Edward Witten. *Superstring Theory. Vol. 1: Introduction*. 1988. ISBN: 978-0-521-35752-4. URL: http://www.cambridge.org/us/academic/subjects/physics/theoretical-physics-and-mathematical-physics/superstring-theory-volume-1.

[36] Michael B. Green, J. H. Schwarz and Edward Witten. *Superstring Theory. Vol. 2: Loop Amplitudes, Anomalies and Phenomenology*. 1988. ISBN: 978-0-521-35753-1. URL: http://www.cambridge.org/us/academic/subjects/physics/theoretical-physics-and-mathematical-physics/superstring-theory-volume-2.

[37] A. Ashtekar. 'New Variables for Classical and Quantum Gravity'. In: *Phys. Rev. Lett.* 57 (1986), pp. 2244–2247. DOI: 10.1103/PhysRevLett.57.2244.

[38] Daniel Z. Freedman, P. van Nieuwenhuizen and S. Ferrara. 'Progress Toward a Theory of Supergravity'. In: *Phys. Rev.* D13 (1976), pp. 3214–3218. DOI: 10.1103/PhysRevD.13.3214.

[39] Steven Weinberg. 'Critical Phenomena for Field Theorists'. In: *Erice Subnucl.Phys.1976:1.* 1976, p. 1.

[40] Steven Weinberg. 'Ultraviolet Divergences in Quantum Theories of Gravitation'. In: *General Relativity: An Einstein Centenary Survey.* 1980, pp. 790–831.

[41] M. Reuter. 'Nonperturbative evolution equation for quantum gravity'. In: *Phys. Rev.* D57 (1998), pp. 971–985. DOI: 10.1103/PhysRevD.57.971. arXiv: hep-th/9605030 [hep-th].

[42] Jogesh C. Pati and Abdus Salam. 'Lepton Number as the Fourth Color'. In: *Phys. Rev.* D10 (1974). [Erratum: Phys. Rev.D11,703(1975)], pp. 275–289. DOI: 10.1103/PhysRevD.10.275,10.1103/PhysRevD.11.703.2.

[43] H. Georgi and S. L. Glashow. 'Unity of All Elementary Particle Forces'. In: *Phys. Rev. Lett.* 32 (1974), pp. 438–441. DOI: 10.1103/PhysRevLett.32.438.

[44] K. G. Wilson and John B. Kogut. 'The Renormalization group and the epsilon expansion'. In: *Phys. Rept.* 12 (1974), pp. 75–200. DOI: 10.1016/0370-1573(74)90023-4.

[45] David J. E. Callaway. 'Triviality Pursuit: Can Elementary Scalar Particles Exist?' In: *Phys. Rept.* 167 (1988), p. 241. DOI: 10.1016/0370-1573(88)90008-7.

[46] M. Luscher and P. Weisz. 'Scaling Laws and Triviality Bounds in the Lattice phi**4 Theory. 2. One Component Model in the Phase with Spontaneous Symmetry Breaking'. In: *Nucl. Phys.* B295 (1988), p. 65. DOI: 10.1016/0550-3213(88)90228-3.

[47] M. Luscher and P. Weisz. 'Scaling Laws and Triviality Bounds in the Lattice phi**4 Theory. 3. N Component Model'. In: *Nucl. Phys.* B318 (1989), p. 705. DOI: 10.1016/0550-3213(89)90637-8.

[48] Anna Hasenfratz et al. 'The Triviality Bound of the Four Component phi**4 Model'. In: *Phys. Lett.* B199 (1987), p. 531. DOI: 10.1016/0370-2693(87)91622-4.

[49] Urs M. Heller, Herbert Neuberger and Pavlos M. Vranas. 'Large N analysis of the Higgs mass triviality bound'. In: *Nucl. Phys.* B399 (1993), pp. 271–348. DOI: 10.1016/0550-3213(93)90499-F. arXiv: hep-lat/9207024 [hep-lat].

[50] Urs M. Heller et al. 'Numerical analysis of the Higgs mass triviality bound'. In: *Nucl. Phys.* B405 (1993), pp. 555–573. DOI: 10.1016/0550-3213(93)90559-8. arXiv: hep-ph/9303215 [hep-ph].

[51] Oliver J. Rosten. 'Triviality from the Exact Renormalization Group'. In: *JHEP* 07 (2009), p. 019. DOI: 10.1088/1126-6708/2009/07/019. arXiv: 0808.0082 [hep-th].

[52] Holger Gies and Michael M. Scherer. 'Asymptotic safety of simple Yukawa systems'. In: *Eur. Phys. J.* C66 (2010), pp. 387–402. DOI: 10.1140/epjc/s10052-010-1256-z. arXiv: 0901.2459 [hep-th].

[53] Holger Gies, Stefan Rechenberger and Michael M. Scherer. 'Towards an Asymptotic-Safety Scenario for Chiral Yukawa Systems'. In: *Eur. Phys. J.* C66 (2010), pp. 403–418. DOI: 10.1140/epjc/s10052-010-1257-y. arXiv: 0907.0327 [hep-th].

[54] Gian Paolo Vacca and Luca Zambelli. 'Multimeson Yukawa interactions at criticality'. In: *Phys. Rev.* D91.12 (2015), p. 125003. DOI: 10.1103/PhysRevD.91.125003. arXiv: 1503.09136 [hep-th].

[55] Daniel F. Litim and Francesco Sannino. 'Asymptotic safety guaranteed'. In: *JHEP* 12 (2014), p. 178. DOI: 10.1007/JHEP12(2014)178. arXiv: 1406.2337 [hep-th].

[56] Holger Gies et al. 'An asymptotic safety scenario for gauged chiral Higgs-Yukawa models'. In: *Eur. Phys. J.* C73 (2013), p. 2652. DOI: 10.1140/epjc/s10052-013-2652-y. arXiv: 1306.6508 [hep-th].

[57] Bob Holdom, Jing Ren and Chen Zhang. 'Stable Asymptotically Free Extensions (SAFEs) of the Standard Model'. In: *JHEP* 03 (2015), p. 028. DOI: 10.1007/JHEP03(2015)028. arXiv: 1412.5540 [hep-ph].

[58] Holger Gies and Luca Zambelli. 'Asymptotically free scaling solutions in non-Abelian Higgs models'. In: *Phys. Rev.* D92.2 (2015), p. 025016. DOI: 10.1103/PhysRevD.92.025016. arXiv: 1502.05907 [hep-ph].

[59] L. Maiani, G. Parisi and R. Petronzio. 'Bounds on the Number and Masses of Quarks and Leptons'. In: *Nucl. Phys.* B136 (1978), p. 115. DOI: 10.1016/0550-3213(78)90018-4.

[60] N. Cabibbo et al. 'Bounds on the Fermions and Higgs Boson Masses in Grand Unified Theories'. In: *Nucl. Phys.* B158 (1979), pp. 295–305. DOI: 10.1016/0550-3213(79)90167-6.

[61] M. Lindner. 'Implications of Triviality for the Standard Model'. In: *Z. Phys.* C31 (1986), p. 295. DOI: 10.1007/BF01479540.

[62] Julius Kuti, Lee Lin and Yue Shen. 'Upper Bound on the Higgs Mass in the Standard Model'. In: *Phys. Rev. Lett.* 61 (1988), p. 678. DOI: 10.1103/PhysRevLett.61.678.

[63] Thomas Hambye and Kurt Riesselmann. 'Matching conditions and Higgs mass upper bounds revisited'. In: *Phys. Rev.* D55 (1997), pp. 7255–7262. DOI: 10.1103/PhysRevD.55.7255. arXiv: hep-ph/9610272 [hep-ph].

[64] Zoltan Fodor et al. 'New Higgs physics from the lattice'. In: *PoS* LAT2007 (2007), p. 056. arXiv: 0710.3151 [hep-lat].

[65] I. V. Krive and Andrei D. Linde. 'On the Vacuum Stability Problem in Gauge Theories'. In: *Nucl. Phys.* B117 (1976), p. 265. DOI: 10.1016/0550-3213(76)90573-3.

[66] N. V. Krasnikov. 'Restriction of the Fermion Mass in Gauge Theories of Weak and Electromagnetic Interactions'. In: *Yad. Fiz.* 28 (1978), pp. 549–551.

[67] Pham Quang Hung. 'Vacuum Instability and New Constraints on Fermion Masses'. In: *Phys. Rev. Lett.* 42 (1979), p. 873. DOI: 10.1103/PhysRevLett.42.873.

[68] H. David Politzer and Stephen Wolfram. 'Bounds on Particle Masses in the Weinberg-Salam Model'. In: *Phys. Lett.* B82 (1979). [Erratum: Phys. Lett.83B,421(1979)], pp. 242–246. DOI: 10.1016/0370-2693(79)90746-9.

[69] Andrei D. Linde. 'Vacuum Instability, Cosmology and Constraints on Particle Masses in the Weinberg-Salam Model'. In: *Phys. Lett.* B92 (1980), p. 119. DOI: 10.1016/0370-2693(80)90318-4.

[70] Manfred Lindner, Marc Sher and Helmut W. Zaglauer. 'Probing Vacuum Stability Bounds at the Fermilab Collider'. In: *Phys. Lett.* B228 (1989), p. 139. DOI: 10.1016/0370-2693(89)90540-6.

[71] Marc Sher. 'Electroweak Higgs Potentials and Vacuum Stability'. In: *Phys. Rept.* 179 (1989), pp. 273–418. DOI: 10.1016/0370-1573(89)90061-6.

[72] Peter Brockway Arnold. 'Can the Electroweak Vacuum Be Unstable?' In: *Phys. Rev.* D40 (1989), p. 613. DOI: 10.1103/PhysRevD.40.613.

[73] Peter Brockway Arnold and Stamatis Vokos. 'Instability of hot electroweak theory: bounds on m(H) and M(t)'. In: *Phys. Rev.* D44 (1991), pp. 3620–3627. DOI: 10.1103/PhysRevD.44.3620.

[74] C. Ford et al. 'The Effective potential and the renormalization group'. In: *Nucl. Phys.* B395 (1993), pp. 17–34. DOI: 10.1016/0550-3213(93)90206-5. arXiv: hep-lat/9210033 [hep-lat].

[75] Marc Sher. 'Precise vacuum stability bound in the standard model'. In: *Phys. Lett.* B317 (1993). [Addendum: Phys. Lett.B331,448(1994)], pp. 159–163. DOI: 10.1016/0370-2693(93)91586-C. arXiv: hep-ph/9307342 [hep-ph].

[76] Guido Altarelli and G. Isidori. 'Lower limit on the Higgs mass in the standard model: An Update'. In: *Phys. Lett.* B337 (1994), pp. 141–144. DOI: 10.1016/0370-2693(94)91458-3.

[77] J. R. Espinosa and M. Quiros. 'Improved metastability bounds on the standard model Higgs mass'. In: *Phys. Lett.* B353 (1995), pp. 257–266. DOI: 10.1016/0370-2693(95)00572-3. arXiv: hep-ph/9504241 [hep-ph].

[78] Gino Isidori, Giovanni Ridolfi and Alessandro Strumia. 'On the metastability of the standard model vacuum'. In: *Nucl. Phys.* B609 (2001), pp. 387–409. DOI: 10.1016/S0550-3213(01)00302-9. arXiv: hep-ph/0104016 [hep-ph].

[79] Martin B. Einhorn and D. R. Timothy Jones. 'The Effective potential, the renormalisation group and vacuum stability'. In: *JHEP* 04 (2007), p. 051. DOI: 10.1088/1126-6708/2007/04/051. arXiv: hep-ph/0702295 [HEP-PH].

[80] J. Ellis et al. 'The Probable Fate of the Standard Model'. In: *Phys. Lett.* B679 (2009), pp. 369–375. DOI: 10.1016/j.physletb.2009.07.054. arXiv: 0906.0954 [hep-ph].

[81] Martin Holthausen, Kher Sham Lim and Manfred Lindner. 'Planck scale Boundary Conditions and the Higgs Mass'. In: *JHEP* 02 (2012), p. 037. DOI: 10.1007/JHEP02(2012)037. arXiv: 1112.2415 [hep-ph].

[82] S. Alekhin, A. Djouadi and S. Moch. 'The top quark and Higgs boson masses and the stability of the electroweak vacuum'. In: *Phys. Lett.* B716 (2012), pp. 214–219. DOI: 10.1016/j.physletb.2012.08.024. arXiv: 1207.0980 [hep-ph].

[83] Dario Buttazzo et al. 'Investigating the near-criticality of the Higgs boson'. In: *JHEP* 12 (2013), p. 089. DOI: 10.1007/JHEP12(2013)089. arXiv: 1307.3536 [hep-ph].

[84] Emidio Gabrielli et al. 'Towards Completing the Standard Model: Vacuum Stability, EWSB and Dark Matter'. In: *Phys. Rev.* D89.1 (2014), p. 015017. DOI: 10.1103/PhysRevD.89.015017. arXiv: 1309.6632 [hep-ph].

[85] Florian Loebbert and Jan Plefka. 'Quantum Gravitational Contributions to the Standard Model Effective Potential and Vacuum Stability'. In: *Mod. Phys. Lett.* A30.34 (2015), p. 1550189. DOI: 10.1142/S0217732315501898. arXiv: 1502.03093 [hep-ph].

[86] J. R. Espinosa and M. Quiros. 'On Higgs boson masses in nonminimal supersymmetric standard models'. In: *Phys. Lett.* B279 (1992), pp. 92–97. DOI: 10.1016/0370-2693(92)91846-2.

[87] J. A. Casas, J. R. Espinosa and M. Quiros. 'Improved Higgs mass stability bound in the standard model and implications for supersymmetry'. In: *Phys. Lett.* B342 (1995), pp. 171–179. DOI: 10.1016/0370-2693(94)01404-Z. arXiv: hep-ph/9409458 [hep-ph].

[88] J. A. Casas, J. R. Espinosa and M. Quiros. 'Standard model stability bounds for new physics within LHC reach'. In: *Phys. Lett.* B382 (1996), pp. 374–382. DOI: 10.1016/0370-2693(96)00682-X. arXiv: hep-ph/9603227 [hep-ph].

[89] Joan Elias-Miro et al. 'Stabilization of the Electroweak Vacuum by a Scalar Threshold Effect'. In: *JHEP* 06 (2012), p. 031. DOI: 10.1007/JHEP06(2012)031. arXiv: 1203.0237 [hep-ph].

[90] Luis A. Anchordoqui et al. 'Vacuum Stability of Standard Model^{++}'. In: *JHEP* 02 (2013), p. 074. DOI: 10.1007/JHEP02(2013)074. arXiv: 1208.2821 [hep-ph].

[91] Mario Kadastik et al. 'Implications of the 125 GeV Higgs boson for scalar dark matter and for the CMSSM phenomenology'. In: *JHEP* 05 (2012), p. 061. DOI: 10.1007/JHEP05(2012)061. arXiv: 1112.3647 [hep-ph].

[92] Oleg Lebedev. 'On Stability of the Electroweak Vacuum and the Higgs Portal'. In: *Eur. Phys. J.* C72 (2012), p. 2058. DOI: 10.1140/epjc/s10052-012-2058-2. arXiv: 1203.0156 [hep-ph].

[93] Chian-Shu Chen and Yong Tang. 'Vacuum stability, neutrinos, and dark matter'. In: *JHEP* 04 (2012), p. 019. DOI: 10.1007/JHEP04(2012)019. arXiv: 1202.5717 [hep-ph].

[94] Isabella Masina. 'Higgs boson and top quark masses as tests of electroweak vacuum stability'. In: *Phys. Rev.* D87.5 (2013), p. 053001. DOI: 10.1103/PhysRevD.87.053001. arXiv: 1209.0393 [hep-ph].

[95] Bastian Bergerhoff, Manfred Lindner and Manfred Weiser. 'Dynamics of metastable vacua in the early universe'. In: *Phys. Lett.* B469 (1999), pp. 61–68. DOI: 10.1016/S0370-2693(99)01273-3. arXiv: hep-ph/9909261 [hep-ph].

[96] J. R. Espinosa, G. F. Giudice and A. Riotto. 'Cosmological implications of the Higgs mass measurement'. In: *JCAP* 0805 (2008), p. 002. DOI: 10.1088/1475-7516/2008/05/002. arXiv: 0710.2484 [hep-ph].

[97] Nima Arkani-Hamed et al. '(No) Eternal Inflation and Precision Higgs Physics'. In: *JHEP* 03 (2008), p. 075. DOI: 10.1088/1126-6708/2008/03/075. arXiv: 0801.2399 [hep-ph].

[98] Joan Elias-Miro et al. 'Higgs mass implications on the stability of the electroweak vacuum'. In: *Phys. Lett.* B709 (2012), pp. 222–228. DOI: 10.1016/j.physletb.2012.02.013. arXiv: 1112.3022 [hep-ph].

[99] Giuseppe Degrassi et al. 'Higgs mass and vacuum stability in the Standard Model at NNLO'. In: *JHEP* 08 (2012), p. 098. DOI: 10.1007/JHEP08(2012)098. arXiv: 1205.6497 [hep-ph].

[100] Oleg Lebedev and Alexander Westphal. 'Metastable Electroweak Vacuum: Implications for Inflation'. In: *Phys. Lett.* B719 (2013), pp. 415–418. DOI: 10.1016/j.physletb.2012.12.069. arXiv: 1210.6987 [hep-ph].

[101] Fedor Bezrukov et al. 'Higgs Boson Mass and New Physics'. In: *JHEP* 10 (2012), p. 140. DOI: 10.1007/JHEP10(2012)140. arXiv: 1205.2893 [hep-ph].

[102] Fedor Bezrukov and Mikhail Shaposhnikov. 'Why should we care about the top quark Yukawa coupling?' In: *J. Exp. Theor. Phys.* 120 (2015), pp. 335–343. DOI: 10.1134/S1063776115030152. arXiv: 1411.1923 [hep-ph].

[103] Ian G. Moss. 'Vacuum stability and the scaling behaviour of the Higgs-curvature coupling'. In: (2015). arXiv: 1509.03554 [hep-th].

[104] Nobuchika Okada and Digesh Raut. 'Running Non-Minimal Inflation with Stabilized Inflaton Potential'. In: (2015). arXiv: 1509.04439 [hep-ph].

[105] Olga Czerwińska, Zygmunt Lalak and Łukasz Nakonieczny. 'Stability of the effective potential of the gauge-less top-Higgs model in curved spacetime'. In: (2015). arXiv: 1508.03297 [hep-th].

[106] José R. Espinosa, Jean-François Fortin and Maxime Trépanier. 'Consistency of Scalar Potentials from Quantum de Sitter Space'. In: (2015). arXiv: 1508.05343 [hep-th].

[107] K. Holland and J. Kuti. 'How light can the Higgs be?' In: *Nucl. Phys. Proc. Suppl.* 129 (2004). [,765(2003)], pp. 765–767. DOI: 10.1016/S0920-5632(03)02706-3. arXiv: hep-lat/0308020 [hep-lat].

[108] K. Holland. 'Triviality and the Higgs mass lower bound'. In: *Nucl. Phys. Proc. Suppl.* 140 (2005). [,155(2004)], pp. 155–161. DOI: 10.1016/j.nuclphysbps.2004.11.293. arXiv: hep-lat/0409112 [hep-lat].

[109] José Ramón Espinosa. 'Vacuum Stability and the Higgs Boson'. In: *PoS* LATTICE2013 (2014), p. 010. arXiv: 1311.1970 [hep-lat].

[110] Vincenzo Branchina and Hugo Faivre. 'Effective potential (in)stability and lower bounds on the scalar (Higgs) mass'. In: *Phys. Rev.* D72 (2005), p. 065017. DOI: 10.1103/PhysRevD.72.065017. arXiv: hep-th/0503188 [hep-th].

[111] Vincenzo Branchina, Hugo Faivre and Vincent Pangon. 'Effective potential and vacuum stability'. In: *J. Phys.* G36 (2009), p. 015006. DOI: 10.1088/0954-3899/36/1/015006. arXiv: 0802.4423 [hep-ph].

[112] Holger Gies, Clemens Gneiting and René Sondenheimer. 'Higgs Mass Bounds from Renormalization Flow for a simple Yukawa model'. In: *Phys. Rev.* D89.4 (2014), p. 045012. DOI: 10.1103/PhysRevD.89.045012. arXiv: 1308.5075 [hep-ph].

[113] P. Q. Hung and Marc Sher. 'Implications of a Higgs discovery at LEP'. In: *Phys. Lett.* B374 (1996), pp. 138–144. DOI: 10.1016/0370-2693(96)00123-2. arXiv: hep-ph/9512313 [hep-ph].

[114] J. A. Casas, V. Di Clemente and M. Quiros. 'The Standard model instability and the scale of new physics'. In: *Nucl. Phys.* B581 (2000), pp. 61–72. DOI: 10.1016/S0550-3213(00)00199-1. arXiv: hep-ph/0002205 [hep-ph].

[115] C. P. Burgess, V. Di Clemente and J. R. Espinosa. 'Effective operators and vacuum instability as heralds of new physics'. In: *JHEP* 01 (2002), p. 041. DOI: 10.1088/1126-6708/2002/01/041. arXiv: hep-ph/0201160 [hep-ph].

[116] Holger Gies and René Sondenheimer. 'Higgs Mass Bounds from Renormalization Flow for a Higgs-top-bottom model'. In: *Eur. Phys. J.* C75.2 (2015), p. 68. DOI: 10.1140/epjc/s10052-015-3284-1. arXiv: 1407.8124 [hep-ph].

[117] P. Gerhold and K. Jansen. 'The Phase structure of a chirally invariant lattice Higgs-Yukawa model for small and for large values of the Yukawa coupling constant'. In: *JHEP* 09 (2007), p. 041. DOI: 10.1088/1126-6708/2007/09/041. arXiv: 0705.2539 [hep-lat].

[118] P. Gerhold and K. Jansen. 'The Phase structure of a chirally invariant lattice Higgs-Yukawa model - numerical simulations'. In: *JHEP* 10 (2007), p. 001. DOI: 10.1088/1126-6708/2007/10/001. arXiv: 0707.3849 [hep-lat].

[119] P. Gerhold and K. Jansen. 'Lower Higgs boson mass bounds from a chirally invariant lattice Higgs-Yukawa model with overlap fermions'. In: *JHEP* 07 (2009), p. 025. DOI: 10.1088/1126-6708/2009/07/025. arXiv: 0902.4135 [hep-lat].

[120] P. Gerhold and K. Jansen. 'Upper Higgs boson mass bounds from a chirally invariant lattice Higgs-Yukawa model'. In: *JHEP* 04 (2010), p. 094. DOI: 10.1007/s13130-010-0464-1. arXiv: 1002.4336 [hep-lat].

[121] John Bulava et al. 'Higgs-Yukawa model in chirally-invariant lattice field theory'. In: *Adv. High Energy Phys.* 2013 (2013), p. 875612. DOI: 10.1155/2013/875612. arXiv: 1210.1798 [hep-lat].

[122] P. Gerhold, K. Jansen and J. Kallarackal. 'Higgs boson mass bounds in the presence of a very heavy fourth quark generation'. In: *JHEP* 01 (2011), p. 143. DOI: 10.1007/JHEP01(2011)143. arXiv: 1011.1648 [hep-lat].

[123] J. Bulava, K. Jansen and A. Nagy. 'Constraining a fourth generation of quarks: non-perturbative Higgs boson mass bounds'. In: *Phys. Lett.* B723 (2013), pp. 95–99. DOI: 10.1016/j.physletb.2013.04.041. arXiv: 1301.3416 [hep-lat].

[124] Abdelhak Djouadi and Alexander Lenz. 'Sealing the fate of a fourth generation of fermions'. In: *Phys. Lett.* B715 (2012), pp. 310–314. DOI: 10.1016/j.physletb.2012.07.060. arXiv: 1204.1252 [hep-ph].

[125] David Y. -J. Chu et al. 'A lattice study of a chirally invariant Higgs–Yukawa model including a higher dimensional Φ^6-term'. In: *Phys. Lett.* B744 (2015), pp. 146–152. DOI: 10.1016/j.physletb.2015.03.050. arXiv: 1501.05440 [hep-lat].

[126] Oscar Akerlund and Philippe de Forcrand. 'The Higgs-Yukawa model with higher dimension operators via EMFT'. In: (2015). arXiv: 1508.07959 [hep-lat].

[127] Astrid Eichhorn and Michael M. Scherer. 'Planck scale, Higgs mass, and scalar dark matter'. In: *Phys. Rev.* D90.2 (2014), p. 025023. DOI: 10.1103/PhysRevD.90.025023. arXiv: 1404.5962 [hep-ph].

[128] Astrid Eichhorn et al. 'The Higgs Mass and the Scale of New Physics'. In: *JHEP* 04 (2015), p. 022. DOI: 10.1007/JHEP04(2015)022. arXiv: 1501.02812 [hep-ph].

[129] Arthur Hebecker, Alexander K. Knochel and Timo Weigand. 'The Higgs mass from a String-Theoretic Perspective'. In: *Nucl. Phys.* B874 (2013), pp. 1–35. DOI: 10.1016/j.nuclphysb.2013.05.004. arXiv: 1304.2767 [hep-th].

[130] Michael E. Peskin and Daniel V. Schroeder. *An Introduction to quantum field theory*. 1995. ISBN: 9780201503975, 0201503972. URL: http://www.slac.stanford.edu/spires/find/books/www?cl=QC174.45:P4.

[131] M. Bohm, Ansgar Denner and H. Joos. *Gauge theories of the strong and electroweak interaction*. 2001.

[132] Taichiro Kugo. *Eichtheorie*. 1997. DOI: 10.1007/978-3-642-59128-0.

[133] K. A. Olive et al. 'Review of Particle Physics'. In: *Chin. Phys.* C38 (2014), p. 090001. DOI: 10.1088/1674-1137/38/9/090001.

[134] Nicola Cabibbo. 'Unitary Symmetry and Leptonic Decays'. In: *Phys. Rev. Lett.* 10 (1963), pp. 531–533. DOI: 10.1103/PhysRevLett.10.531.

[135] Makoto Kobayashi and Toshihide Maskawa. 'CP Violation in the Renormalizable Theory of Weak Interaction'. In: *Prog. Theor. Phys.* 49 (1973), pp. 652–657. DOI: 10.1143/PTP.49.652.

[136] B. Pontecorvo. 'Mesonium and anti-mesonium'. In: *Sov. Phys. JETP* 6 (1957). [Zh. Eksp. Teor. Fiz.33,549(1957)], p. 429.

[137] Ziro Maki, Masami Nakagawa and Shoichi Sakata. 'Remarks on the unified model of elementary particles'. In: *Prog. Theor. Phys.* 28 (1962), pp. 870–880. DOI: 10.1143/PTP.28.870.

[138] Walter E. Thirring. 'A Soluble relativistic field theory?' In: *Annals Phys.* 3 (1958), pp. 91–112. DOI: 10.1016/0003-4916(58)90015-0.

[139] Julian S. Schwinger. 'Gauge Invariance and Mass. 2.' In: *Phys. Rev.* 128 (1962), pp. 2425–2429. DOI: 10.1103/PhysRev.128.2425.

[140] F. J. Dyson. 'The S matrix in quantum electrodynamics'. In: *Phys. Rev.* 75 (1949), pp. 1736–1755. DOI: 10.1103/PhysRev.75.1736.

[141] Julian S. Schwinger. 'On the Green's functions of quantized fields. 1.' In: *Proc. Nat. Acad. Sci.* 37 (1951), pp. 452–455. DOI: 10.1073/pnas.37.7.452.

[142] Julian S. Schwinger. 'On the Green's functions of quantized fields. 2.' In: *Proc. Nat. Acad. Sci.* 37 (1951), pp. 455–459. DOI: 10.1073/pnas.37.7.455.

[143] Craig D. Roberts and Anthony G. Williams. 'Dyson-Schwinger equations and their application to hadronic physics'. In: *Prog. Part. Nucl. Phys.* 33 (1994), pp. 477–575. DOI: 10.1016/0146-6410(94)90049-3. arXiv: hep-ph/9403224 [hep-ph].

[144] Reinhard Alkofer and Lorenz von Smekal. 'The Infrared behavior of QCD Green's functions: Confinement dynamical symmetry breaking, and hadrons as relativistic bound states'. In: *Phys. Rept.* 353 (2001), p. 281. DOI: 10.1016/S0370-1573(01)00010-2. arXiv: hep-ph/0007355 [hep-ph].

[145] Christian S. Fischer. 'Infrared properties of QCD from Dyson-Schwinger equations'. In: *J. Phys.* G32 (2006), R253–R291. DOI: 10.1088/0954-3899/32/8/R02. arXiv: hep-ph/0605173 [hep-ph].

[146] Jean Zinn-Justin. 'Quantum field theory and critical phenomena'. In: *Int. Ser. Monogr. Phys.* 77 (1989), pp. 1–914.

[147] L. P. Kadanoff. 'Scaling laws for Ising models near T(c)'. In: *Physics* 2 (1966), pp. 263–272.

[148] Sidney R. Coleman and Erick J. Weinberg. 'Radiative Corrections as the Origin of Spontaneous Symmetry Breaking'. In: *Phys. Rev.* D7 (1973), pp. 1888–1910. DOI: 10.1103/PhysRevD.7.1888.

[149] A. Djouadi and R. M. Godbole. 'Electroweak symmetry breaking at the LHC'. In: *Physics at the Large Hadron Collider*. Ed. by Amitava Datta et al. 2009, pp. 47–74. DOI: 10.1007/978-81-8489-295-6_5. arXiv: 0901.2030 [hep-ph]. URL: http://inspirehep.net/record/810987/files/arXiv:0901.2030.pdf.

[150] Vincenzo Branchina and Emanuele Messina. 'Stability, Higgs Boson Mass and New Physics'. In: *Phys. Rev. Lett.* 111 (2013), p. 241801. DOI: 10.1103/PhysRevLett.111.241801. arXiv: 1307.5193 [hep-ph].

[151] Vincenzo Branchina, Emanuele Messina and Alessia Platania. 'Top mass determination, Higgs inflation, and vacuum stability'. In: *JHEP* 09 (2014), p. 182. DOI: 10.1007/JHEP09(2014)182. arXiv: 1407.4112 [hep-ph].

[152] Vincenzo Branchina, Emanuele Messina and Marc Sher. 'Lifetime of the electroweak vacuum and sensitivity to Planck scale physics'. In: *Phys. Rev.* D91 (2015), p. 013003. DOI: 10.1103/PhysRevD.91.013003. arXiv: 1408.5302 [hep-ph].

[153] Kenneth G. Wilson. 'Renormalization group and critical phenomena. 1. Renormalization group and the Kadanoff scaling picture'. In: *Phys. Rev.* B4 (1971), pp. 3174–3183. DOI: 10.1103/PhysRevB.4.3174.

[154] Kenneth G. Wilson. 'Renormalization group and critical phenomena. 2. Phase space cell analysis of critical behavior'. In: *Phys. Rev.* B4 (1971), pp. 3184–3205. DOI: 10.1103/PhysRevB.4.3184.

[155] Franz J. Wegner and Anthony Houghton. 'Renormalization group equation for critical phenomena'. In: *Phys. Rev.* A8 (1973), pp. 401–412. DOI: 10.1103/PhysRevA.8.401.

[156] Joseph Polchinski. 'Renormalization and Effective Lagrangians'. In: *Nucl. Phys.* B231 (1984), pp. 269–295. DOI: 10.1016/0550-3213(84)90287-6.

[157] Christof Wetterich. 'Exact evolution equation for the effective potential'. In: *Phys. Lett.* B301 (1993), pp. 90–94. DOI: 10.1016/0370-2693(93)90726-X.

[158] Tim R. Morris. 'Elements of the continuous renormalization group'. In: *Prog. Theor. Phys. Suppl.* 131 (1998), pp. 395–414. DOI: 10.1143/PTPS.131.395. arXiv: hep-th/9802039 [hep-th].

[159] C. Bagnuls and C. Bervillier. 'Exact renormalization group equations. An Introductory review'. In: *Phys. Rept.* 348 (2001), p. 91. DOI: 10.1016/S0370-1573(00)00137-X. arXiv: hep-th/0002034 [hep-th].

[160] Juergen Berges, Nikolaos Tetradis and Christof Wetterich. 'Nonperturbative renormalization flow in quantum field theory and statistical physics'. In: *Phys. Rept.* 363 (2002), pp. 223–386. DOI: 10.1016/S0370-1573(01)00098-9. arXiv: hep-ph/0005122 [hep-ph].

[161] K. Aoki. 'Introduction to the nonperturbative renormalization group and its recent applications'. In: *Int. J. Mod. Phys.* B14 (2000), pp. 1249–1326. DOI: 10.1016/S0217-9792(00)00092-3.

[162] Janos Polonyi. 'Lectures on the functional renormalization group method'. In: *Central Eur. J. Phys.* 1 (2003), pp. 1–71. DOI: 10.2478/BF02475552. arXiv: hep-th/0110026 [hep-th].

[163] Jan M. Pawlowski. 'Aspects of the functional renormalisation group'. In: *Annals Phys.* 322 (2007), pp. 2831–2915. DOI: 10.1016/j.aop.2007.01.007. arXiv: hep-th/0512261 [hep-th].

[164] Holger Gies. 'Introduction to the functional RG and applications to gauge theories'. In: *Lect. Notes Phys.* 852 (2012), pp. 287–348. DOI: 10.1007/978-3-642-27320-9_6. arXiv: hep-ph/0611146 [hep-ph].

[165] Bertrand Delamotte. 'An Introduction to the nonperturbative renormalization group'. In: *Lect. Notes Phys.* 852 (2012), pp. 49–132. DOI: 10.1007/978-3-642-27320-9_2. arXiv: cond-mat/0702365 [cond-mat.stat-mech].

[166] Oliver J. Rosten. 'Fundamentals of the Exact Renormalization Group'. In: *Phys. Rept.* 511 (2012), pp. 177–272. DOI: 10.1016/j.physrep.2011.12.003. arXiv: 1003.1366 [hep-th].

[167] T. Papenbrock and C. Wetterich. 'Two loop results from one loop computations and nonperturbative solutions of exact evolution equations'. In: *Z. Phys.* C65 (1995), pp. 519–535. DOI: 10.1007/BF01556140. arXiv: hep-th/9403164 [hep-th].

[168] Daniel F. Litim and Jan M. Pawlowski. 'Completeness and consistency of renormalisation group flows'. In: *Phys. Rev.* D66 (2002), p. 025030. DOI: 10.1103/PhysRevD.66.025030. arXiv: hep-th/0202188 [hep-th].

[169] Daniel F. Litim. 'Optimization of the exact renormalization group'. In: *Phys. Lett.* B486 (2000), pp. 92–99. DOI: 10.1016/S0370-2693(00)00748-6. arXiv: hep-th/0005245 [hep-th].

[170] Daniel F. Litim. 'Optimized renormalization group flows'. In: *Phys. Rev.* D64 (2001), p. 105007. DOI: 10.1103/PhysRevD.64.105007. arXiv: hep-th/0103195 [hep-th].

[171] Richard D. Ball et al. 'Scheme independence and the exact renormalization group'. In: *Phys. Lett.* B347 (1995), pp. 80–88. DOI: 10.1016/0370-2693(95)00025-G. arXiv: hep-th/9411122 [hep-th].

[172] Sen-Ben Liao, Janos Polonyi and Michael Strickland. 'Optimization of renormalization group flow'. In: *Nucl. Phys.* B567 (2000), pp. 493–514. DOI: 10.1016/S0550-3213(99)00496-4. arXiv: hep-th/9905206 [hep-th].

[173] Leonie Canet et al. 'Optimization of the derivative expansion in the nonperturbative renormalization group'. In: *Phys. Rev.* D67 (2003), p. 065004. DOI: 10.1103/PhysRevD.67.065004. arXiv: hep-th/0211055 [hep-th].

[174] Leonie Canet et al. 'Nonperturbative renormalization group approach to the Ising model: A Derivative expansion at order partial**4'. In: *Phys. Rev.* B68 (2003), p. 064421. DOI: 10.1103/PhysRevB.68.064421. arXiv: hep-th/0302227 [hep-th].

[175] M. Reuter and Frank Saueressig. 'Renormalization group flow of quantum gravity in the Einstein-Hilbert truncation'. In: *Phys. Rev.* D65 (2002), p. 065016. DOI: 10.1103/PhysRevD.65.065016. arXiv: hep-th/0110054 [hep-th].

[176] Max Niedermaier and Martin Reuter. 'The Asymptotic Safety Scenario in Quantum Gravity'. In: *Living Rev. Rel.* 9 (2006), pp. 5–173. DOI: 10.12942/lrr-2006-5.

[177] Jan-Eric Daum, Ulrich Harst and Martin Reuter. 'Running Gauge Coupling in Asymptotically Safe Quantum Gravity'. In: *JHEP* 01 (2010), p. 084. DOI: 10.1007/JHEP01(2010)084. arXiv: 0910.4938 [hep-th].

[178] Pietro Donà, Astrid Eichhorn and Roberto Percacci. 'Matter matters in asymptotically safe quantum gravity'. In: *Phys. Rev.* D89.8 (2014), p. 084035. DOI: 10.1103/PhysRevD.89.084035. arXiv: 1311.2898 [hep-th].

[179] Holger Gies, Benjamin Knorr and Stefan Lippoldt. 'Generalized Parametrization Dependence in Quantum Gravity'. In: (2015). arXiv: 1507.08859 [hep-th].

[180] Holger Gies. 'Running coupling in Yang-Mills theory: A flow equation study'. In: *Phys. Rev.* D66 (2002), p. 025006. DOI: 10.1103/PhysRevD.66.025006. arXiv: hep-th/0202207 [hep-th].

[181] Holger Gies. 'Renormalizability of gauge theories in extra dimensions'. In: *Phys. Rev.* D68 (2003), p. 085015. DOI: 10.1103/PhysRevD.68.085015. arXiv: hep-th/0305208 [hep-th].

[182] Christian S. Fischer and Holger Gies. 'Renormalization flow of Yang-Mills propagators'. In: *JHEP* 10 (2004), p. 048. DOI: 10.1088/1126-6708/2004/10/048. arXiv: hep-ph/0408089 [hep-ph].

[183] Jens Braun et al. 'On the Nature of the Phase Transition in SU(N), Sp(2) and E(7) Yang-Mills theory'. In: *Eur. Phys. J.* C70 (2010), pp. 689–702. DOI: 10.1140/epjc/s10052-010-1485-1. arXiv: 1007.2619 [hep-ph].

[184] Holger Gies and Joerg Jaeckel. 'Chiral phase structure of QCD with many flavors'. In: *Eur. Phys. J.* C46 (2006), pp. 433–438. DOI: 10.1140/epjc/s2006-02475-0. arXiv: hep-ph/0507171 [hep-ph].

[185] Christian S. Fischer and Jan M. Pawlowski. 'Uniqueness of infrared asymptotics in Landau gauge Yang-Mills theory'. In: *Phys. Rev.* D75 (2007), p. 025012. DOI: 10.1103/PhysRevD.75.025012. arXiv: hep-th/0609009 [hep-th].

[186] Jens Braun and Holger Gies. 'Chiral phase boundary of QCD at finite temperature'. In: *JHEP* 06 (2006), p. 024. DOI: 10.1088/1126-6708/2006/06/024. arXiv: hep-ph/0602226 [hep-ph].

[187] Jens Braun, Holger Gies and Jan M. Pawlowski. 'Quark Confinement from Color Confinement'. In: *Phys. Lett.* B684 (2010), pp. 262–267. DOI: 10.1016/j.physletb.2010.01.009. arXiv: 0708.2413 [hep-th].

[188] Christian S. Fischer, Axel Maas and Jan M. Pawlowski. 'On the infrared behavior of Landau gauge Yang-Mills theory'. In: *Annals Phys.* 324 (2009), pp. 2408–2437. DOI: 10.1016/j.aop.2009.07.009. arXiv: 0810.1987 [hep-ph].

[189] Christian S. Fischer and Jan M. Pawlowski. 'Uniqueness of infrared asymptotics in Landau gauge Yang-Mills theory II'. In: *Phys. Rev.* D80 (2009), p. 025023. DOI: 10.1103/PhysRevD.80.025023. arXiv: 0903.2193 [hep-th].

[190] Jens Braun et al. 'Phase Structure of Two-Flavor QCD at Finite Chemical Potential'. In: *Phys. Rev. Lett.* 106 (2011), p. 022002. DOI: 10.1103/PhysRevLett.106.022002. arXiv: 0908.0008 [hep-ph].

[191] Lisa M. Haas et al. 'Improved Polyakov-loop potential for effective models from functional calculations'. In: *Phys. Rev.* D87.7 (2013), p. 076004. DOI: 10.1103/PhysRevD.87.076004. arXiv: 1302.1993 [hep-ph].

[192] Franziska Synatschke et al. 'Flow Equation for Supersymmetric Quantum Mechanics'. In: *JHEP* 03 (2009), p. 028. DOI: 10.1088/1126-6708/2009/03/028. arXiv: 0809.4396 [hep-th].

[193] Marianne Heilmann et al. 'Convergence of Derivative Expansion in Supersymmetric Functional RG Flows'. In: *JHEP* 02 (2015), p. 109. DOI: 10.1007/JHEP02(2015)109. arXiv: 1409.5650 [hep-th].

[194] Tobias Hellwig, Andreas Wipf and Omar Zanusso. 'Scaling and superscaling solutions from the functional renormalization group'. In: (2015). arXiv: 1508.02547 [hep-th].

[195] Holger Gies and Christof Wetterich. 'Renormalization flow of bound states'. In: *Phys. Rev.* D65 (2002), p. 065001. DOI: 10.1103/PhysRevD.65.065001. arXiv: hep-th/0107221 [hep-th].

[196] Florian Schutz, Lorenz Bartosch and Peter Kopietz. 'Collective fields in the functional renormalization group for fermions, Ward identities, and the exact solution of the Tomonaga-Luttinger model'. In: *Phys. Rev.* B72 (2005), p. 035107. DOI: 10.1103/PhysRevB.72.035107. arXiv: cond-mat/0409404 [cond-mat].

[197] Koji Harada, Kenzo Inoue and Hirofumi Kubo. 'Wilsonian RG and redundant operators in nonrelativistic effective field theory'. In: *Phys. Lett.* B636 (2006), pp. 305–309. DOI: 10.1016/j.physletb.2006.03.072. arXiv: nucl-th/0511020 [nucl-th].

[198] S. Diehl et al. 'Functional renormalization group approach to the BCS-BEC crossover'. In: *Annalen Phys.* 522 (2010), pp. 615–656. DOI: 10.1002/andp.201010458. arXiv: 0907.2193 [cond-mat.quant-gas].

[199] Igor Boettcher, Jan M. Pawlowski and Christof Wetterich. 'Critical temperature and superfluid gap of the Unitary Fermi Gas from Functional Renormalization'. In: *Phys. Rev.* A89.5 (2014), p. 053630. DOI: 10.1103/PhysRevA.89.053630. arXiv: 1312.0505 [cond-mat.quant-gas].

[200] I. Boettcher et al. 'Phase structure of spin-imbalanced unitary Fermi gases'. In: *Phys. Rev.* A91.1 (2015), p. 013610. DOI: 10.1103/PhysRevA.91.013610. arXiv: 1409.5070 [cond-mat.quant-gas].

[201] Holger Gies and Lukas Janssen. 'UV fixed-point structure of the three-dimensional Thirring model'. In: *Phys. Rev.* D82 (2010), p. 085018. DOI: 10.1103/PhysRevD.82.085018. arXiv: 1006.3747 [hep-th].

[202] Walter Metzner et al. 'Functional renormalization group approach to correlated fermion systems'. In: *Rev. Mod. Phys.* 84 (2012), p. 299. DOI: 10.1103/RevModPhys.84.299. arXiv: 1105.5289 [cond-mat.str-el].

[203] Laura Classen et al. 'Mott multicriticality of Dirac electrons in graphene'. In: *Phys. Rev.* B92.3 (2015), p. 035429. DOI: 10.1103/PhysRevB.92.035429. arXiv: 1503.05002 [cond-mat.str-el].

[204] Holger Gies, Joerg Jaeckel and Christof Wetterich. 'Towards a renormalizable standard model without fundamental Higgs scalar'. In: *Phys. Rev.* D69 (2004), p. 105008. DOI: 10.1103/PhysRevD.69.105008. arXiv: hep-ph/0312034 [hep-ph].

[205] A. Jakovac, I. Kaposvari and A. Patkos. 'Scalar mass stability bound in a simple Yukawa-theory from renormalisation group equations'. In: (2015). arXiv: 1508.06774 [hep-th].

[206] Mikhail Shaposhnikov and Christof Wetterich. 'Asymptotic safety of gravity and the Higgs boson mass'. In: *Phys. Lett.* B683 (2010), pp. 196–200. DOI: 10.1016/j.physletb.2009.12.022. arXiv: 0912.0208 [hep-th].

[207] J. Frohlich, G. Morchio and F. Strocchi. 'Higgs phenomenon without a symmetry breaking order parameter'. In: *Nucl. Phys.* B190 (1981), pp. 553–582. DOI: 10.1016/0550-3213(81)90448-X.

[208] Axel Maas. 'Bound-state/elementary-particle duality in the Higgs sector and the case for an excited 'Higgs' within the standard model'. In: *Mod. Phys. Lett.* A28 (2013), p. 1350103. DOI: 10.1142/S0217732313501034. arXiv: 1205.6625 [hep-lat].

[209] Michael Thies. 'From relativistic quantum fields to condensed matter and back again: Updating the Gross-Neveu phase diagram'. In: *J. Phys.* A39 (2006), pp. 12707–12734. DOI: 10.1088/0305-4470/39/41/S04. arXiv: hep-th/0601049 [hep-th].

[210] M. P. Fry. 'Stability of QED'. In: *Phys. Rev.* D84 (2011), p. 065021. DOI: 10.1103/PhysRevD.84.065021. arXiv: 1108.4345 [hep-th].

[211] D. U. Jungnickel and C. Wetterich. 'Effective action for the chiral quark-meson model'. In: *Phys. Rev.* D53 (1996), pp. 5142–5175. DOI: 10.1103/PhysRevD.53.5142. arXiv: hep-ph/9505267 [hep-ph].

[212] L. Rosa, P. Vitale and C. Wetterich. 'Critical exponents of the Gross-Neveu model from the effective average action'. In: *Phys. Rev. Lett.* 86 (2001), pp. 958–961. DOI: 10.1103/PhysRevLett.86.958. arXiv: hep-th/0007093 [hep-th].

[213] F. Hofling, C. Nowak and C. Wetterich. 'Phase transition and critical behavior of the D = 3 Gross-Neveu model'. In: *Phys. Rev.* B66 (2002), p. 205111. DOI: 10.1103/PhysRevB.66.205111. arXiv: cond-mat/0203588 [cond-mat].

[214] S. Diehl et al. 'Flow equations for the BCS-BEC crossover'. In: *Phys. Rev.* A76 (2007), p. 021602. DOI: 10.1103/PhysRevA.76.021602. arXiv: cond-mat/0701198 [cond-mat].

[215] S. Floerchinger et al. 'Particle-hole fluctuations in the BCS-BEC Crossover'. In: *Phys. Rev.* B78 (2008), p. 174528. DOI: 10.1103/PhysRevB.78.174528. arXiv: 0808.0150 [cond-mat.supr-con].

[216] Jens Braun. 'The QCD Phase Boundary from Quark-Gluon Dynamics'. In: *Eur. Phys. J.* C64 (2009), pp. 459–482. DOI: 10.1140/epjc/s10052-009-1136-6. arXiv: 0810.1727 [hep-ph].

[217] Jens Braun, Holger Gies and Daniel D. Scherer. 'Asymptotic safety: a simple example'. In: *Phys. Rev.* D83 (2011), p. 085012. DOI: 10.1103/PhysRevD.83.085012. arXiv: 1011.1456 [hep-th].

[218] Alfio Bonanno and Dario Zappala. 'Two loop results from the derivative expansion of the blocked action'. In: *Phys. Rev.* D57 (1998), pp. 7383–7387. DOI: 10.1103/PhysRevD.57.7383. arXiv: hep-th/9712038 [hep-th].

[219] Stefano Arnone et al. 'Exact scheme independence at two loops'. In: *Phys. Rev.* D69 (2004), p. 065009. DOI: 10.1103/PhysRevD.69.065009. arXiv: hep-th/0309242 [hep-th].

[220] Alessandro Codello, Maximilian Demmel and Omar Zanusso. 'Scheme dependence and universality in the functional renormalization group'. In: *Phys. Rev.* D90.2 (2014), p. 027701. DOI: 10.1103/PhysRevD.90.027701. arXiv: 1310.7625 [hep-th].

[221] Erick J. Weinberg and Ai-qun Wu. 'Understanding complex perturbative effective potentials'. In: *Phys. Rev.* D36 (1987), p. 2474. DOI: 10.1103/PhysRevD.36.2474.

[222] J. Berges and C. Wetterich. 'Equation of state and coarse grained free energy for matrix models'. In: *Nucl. Phys.* B487 (1997), pp. 675–720. DOI: 10.1016/S0550-3213(96)00670-0. arXiv: hep-th/9609019 [hep-th].

[223] J. Berges, N. Tetradis and C. Wetterich. 'Coarse graining and first order phase transitions'. In: *Phys. Lett.* B393 (1997), pp. 387–394. DOI: 10.1016/S0370-2693(96)01654-1. arXiv: hep-ph/9610354 [hep-ph].

[224] Bernd-Jochen Schaefer and Jochen Wambach. 'The Phase diagram of the quark meson model'. In: *Nucl. Phys.* A757 (2005), pp. 479–492. DOI: 10.1016/j.nuclphysa.2005.04.012. arXiv: nucl-th/0403039 [nucl-th].

[225] Kenji Fukushima, Kazuhiko Kamikado and Bertram Klein. 'Second-order and Fluctuation-induced First-order Phase Transitions with Functional Renormalization Group Equations'. In: *Phys. Rev.* D83 (2011), p. 116005. DOI: 10.1103/PhysRevD.83.116005. arXiv: 1010.6226 [hep-ph].

[226] C. Wetterich. 'Fine Tuning Problem and the Renormalization Group'. In: *Phys. Lett.* B140 (1984), p. 215. DOI: 10.1016/0370-2693(84)90923-7.

[227] K. G. Chetyrkin and M. Steinhauser. 'The Relation between the MS-bar and the on-shell quark mass at order alpha(s)**3'. In: *Nucl. Phys.* B573 (2000), pp. 617–651. DOI: 10.1016/S0550-3213(99)00784-1. arXiv: hep-ph/9911434 [hep-ph].

[228] C. Wetterich. 'THE MASS OF THE HIGGS PARTICLE'. In: *Search for Scalar Particles: Experimental and Theoretical Aspects Trieste, Italy, July 23-24, 1987*. 1987. URL: http://alice.cern.ch/format/showfull?sysnb=0094536.

[229] C. Wetterich. 'GAUGE HIERARCHY DUE TO STRONG INTERACTIONS?' In: *Phys. Lett.* B104 (1981), p. 269. DOI: 10.1016/0370-2693(81)90124-6.

[230] Jennifer A. Adams et al. 'Solving nonperturbative flow equations'. In: *Mod. Phys. Lett.* A10 (1995), pp. 2367–2380. DOI: 10.1142/S0217732395002520. arXiv: hep-th/9507093 [hep-th].

[231] O. Bohr, B. J. Schaefer and J. Wambach. 'Renormalization group flow equations and the phase transition in O(N) models'. In: *Int. J. Mod. Phys.* A16 (2001), pp. 3823–3852. DOI: 10.1142/S0217751X0100502X. arXiv: hep-ph/0007098 [hep-ph].

[232] Thomas Fischbacher and Franziska Synatschke-Czerwonka. 'FlowPy: A Numerical solver for functional renormalization group equations'. In: *Comput. Phys. Commun.* 184 (2013), pp. 1931–1945. DOI: 10.1016/j.cpc.2013.03.002. arXiv: 1202.5984 [physics.comp-ph].

[233] Clemens Gneiting. 'Diploma thesis'. Heidelberg 2005.

[234] L. O'Raifeartaigh, A. Wipf and H. Yoneyama. 'The Constraint Effective Potential'. In: *Nucl. Phys.* B271 (1986), p. 653. DOI: 10.1016/S0550-3213(86)80031-1.

[235] R.E. Robson and A. Prytz. 'The discrete ordinate/pseudo-spectral method: review and application from a physicist's perspective'. In: *Australian Journal of Physics* 46 (1993).

[236] Rodrigo Panosso Macedo and Marcus Ansorg. 'Axisymmetric fully spectral code for hyperbolic equations'. In: *J. Comput. Phys.* 276 (2014), pp. 357–379. DOI: 10.1016/j.jcp.2014.07.040. arXiv: 1402.7343 [physics.comp-ph].

[237] Julia Borchardt and Benjamin Knorr. 'Global solutions of functional fixed point equations via pseudospectral methods'. In: *Phys. Rev.* D91.10 (2015), p. 105011. DOI: 10.1103/PhysRevD.91.105011. arXiv: 1502.07511 [hep-th].

[238] John P. Boyd. *Chebyshev and Fourier Spectral Methods*. 2nd. Dover Publications, 2000.

[239] Julia Borchardt, Holger Gies and René Sondenheimer. 'Global flow of the Higgs potential in a Yukawa model'. in preparation.

[240] Jan M. Pawlowski and Fabian Rennecke. 'Higher order quark-mesonic scattering processes and the phase structure of QCD'. In: *Phys. Rev.* D90.7 (2014), p. 076002. DOI: 10.1103/PhysRevD.90.076002. arXiv: 1403.1179 [hep-ph].

[241] Jens Braun et al. 'From Quarks and Gluons to Hadrons: Chiral Symmetry Breaking in Dynamical QCD'. In: (2014). arXiv: 1412.1045 [hep-ph].

[242] O. Zanusso et al. 'Gravitational corrections to Yukawa systems'. In: *Phys. Lett.* B689 (2010), pp. 90–94. DOI: 10.1016/j.physletb.2010.04.043. arXiv: 0904.0938 [hep-th].

[243] G. P. Vacca and O. Zanusso. 'Asymptotic Safety in Einstein Gravity and Scalar-Fermion Matter'. In: *Phys. Rev. Lett.* 105 (2010), p. 231601. DOI: 10.1103/PhysRevLett.105.231601. arXiv: 1009.1735 [hep-th].

[244] Jan M. Pawlowski. 'Geometrical effective action and Wilsonian flows'. In: (2003). arXiv: hep-th/0310018 [hep-th].

[245] Stefano Arnone, Tim R. Morris and Oliver J. Rosten. 'Manifestly gauge invariant QED'. In: *JHEP* 10 (2005), p. 115. DOI: 10.1088/1126-6708/2005/10/115. arXiv: hep-th/0505169 [hep-th].

[246] Stefano Arnone, Tim R. Morris and Oliver J. Rosten. 'A Generalised manifestly gauge invariant exact renormalisation group for SU(N) Yang-Mills'. In: *Eur. Phys. J.* C50 (2007), pp. 467–504. DOI: 10.1140/epjc/s10052-007-0258-y. arXiv: hep-th/0507154 [hep-th].

[247] Tim R. Morris and Oliver J. Rosten. 'Manifestly gauge invariant QCD'. In: *J. Phys.* A39 (2006), pp. 11657–11681. DOI: 10.1088/0305-4470/39/37/020. arXiv: hep-th/0606189 [hep-th].

[248] Ulrich Ellwanger, Manfred Hirsch and Axel Weber. 'Flow equations for the relevant part of the pure Yang-Mills action'. In: *Z. Phys.* C69 (1996), pp. 687–698. DOI: 10.1007/s002880050073. arXiv: hep-th/9506019 [hep-th].

[249] Holger Gies and Christof Wetterich. 'Universality of spontaneous chiral symmetry breaking in gauge theories'. In: *Phys. Rev.* D69 (2004), p. 025001. DOI: 10.1103/PhysRevD.69.025001. arXiv: hep-th/0209183 [hep-th].

[250] Axel Maas and Tajdar Mufti. 'Two- and three-point functions in Landau gauge Yang-Mills-Higgs theory'. In: *JHEP* 04 (2014), p. 006. DOI: 10.1007/JHEP04(2014)006. arXiv: 1312.4873 [hep-lat].

[251] T. Appelquist and Helen R. Quinn. 'Divergence cancellations in a simplified weak interaction model'. In: *Phys. Lett.* B39 (1972), pp. 229–232. DOI: 10.1016/0370-2693(72)90783-6.

[252] S. Y. Lee. 'Higher-order corrections to leptonic processes and the renormalization of weinberg's theory of weak interactions in the unitary gauge'. In: *Phys. Rev.* D6 (1972), pp. 1701–1717. DOI: 10.1103/PhysRevD.6.1701.

[253] S. Y. Lee. 'Finite higher-order weak and electromagnetic corrections to the strangeness-conserving hadronic beta decay in weinberg's theory of weak interactions'. In: *Phys. Rev.* D6 (1972), pp. 1803–1807. DOI: 10.1103/PhysRevD.6.1803.

[254] D. Ross. 'Renormalization of a spontaneous symmetry-breaking model in the unitary gauge'. In: *Nucl. Phys.* B59 (1973), pp. 23–33. DOI: 10.1016/0550-3213(73)90472-0.

[255] Gerard 't Hooft. 'Renormalizable Lagrangians for Massive Yang-Mills Fields'. In: *Nucl. Phys.* B35 (1971), pp. 167–188. DOI: 10.1016/0550-3213(71)90139-8.

[256] Gerard 't Hooft and M. J. G. Veltman. 'Regularization and Renormalization of Gauge Fields'. In: *Nucl. Phys.* B44 (1972), pp. 189–213. DOI: 10.1016/0550-3213(72)90279-9.

[257] J. Frohlich, G. Morchio and F. Strocchi. 'Higgs phenomenon without a symmetry breaking order parameter'. In: *Phys. Lett.* B97 (1980), p. 249. DOI: 10.1016/0370-2693(80)90594-8.

[258] Axel Maas and Tajdar Mufti. 'Spectroscopic analysis of the phase diagram of Yang-Mills-Higgs theory'. In: *Phys. Rev.* D91.11 (2015), p. 113011. DOI: 10.1103/PhysRevD.91.113011. arXiv: 1412.6440 [hep-lat].

[259] Axel Maas. 'Field theory as a tool to constrain new physics models'. In: *Mod. Phys. Lett.* A30.29 (2015), p. 1550135. DOI: 10.1142/S0217732315501357. arXiv: 1502.02421 [hep-ph].

[260] Pascal Törek and Axel Maas. 'Towards the spectrum of a GUT from gauge invariance'. In: *27th International Symposium on Lepton Photon Interactions at High Energy (LP15) Ljubljana, Slovenia, August 17-22, 2015*. 2015. arXiv: 1509.06497 [hep-ph]. URL: https://inspirehep.net/record/1394398/files/arXiv:1509.06497.pdf.

[261] Yoichiro Nambu. 'Quasiparticles and Gauge Invariance in the Theory of Superconductivity'. In: *Phys. Rev.* 117 (1960), pp. 648–663. DOI: 10.1103/PhysRev.117.648.

[262] J. Goldstone. 'Field Theories with Superconductor Solutions'. In: *Nuovo Cim.* 19 (1961), pp. 154–164. DOI: 10.1007/BF02812722.

[263] Jeffrey Goldstone, Abdus Salam and Steven Weinberg. 'Broken Symmetries'. In: *Phys. Rev.* 127 (1962), pp. 965–970. DOI: 10.1103/PhysRev.127.965.

[264] L. D. Faddeev and V. N. Popov. 'Feynman Diagrams for the Yang-Mills Field'. In: *Phys. Lett.* B25 (1967), pp. 29–30. DOI: 10.1016/0370-2693(67)90067-6.

[265] V. N. Gribov. 'Quantization of Nonabelian Gauge Theories'. In: *Nucl. Phys.* B139 (1978), p. 1. DOI: 10.1016/0550-3213(78)90175-X.

[266] I. M. Singer. 'Some Remarks on the Gribov Ambiguity'. In: *Commun. Math. Phys.* 60 (1978), pp. 7–12. DOI: 10.1007/BF01609471.

[267] J. C. Taylor. *Gauge Theories of Weak Interactions*. Cambridge Monographs on Mathematical Physics. Cambridge, UK: Cambridge Univ. Press, 1979. ISBN: 9780521295185. URL: http://www.cambridge.org/uk/catalogue/catalogue.asp?isbn=0521208963.

[268] Lowell S. Brown. 'Stress Tensor Trace Anomaly in a Gravitational Metric: Scalar Fields'. In: *Phys. Rev.* D15 (1977), p. 1469. DOI: 10.1103/PhysRevD.15.1469.

[269] M. Luscher. 'Dimensional Regularization in the Presence of Large Background Fields'. In: *Annals Phys.* 142 (1982), p. 359. DOI: 10.1016/0003-4916(82)90076-8.

[270] Alexander Spencer-Smith. 'Higgs Vacuum Stability in a Mass-Dependent Renormalisation Scheme'. In: (2014). arXiv: 1405.1975 [hep-ph].

[271] Roberto Percacci. 'Asymptotic Safety'. In: (2007). arXiv: 0709.3851 [hep-th].

[272] F. Bazzocchi et al. 'Fermions and Goldstone bosons in an asymptotically safe model'. In: *Phys. Lett.* B705 (2011), pp. 388–392. DOI: 10.1016/j.physletb.2011.10.029. arXiv: 1105.1968 [hep-ph].

Danksagung

Zunächst möchte ich mich herzlich bei Prof. Holger Gies bedanken. Sowohl für die vielen erhellenden Gespräche und Anregungen sowie die hervorragende Betreuung, als auch die Möglichkeit eigenen Ideen und Vorhaben nachgehen zu können.

Weiterhin bedanke ich mich bei Julia Borchardt, Astrid Eichhorn, Jörg Jäckel, Tilman Plehn, Michael Scherer und Matthias Warschinke für die fruchtbare und Erkenntnis gewinnende Zusammenarbeit bezüglich verschiedener Teilaspekte der Higgs-Physik.

Darüber hinaus gilt mein Dank den Mitgliedern des TPI Jena, im Besonderen Martin Ammon, Alexander Blinne, Tobias Hellwig, Benjamin Knorr, Julian Leiber, Stefan Lippoldt, Daniel Schmidt, Andre Sternbeck, Andreas Wipf, Luca Zambelli und Omar Zanusso für Diskussionen bezüglich der theoretischen Physik und darüber hinaus.

Zusätzlicher Dank gilt Tobias Hellwig und Luca Zambelli für ihre kritischen Kommentare bezüglich des Manuskripts.

Auf diversen Konferenzen und Workshops hatte ich das Glück lehrreiche Diskussionen mit Axel Maas, Jan Pawlowski, Jens Braun, Gerald Dunne, Karl Jansen, Lukas Janssen, Manfred Lindner, Stefan Rechenberger, Dietrich Roscher, Francesco Sannino, Pascal Törek und Gian Paolo Vacca führen zukönnen. Ihnen sei dafür gedankt.

Ebenso gilt mein Dank meinen Eltern, meiner Schwester und meiner Oma für ihre Unterstützung jenseits der Physik. Schlussendlich möchte ich mich am meisten bei Marie bedanken, für die vielen schönen Momente und vor allem für ihre schier endlose Geduld mit mir beim Erstellen dieser Arbeit.

Ehrenwörtliche Erklärung

Ich erkläre hiermit ehrenwörtlich, dass ich die vorliegende Arbeit selbstständig, ohne unzulässige Hilfe Dritter und ohne Benutzung anderer als der angegebenen Hilfsmittel und Literatur angefertigt habe. Die aus anderen Quellen direkt oder indirekt übernommenen Daten und Konzepte sind unter Angabe der Quelle gekennzeichnet.

Ergebnisse und Veröffentlichungen, die in Zusammenarbeit mit meinem betreuenden Hochschullehrer Prof. Dr. Holger Gies sowie mit anderen Mitgliedern des Lehrstuhles fur Quantenfeldtheorie in Jena und anderen Kooperationen entstanden sind, sind in der Arbeit entsprechend benannt.

Weitere Personen waren an der inhaltlich-materiellen Erstellung der vorliegenden Arbeit nicht beteiligt. Insbesondere habe ich hierfür nicht die entgeltliche Hilfe von Vermittlungs- bzw. Beratungsdiensten (Promotionsberater oder andere Personen) in Anspruch genommen. Niemand hat von mir unmittelbar oder mittelbar geldwerte Leistungen für Arbeiten erhalten, die im Zusammenhang mit dem Inhalt der vorgelegten Dissertation stehen.

Die Arbeit wurde bisher weder im In- noch im Ausland in gleicher oder ähnlicher Form einer anderen Prüfungsbehörde vorgelegt.

Die geltende Promotionsordnung der Physikalisch-Astronomischen Fakultät ist mir bekannt.

Ich versichere ehrenwörtlich, dass ich nach bestem Wissen die reine Wahrheit gesagt und nichts verschwiegen habe.

Ort, Datum René Sondenheimer